Syntheses, Characterization and Kinetics of Nickel-Tungsten Nitride Catalysts for Hydrotreating of Gas Oil

A Thesis Submitted to the College of Graduate Studies and Research
in Partial Fulfillment of the Requirements for the
Degree of Doctor of Philosophy
in the Department of Chemical Engineering
University of Saskatchewan
Saskatoon

By

Christian Botchwey

COPYRIGHT

ABSTRACT

This thesis summarizes the methods and major findings of Ni-W(P)/γ-Al_2O_3 nitride catalyst synthesis, characterization, hydrotreating activity, kinetic analysis and correlation of the catalysts' activities to their synthesis parameters and properties.

The range of parameters for catalyst synthesis were W (15-40 wt%), Ni (0-8 wt%), P (0-5 wt%) and nitriding temperature (T_N) (500-900 °C). Characterization techniques used included: N_2 sorption studies, chemisorption, elemental analysis, temperature programmed studies, x-ray diffraction, scanning electron microscopy, energy dispersive x-ray, infrared spectroscopy, transmission electron microscopy and x-ray absorption near edge structure. Hydrodesulfurization (HDS), hydrodenitrogenation (HDN) and hydrodearomatization (HDA) were performed at: temperature (340-380 °C), pressure (6.2-9.0 MPa), liquid hourly space velocity (1-3 h^{-1}) and hydrogen to oil ratio (600 ml/ml, STP).

The predominant species on the catalyst surface were Ni_3N, W_2N and bimetallic Ni_2W_3N. The bimetallic Ni-W nitride species was more active than the individual activities of the Ni_3N and W_2N. P increased weak acid sites while nitriding temperature decreased amount of strong acid sites. Low nitriding temperature enhanced dispersion of metal particles. P interacted with Al_2O_3 which increased the dispersion of metal nitrides on the catalyst surface. HDN activity increased with Ni and P loading but decreased with increase in nitriding temperature (optimum conversion; 60 wt%). HDS and HDA activities went through a maximum with increase in the synthesis parameters (optimum conversions; 88. wt% for HDS and 47 wt% for HDA). Increase in W loading led to increase in catalyst activity. The catalysts were stable to deactivation and had the nitride structure conserved during hydrotreating in the presence of hydrogen sulfide.

The results showed good correlation between hydrotreating activities (HDS and HDN) and the catalyst nitrogen content, number of exposed active sites, catalyst particle size and BET surface area.

HDS and HDN kinetic analyses, using Langmuir-Hinshelwood models, gave activation energies of 66 and 32 kJ/mol, respectively. There were no diffusion limitations in the reaction process. Two active sites were involved in HDS reaction while one site was used for HDN.

HDS and HDN activities of the Ni-W(P)/γ-Al_2O_3 nitride catalysts were comparable to the corresponding sulfides.

ACKNOWLEDGEMENT

I wish to acknowledge the input and contribution of a number of persons who helped in diverse ways to bring this thesis to fruition.

First and foremost, I render my sincere gratitude to my supervisors, Drs A. K. Dalai and J. Adjaye for their invaluable assistance and guidance in my entire experimental work and in my thesis write up. Secondly, I wish to express my profound gratitude to the members of my advisory committee: Drs. G. A. Hill, T. Pugsley, H. Wang and J. Sharma for their time, reviews and contribution. I'm grateful that in the midst of all their busy schedules, they accepted to be members of my advisory committee. Other personalities whose assistance I wish to recognize are the support staff in the Chemical Engineering department (particularly Mrs. Blondin Richard and Mr. T. B. Wellentiny), and the technical staff at Syncrude Canada research centre who helped analyze my samples and maintain the equipment for my experiments. Many thanks go to the support my colleagues in the chemical reaction and engineering lab for availing themselves in the time of need. Financial assistances from NSERC, the University of Saskatchewan, Syncrude Canada, and the CRC award to Dr. Dalai are gratefully acknowledged

Above all, I acknowledge the guidance and protection of God, without whom this feat could not have been achieved.

DEDICATION

This work is dedicated to
my wife Agnes,
my two girls Elsa and Darlene and
my mum Agnes

TABLE OF CONTENTS

COPYRIGHT i

ABSTRACT ii

ACKNOWLEDGEMENT iv

DEDICATION v

TABLE OF CONTENTS vi

LIST OF TABLES xiii

LIST OF FIGURES xv

NOMENCLATURE xxii

CHAPTER 1 INTRODUCTION 1

1.1 Research Background 1

1.2 Industrial Challenge 2

1.3 Novel Catalyst Development 4

1.3.1 Catalyst Supports 5

1.3.2 Studies with Non-Metallic Additives 5

1.3.3 Preparation with Different Precursors 6

1.3.4 Transition Metal Sulfides 6

1.3.5 Active Phases other than Sulfides 6

CHAPTER 2 LITERATURE REVIEW 8

2.1. Feed Properties and Reactivities 8

2.1.1. Sulfur Compounds 8

2.1.2. Nitrogen Heterocyclic Compounds and their Reactivities 12

2.1.3. Aromatic Hydrocarbons and their Reactivities 15

2.2. Nitride Catalysts 17

2.2.1. Bulk Nitride Catalysts 19
2.2.2. Supported Nitride Catalysts 20
2.2.3. Oxynitride Catalysts 22
2.2.4. Cooling and Passivation of Nitride Catalysts 22
2.2.5. Synthesis Gases for Nitride Catalyst Preparations 23
2.2.6. Stability of Nitride Catalysts in HDS Environment 23
2.3. Catalyst Characterization 24
2.3.1. Surface Area, Pore Diameter and Pore Volume Analyses 24
2.3.2. Elemental Analyses (ICP-MS, EDX, CHN) 28
2.3.3. Chemisorption Studies 29
2.3.4. Temperature Programmed Techniques 30
2.3.5. Thermogravimetric Analysis (TGA) 34
2.3.6. X-ray Diffraction (XRD) Analyses 35
2.3.7. Scanning Electron Microscopy (SEM) 37
2.3.8. Energy Dispersive X-ray (EDX) 38
2.3.9. Transmission Electron Microscopy (TEM) 38
2.3.10. Infrared Spectroscopy 40
2.3.11. X-ray Absorption near Edge Structure (XANES) 40
2.4. Kinetic Analysis 42
2.4.1. Limitations in Catalytic Reactions 46
2.4.2. Analyses of Catalyst Utilization 47
2.4.3. HDS and HDN Kinetic 49
2.4.4. Solving Rate Equations and Evaluating Kinetic Parameters 52
2.5. Knowledge Gaps 52
2.6. Hypothesis 53
2.7. Research Objectives 53
2.7.1. Main Objective 53
2.7.2. Sub-Objectives 54
CHAPTER 3 EXPERIMENTAL 55

3.1 Catalyst Syntheses 55
3.1.1 Overview of Catalyst Synthesis Work 55
3.1.2 Catalyst Impregnation and Calcination Processes 59
3.1.3 Nitriding and Passivation Processes 59
3.1.4 Sulfide Catalyst Synthesis 61
3.2 Catalyst Characterization 62
3.2.1 Surface Area, Pore Diameter and Pore Volume Analyses 62
3.2.2 Catalyst Nitrogen and Sulfur Analyses 62
3.2.3 Temperature Programmed Techniques 63
3.2.4 Temperature Programmed Oxidation (TPO) 63
3.2.5 X-ray Diffraction (XRD) Analyses 63
3.2.6 Scanning Electron Microscopy (SEM) 63
3.2.7 Transmission Electron Microscopy (TEM) 64
3.2.8 Infrared Spectroscopy (IR) 64
3.2.9 X-ray Absorption near Edge Structure (XANES) 64
3.3 Hydrotreating Experimental Setup and Activity Studies 65
3.3.1 Reactor Loading 65
3.3.2 Reactor Pressure Testing 68
3.3.3 Catalyst Pretreatment 69
3.3.4 Catalyst Activity Stabilization 69
3.3.5 Catalyst Activity Test Runs 70
CHAPTER 4 CATALYST CHARACTERIZATION 73
4.1 N_2 Sorption Studies 73
4.1.1 Surface Area, Pore Volume and Pore Diameter of Cat-P Nitrides 75
4.1.2 Surface Area, Pore Volume and Pore Diameter of Cat-Ni Nitrides 76
4.1.3 Surface Area, Pore Volume and Pore Diameter of Cat-W Nitrides 76
4.1.4 Surface Area, Pore Volume and Pore Diameter of Cat-T_N Nitrides 77
4.2 Temperature Programmed Desorption (TPD) 77
4.2.1 Temperature Programmed Desorption of Cat-P Nitrides 81

4.2.2 Temperature Programmed Desorption of Cat-Ni Nitrides 82
4.2.3 Temperature Programmed Desorption of Cat-W Nitrides 82
4.2.4 Temperature Programmed Desorption of Cat-T_N Nitrides 82
4.3 Temperature Programmed Reduction (TPR) 83
4.3.1 Temperature Programmed Reduction of Cat-P Nitrides 85
4.3.2 Temperature Programmed Reduction of Cat-Ni Nitrides 87
4.3.3 Temperature Programmed Reduction of Cat-W Nitrides 87
4.3.4 Temperature Programmed Reduction of Cat-T_N Nitrides 89
4.4 Temperature Programmed Oxidation (TPO) 89
4.4.1 Temperature Programmed Oxidation of Cat-P Nitrides 90
4.4.2 Temperature Programmed Oxidation of Cat-Ni Nitrides 93
4.4.3 Temperature Programmed Oxidation of Cat-W and Cat-T_N Nitrides 93
4.5 X-Ray Diffraction (XRD) 95
4.5.1 X-ray Diffraction of Cat-P Nitrides 95
4.5.2 X-ray Diffraction of Cat-Ni Nitrides 98
4.5.3 X-ray Diffraction of Cat-W and Cat-T_N Nitrides 98
4.6 SEM and EDX of Ni-W(P)/γ-Al_2O_3 Nitride Catalyst Samples 100
4.6.1 Scanning Electron Microscopy of Cat-P Nitrides 100
4.6.2 Scanning Electron Microscopy of Cat-Ni Nitrides 103
4.6.3 Scanning Electron Microscopy of Cat-W Nitrides 103
4.6.4 Scanning Electron Microscopy of Cat-T_N Nitrides 103
4.7 Energy Dispersive X-ray 107
4.8 Transmission Electron Microscopy (TEM) 107
4.9 Infrared Spectroscopy (IR) 116
4.10 X-ray Absorption Near Edge Structure (XANES) 118
CHAPTER 5 HYDROTREATING OF GAS OIL OVER NITRIDE CATALYSTS 121
5.1 Catalyst Precoking 121
5.2 Effect of Catalyst Synthesis Parameters on HDS, HDN and HDA 123

5.2.1 Catalyst Screening: HDS 124
5.2.2 Catalyst Screening: HDA 126
5.2.3 Catalyst Screening: HDN 126
5.2.4 Catalyst Screening: Effect of Tungsten Loading 129
5.3 Effect of Process Conditions on HDS and HDN 132
5.3.1 Effect of Process Conditions on HDS 132
5.3.2 Effect of Process Conditions on HDN 135
5.4 Stability of Tungsten Nitride Catalysts to Deactivation 138
5.5 Effect of H_2S on Hydrotreating 139
CHAPTER 6 CORRELATION OF ACTIVITY TO CATALYST PROPERTIES 150
6.1 Correlation of Activity to Catalyst Properties: Effect of Phosphorus 150
6.2 Correlation of Activity to Catalyst Properties: Effect of Nickel 152
6.3 Correlation of Activity to Catalyst Properties: Effect of Tungsten 154
6.4 Correlation of Activity to Catalyst Properties: Effect of Nitriding Temperature 156
CHAPTER 7 KINETIC ANALYSES 159
7.1 Kinetic Model Considerations 159
7.2 Evaluation of Parameters and Model Discrimination 161
7.2.1 Analyses of HDS Kinetics 161
7.2.2 Analyses of HDN Kinetics 164
7.3 Mass Transfer Considerations 166
7.3.1 External Mass Transfer Limitations 166
7.3.2 Internal Mass Transfer Limitations 168
CHAPTER 8 CONCLUSIONS AND RECOMMENDATIONS 170
8.1 Conclusions 170
8.1.1 Nitride Catalyst Syntheses 170
8.1.2 Nitride Catalyst Characterization 170

8.1.3 Hydrotreating of Gas oil 171
8.1.4 Correlation of Catalyst Surface Properties to Activity 172
8.1.5 Kinetic Analyses 173
8.2 Recommendations 173
REFERENCES 175
APPENDICES 194
APPENDIX A EXPERIMENTAL CALIBRATIONS 195
A.1 Reactor Temperature Controller Calibration 195
A.2 Mass Flow Meter Calibration 195
A.3 Pump Calibration 198
APPENDIX B STATISTICAL EXPERIMENTAL DESIGN 202
B.1 Central Composite Design 202
B.2 Statistical Model Development 203
B.2.1 Modeling of Catalyst Screening Results: HDS 204
B.2.2 Modeling of Catalyst Screening Results: HDA 204
B.2.3 Modeling of Catalyst Screening Results: HDN 206
B.2.4 Effect of Process Conditions on HDS of LGO 208
APPENDIX C SAMPLE CALCULATIONS 210
C.1 Calculation for Amounts of Precursors in Catalyst Synthesis 210
C.2 Mass Transfer Calculations 212
C.2.1 External Mass Transfer Limitations 212
C.2.2 Internal Mass Transfer Limitations 219
C.2.3 Particle Peclet Number Calculations 228
APPENDIX D THERETICAL ANALYSES OF ANALYTICAL TECHNIQUES AND KINETICS 230

D.1 Electron Microscopy 230
D.2 Vibrational Spectroscopies 230
D.3 Developing Langmuir-Hinshelwood Kinetic Models 233
D.4 Evaluation of Kinetic Parameters 234
D.4.1 Differential Method 234
D.4.2 Integral Method 235
D.4.3 Non-linear Least Squares Analysis 236
D.4.4 Evaluation of Activation Energy and Heat of Adsorption 237
APPENDIX E FEED AND PRODUCT ANALYSES 238
E.1 Sulfur Analysis 238
E.2 Nitrogen Analysis 238
E.3 Aromatic Hydrocarbon Analysis 239
APPENDIX F EXPERIMENTAL RESULTS 240
F.1 Preliminary Characterization Results 240
F.1.1 BET Surface Area Analyses 240
F.2 SEM and EDX Results 242
F.2.1 Reference Samples 242
F.2.2 SEM and EDX of Cat-P Samples 243
F.2.3 SEM and EDX of Cat-Ni Samples 244
F.2.4 SEM and EDX of Cat-W Samples 245
F.2.5 SEM and EDX of Cat-T_N Samples 246
F.3 Transmission Electron Microscopy Results 247
F.4 Infrared Spectroscopy Results 251

LIST OF TABLES

Table 1.1: Conventional and unconventional crude oil qualities (McKetta, 1992). 3
Table 2.1: Bond energies of heterocyclic compounds in petroleum (Kabe et al., 1999). 14
Table 2.2: Relative rate constants for hydrogenation of aromatic hydrocarbons over sulfided catalysts. (Yang and Stock, 1996). 18
Table 2.3: Some techniques commonly used in catalyst characterization and their relevance to hydrotreating. 26
Table 2.4: Common infrared bands relevant to nitride catalysts. 41
Table 3.1: Parameter values for nitride catalyst synthesis based on statistical experimental design; W loading, 15 wt%. 58
Table 3.2: Elemental composition and nitriding temperature of synthesized nitride catalysts. 60
Table 3.3: Properties of Light Gas Oil feed used for the experimental work. 71
Table 4.1: BET surface area, pore volume and pore diameter of Ni-W(P)/γ-Al_2O_3 nitride catalyst. 74
Table 4.2: Elemental composition from EDX analyses of Cat-P and Cat-W nitride samples 109
Table 5.1 BET, chemisorption and nitrogen content of tungsten nitride catalysts 131
Table 5.2: Design factors, levels and conversions for HDS and HDN of light gas oil (coded values in brackets) 133
Table 5.3: HDS and HDN reaction rate constants for Stages II and IV of tungsten nitride catalyst stability studies. 141
Table 5.4: Simulated distillation data for feed and sample hydrotreated at 385 ºC, 9.0 MPa and 2 h^{-1} 142
Table 5.5: Nitrogen and sulfur content of nitride and sulfided nitride catalysts 146
Table 7.1: Kinetic parameters for HDS of LGO using Ni-W(P)/γ-Al_2O_3 nitride catalyst 162
Table 7.2: Kinetic parameters for HDN of light gas oil using Ni-W(P)/γ-Al_2O_3 nitride catalyst. 165
Table B.1: Modeling statistics for effects of process conditions on HDS and HDN 209
Table C.1: Precursors used for catalyst syntheses and their molecular weights 211
Table C.2: Thermodynamic properties of three sulfur-containing compounds in petroleum (Data from ChemDraw) 217

Table C.3: Evaluated results of specific molar volume for three sulfur-containing compounds in petroleum 218
Table C.4: Thermodynamic properties of reactants and products of hydrodesulfurization reaction (all data – at 298.15 K and 1 atm – obtained from ChemDraw) 227
Table F.1: HDS, HDN and HDA responses for nitride catalyst activity screening studies..... 253

LIST OF FIGURES

Figure 2.1: Total world oil reserves. Unconventional = oil sands bitumen, heavy oil and extra heavy oil (Alboudwarej et al., 2006). 9
Figure 2.2: Some organosulfur compounds in petroleum (Girgis and Gates, 1991). 10
Figure 2.3: Some organonitrogen compounds in petroleum (Girgis and Gates, 1991) 13
Figure 2.4: Some aromatic hydrocarbons in petroleum feedstock (Girgis and Gates, 1991)..... 16
Figure 2.5: Diagram showing examples of catalyst contact with sub-atomic particles or electromagnetic radiation and emissions obtained. (em = electromagnetic) 25
Figure 2.6: Schematic representation of the structure of activated carbon (Wood and Gladden, 2002)..... 44
Figure 2.7: External and internal mass transfer of reactant molecule during reaction. 45
Figure 3.1: Overview of syntheses procedures for nitride and sulfide catalysts. 56
Figure 3.2: Different groups of catalysts prepared for various experimental work..... 57
Figure 3.3: Schematic Diagram of Experimental Setup (TC: Temperature Controller, PG: Pressure gauge). 66
Figure 3.4: Schematic diagram of a loaded micro-reactor prior to hydrotreating. 67
Figure 4.1: Temperature programmed desorption of NH_3 from reference nitride catalysts. Conditions: 30 wt% W, 10 wt% Ni, T_N of 700 °C and adsorption temperature of 30 °C. 78
Figure 4.2: TPD profiles of NH_3 from (A) Cat-P and (B) Cat-Ni nitride samples. Conditions: 30 wt% W, T_N of 700 °C and adsorption temperature of 30 °C; (A) 4 wt% Ni; (B) 2 wt% P. 79
Figure 4.3: TPD profiles of (A) Cat-W and (B) Cat-T_N nitride samples. Conditions: 4 wt% Ni, 2 wt%, P and adsorption temperature of 30 °C; (A) T_N of 700 °C, (B) 30 wt% W..... 80
Figure 4.4: Temperature programmed reduction of reference nitride catalysts and γ-Al_2O_3. Conditions: 30 wt% W, 10 wt% Ni and T_N of 700 °C. 84
Figure 4.5: TPR profiles of (A) Cat-P and (B) Cat-Ni nitride samples. Conditions: 30 wt% W, T_N of 700 °C and (A) 4 wt% Ni; (B) 2 wt% P..... 86

Figure 4.6: TPR profiles of (A) Cat-W and (B) Cat-T_N nitride samples. Conditions: 4 wt% Ni, 2 wt%, P (A) T_N of 700 °C and (B) 30 wt% W. 88
Figure 4.7: Temperature programmed oxidation of reference nitride catalysts and γ-Al_2O_3. Conditions: 30 wt% W, 10 wt% Ni and T_N of 700 °C. 91
Figure 4.8: Temperature programmed oxidation profiles of (A) Cat-P and (B) Cat-Ni nitride samples. Conditions: 30 wt% W, T_N of 700 °C and (A) 4 wt% Ni; (B) 2 wt% P. 92
Figure 4.9: Temperature programmed oxidation profiles of (A) Cat-W and (B) Cat-T_N nitride samples. Conditions: 4 wt% Ni, 2 wt% P and (A) 700 °C T_N; (B) 30 wt% W. 94
Figure 4.10: X-ray diffraction patterns of reference samples. (o) γ-Al_2O_3, (+) W_2N, (*) Ni_3N, ( ) Ni metal. Conditions: 30 wt% W, 10 wt% Ni and T_N of 700 °C. 96
Figure 4.11: X-ray diffraction patterns of (A) Cat-P nitrides and (B) Cat-Ni nitrides. Peaks: - (o) γ-Al_2O_3; (+) W_2N; (*) Ni_3N; (Δ) Ni_2W_3N. Conditions: 30 wt% W, T_N, of 700 °C and (A) 4 wt% Ni; (B) 2 wt% P. 97
Figure 4.12: X-ray diffraction patterns of (A) Cat-W nitrides and (B) Cat-T_N nitrides. Peaks: - (o) γ-Al_2O_3; (+) W_2N; (*) Ni_3N; (Δ) Ni_2W_3N, (•) W metal, (-) Ni metal. Conditions: 4 wt% Ni, 2 wt% P and (A) T_N of 700 °C; (B) 30 wt% W. 99
Figure 4.13: SEM micrographs of W/γAl_2O_3 nitride catalysts. Conditions: 30 wt% Wand T_N of 700 °C. 101
Figure 4.14: SEM micrographs of Cat-P nitride samples. (A) 0%-P; (B) W(P)/γAl_2O_3; (C, D) 2%-P; (E,F) 4%-P. Conditions: 30 wt% W, 4 wt% Ni and T_N of 700 °C. 102
Figure 4.15: SEM micrographs of Cat-Ni nitride samples. (A) 0%-Ni; (B) Ni-W/γAl_2O_3; (C, D) 2%-Ni; (E, F) 4%-Ni. Conditions: 30 wt% W, 2 wt% P and T_N of 700 °C. 104
Figure 4.16: SEM micrographs of Cat-W nitride samples. (A, B) 15%-W; (C, D) 30%-W; (E F) 40%-W. Conditions: 4 wt% Ni, 2 wt% P and T_N of 700 °C. 105
Figure 4.17: SEM micrographs of Cat-T_N nitride samples. (A, B) 500°-T_N; (C, D) 700°-T_N; (E, F) 900°-T_N. Conditions: 30 wt% W, 4 wt%, Ni and 2 wt% P. 106
Figure 4.18: EDX spectra of 2%-P nitride catalyst. Conditions: 30 wt% W, 4 wt% Ni, 2 wt% P and T_N of 700 °C. 108

Figure 4.19: Transmission electron micrographs of Ni-W(P)/γ-Al_2O_3 oxide. Conditions: 30 wt% W, 4 wt% Ni and 2 wt% P. 110
Figure 4.20: Transmission electron micrographs of W/γ-Al_2O_3 nitride. Conditions: 30 wt% W and T_N of 700 °C 111
Figure 4.21: Transmission electron micrographs of W(P)/γ-Al_2O_3 nitride. Conditions: 30 wt% W, 2 wt% P and T_N of 700 °C 112
Figure 4.22: Transmission electron micrographs of Ni-W/γ-Al_2O_3 nitride. Conditions: 30 wt% W, 4 wt% Ni and T_N of 700 °C. 113
Figure 4.23: Transmission electron micrographs of Ni-W(P)/γ-Al_2O_3 nitride. Conditions: 30 wt% W, 4 wt% Ni, 2 wt% P and T_N of 700 °C. 114
Figure 4.24: Transmission electron micrographs of Ni-W(P)/γ-Al_2O_3 nitride. Conditions: 30 wt% W, 4 wt% Ni, 2 wt% P and T_N of 900 °C. 115
Figure 4.25: Infrared spectra of (A) reference oxide (P, 2 wt%) and nitrides (Ni, 10 wt%), and (B) Cat-P nitride samples in the 400-4000 cm^{-1} region. Conditions: 30 wt% W, 4 wt% Ni and T_N of 700 °C. 117
Figure 4.26: P L-edge XANES spectra of selected Cat-P nitride. Conditions: 30 wt% W, 4 wt% Ni, (I) 2 wt% P and T_N of 700 °C; (II) 4 wt% P and T_N of 700 °C; (III) 2 wt% P and T_N of 500 °C. 119
Figure 5.1: HDN activity for nitride catalyst precoking. Conditions: T, 375°C; P_H, 9.0 MPa; LHSV, 1 h^{-1} and H_2/oil: 600 ml/ml. 15 wt% W, (Cat-2) 6.4 wt% Ni, 1 wt% P and T_N of 739 °C; (Cat-3) 4 wt% Ni, 2.5 wt% P and T_N of 650 °C; (Cat-4) 1.6 wt% Ni, 4 wt% P and T_N of 739 °C; (Cat-14) 1.6 wt% Ni, 1 wt% P and T_N of 561 °C. 122
Figure 5.2: (A) Perturbation and (B) parity plots for Effects of synthesis parameters on HDS of LGO hydrotreated at 350 °C, 9.0 MPa, LHSV of 2 h^{-1} and H_2/Oil of 600 ml/ml. Reference Points: 4.0 wt% Ni, 2.5 wt% P and T_N of 650 °C..... 125
Figure 5.3: (A) Perturbation and (B) parity plots for Effects of synthesis parameters on HDA of LGO hydrotreated at 350 °C, 9.0 MPa, LHSV of 2 h^{-1} and H_2/Oil of 600 ml/ml. Reference Points: Ni = 4.0 wt%, P_H = 2.5 wt%, T_N = 650 °C..... 127
Figure 5.4: (A) Perturbation and (B) parity plots for Effects of synthesis parameters on HDN of LGO hydrotreated at 350 °C, 9.0 MPa, LHSV of 2 h^{-1} and H_2/Oil of 600 ml/ml. Reference Points: 4.0 wt% Ni, 2.5 wt% P and T_N of 650 °C..... 128

Figure 5.5: Effect of tungsten loading on HDS and HDN of LGO using Ni-W(P)/γ-Al_2O_3 nitride catalyst at (A) 350 °C and (B) 360 °C. Conditions: 2.5 wt% Ni, 1 wt% P and T_N of 560 °C. Process conditions: P_H = 9.0 MPa, LHSV= 2 h^{-1}, H_2/oil = 600 ml/ml. 130

Figure 5.6: (A) Perturbation and (B) parity plots for effects of process conditions on HDS of LGO over Ni-W(P)/γ-Al_2O_3 nitride catalyst. Process conditions: 340 - 385 °C, 6.2 – 9.0 MPa, LHSV of 1 - 3 h^{-1} and hydrogen/oil of 600 ml/ml (STP). Catalyst conditions: 2.5 wt% Ni, 1 wt%, P and T_N of 560 °C. 134

Figure 5.7: HDS Interaction effect between temperature and LHSV over Ni-W/γ-Al_2O_3 nitride using light gas oil. P_H, 7.6 MPa; Hydrogen/oil, 600 ml/ml (STP). 136

Figure 5.8: Perturbation plot for HDN of light gas oil using tungsten nitride catalyst. Reference conditions: 340 - 385 °C, 6.2 - 9.0 MPa, LHSV of 1 - 3 h^{-1} and hydrogen/oil: 600 ml/ml (STP). 137

Figure 5.9: Ni-W(P)/γ-Al_2O_3 nitride catalyst stability to HDS and HDN reaction using light gas oil. Conditions: 330 to 385 °C, 9.0 MPa, LHSV of 2 h^{-1} and hydrogen/oil, 600 ml/ml (STP). 140

Figure 5.10: (A) HDN at 15 wt% W loading and (B) HDS at 25 wt% W loading of LGO using Ni-W(P)/γ-Al_2O_3 nitride catalyst. N = nitride; SN = sulfided nitride; P_H, 9.0 MPa; LHSV, 2 h^{-1}; H_2/oil, 600 ml/ml; Ni, 2.5 wt%; P, 1wt%; T_N, 560 °C. 144

Figure 5.11: HDS and HDN of LGO using Ni-W(P)/γ-Al_2O_3 nitride catalyst at LHSV of (A) 1 h^{-1} and (B) 2 h^{-1}. N = nitride; NS = sulfided nitride; S = sulfide; P_H, 9.0 MPa; H_2/oil, 600 ml/ml; W, 15 wt%; Ni, 2.5 wt%; P, 1wt%; T_N, 560 °C. 145

Figure 5.12: (A) FTIR spectroscopy of nitride and sulfided W(P)/γ-Al_2O_3 nitride catalyst and (B) sulphur L-edge XANES of fresh and spent nitride catalysts at 25 wt% W, 2.5 wt% Ni, 1 wt% P and T_N of 560 °C. 148

Figure 5.13: X-ray diffraction patterns of (A) sulfided nitride and (B) nitride catalysts. Conditions: 2.5 wt% Ni, 1 wt% P and,25 wt% W and T_N of 560 °C. 149

Figure 6.1: (A) Effect of P loading on HDS and HDN of light gas oil at 350 °C, 9.0 MPa, LHSV of 2 h^{-1} and H_2/oil of 600 ml/ml. (B) Correlation between amount of chemisorbed oxygen, surface area (S.A.), nitrogen content (N) and average particle

size (P.S.) to catalyst P loading. Conditions: 30 wt% W, 4 wt% Ni and T_N of 700 °C. 151
Figure 6.2: (A) Effect of Ni on HDS and HDN of light gas oil at T, 350 °C; P_H, 9.0 MPa; LHSV, 2 h^{-1}; H_2/oil, 600 ml/ml. (B) Correlation of surface area (S.A.), nitrogen content (N) and average TEM particle size (P.S.) to catalyst T_N. Conditions: 30 wt% W, 2 wt% P and T_N of 700 °C. 153
Figure 6.3: (A) Effect of W loading on HDS and HDN of light gas oil at T, 350 °C; P_H, 9.0 MPa; LHSV, 2 h^{-1}; H_2/oil, 600 ml/ml. (B) Correlation of amount of chemisorbed oxygen (chemi), surface area (S.A.), nitrogen content (N) and average particle size (P.S.) to catalyst W loading. Conditions: 2 wt% P, 4 wt% Ni and T_N of 700 °C..... 155
Figure 6.4: (A) Effect of T_N on HDS and HDN of light gas oil at T, 350 °C; P_H, 9.0 MPa; LHSV, 2 h^{-1}; H_2/oil, 600 ml/ml. (B) Correlation of amount of chemisorbed oxygen, surface area (S.A.), nitrogen content (N) and average particle size (P.S.) to catalyst T_N. Conditions: 30 wt% W, 2 wt% P and 4 wt% Ni. 157
Figure 7.1: Parity plot for the experimental and model-predicted product sulfur concentrations of the HDS of light gas oil using Ni-W(P)/γ-Al_2O_3 catalyst. T, 340 to 385 ºC; P_H, 9.0 MPa; LHSV, 2 h^{-1}; H_2/oil, 600 ml/ml (STP); 15 wt% W, 2.5 wt% Ni, 1 wt% P and T_N, of 560 °C. 163
Figure 7.2: Parity plot for the experimental and model-predicted product nitrogen concentrations of the HDN of light gas oil using Ni-W(P)/γ-Al_2O_3 catalyst at 340 to 385 ºC, 9.0 MPa, LHSV of 2 h^{-1} and H_2/oil, 600 ml/ml (STP). Catalyst properties: 15 wt% W, 2.5 wt% Ni, 1 wt% P and T_N of 560 °C. 167
Figure A.1: Temperature pattern along the length of the reactor. 196
Figure A.2: Reactor average temperature curve. 197
Figure A.3: Calibration curve for hydrogen mass flow controller..... 199
Figure A.4: Pump calibration curve. 200
Figure A.5: (A) Temperature and (B) mass flow controller calibrations for temperature programmed nitriding set up. 201
Figure B.1: Structure of central composite design..... 202
Figure B.2: (A) HDS and (B) HDA of LGO over Ni-W(P)/γ-Al_2O_3 nitride catalysts. Conditions: 30 wt% W, (A) T_N of 650 °C and (B) 2.5 wt% P. 205

Figure B.3: HDN of LGO over Ni-W(P)/γ-Al_2O_3 nitride catalysts at T_N of 560 ^oC. 207
Figure B.4: Effect of process conditions on HDS of LGO over Ni-W(P)/γ-Al_2O_3 nitride catalyst. H_2/oil, 600 ml/ml (STP); (A) LHSV = 2 h^{-1}; (B) P_H = 7.6 MPa. Catalyst conditions: Ni = 2.5 wt%, P_H = 1 wt%, T_N = 560 °C. 208
Figure D.1: Schematic set ups of TEM and SEM (Niemantsverdriet, 1993) 231
Figure D.2: Different forms of infrared spectroscopy: transmission infrared and diffuse reflectance infrared spectroscopy. 232
Figure F.1: BET surface area of Ni-W(P)/γ-Al_2O_3 nitride catalyst at varying T_N, Ni and P loadings. Conditions: 15 wt% W, (A) 2.5 wt% P and (B) 4 wt% Ni. 241
Figure F.2: (A) SEM micrograph and (B) EDX of W/γ-Al_2O_3 nitride catalyst. Conditions: 30 wt% W, 4 wt% Ni, 2 wt% P and T_N of 700 °C. 242
Figure F.3: (A) SEM micrograph and (B) EDX of W/γ-Al_2O_3 nitride catalyst. Conditions: W, 30 wt%; Ni, 4 wt%; P, 2 wt%; 700 °C 243
Figure F.4: SEM micrographs and EDX spectra of Cat-Ni nitride samples. (A, B) 0%-Ni; (C, D) 2%-Ni; (E,F) 4%-Ni. Conditions: 30 wt% W, 2 wt% P and T_N of 700 °C. 244
Figure F.5: SEM micrographs and EDX spectra of Cat-W nitride samples. (A, B) 15%-W; (C, D) 30%-W; (E, F) 40%-W. Conditions: 4 wt% Ni, 2 wt% P and T_N of 700 °C. 245
Figure F.6: SEM micrographs and EDX spectra of Cat-T_N nitride samples. (A, B) 500°-T_N; (C, D) 700°-T_N; (E, F) 900°-T_N. Conditions: 30 wt% W, 4 wt% Ni and 2 wt% P. 246
Figure F.7: Transmission electron micrographs of (A) W/γ-Al_2O_3 and (B) 4%-P nitride catalysts. Conditions: 30 wt% W, 4 wt% Ni, 4 wt% P and T_N, 700 °C. 247
Figure F.8: Transmission electron micrographs of 2%-Ni nitride catalyst. Conditions: 30 wt% W, 2 wt% Ni, 2 wt% P and T_N, 700 °C. 248
Figure F.9: Transmission electron micrographs of 40% W nitrides catalyst. Conditions: 40 wt% W, 4 wt% Ni, 2 wt% P and T_N of 700 °C. 249
Figure F.10: Transmission electron micrographs of 500°-T_N nitrides catalyst. Conditions: 30 wt% W, 4 wt% Ni, 2 wt% P and T_N of 500 °C. 250
Figure F.11: Infrared spectra of Cat-Ni nitride samples in the 400-4000 cm^{-1} region. Conditions: W, 30 wt%; P, 2 wt%; T_N, 700 °C. 251

Figure F.12: IR spectra of (A) Cat-W and (B) Cat-T_N nitride samples in the 400-4000 cm^{-1} region. Conditions: 4 wt% Ni, 2 wt% P, (A) T_N of 700 °C, (B) 30 wt% W. 252

NOMENCLATURE

A	reactant
BET	Brunauer, Emmett and Teller
C	concentration (ppm or wt%)
C_{ib}	bulk concentration of reactant (kmol/m^3)
C_{As}	catalyst surface concentration of reactant A (kmol/m^3)
C_m	ratio of reaction rate to the external diffusion rate (dimensionless)
C_o	feed sulfur concentration (ppm or wt%)
C_{WP}	ratio of actual reaction rate to diffusion rate
Cat-Ni	catalysts with varying nickel loading
Cat-P	catalysts with varying phosphorus loading
Cat-T_N	catalysts with varying nitriding temperature
Cat-W	catalysts with varying tungsten loading
d_c	catalyst particle diameter (m)
d_p	catalyst pore diameter (m)
D_b	bulk diffusivity (m^2/s)
D_e	effective diffusivity (m^2/s)
DTA	differential thermal analysis
E	activation energy (kJ/mole)
EDX	energy dispersive x-ray spectroscopy
H	hydrogen gas
HDA	removal of aromatic compounds in petroleum feedstock by reacting with H_2
HDN	the removal of nitrogen from nitrogen-containing compounds in petroleum feedstock by reacting with H_2 to give off a hydrocarbon product and NH_3
HDS	the removal of sulfur from sulfur-containing compounds in petroleum feedstock by reacting with H_2 to give off a hydrocarbon product and H_2S

i	sulfur or nitrogen compound present in light gas oil
I	inhibitor
IR	infrared
k	reaction rate constant ($Pa^{-1}.\ h^{-(1+n)}$ or $wt\%^{(1-x)}.Pa^{-y}.h^{-(1+n)}$)
k'	reaction rate constant for desorption reaction
k_c	mass transfer coefficient (m/s)
K	adsorption rate constant ($ppm^{-1}*10^4$ or Pa^{-1})
K_s	constant in the Scherrer equation (dimensionless)
L	liquid hourly space velocity (h^{-1})
LGO	light gas oil
$LHSV$	liquid hourly space velocity
n	reaction order
Ni	nickel
P	phosphorus
P_H	hydrogen pressure (Pa)
Q	adsorption energy (kJ/mole)
r	rate of reaction ($ppm*10^4.h^{-1}$)
r_i'	reaction rate per unit mass of catalyst (kmol/kg-s)
R	catalyst particle radius
$\mathbf{Re}$	Reynolds numbers
R_g	gas constant ($KJmol^{-1}K^{-1}$)
Sc	Schmidt numbers
SEM	scanning electron microscopy
S_g	Specific surface area (m^2/g)
Sh	Sherwood number
t	time
T	hydrotreating temperature (ºC or K)
T_N	nitriding temperature (ºC)

TEM	transmission electron microscopy
TG	thermogravimetry
TPD	temperature programmed desorption
TPO	temperature programmed oxidation
TPR	temperature programmed reduction
U	superficial velocity (m/s)
v	molar volume (cm^3/mol)
v_c	specific critical volume (cm^3/mol)
V_p	catalyst specific pore volume (m^3/kg)
v_s	molar volume of sulfur compounds at normal boiling conditions (cm^3/mol)
W	tungsten
x	reaction order
XANES	x-ray absorption near edge structure
XRD	x-ray diffraction
y	reaction order

Greek Alphabets

β_s	peak width at half maximum
ε_b	catalyst bed porosity
ε_p	catalyst pellet porosity
λ	wavelength
μ	dynamic viscosity (kg/m.s)
ρ_b	bulk density of catalyst bed (kg/m^3)
ρ_c	density of catalyst pellet (kg/m^3)
ρ_f	fluid density (kg/m^3)
ρ_p	bulk density of catalyst pellet (kg/m^3)
σ	sum of squares

Φ	minimized error
θ	angle (°)
Θ	fraction of adsorbed catalyst sites covered by reactant
τ	tortuosity

CHAPTER 1
INTRODUCTION

1.1 Research Background

Hydrotreating is a hydrogenation process designed to remove contaminants such as sulfur, nitrogen, metals or oxygen from petroleum fractions and to saturate aromatics. If not removed, the contaminants can have negative effects on the equipment, the catalysts, and the quality of the finished product as they travel through the refinery processing units. For example, hydrotreating is performed to reduce sulfur and nitrogen contaminants that may poison catalysts for catalytic cracking. It is also used to upgrade middle-distillate petroleum fractions into products such as kerosene, diesel fuel, and heating fuel oils. Typically, hydrotreating is used to reduce sulfur in petroleum fractions so as to reduce sulfur dioxide emissions that result from using fuels in automotive vehicles, aircraft, railroad locomotives, ships, gas or oil burning power plants, residential and industrial furnaces, and other forms of fuel combustion.

Feedstocks for hydrotreating processes range from naphtha to vacuum residue. A typical hydrotreating process is carried out at high temperatures (317 – 427 °C) and pressures (9 – 14 MPa) (McKetta, 1992) over sulfided Co(Ni)-Mo(W)/Al_2O_3 catalyst to produce hydrocarbon products and H_2S and NH_3 as byproducts. As stated above, when contaminants end up in fuels, they are emitted as SO_x, NO_x, CO gases and particulates after combustion. Emission of these gases results in the formation of acid rain, smog and poison catalysts in catalytic converters (Whitehurst et al., 1998). As a result, the amount of contaminants in fuels is regulated by environmental agencies (Pille and Yu, 1994). For example, the maximum amount of sulfur permitted in diesel fuels in North America as of year 2005 was 500 parts per million (ppm) (Hunter et al., 2001; Milbourn, 2001). In a quest to create a cleaner environment, more stringent measures on sulfur specifications are being imposed over time (Siewe and Ng, 1998; Lee and de Wind, 1992). In the USA, the environmental protection agency (EPA) has mandated that refiners produce highway diesel fuel with maximum sulfur content of 15 ppm (ultra low sulfur diesel – ULSD) since June 1, 2006. In Canada, the concentration of sulfur in diesel fuel produced or imported for use in off-road engines is currently regulated not to exceed 500 ppm. This is expected to change to 15 ppm (ULSD) from 31 May 2010.

1.2 Industrial Challenge

Meeting the new sulfur emission standards poses a great challenge to refiners. Reducing the current sulfur specification by 97% can in no means be achieved by the current hydrotreating processes and facilities in place. It will surely require much more severe hydrodenitrogenation (HDN) and hydrodesulfurization (HDS) of petroleum fractions. Synthetic crude producers will no doubt face the greatest challenge, as they have to produce high quality fuel from low quality feedstock. Factors that affect hydrotreating product quality include operating conditions, feed oil and type of catalyst.

Severe operating conditions such as high operating temperature and pressures as well as low flow rates can be used to increase the quality of hydrotreating products. There is however a limit to how much operating conditions can be varied. Excessive increase in temperature will result in sintering and subsequent deactivation of catalysts (Speight, 2000). It will also lead to severe side reactions such as cracking to form gaseous products (Gray et al., 1994). Another issue with excessive increase in temperature is the risk of reduction in yield due to thermodynamic constraints (Whitehurst et al., 1998). Increase in hydrogen partial pressures often increases the overall hydrotreating reaction (Frost and Jensen, 1973; Gioia and Lee, 1986). High hydrogen partial pressures can reduce the rate of formation of coke during hydrotreating and increase activity (Girgis and Gates, 1991). It can also reduce the partial pressures of H_2S and NH_3 leading to increase in activity (Whitehurst et al., 1998). However, pressure is limited by the strength of current hydrotreating reactors. Although lowering flow rates will increase the overall quality of the product, excessive reduction in flow rate will not be economically favourable.

The type of feed used in hydrotreating has a great effect on the end product. The heavier the feed, the higher the level of contaminants (e.g. sulfur) and the more difficult it is to hydrotreat. Heavier feeds abound in refractory sulfur and nitrogen compounds and so make them difficult to hydrotreat (Girgis and Gates, 1991). Table 1.1 shows the relative sulfur and nitrogen contents of selected conventional and unconventional feedstock. With reports of continuous decline in both the quantity and quality of conventional feedstock supply to refineries (Siewe and Ng, 1998), manipulating the feedstock to meet the ULSD standard may not be possible. Another factor that may be manipulated to enhance the quality of hydrotreating products is enhancement in activity of hydrotreating catalysts. Commercial hydrotreating catalysts are currently Co(Ni)-Mo(W) sulfides supported on gamma alumina (γ-Al_2O_3) (Whitehurst et al.,

Table 1.1: Conventional and unconventional crude oil qualities (McKetta, 1992).

	Atha-basca***	Kuwait**	Ah-Safaniya**	Maya**	Bachaquero**
Specific gravity	0.99	0.871	0.889	0.913	0.955
^{o}API	12.4	30.9	27.7	23.5	16.7
Sulfur* [wt %]	4.0	2.5	2.9	3.0	2.3
Nitrogen [ppm]	2986	1300	1300	300	4300
Simulated Distillation, [vol %]					
15-18^{o}C	0	6.4	5.6	3.8	1.6
80-190^{o}C	0	17.6	15.6	15.3	6.4
190-340^{o}C	21.1	25.0	24.0	21.9	20.6
340-FBP °C	78.9	48.5	52.9	58.1	70.9
Aromatics [wt%]					
Mono-	20.7	17.7	-	-	-
Di-	12.2	11.5	-	-	-
Poly-	3.6	4.5	-	-	-

***Unconventional crude oil, **Conventional crude oil, *Heteroatoms.

1998). These conventional catalysts have been in use for over 80 years as hydrotreating catalysts but their activities have not improved much over the period. They are unable to completely eliminate sulfur from petroleum fuels (Whitehurst et al., 1998). The 500 ppm sulfur specification standard was achieved, not only through improvements in the activity of commercial catalysts, but in combination with the use of high-pressure vessels. More improvements in activity may be required especially now that even more stringent sulfur standards are being enforced.

Revamping hydrotreating facilities is costly. It is reported (EnviroFuels, 2007) in the U.S. that billions of dollars have already been invested in refinery upgrades to help meet the sulfur standards. Refiners do not have much control over the composition of feedstock. Options in this area will be to recycle the feedstock multiple times to reduce sulfur in the end product but that is not economical. Manipulating the catalyst may be the easiest and most economically favourable choice to improving hydrotreating product quality (Pille and Yu, 1994). However, commercial catalysts are approaching their peak in terms of activity, if not already there. Proposed options to meet the stringent sulfur emission standards include developing other active catalyst to replace the commercial ones. This has spurred hydrotreating catalyst research in a variety of areas as discussed below.

1.3 Novel Catalyst Development

To be able to develop more active catalysts, it is essential to understand the functionality of current conventional catalysts, efforts made to improve their activity and the outcome of such studies. Some of the areas investigated are:

1. Modification of catalyst support (Calafat et al., 1996; Eijsbouts et al., 1991a; Fish et al., 1990).
2. The use of different precursors for catalyst preparation (Maezawa et al., 1988).
3. The effects of additives such as phosphorus (P), fluorine (F) and boron (B) on conventional catalysts.
4. The use of transition metals other than the conventional Mo and W used in commercial catalysts (Eijsbouts et al., 1991a; Lacroix et al., 1089; Pecoraro and Chianelli, 1981).
5. The use of active phases such as nitrides and carbides other than the traditional sulfide active phase for commercial catalysts (Nagai et al., 1998; Aegerter et al., 1996).

1.3.1 Catalyst Supports

A catalyst support or carrier is an inert material that provides a good dispersion of the often expensive active metallic species by way of its large surface area (Satterfield, 1980). Other characteristics of a good support include: desirable mechanical properties such as hardness and high compressive strength, high stability under both reaction and catalyst regeneration, and low cost. Alumina has been widely used as support for conventional hydrotreating catalyst because it possesses almost all the above qualities. Recent studies on hydrotreating catalysts development have sought to modify the catalyst support or carrier to see its effect on activity. Supports such as carbon, oxides, zeolites and mixed oxides for hydrotreating reaction studies have been reported in the literature (Calafat et al., 1996; Ramirez et al., 1991). In other instances, bulk metallic catalysts without supports have also been reported (Lee et al., 1991).

Carbon supported catalysts have been extensively studied and are reported to be more active in hydrodesulfurization (HDS) than the corresponding alumina-supported ones (Calafat et al., 1996). Hydrodenitrogenation (HDN) catalyzed by carbon-supported catalysts has also been reported (Eijsbouts et al., 1991b). The use of oxides such as titania (TiO_2), zirconia (ZrO_2), silica (SiO_2) and magnesia (MgO) have received much investigation (Ramirez et al., 1991; Vrinat et al., 1994; Shimada et al., 1988). Supports formed from a combination of these oxides such as SiO_2-Al_2O_3, TiO_2-Al_2O_3 and TiO_2-ZrO_2, have all been reported (Breysse et al., 1991; Tanaka et al., 1996; Olguin et al., 1997; Daly, 1989). There have been reports on the use of Ni- and Mg-aluminates ($Ni(Mg)Al_2O_4$) as hydrotreating catalyst supports (Duchet et al., 1991). While $NiAl_2O_4$ is higher in activity, $MgAl_2O_4$ is said to be lower in activity compared to conventional alumina-supported hydrotreating catalysts. By virtue of their high surface area, shape selectivity, acid-base properties and high thermal stability, zeolites are considered potential supports for hydrotreating catalysts (Tatsumi et al., 1996). Studies performed on zeolite-supported hydrotreating catalysts indicate comparable or higher activity than conventional alumina-supported catalysts.

1.3.2 Studies with Non-Metallic Additives

Addition of other ingredients to modify the support or alter the surface structure of catalysts has also been reported. The addition of phosphorus (P), boron (B) and fluorine (F) have been commonly used to modify the HDN and HDS reactivities of hydrotreating catalysts (Rami-

rez et al., 1991; Kim and Woo, 1992; Ferdous et al., 2004a). The addition of P, for instance, is reported to change the number and reactivity of active sites, active phase dispersion, surface structure and morphology of the catalyst. The current commercial catalysts, for instance, contain P which helps to disperse the active phase on the support and enhances the activity. These are designated as Ni-Mo-P/Al_2O_3 or Co-Mo-P/Al_2O_3 (Eijsbouts et al., 1991a). Boron-modified commercial NiMo/Al_2O_3 catalyst has been effective for HDS and HDN of light gas oil (LGO) (DeCanio and Weissman, 1995; Ferdous et al., 2004b). Catalysts with boron addition are reported to be more active in HDS and hydrodemetallation (HDM) than conventional hydrotreating catalysts (Tsai et al., 1991). Fluorine, on the other hand, decreases the HDS of gas oil and slightly increases HDN of pyridine (Ramirez et al., 1991).

1.3.3 Preparation with Different Precursors

Another area of study in terms of hydrotreating catalyst development is the use of new preparatory methods. Generally, Mo and W base conventional hydrotreating catalysts are prepared from ammonium heptamolybdate and ammonium metatungstate precursors. Other materials that have been used in catalyst preparation in a bid to increase the reactivity are metal carbonyl complexes. Some of the commonly used metal complexes are $Cr(CO)_6$, $W(CO)_6$, $Mo(CO)_6$, $Co_2(CO)_8$, etc. Okamoto et al. (1995) reported that $Mo(Co)_2/Al_2O_3$ was more active than the corresponding MoO_3/Al_2O_3 in the HDS of thiophene.

1.3.4 Transition Metal Sulfides

Hydrotreating activities of transition metals besides molybdenum (Mo) and tungsten (W) have been investigated (Kim and Woo, 1992). Both mono- and bimetallic transition metal sulfides (M-S and M_I-M_{II}-S where M, M_I and M_{II} are transition metals) have been studied. A study by Pecoraro and Chianelli (1981) revealed that ruthenium sulfide is the most active among transition metal sulfides. This has generated a keen interest in the study of hydrotreating reactions catalyzed by noble metals especially ruthenium (Vrinat et al., 1989).

1.3.5 Active Phases other than Sulfides

The use of active phases other than the traditional sulfide phase has been the subject of study by a number of researchers. Phases such as the oxide phase, the metallic (reduced) phase, nitride and carbide phases have been reported in the literature (Nagai et al., 1988; Nagai et al.,

1998a)). It is reported that the sulfide phase is more active than the oxide and the reduced phases. However, reports on nitride and carbide phases indicate that they are more active than the sulfide phase (Nagai et al., 2000a; Aegerter et al., 1996; Chu et al., 1999). Detailed review of the literature on nitrides is discussed in Chapter 2.

CHAPTER 2
LITERATURE REVIEW

2.1. Feed Properties and Reactivities

The feed for hydrotreating (petroleum) is a complex mixture of hydrocarbons (both aliphatic and aromatic), heteroatomic compounds of nitrogen, oxygen and sulfur, and trace amounts of metals such as iron, nickel, copper and vanadium. It can be classified into two groups; conventional and unconventional. Most of the world's oils are unconventional (see Figure 2.1). As shown in Table 1.1, the elemental composition of the feed depends largely on the type of feed, whether conventional or unconventional. Heteroatoms, which are compounds in petroleum other than carbon and hydrogen (Gray et al., 1994), e.g. sulfur and nitrogen, are higher in unconventional feeds than in conventional feeds. The molecular composition varies widely depending on the formation and type of feed. The heavier the feed, the lesser the hydrogen to carbon ratio and the more condensed or aromatic the constituent molecules.

2.1.1. Sulfur Compounds

Sulfur compounds in petroleum include thiophene homologs, some of which are shown in Figure 2.2. Other sulfur compounds present in petroleum are: sulfides or thioethers (R_1-CH_2-S-CH_2-R_2), disulfides (R_1-CH_2-S-S-CH_2-R_2) and thiols or mercaptans (R-SH). The sulfides, disulfides and thiols are quite reactive and are more readily desulfurized than the thiophenic compounds.

2.1.1.1. Reactivities of Sulfur Heterocyclic Compounds

Research has shown that the least reactive sulfur compounds in petroleum fractions are thiophenic compounds (Girgis and Gates, 1991). Thiophenic compounds are organosulfur compounds with a sulfur atom contained in at least one five-ringed structure. The amount of sulfur in heavy gas oil is low compared to the hydrocarbon components. In hydrotreating, some sulfur species are easily removed while others remain refractory (Prins et al., 1989). Under typical industrial processing conditions, e.g. (317 – 427 °C) and pressures (9 – 14 MPa) (McKetta, 1992), HDS reactions are exothermic and irreversible (Speight, 1981). As temperature increases, the equilibrium constants decrease in agreement with the exothermicity of the reactions. Speight

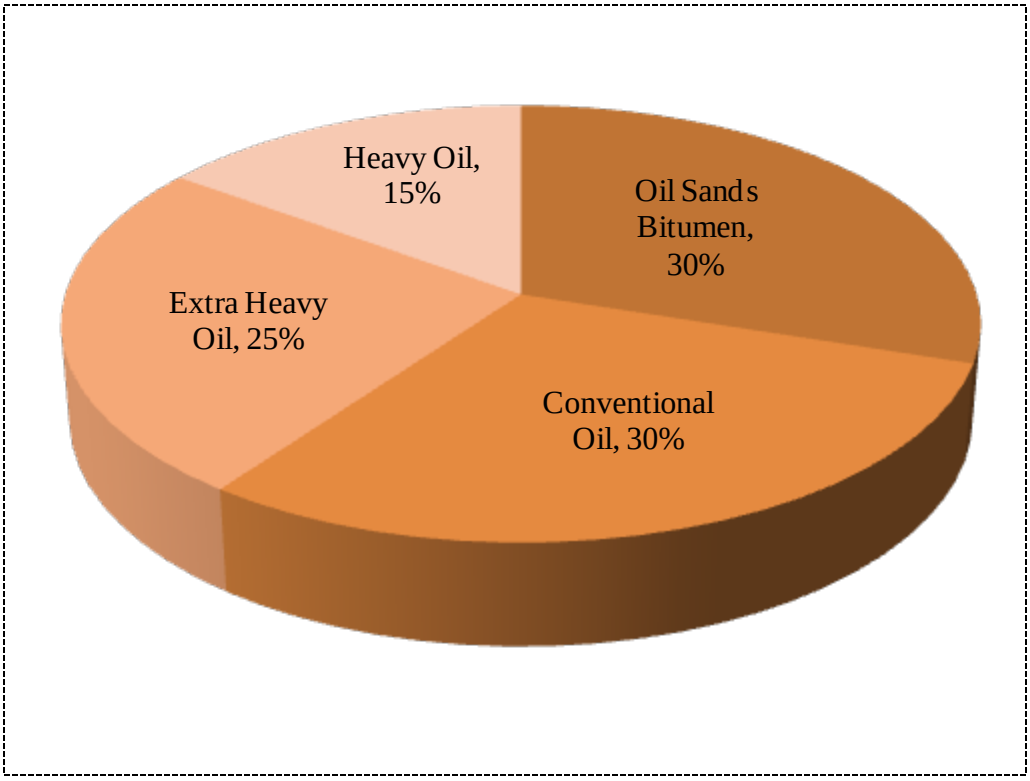

Figure 2.1: Total world oil reserves. Unconventional = oil sands bitumen, heavy oil and extra heavy oil (Alboudwarej et al., 2006).

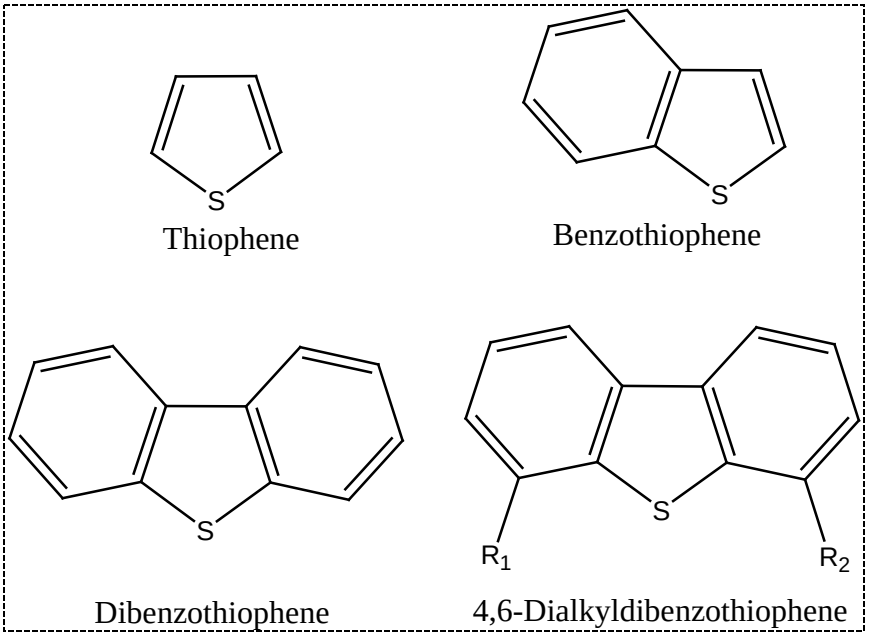

Figure 2.2: Some organosulfur compounds in petroleum (Girgis and Gates, 1991).

(1981) has shown that the equilibrium constant for hydrodesulfurization of 2-propanethiol decreases from 6.05 to 4.45 when temperature increases from 317 to 427 °C. The reactivities of organosulfur compounds also decrease with increase in the number of aromatic rings (Ma et al., 1994a). Singhal (1981) reported that among organosulfur compounds, dibenzothiophene has the least HDS conversion. The reactivity further decreases when there are methyl substituents in the 4^{th} and 6^{th} positions as in 4,6-dimethyldibenzothiophene (4,6-DMDBT). The low reactivity of 4,6-DMDBT in particular is attributed to the inability of the molecule to adsorb to active sites of catalysts due to steric effects. There are two main pathways by which HDS of thiophenic compounds occur:

1. an initial step of ring hydrogenation followed by sulfur extraction and
2. by direct sulfur extraction.

Equations (2.1) and (2.2) illustrate the two possible pathways for hydrodesulfurization of thiophene (Girgis and Gates, 1991). In pathway (1), the ring containing the sulfur atom is hydrogenated prior to breaking the sulfur-carbon bonds. However, in pathway (2), the sulfur atom is directly abstracted without prior hydrogenation of the sulfur-containing ring. Depending on the reaction conditions and the type of catalyst being used, either pathway can be favoured. For example, at high hydrogen pressures, the pathway with initial hydrogenation (path 1) appears to be favoured. It has been reported (Girgis and Gates, 1991) that Ni-Mo/Al_2O_3, in particular, favours the pathway with initial hydrogenation. However, generally, the pathway with direct sulfur extraction (path 2) appears to be the most favoured reaction pathway. Pathway (1) could be affected

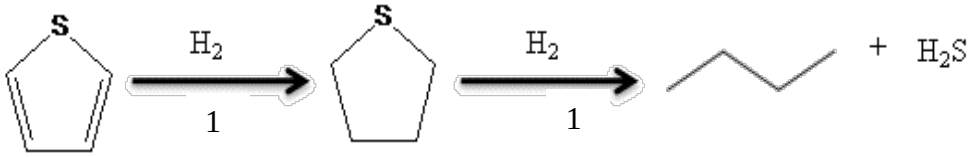

(2.1)

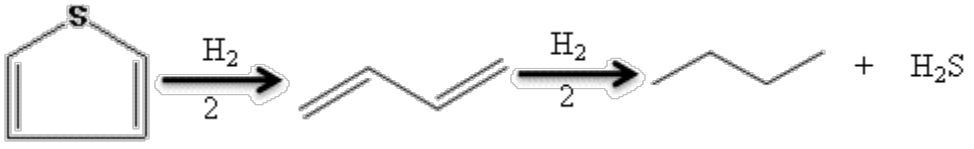

(2.2)

by equilibrium limitations, especially at high temperatures since equilibrium constants decrease with increase in temperature. For highly substituted dibenzothiophene, pathway (1) is the main route due to steric hindrance to catalyst adsorption by the substituents. The presence of substitu-

ents on dibenzothiophene (especially in the 4^{th} and 6^{th} positions) reduces its accessibility to the catalyst site.

2.1.2. Nitrogen Heterocyclic Compounds and their Reactivities

Nitrogen is mainly present in petroleum as heterocyclic aromatic compounds. Other compounds present in smaller amounts include aliphatic amines and nitriles. The aliphatic amines and nitriles are very reactive and are denitrogenated more rapidly (Girgis and Gates, 1991). Heterocyclic nitrogen compounds can be classified in two forms: basic and non-basic nitrogen compounds. Basic nitrogen compounds have the nitrogen atom contained in a six-ringed structure. Examples of such compounds are pyridine and quinoline (see Figure 2.3). Compounds with the nitrogen atom contained in at least one five-ringed member are referred to as non-basic nitrogen compounds. Examples of non-basic nitrogen compounds are pyrrole, indole and carbazole (see Figure 2.3).

The basicity of basic nitrogen compounds stems from the fact that the lone pair of electrons on the nitrogen atom is not delocalized in the ring containing the atom and so makes it readily available for reaction with acidic catalyst as a Lewis base. In other words, the nitrogen-containing ring is electron deficient due to the electron withdrawing tendency of the nitrogen atom. As a result, basic nitrogen compounds are more reactive than their corresponding homocyclic aromatic compounds. For example, pyridine is more reactive than benzene. On the other hand, the lone pair of electrons on the ring nitrogen of non-basic nitrogen compounds is delocalized in the nitrogen-containing ring. This renders the ring relatively richer in electrons than the corresponding homocyclic aromatic compounds. Non-basic nitrogen compounds (e.g. pyrrole) are therefore less reactive compared to their benzenoid counterparts (Ho, 1988; Kabe et al., 1999).

Contrary to the HDS reactions, HDN reactions of heterocyclic compounds follow one reaction pathway. The nitrogen-containing ring is always hydrogenated (hydrogenation reaction) prior to nitrogen extraction (hydrogenolysis reaction) (Girgis and Gates, 1991; Malkani et al, 1987). This is partly due to the fact that the C=N bond is stronger than the C-N bond (Kabe et al., 1999; Katzer and Sivasubramanian, 1979). Table 2.1 shows the bond strengths in heterocyclic organic compounds. Equation (2.3) illustrates the process of hydrodenitrogenation in heterocyclic nitrogen compounds. The hydrogenation step reduces the large energy of the C=N bonds

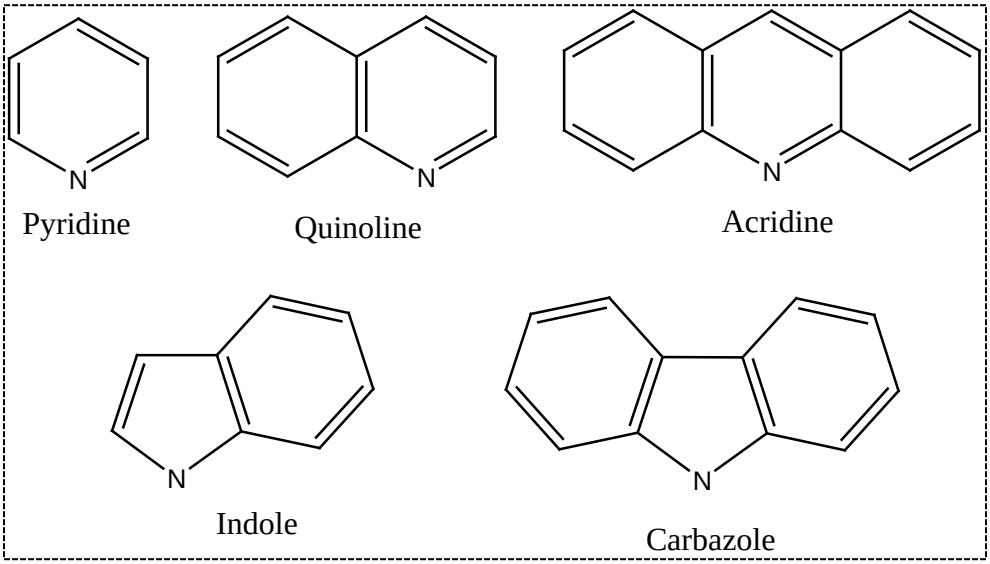

Figure 2.3: Some organonitrogen compounds in petroleum (Girgis and Gates, 1991)

Table 2.1: Bond energies of heterocyclic compounds in petroleum (Kabe et al., 1999).

Bond	Energy [kJ/mol]
C-S	322
C-C	347
C=C	611
C-C triple bond	837
N-H	389
C-H	414
C-N	305
C=N	615
C=S	536
C-N triple bond	891
S-H	347

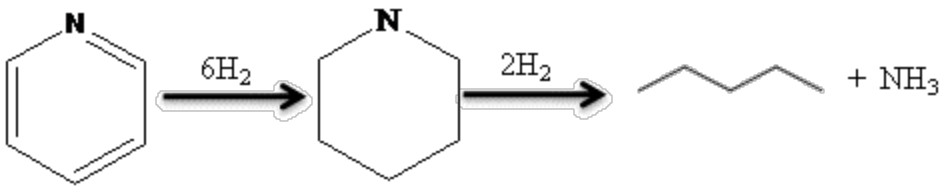

(2.3)

in the ring and enhances ease of the C-N bond cleavage.

In their study on the hydrogenation of heterocyclic compounds in quinoline network, Satterfield and Cocchetto (1981) reported that although equilibrium is not favoured for the hydrogenation step in HDN processes, the hydrogenolysis (denitrogenation) step and the overall HDN are thermodynamically favoured even at 500 °C. They observed that the equilibrium constants are less than unity for aromatic ring saturation and become smaller with increasing temperature. They also observed that the ring hydrogenations are exothermic. Due to the unfavourable hydrogenation step, high hydrogen partial pressures are used in the industry to force the equilibrium towards the products. HDN process is therefore irreversible under industrial processing conditions (Girgis and Gates, 1991)

The equilibrium position of the hydrogenation step can affect the overall rate of HDN. If the rate of hydrogenolysis was the rate-limiting step, then low hydrogenation equilibrium levels would affect the rate of hydrogenolysis as only low amounts of hydrogenated products would be available for denitrogenation. Increasing the equilibrium amount will therefore increase the rate of hydrogenolysis. Increase in hydrogen partial pressure increases the equilibrium concentration of hydrogenated products thereby increasing HDN. Increasing temperature decreases the equilibrium concentration of the intermediate, thereby decreasing overall HDN.

2.1.3. Aromatic Hydrocarbons and their Reactivities

Aromatic hydrocarbons are hydrocarbons with conjugated cyclic molecular structure with higher stability than expected in the hypothetical localized structure. They derive their stability from the delocalization of six electrons among the carbon atoms in the cycle. They can be classified as mono- (one ring structure) di- (two-ring structure) and poly-aromatics (more than two ring structures). Figure 2.4 shows sample aromatic hydrocarbons in petroleum feedstock. As shown in Table 1.1, unconventional petroleum feedstock has higher aromatic content than conventional ones (Yui and Snaford, 1987). Hydrogenation of aromatic hydrocarbons is reversible (see Equation (2.4)) and exothermic. This means the extent of reaction decreases with increase

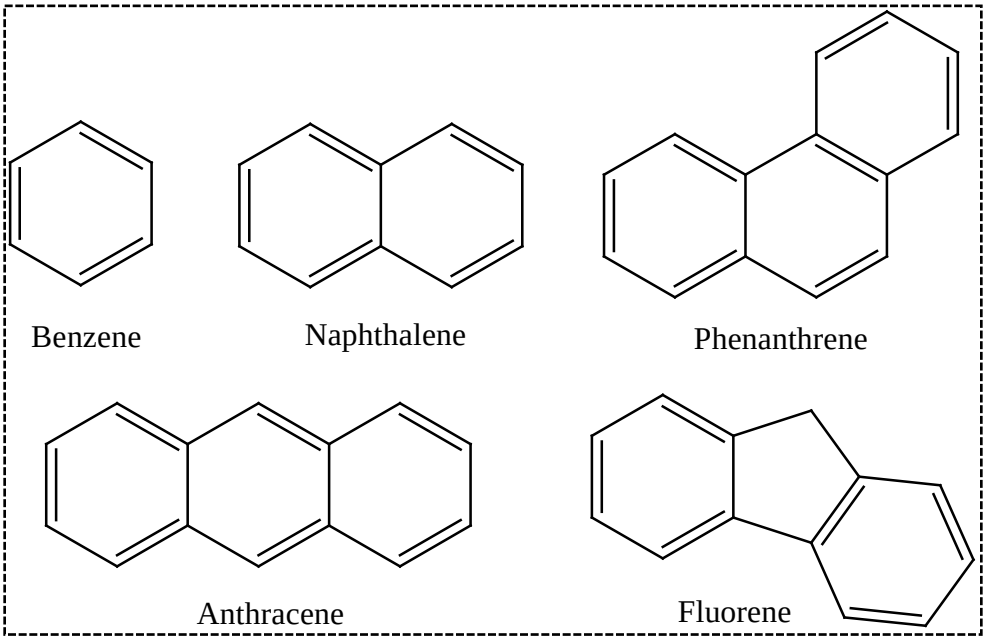

Figure 2.4: Some aromatic hydrocarbons in petroleum feedstock (Girgis and Gates, 1991)

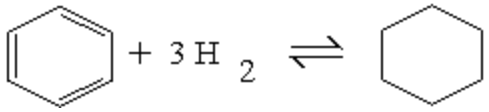

(2.4)

in operating temperature (Girgis and Gates, 1991). In real feedstock, sulfur and nitrogen compounds may be present and increasing operating temperature may increase the reaction rates of the sulfur and nitrogen compounds but decrease that of aromatic hydrocarbons. The lower equilibrium conversions are more significant at lower operating pressures. It is reported (Gray et al., 1994; Girgis and Gates, 1991) that the reactivity of aromatic hydrocarbons increases with increase in the number of aromatic rings. Mono aromatics are the least reactive due to their high resonance stabilization (see Table 2.2). Hydrogenation of poly-aromatic hydrocarbons are normally sequential i.e. one ring is hydrogenated prior to the other. The rate of hydrogenation for subsequent rings are lower than that for initial rings, meaning high operating conditions are required to increase the hydrogenation rates in subsequent hydrogenations (Girgis and Gates, 1991; Stanislaus and Cooper 1996; Yang and Stock, 1996).

2.2. Nitride Catalysts

Nitride catalysts have been widely used for hydrotreating operations in a bid to find catalysts with better activity than sulfided Co(Ni)-Mo(W)/Al_2O_3. Besides hydrotreating, nitride catalysts find application in processes like CO hydrogenation, unsaturated hydrocarbon hydrogenation (Ranhotra et al., 1987) and ammonia synthesis (Liang et al., 2000). Before Volpe and Boudart (1985) reported the synthesis of nitride catalysts via the temperature programmed reaction method, transition metal nitrides had long been known as hard, refractory materials with electronic and magnetic properties of metals. They had low specific surface area and so were not considered as catalyst materials. After the work of Volpe and Boudart (1985), which produced high specific surface area nitride materials, there has been interest in the synthesis, characterization and reactivity studies of these materials.

Temperature Programmed Reaction (TPr) synthesis of nitride catalysts is the reaction of the catalyst precursor (often in oxide phase) with NH_3 using a ramped temperature program. A slow temperature ramping is recommended to avoid sintering (the agglomeration of catalyst surfaces and pores at high temperatures) of the catalyst. Due to high operating temperatures, and the inability of hydrotreating reactors to withstand such high temperatures, TPr is performed in quartz reactors before transfer into the hydrotreating reactor for hydrotreating runs. The concern

Table 2.2: Relative rate constants for hydrogenation of aromatic hydrocarbons over sulfided catalysts. (Yang and Stock, 1996).

Hydrogenation Reaction	Relative Rate Constant			Total Resonance Energy (Kcal/mol)	Resonance Energy Per Ring (Kcal/mol)
	NiMo/ Al_2O_3	NiW/ Al_2O_3	WS_2		
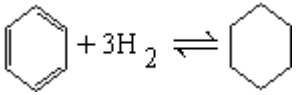	1	1	1	36-40	40
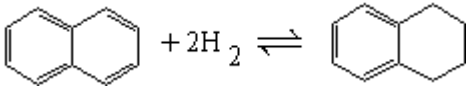	10	18	23	59-75	28
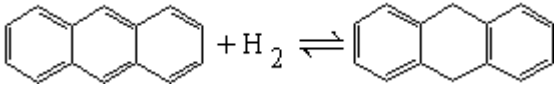	36	40	62	71-105	-

is that the fresh nitride catalysts are pyrophoric (react with air) and would need to be passivated in low concentrated O_2 flow before exposure to air. Once in the hydrotreater, the passive layer would need to be removed to reactivate the catalyst. Various aspects of nitride catalysts have been studied which are discussed below.

2.2.1. Bulk Nitride Catalysts

Most work carried out on nitride catalysts have focused on unsupported (bulk) catalysts. Colling et al., (1996) studied the surface chemistry of bulk molybdenum nitride catalysts with specific surface area of up to 193 m^2/g by the TPr of MoO_3 with NH_3 from room temperature to 500 °C. The catalysts were characterized by temperature programmed desorption (TPD) measurements. They reported that oxygen on the surface of the passivated catalyst was removed by reaction with decomposed NH_3 and H_2 gas left on the surface of the catalyst at temperatures < ~ 277 °C or with H_2 gas at higher temperatures. They concluded that NH_3 desorbed from the surface of the catalyst either molecularly (27-227 °C) or in the form of H_2 and N_2 (227-427 °C). The ratio of desorbed molecular NH_3 to decomposed NH_3 was 3:1 and the pyridine HDN activity studied increased linearly with the amount of NH_3 chemisorbed.

Lee et al., (1993) investigated the hydrogenation of quinoline over high-surface-area bulk molybdenum nitride catalyst by the temperature programmed reaction of the oxide precursor MoO_3 and NH_3 from 395 to 700 °C in a quartz reactor. X-ray diffraction (XRD) results showed no evidence of the presence of MoO_3 on the freshly prepared catalyst indicating a total conversion to the nitride phase while BET analysis gave surface area in excess of 200 m^2/g. Neylon et al. (1999) also investigated the catalytic properties of transition metal nitrides synthesized by the method of temperature programmed reaction of metal oxides with NH_3. The fresh catalyst was passivated before exposure to air to avoid bulk oxidation. The techniques for characterization included XRD and sorption analysis. They observed that the nitrides were mostly mesoporous (2-50 nm catalyst pore diameter) with specific surface area up to 81 m^2/g.

Nitride of the transition metals Mo, W, V, Nb and Ti were studied by Ramanathan and Oyama (1995). The catalysts were prepared by temperature programmed reaction of oxide precursors with 100% NH_3 and characterized by XRD, x-ray photoelectron spectroscopy (XPS), BET surface area and CO chemisorption. The HDN, HDS and hydrodeoxygenation (HDO) activities studied were based on model compounds such as quinoline, dibenzothiophene and benzo-

furan, respectively. They concluded that the activities for HDN and HDS followed the order: group 6 > group 5 > group 4. While XRD showed no change in the catalyst structure, XPS indicated the presence of little sulfur on the catalyst surface

Although bulk metal nitrides have proved to have high activity for HDS and HDN, high amounts of metal are required to produce enough catalyst for hydrotreating processes. Secondly, bulk catalysts normally have low surface areas (Neylon et al., 1999) compared to those of supported catalysts (Speight, 2000) but high surface area is known to enhance catalyst activity (Satterfield, 1980). To enhance the catalyst surface area, improve the dispersion and yet reduce the amounts of metal used in the synthesis, catalyst supports would have to be incorporated in the synthesis process. These studies have been reported in the literature and are discussed below.

2.2.2. Supported Nitride Catalysts

Supported catalysts are catalysts in which metal components are dispersed on inorganic oxide materials with high porosity. In conventional catalysts, metals commonly used are mixtures of cobalt (Co) or nickel (Ni) with molybdenum (Mo) or tungsten (W). Examples of the inorganic supports are alumina, silica, silica-alumina, kiesulguhr, magnesia, zeolites and activated carbon (Satterfield, 1980; Speight, 2000). The supports are normally formed into a variety of shapes or could be made into powder. The dispersed metal component of the catalyst can be a single metal (Aegerter et al., 1996; Dolce et al., 1997) or coupled with another metal (Hada et al., 2002; Chu et al., 1999). Catalysts with more than two metal components have also been reported (Sigurdson et al., 2008).

2.2.2.1. Supported Mono-Metallic Nitride Catalysts

Supported nitride catalysts have been investigated and reported. Aegerter et al. (1996) studied thiophene HDS over alumina-supported molybdenum nitride catalysts with Mo loading of 10 wt%. The catalysts were characterized by XRD, pulse chemisorption, infrared spectroscopy (IR) and temperature programmed desorption (TPD) measurements. Although the XRD of their tested catalysts indicated the bulk structure of the nitride (γ-Mo_2N) particles was retained, IR spectroscopy showed the presence of sulfides under reaction conditions. Activities of the nitrides were observed to be higher than those of the corresponding sulfides. Dolce et al. (1997) studied hydrotreating of quinoline and benzothiophene using supported molybdenum nitride catalysts synthesized via temperature programmed reaction of precursor oxides with NH_3. XRD,

elemental analysis and neutron activation analysis were among the techniques used to determine the phase constituent and composition while O_2 chemisorption was used to probe the catalyst surface properties. From product distribution analysis, the catalysts were found to be more efficient than sulfide catalysts.

Nagai et al. (2000) investigated surface properties and activity of nitrided Mo/Al_2O_3 (12.5 wt%) catalyst through temperature programmed reduction, XPS, diffuse reflectance and Fourier transform infrared spectroscopy (FTIR) analyses. Mo/Al_2O_3 was reported to have six nitrogen peaks, four of which were due to adsorbed nitrogen on surface Mo species (MoO_2, γ-Mo_2N, Mo metal) and Al_2O_3. The other two peaks were due to nitrogen released from bulk Mo_2N. Catalysts nitrided at 900 °C were less acidic compared to those nitrided at 500 °C.

2.2.2.2. Supported Bimetallic Nitride Catalysts

The objective of using two metals in catalyst synthesis is to enhance the activity of the catalyst. In other words, one of the component metals of the catalyst acts as an activity promoter of the main active component of the catalysts. In conventional catalysts, Ni and Co are frequently used as promoters of Mo or W sulfides (Speight, 2000).

Chu et al. (1999) prepared a series of nickel molybdenum nitride catalysts ($NiMoN_X/\gamma$-Al_2O_3) by temperature programmed reaction of $NiO\text{-}MoO_3/\gamma\text{-}Al_2O_3$ precursor and NH_3. The characterization techniques included: BET, XRD and H_2-temperature programmed reduction. Three different phases were observed on the surface of $NiMoN_X/\gamma\text{-}Al_2O_3$ in the form of metallic Ni, Mo_2N and Ni_3Mo_3N. The catalyst with precursor combination of 5.0 wt% NiO and 15.0 wt% MoO_3 gave the highest HDN of pyridine activity. Activities of the catalysts reduced in the order: reduced $NiMo/\gamma\text{-}Al_2O_3 \geq$ nitrided $NiMo/\gamma\text{-}Al_2O_3 >$ partially reduced $NiMo/\gamma\text{-}Al_2O_3$ and sulfided $NiMo/\gamma\text{-}Al_2O_3$. Kojima and Aika (2001) investigated the activity of cesium-promoted cobalt molybdenum nitride catalysts. The catalysts were synthesized by the nitridation of molybdenum trioxide and molybdenum bimetallic oxide precursors with NH_3 in a temperature programmed reaction up to 700 °C. Kojima and Aika (2001) again investigated catalytic properties of supported nickel molybdenum nitrides for HDN analysis using 3-methyl pyridine as feed. Characterization techniques such as XRD, TPR and XPS were used to illustrate structure, surface reaction properties and role of Ni in the reaction. They found $NiMoN_X/\gamma\text{-}Al_2O_3$ to be more active than $Mo_2N/\gamma\text{-}Al_2O$ HDN activity decreased in the order: $NiMoN_X$ (5 wt%, 15 wt%) >

Mo_2N (15 wt%) > Mo_2N (10 wt%) > Mo_2N (5 wt%). It was also observed that Mo_2N, Ni_3Mo_3N and Ni metal were formed on the $NiMoN_X/\gamma\text{-}Al_2O_3$. The high activity was attributed to synergy between components in the species. Ni was found to decrease the reducing temperature of the oxygen passive layer on the catalyst surface through TPR studies. Hada et al. (2002) studied the nitrides of Co and Mo mixtures at Co/(Co+Mo) ratios of 0, 0.25 and 0.5 and found that the species formed at 750 °C were Co_3Mo_3N, $\gamma\text{-}Mo_2N$ and $\beta\text{-}Mo_2N_{0.78}$. The rate of thiophene HDS depended on Co/Mo ratio and the surface area of the catalyst.

2.2.3. Oxynitride Catalysts

Nitride catalysts in the form $M_I\text{-}M_{II}\text{-}O\text{-}N$ have also been synthesized and characterized (Yu et al., 1998). Oxygen is able to populate interstitial sites of nitrides resulting in oxynitrides structures. These oxy- compounds have structures similar to the nitrides (Neylon et al., 19990. The synthesis procedure of Yu et al. (1998) involved nitriding bimetallic oxide precursors with NH_3 gas by temperature programmed reaction methods at temperatures below 747 °C. The precursors were prepared by solid state reaction of monometallic oxides which involved mixing, grinding pelletizing and firing together of the monometallic oxides at various temperatures. The catalysts were passivated before exposure to air and their surface activities measured by CO chemisorption. The authors concluded that the catalysts were face centered cubic structured and had specific surface areas between 37 and 121 m^2/g. In a similar work, Ramanathan et al. (1998) conducted hydroprocessing reactivity studies on bimetallic oxynitrides of the form $M_IM_{II}O_XN_y$. All the catalyst contained either MoO_3 or WO_3 as one of the precursors. Activity was tested on a mixture of heteroatomic model compounds including: dibenzothiophene, quinoline, benzofuran, tetralin and aliphatic compounds. HDN activity of V-Mo-O-N was found to be higher than Ni-Mo-S/Al_2O_3 catalyst with Co-Mo-O-N being the most active HDS catalyst.

2.2.4. Cooling and Passivation of Nitride Catalysts

Nitride catalysts are normally prepared at high temperatures after which they are cooled rapidly to ambient temperature and passivated. The cooling process and the effect it has on catalyst activity have been investigated by Nagai et al. (1998). The catalysts were synthesized at 500, 700 and 900 °C, and cooled to room temperature in either NH_3 or He flow. The specific surface area decreased as the final nitriding temperature increased and activity per specific area

for He-cooled catalyst was higher than the NH_3-cooled ones for both overall HDN and hydrogenation. However, the NH_3-cooled catalyst was more active for carbon-nitrogen (C-N) bond breakage. In a related study, Nagai et al. (1998) observed that the specific area of He-cooled 12.5 % MoO_3/Al_2O_3 catalyst was lower than that of NH_3-cooled catalyst. The NH_3-cooled catalyst at 900 °C was the most active catalyst while the He-cooled catalyst at 500 °C was the least active. In general, HDN rate of carbazole increased with nitriding temperature.

In their study of surface species of passivated and non-passivated Mo_2N catalyst samples Wei et al. (1997) observed two types of NH_X adsorbed on the freshly prepared catalysts. The weakly adsorbed NH_X desorbed at 200-300 °C while the strongly adsorbed ones decomposed to H_2 and N_2 at 610 °C. They also observed a change in phase of Mo_2N when heated at 850 °C in He but no such change was observed for the passivated samples. Reduction of Mo_2N to the metallic form (Mo) occurred at 880 °C.

2.2.5. Synthesis Gases for Nitride Catalyst Preparations

Nitride catalysts are usually prepared by reacting an oxide precursor with NH_3 gas (Dolce et al., 1997; Chu et al., 1999; Yu et al., 1998; Kojima and Aika, 2001). However, preparations using different synthesis gases have been reported. Liu et al. (2002) investigated the HDS of dibenzothiophene over Co-Mo-N and γ-Mo_2N catalysts prepared from the reaction of MoO_3 and Co-Mo oxides with H_2/N_2 mixture instead of the traditional NH_3. Wise and Markel (1994) also investigated production of high surface area (150 m^2g^{-1}) passivated unsupported γ–Mo_2N by temperature programmed reaction of MoO_3 powder with mixtures of H_2 and N_2. Addition of water to the synthesis gas reduced the product surface area. Nitride phase was formed only in synthesis where the partial pressure of nitrogen was higher than 4 kPa. They concluded that the use of H_2/N_2 gas mixture offered an advantage over the use of NH_3 as synthesis gas, in that it eliminated the problem of endothermic decomposition of NH_3 in large reactant beds.

2.2.6. Stability of Nitride Catalysts in HDS Environment

Another area of nitride catalysts that has generated interest is the stability of the nitride phase after exposure to HDS reaction. The performance and post reaction characterization of unsupported γ-Mo_2N catalysts in HDS and HDN was reported by Ozkan et al. (1997). Characterization techniques for pre- and post-reaction were XPS, TPD, TPR, XRD and BET. Their

post reaction XPS analysis indicated the presence of MoS_2 over the Mo_2N surface although the bulk was still in the nitride phase. XRD results did not show any difference between the fresh and spent catalysts. They concluded that the nitride phase acted as support for the formation of the sulfide phase. From their XPS studies of bimetallic oxynitrides, Ramanathan et al. (1998) observed the presence of S on the catalyst surface after prolonged exposure to the reactant. However, in a related study of transition metal nitrides, Ramanathan and Oyama (1995) demonstrated from XRD of their spent catalysts that the nitrides were stable and there were no sulfides present. The difference in the two studies may be due to the difference in catalysts; one a nitride and the other an oxynitrides.

2.3. Catalyst Characterization

The surface properties and activity of a catalyst depend on its composition and structure at the atomic level. It is therefore important to know and understand the structure, shape, size, as well as defects, and the location of the composite metals. Various characterization techniques that provide information on both catalyst surface and bulk properties have been used to acquire knowledge on catalyst samples. Since reactions mainly take place on catalyst surfaces, it is possible to correlate the activity and selectivity of catalysts to the surface structural information obtained from characterization studies.

Several options are available to obtain information from a catalyst. Spectroscopies are obtained based on a form of excitation which a catalyst responds to after being contacted with sub-atomic particles such as electrons, ions, neutrons or some form of electromagnetic radiation such as photon or heat (see Figure 2.5). The information is obtained from scattering, emission or absorption of the encountered particle or radiation. Techniques often used in catalyst characterization (see Table 2.3) also show some common characterization techniques and information obtainable from such techniques.

2.3.1. Surface Area, Pore Diameter and Pore Volume Analyses

Surface area, pore size distribution and pore volume analyses are characterization techniques that are frequently used to study the surface areas available for reaction and the pore size and distribution of hydrotreating catalysts. Two main methods are used for analysis, i.e. nitrogen adsorption and mercury porosimetry methods.

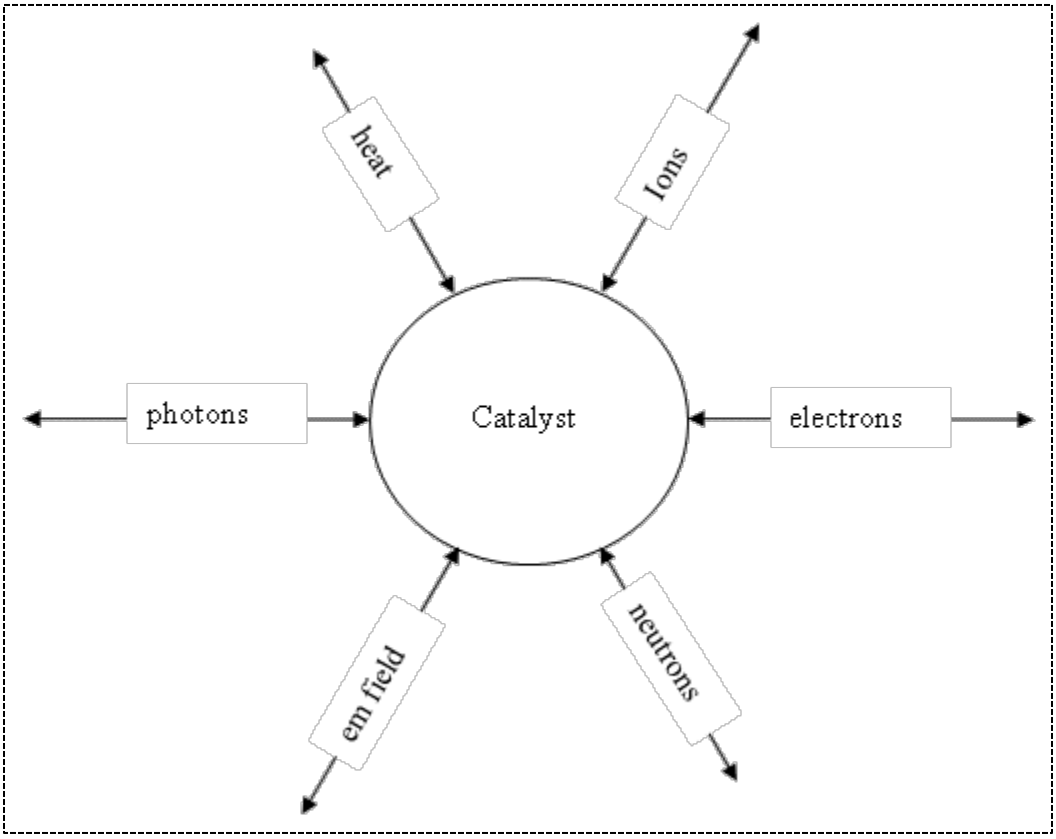

Figure 2.5: Diagram showing examples of catalyst contact with sub-atomic particles or electromagnetic radiation and emissions obtained. (em = electromagnetic)

Table 2.3: Some techniques commonly used in catalyst characterization and their relevance to hydrotreating.

Acronym	Full Name	Input	Output	Information
AES	Auger Electron Spectroscopy	e^-	e^-	Surface Composition
AFM	Atomic Force Microscopy	-	-	Surface Morphology
	Chemisorption	Gas	Gas	Number of active sites
BET	Brunner, Emett and Teller	Pressure + Gas	Gas/Liquid	Surface Area, Pore Volume and Pore Size
EDX	Energy Dispersive X-Ray	e^-	X-Ray	Composition
EXAFS	Extended X-Ray Absorption Fine Structure	X-Rays	X-Rays	Local Structure
IR	Infrared Spectroscopy	Photon	Photon	Molecular Vibrations
MAS & MES	Mossbauer Absorption and Emission Spectroscopy	γ-Rays	γ-Rays	Oxidation State and Magnetic Properties
NMR	Nuclear Magnetic Resonance	Magnetic Field	Magnetic Field	Strength and number of acid sites
SEM	Scanning Electron Microscopy	e^-	e^-	Morphology
TDS	Thermal desorption Spec.	Heat	Gas	Adsorption Strength
TEM	Transmission Electron Microscopy	e^-	e^-	Size, Structure
	Temperature Programmed:			
TPD	Desorption	Heat +		Acid and Basic Sites
TPO	Oxidation	Gas	Gas	Oxidizability
TPR	Reduction			Reducibility
XPS	X-Ray Photoelectron Spec.	X-Ray	e^-	Composition, Oxidation Stat and Dispersion
XRD	X-Ray Diffraction	X-Ray	X-Ray	Bulk Structure, Particle Size

Nitrogen adsorptions method is used for catalyst with micropores (pore diameter < 2nm) and mesopores (pore diameter 2 – 50 nm) while mercury porosimetry is used for catalyst with mesopores and macropores (pore diameter > 50nm). The nitrogen adsorption method is the most widely used technique because high catalyst surface area enhances catalyst activity and for high surface area, a catalyst must have pores in the micropore and mesopore region.

Various authors have used the nitrogen adsorption method to investigate catalyst surface area, pore size and pore volume (Chu et al., 1999; Kojima and Aika, 2001; Ozkan et al., 1997). Neylon et al. (1999) determined BET surface areas of their bulk, early transition metal nitride and carbide catalysts by N_2 adsorption at≈ -196 °C using a Micromeritics ASAP 2010 and Quantasorb analyzer. The surface areas were then used to estimate the average particle sizes, assuming spherical sizes, from the equation;

$$d_p = \frac{6}{\rho_p S_g} \tag{2.5}$$

where ρ_b is the bulk density and S_g is the surface area. Pore size distributions were determined from the nitrogen desorption isotherms using the Barrett, Joyner, and Halenda cylindrical pore models. They observed that surface areas for the nitrides and carbides were substantially higher than those for their parent oxides (W_2N was 81 m^2/g). The particle size estimates from the surface area (W_2N was 4 nm) were similar to the crystallite sizes estimated from their XRD line broadening analyses (W_2N was 5 nm) suggesting that the particles were single crystalline. Pore size distribution showed Group VI (Mo and W) nitrides and carbides had some degree of microporosity with the highest density of pores in the mesopore region. Pore size distribution for W_2N in particular was found to be bimodal.

Yu et al. (1998) obtained surface areas in the order of 37 to 121 m^2g^{-1} and calculated particle size of oxynitride samples using Equation (2.5) where ρ_b was taken as 19.9 gcm^{-3} for W oxynitride samples (assuming perfect rock structure). The particle size calculations from BET surface area measurements (4-16 nm) were comparable to the crystallite size calculations from XRD line broadening (3 - 11 nm).

Perez-Romo et al. (2002) observed in their study that pore size distribution was bimodal for some samples while others were in the mesopore region between 2 and 4 nm. As P/W ratio increased, the surface area went through a maximum and then decreased. The measured surface areas were between 33 and 84 m^2g^{-1}.

For NiW/Al_2O_3 samples, Kordulis et al. (2001) observed little difference between the specific surface area of the support (234 m^2/g) and the catalyst samples (224 and 220 m^2/g). They suggested that the metal deposits did not plug the mesopores of the support.

2.3.2. Elemental Analyses (ICP-MS, EDX, CHN)

Elemental analysis of catalysts is another important characterization technique that is employed to investigate the composition of elements in the catalyst, both on the surface and in the bulk. Methods that have been used for elemental analyses include: inductively coupled plasma (ICP) analyses (Yu et al., 1998; Korlann et al., 2002), neutron activation analyses (NAA) (Dolce et al., 1997) x-ray photoelectric spectroscopy (XPS), carbon, hydrogen, nitrogen micro-analyses (CHN), energy dispersive x-ray (EDX), and neutron activation analyses (NAA). Techniques such as x-ray absorption near edge structure (XANES) and x-ray diffraction (XRD) could also be used to identify constituent elements in a sample (Niemantsverdriet, 1993).

Yu et al. (1998) determined the elemental composition of oxynitride catalysts using inductively coupled plasma (ICP) analyses. Results confirmed the initial oxide compositions used. Deviation was, however, observed with the highest temperature (840 °C) samples which was consistent with volatilization of the lower melting point oxides. Perez-Romo et al. (2002) observed in their elemental analyses the amount of oxygen in all samples was higher making the metal/(N+O) ratio lower than expected. Their P/W ratios were however the same before and after the nitridation process.

Some authors have used NAA to measure the composition of elements in catalyst samples. Dolce et al. (1997) employed neutron activation analyses to measure Al and Mo contents in their Al_2O_3-supported nitride and carbide catalyst materials. This involved bombarding the materials with neutrons and measuring the emitted radiation as the radioisotope decayed. To estimate the carbon-hydrogen-nitrogen (CHN) content of the catalysts, Dolce et al. (1997) further performed CHN microanalyses using Perkin-Elmer 2400 CHN elemental analyzer equipped with a thermal conductivity detector. Overall results showed that the Mo loading was lower than expected but the percent error was not reported. The deviation was attributed to two main factors:

1. Removal of some Mo during calcination in the form of volatile molybdates and,
2. Experimental errors in determining the point of incipient wetness during impregnation.

N/Mo ratios were found to be higher than stoichiometric Mo_2N ratios but agreed with literature

(Colling et al., 1996). About 0.75-1.26 N/Mo ratio was obtained instead of 0.5. Besides, about 0.4 wt% nitrogen was found on nitrided support (Al_2O_3) suggesting that some NH_3 adsorbs on Al_2O_3, evidenced by the presence of hydrogen in the CHN analyses.

Korlann et al. (2002) also obtained nickel and molybdenum compositions lower than expected in the elemental analysis of bulk and supported NiMoN catalysts. The N/Mo ratio was more than expected in agreement with results of Dolce et al. (1997). They attributed the high N content to the presence of nitrogen-containing species on the alumina support or adsorbed N species on the supported bimetallic nitride particles.

From the EDX analysis, Nagai (2007) found the Mo/Al ratio in the l-position for a 4.8% Mo/Al_2O_3 sample was 26 times greater than that of the s-position for the 4.8% Mo/Al_2O_3 sample. Mo nitrides of the 11.6% Mo/Al_2O_3 were partially agglomerated and formed large particles of Mo nitride on the surface

2.3.3. Chemisorption Studies

Chemisorption is a characterization technique that is used to measure dispersion of metal atoms on support surfaces. It is also employed in Fourier Transform Infrared studies to investigate acid sites on catalyst surfaces. Results from chemisorption are often correlated to catalyst activity in terms of the turn over frequency. Common gases used in chemisorption include: CO, NO, O_2, and H_2 (Satterfield, 1980). The use of NH_3 has also been reported in the literature (Furimsky, 2003). The chemisorption gas is used to titrate the catalyst surface and the volume of gas uptake is used as a measure of the number of active metals exposed on the surface (Satterfield, 1980; Yu et al., 1997).

Ramanathan and Oyama (1995) compared the activities of $Ni\text{-}Mo/Al_2O_3$ and Mo_2C based on surface area and chemisorption. In the activity per unit surface area, they observed that the $Ni\text{-}Mo/Al_2O_3$ had higher activity than the Mo_2C. However, based on CO chemisorption for Mo_2C and O_2 for $Ni\text{-}Mo/Al_2O_3$, Mo_2C showed 2.4 times more activity than $Ni\text{-}Mo/Al_2O_3$. The results indicate that the catalyst activity comparisons are critical and dependent on the methods used.

Yu et al. (1998) titrated the accessible surface metal atoms in bimetallic oxynitride catalysts using CO chemisorption. They obtained surface densities in the range of $0.01 – 0.1 \times 10^{15}$ cm^{-2} (the normal for metal and metal alloys is $\sim 1 \times 10^{15}$ cm^{-2}). Migration of oxygen and nitro-

gen atoms from the bulk to the surface after initial reduction at 510 °C hindered the CO chemisorption. The amount of CO chemisorbed was found to correlate well with the surface reducibility.

Perez-Romo et al. (2002) observed CO uptake ranged from 41 to 149 $\mu molg^{-1}$ giving densities of about 0.07 – 0.11 x 1015 cm^{-2}. The results suggested that the surface W species were not stoichiometric (1 x 10^{15} cm^{-2}). The low site density results could also be due to lack of W in the metal lattice (nonstoichiometric relationship). Phosphorus in the sample reduced surface area which resulted in low CO uptake.

Korlann et al. (2002) performed chemisorption studies on alumina-supported bimetallic nitride and carbide catalysts samples. They used low temperature (-77 °C) O_2 probe in a Micromeritics PulseChemisorb 2700 instrument. A calibrated volume of the O_2 (0.101 ml) was injected at 1 min intervals into He flow (15 sccm) until O_2 uptake ceased. Oxygen uptake for pure Co_3Mo_3N/Al_2O_3 (114 μmole/g) was much higher than the impure Co_3Mo_3N/Al_2O_3 (42.3 μmole/g). They concluded that impurities on the surface of the catalyst inhibited O_2 uptake.

2.3.4. Temperature Programmed Techniques

Temperature programmed techniques comprise of reduction and desorption steps. These studies involve the studying of a chemical or physical change in the catalyst with steady increase of the catalyst temperature. In a typical experiment, the reactor (normally a U-tube made of quartz) is loaded with catalyst and heated at rates between 0.1 to 20 °C/min (0.33 °C/s). Both the inlet and outlet gases pass through a thermal conductivity detector (TCD) which measures and compares the difference in conductivities of the gases. Low concentrations of the gases are used in a mixture of an inert carrier gas (e.g. 5% H_2 in He) to optimize the TCD measurements. The spectrum is given in the form of a plot of the gas consumption or desorption as a function of temperature.

2.3.4.1. Temperature Programmed Desorption (TPD)

Temperature programmed desorption is a characterization technique used to study the properties of species that desorb from a catalyst surface at increasing temperature. When an adsorbate (a molecule that adsorbs on a surface) comes into contact with an adsorbent (a surface on which the adsorbate adsorbs), it adsorbs unto the surface and releases energy to increase its stability on the surface. When the adsorbent is heated, the adsorbate absorbs energy and desorbs

from the surface, giving off a signal that is detected by a thermal conductivity detector. The temperature at which desorption takes place is a measure of the adsorption strength and the area under the peak, a measure of the amount of adsorbate desorbed (Kozai et al., 2000). The technique is commonly used in catalyst characterization to measure the strength and amount of acid sites on a catalyst surface. This is done by adsorbing a basic gas (e.g. NH_3 gas) on the surface of acidic catalysts. The use of other adsorbates to characterize catalyst sites such as CO_2 (McGee et al., 2005), NO (Shi et al., 2004) and H_2 (Li et al., 1997; Zhang et al., 1997) have been reported. TPD is also used to study the decomposition properties of catalysts at elevated temperatures. The number of peaks observed in NH_3 TPD identifies the different types of acid sites on the catalyst. Generally, multiple peaks are obtained in the TPD profile signifying different acid centers or decomposing molecules on the catalyst surface. Ferdous et al. (2004a) and, Lewandowskia and Sarbak (2000) classified the acid centers into three groups; weak acids occur below 200 °C; intermediate acids between 200 and 350 °C; strong acids above 350 °C.

Prior to the desorption studies, the sample is often pretreated. That is, the sample is degassed to get rid of any adsorbed species on the catalyst surface such as moisture that may interfere in the adsorption process. In the case of nitride catalysts, the pretreatment process involves reducing the passive layer on the catalyst surface (Sundaramurthy et al., 2008). After desorption, the sample is cooled down to the NH_3 adsorption temperature (normally ambient temperature) for the NH_3 adsorption process. A neutral gas such as helium is then passed over the sample after NH_3 adsorption to romove any residual unadsorbed NH_3 on the catalyst surface. The TPD is then performed in an inert gas flow at a slow ramping temperature rate. The effluent gases can be analyzed to identify the decomposition or desorption products (Bafrali and Bell, 1992).

A number of NH_3 TPD studies are reported in the literature for nitride catalysts. Bafrali and Bell (1992) used TPD studies to characterize bulk Mo-N catalyst. The sample was cooled to ~ -63 °C for adsorption to minimize adsorption of background gases after which it was heated at 0.35 °C/min to desorb the adsorbed gas. The exit gas was monitored with a UTI 100C quadrupole mass spectrometer interfaced to a computer. Results showed that NH_3 can desorb molecularly or dissociatively depending on how much NH_3 is adsorbed. NH_3 desorption from the surface of Mo(100)-N was accompanied by H_2 desorption at 27, 177 and 227 °C. Nitrogen gas (N_2), however, desorbed only above 927 °C. The proposed decomposition of NH_3 during desorption is shown in Equation (2.6).

$$NH_{3,s} \xrightleftharpoons{-H_s} NH_{2,s} \xrightleftharpoons{-Hs} NH_s \xrightleftharpoons{-Hs} N_s \qquad (2.6)$$

Colling et al., (1996) reported that the temperature at which H_2 desorbed during NH_3 TPD was significantly higher than that during H_2 TPD suggesting that the observed H_2 must be due to decomposition of NH_3. NH_3 decomposed on the Mo nitrides at temperatures greater than ~500K and may have adsorbed on nitrogen deficient patches on the Mo nitrides. In a TPD study of nitride 97.1% MoO_3/Al_2O_3 nitrided at 700 °C, Nagai (2007) observed two N_2 desorption peaks at 546 and 728 °C. The N_2 desorption at 546 °C was accompanied by H_2 desorption suggesting decomposition of NH_3. They also confirmed that NH_3 undergoes consecutive dehydrogenation as shown in Equation (2.6). TPD studies by Ozkan et al. (1997) on γ-Mo_2N samples showed a broad N_2 desorption peak covering a temperature range from 240 – 500 °C. The peak was attributed to loss of nitrogen from the surface/subsurface. High temperature N_2 desorption peaks were also observed up to 710 °C. Desorption of NH_3 and H_2O occurred around 330 and 420 °C, respectively. Sundaramurthy et al. (2008) observed increase in the amount of adsorbed NH_3 on NiMo/γ-Al_2O_3 with increase in P loading and attributed it to the formation of P-OH groups on the catalyst surface. Ferdous et al. (2007) reported that for oxide catalysts, most of the ammonia is adsorbed molecularly on Lewis acid sites of aluminum cations and on Bronsted acid sites of Al–OH. Colling et al., (1996) suggested that NH_3 decomposition from their Mo nitrides at temperatures greater than ~500K may have adsorbed on nitrogen deficient patches on the Mo nitrides. This means that the amount of nitrogen in nitride catalyst may be related to the acidity of the catalyst.

2.3.4.2. Temperature Programmed Reduction (TPR)

TPR is widely used to characterize hydrotreating catalysts. It is used to investigate reducible phases in catalyst and their stability to reduction.

Prior to performing the reduction studies, the catalyst is degassed in an inert atmosphere to remove any adsorbed water or impurities that may interfere in the reduction analyses. After cooling down to room temperature, the catalyst is contacted with low hydrogen concentration gas mixture (< 1 vol% H_2 in a neutral gas) at a slow temperature ramping rate (normally ≤ 10 °C/min). Peaks observed are normally attributed to the production of H_2O, NH_3, N_2 and NH_3 decomposition products.

Yu et al. (1998) investigated the surface and bulk reaction properties of oxynitride catalysts using TPR in 10% H_2/He gas. They observed that in all cases, nitrogen peak appeared earlier than ammonia peak with water peak appearing last. The conclusion was that oxygen was held more tightly on the catalyst than nitrogen.

In their TPR studies of Mo_2N samples, Colling et al., (1996) observed that weakly bound NH_3 desorbed molecularly (77 and 277 °C) while more strongly bound NH_3 decomposed into NH_2, NH, and atomic nitrogen and hydrogen. Water was not observed at temperatures below 127 °C and was adjudged to be physisorbed or weakly chemisorbed after desorption. Water that desorbed above 127 °C was believed to be a product of the partial reduction of the passive layer. The samples were degassed at 500 °C and the reduction performed at 15 °C/min in 5.2 % H_2/He.

Shi et al. (2004) performed TPR experiments of W_2N and Mo_2N samples and monitored the effluent by means of a gas chromatography thermal conductivity detector. The samples were degassed up to a maximum of 120 °C and kept at this temperature for 30 min in Ar. They used a heating rate of 10 °C/min in a gas mixture of 5% H_2 in Ar. They observed high temperature (730 °C) peaks that were attributed to reduction of lattice oxygen in W_2N. Peaks observed at 330 °C were assigned to reduction of surface NH_x and/or oxygen species.

Sundaramurthy et al. (2008) also studied the properties of Mo_2N samples with TPR analyses. Samples were purged in He flow up to 400 °C and kept for 1 h to remove impurities on the surface of the sample. The reduction was done at 5 °C/min temperature ramping rate in 3% H_2/N_2 (v/v) gas mixture. Observed peak at 285 °C was assigned to reduction of passive layer on Ni_3Mo_3N. Inclusion of P up to 0.6 wt% reduced the peak intensity. They concluded that P prevented the formation of oxynitrides during passivation.

In the TPR studies of molybdenum and tungsten nitride species, McGee et al. (2005) observed peaks in the temperature range 300-600 °C and assigned to water. Peaks observed above 600 °C were similar to those observed in TPD results and were assigned to decomposition of nitride and oxynitrides species. They used 5% H_2/Ar at a temperature ramping rate of 10 °C/min. Chu et al. (1999) investigated the properties of $NiMoN_x/\gamma\text{-}Al_2O_3$ samples in 5 wt% H_2/Ar at 10 °C/min and reported that Ni in nitride catalysts promoted reduction of the passive layer. This was based on the observation that on increasing Ni loading, the reduction peak shifted to lower temperature (400 °C). An observed peak at 700 °C was associated with reduction of oxidic Ni. The sample was purged at 500 °C to remove adsorbed NHx species. Yuhong et al. (2001) also

attributed TPR peaks at 500 °C to reduction of passive oxygen on the surface of the catalyst. A shift to lower temperature was observed with increase in Ni loading. This was interpreted as Ni facilitating reduction of the passive layer. They purged their samples at 500 °C in order to remove adsorbed NHx species. The TPR was performed in 10% H_2/N_2 mixture at 12 °C/min. Cho et al. (2000) observed peaks at 925 °C in tungsten oxynitrides TPR and assigned them to reduction of highly dispersed surface mono-oxo tungsten oxide species strongly bonded to the Al_2O_3. A shoulder at 752 °C was assigned to peaks for reduction of bulk WO_3

Ozkan et al. (1997) degassed γ-Mo_2N samples at 500 °C prior to TPR experiments. The TPR was performed in a 10% H_2/He at a temperature ramping rate of 15K/min. An observed peak at 130 to 410 °C was assigned to passive layer reduction. Based on this, catalysts were reduced at 400 °C for 12 h prior to hydrotreating. Hada et al. (2000) observed decomposition of Mo_2N during TPR studies to give off N_2 gas at above 827 °C.

2.3.5. Thermogravimetric Analysis (TGA)

TGA is a characterization technique that is performed on samples to determine changes in weight in relation to change in temperature. TGA is used to determine degradation temperatures, absorbed moisture content of materials, decomposition points of materials, amount of species adsorbed on a material and loss or gain in weight due to a chemical reaction (Chen et al., 2004). If coupled with differential thermal analyses (DTA), it is possible to determine whether a change is endothermic or exothermic or none (Kim and Kim, 1999).

Alonso et al. (2004) used TGA – DTA to analyze thermal decomposition points of thiotungstate species. They observed both exothermic and endothermic peaks associated with decompostion. They also found that the observed weight loss of 48% was comparable to the theoretical value of 47.4%. Chen et al. (2004) used TGA-DTA to study the reaction path of hydrazine adsorption and decomposition over Mo_2N/γ -Al_2O_3 catalyst. The catalyst sample weight and rate of weight change were evaluated continuously to determine amount of coke and adsorbed reaction mixture components. Siewe and Ng (1998) analyzed both fresh and spent catalyst by TGA-DTA analyses in oxidizing atmosphere in order to identify the dominant species in the catalysts. They observed that the DTA plots showed little or no accompanying heat of reaction, suggesting that the weight loss was due to desorption of adsorbed material such as H_2O and light hydrocarbons in the spent catalysts. However, there were exothermic reactions associated

weight changes for both MoO_2 and MoS_2 species. Sundaramurthy et al. (2008) also performed TGA analyses of $NiMo/Al_2O_3$ nitride samples in oxidizing atmosphere in which they observed weight loss up to 150 °C. This weight loss was attributed to moisture loss from the surface of the catalyst. Weight gain was observed between 150 and 325 °C which was attributed to oxidation of nitride species.

2.3.6. X-ray Diffraction (XRD) Analyses

X-ray diffraction can be defined as the elastic scattering of x-ray photon by atoms in an ordered lattice. A constructive interference results in a peak from which the d-spacing could be calculated using the Bragg equation (Equation (2.7))

$$\eta\lambda = 2d\sin\theta \tag{2.7}$$

Where λ is the wavelength of the x-rays (Å), d (nm) is the distance between two lattice planes, θ is the angle between the incoming x-rays and the normal to the reflecting lattice plane (°) and η is an integer called order of the reflection.

X-rays are strong enough to penetrate a solid sample and has a wavelength in the range of Ångstrøm. X-ray can be used to estimate crystallite sizes and to identify bulk structures based on the distance between two lattice planes (d-spacing). The Scherrer equation (Equation (2.8)) can also be used to determine crystal size (d_c) and it is based on line broadening.

$$d_c = \frac{K_s\lambda}{\beta_s\cos\theta} \tag{2.8}$$

where K_s is a constant (often taken as 1), λ is the wavelength of the radiation (Å), β_s is the peak width and θ the Bragg angle of the peak (°).

For dimensions below 2-3 nm, x-ray gives little or no information. Amorphous structures are not visible to x–ray diffraction and show broad or no peaks. Line broadening occurs from incomplete destructive interference in cases where the x-rays are out of phase (Niemantsverdriet, 1993). In the XRD experiment, a sample of the powdered material is placed in a holder, then the sample is illuminated with x-rays of a fixed wave-length and the intensity of the reflected radiation and the angle are recorded using a goniometer.

X-ray diffraction has been used widely in the literature to characterize hydrotreating catalysts (Neylon et al., 1999; Ramanathan and Oyama, 1995; Korlann et al., 2002; Claridge et al.,

2000). Neylon et al. (1999) carried out x-ray diffraction studies on bulk, early transition metal nitride using a Rigaku DMAX-B diffractometer with Cu Kα radiation of 1.5405Å wavelength. This gave information on the crystalline structures and a determination of the crystallite size from the Scherrer equation (Equation (2.8)) where K_s was taken to be 0.9. They observed that the peak positions were consistent with crystalline phases, suggesting that the materials were phase-pure. They also observed that there was no evidence of crystalline oxide in any of the materials. Diffraction patterns of spent catalysts were nearly identical to those of the fresh catalysts. This meant that any change that occurred on the catalyst was restricted to the surface and not the bulk material.

Ramanathan and Oyama (1995) identified the bulk structures of transition metal nitride catalysts using Siemens 500 powder diffractometer with Cu kα monochromatized source operated at 40 KV and 30 mA. They observed that the compounds were phase-pure with no evidence of unreacted oxide impurities in the bulk. The x-ray line-broadening of the peaks indicated the materials were composed of small crystallite sizes and which led to high surface area. Using equation (2.8) with β_s defined as the width of the XRD peak at half maximum corrected for instrumental broadening (0.1°) and K_s = 0.9, they obtained the crystallite sizes of the catalyst samples. Mo_2N crystallite size of 8 nm was comparable to the particle size obtained from surface area measurements (7 nm).

XRD analyses of phosphorus-doped tungsten oxynitride catalyst samples were performed by Perez-Romo et al. (20020) using a Siemens D500 automatic diffractometer with Cu Kα monochromated radiation source. Crystallite sizes were determined from the Scherrer equation between d_{111} and d_{200} crystallographic planes. Some of the samples were identified as β-W_2N peaks yielding a lattice parameter of 0.4161 nm (theoretically, 0.4126 nm). The slight increase in lattice parameter was attributed to the presence of oxygen or the nitrogen content being higher than that in β-W_2N. Crystallite sizes decreased with P loading.

Yu et al. (1998) analyzed oxide and oxynitride bimetallic catalysts by XRD using Siemens Model D 500 diffractometer with a Cu Kα monochramatized radiation source for phase identification. They observed from their data that all the oxynitrides had face-centered cubic (fcc) metallic arrangement. Small crystallite size was observed from the XRD peak broadening which suggested high surface area materials.

There have been reports of XRD not detecting amorphous structures (Dezelah et al., 2004; Benitez et al., 1996). Reyes et al. (1994) did not observe any peaks other than alumina for WO_3/Al_2O_3 catalysts with P_2O_5 content $\leq$ 2.5 wt%. WO_3 peak appeared at d-spacing of 3.84 Å at high P_2O_5 content of 6 wt%. Chu et al. (1999) did not observe Mo_2N structures in their XRD studies of $NiMoN_x/\gamma\text{-}Al_2O_3$ samples and attributed it to amorphous nature of the nitrides or small crystallites.

2.3.7. Scanning Electron Microscopy (SEM)

In SEM, electrons are used to probe the sample surface and secondary or backscattered electrons are measured. Information such as the morphology of the particles could be obtained from the samples. Most of the SEM studies in hydrotreating have focused on catalyst particle sizes and shapes.

Ferdous et al. (2004a) examined the surface structures of $NiMo/Al_2O_3$ catalysts using Hitachi S-2700 with Princeton Gamma-Tech Prism EDS Detector. It was observed that an increase in calcination temperature up to 500 °C caused an increase in particle size from ~0.2 to ~0.4 μm. Increase in Ni concentration did not have any visible impact on the particle sizes. Addition of phosphorus resulted in irregular particle sizes and agglomeration. In a bid to investigate the morphology of W_2N species, Hara et al. (2007) performed SEM of the samples with a Hitachi S-4100 scanning electron microscope. They observed partial agglomeration of the W_2N particles with particles clinging together to form large particles. Nagai et al. (1999) monitored the morphology of W_2N samples during synthesis and observed steady growth of the particles in size and shape with time. At 5 min into the chemical vapour deposition (CVD) synthesis process, particles of size o.1 μm were observed. After 60 min, the particles were agglomerated and were rounded, ranging between 0.3 to 0.5 μm. SEM images of $\gamma\text{-}Mo_2N$ samples by Ozkan et al. (19970) showed the presence of highly porous, sponge-like structures. Trawczynski (2001) observed well dispersed Mo_2N samples at synthesis condition of 17 min^{-1} GHSV (gas hourly space velocity) NH_3 flow and heating rate of 2.5 °C/min. However, they observed $\gamma\text{-}Al_2O_3$-supported catalysts formed larger particles due to agglomeration compared to the unsupported catalysts. In a study of the Effect of phosphorus addition on unsupported Ni–Mo–W sulfide samples, Nava et al. (2006) noticed that the morphology of samples appeared partly granulated and had cavities

with diameters of less than 5 μm. Needle-like structures and increased crystallinity was observed as P was added to the sample.

2.3.8. Energy Dispersive X-ray (EDX)

When atoms are bombarded with electrons they give out x-rays. Fluorescence x-rays emitted from an atom due to the ejection of a bound core electron are element specific and are used in determining the composition of the sample. EDX is normally used together with SEM. Although EDX is not as frequently used as SEM to characterize hydrotreating catalysts, there has been a fair number of reports on the use of EDX as characterization tool in the literature.

Researchers (Cruz et al., 2002) have studied dispersion of active phases on catalyst samples by examining the EDX line profiles of the samples. From the line profiles, one can determine whether the species under investigation is homogeneous in the catalyst or non-uniformly distributed. Calafat et al. (1996) performed simultaneous SEM and EDX of sulfide samples using ISI-DS-130 electron microscope. They examined the Mo Lα and Ni Kα line profiles of the sulfided, Mo/C, Ni/C and NiMo/C catalysts and determined that the Mo was homogeneously distributed throughout the catalyst. A similar observation was made for Ni/C but only after the support was treated with acid. Escalona et al. (2007) observed from Kα and Mα EDX line profiles of Ni-promoted Re/Al_2O_3 sulfide samples that homogeneity reduced as the Ni loading increased. The analyses were performed using an ISI DS-130 scanning electron microscope equipped with a Kevex Si/Li detector and a Sun SparcStatiom-5 system.

EDX can also be used to determine catalyst sample composition (Hada et al., 2000; Alonso et al., 2004; Suvanto et al., 1999; Wang et al., 2009). The limitation is that it only determines local composition rather than bulk composition (Ferdous et al., 2004a). Weil (2004) used EDX to determine the composition of Cr_3W_3N catalyst samples and found the ratio to be 1:1:2. Here et al. (1998) also used EDX to determine composition of MnWN species and came up with the formula $MnWN_{1.97\pm0.02}$. In the hydrogenation of tetralin over Mock and WC catalysts, Da Costa et al. (2001) reported that the Mo/Al (0.070) and W/Al (0.065) ratios were homogeneous.

2.3.9. Transmission Electron Microscopy (TEM)

TEM is widely used in catalyst characterization and can give information on the size and structure of particles in a supported catalyst. The contrast between transmitted electrons, the

original electron beam and the blocked electrons help to determine the structure and size of the particles.

Korlann et al. (2002) acquired TEM images of alumina-supported nitride catalysts using Joel 2010 keg. Samples were placed on a 200-mesh copper grid with Formvar and carbon for the analysis. They observed a range of pure Ni_2Mo_3N/Al_2O_3 particle sizes with dimensions in the order of 15 x 21 nm. D-spacing values of 2.11 and 2.80Å for the {310} and {211} crystall o-graphic planes of Ni_2Mo_3N/Al_2O_3 agreed well. Cho et al. (2000) also reported high resolution transmission electron microscopy (HRTEM) results for Mo_2N samples. Sample preparation involved grinding and ultrasonically dispersing the samples in isopropanol. A drop was placed on a carbon-coated 3 mm Cu mesh grid and the microscopy performed at 400 kV using JEOL 4000 EX TEM with resolution of ≤ 2 Å. Crystallite sizes were in agreement with those estimated from XRD line broadening. Particle sizes were in agreement with those obtained from BET analyses. The structures were assumed to be either body-centered cubic (bcc) or face-centered cubic (fcc), giving lattice parameters in the range of 4.32-5.49 and 3.05-3.85 Å, respectively. Claridge et al. (2000) observed from their TEM study of transition metal nitrides and carbides that particles were made of aggregates of smaller particles and was in agreement with BET and XRD results. All the materials maintained the morphology of the parent oxides. In a study of the morphology and composition of cobalt molybdenum nitride catalysts, Hada et al. (2002) observed that the Co_3Mo_3N particles (20 to 30 nm) were surrounded by γ -Mo_2N particles (ca. 4 nm) in the catalyst nitrided at 750 °C. The equipment used was a JEM-2000F transmission electron microscope (JEOL Co.) operating at 200kV and equipped with an energy-dispersive x-ray spectrometer (EDS). TEM of Ni_2Mo_3N samples were studied by Korlann et al. (2002). Their results indicated a range Ni_2Mo_3N particle sizes, but there was no evidence for a crystalline impurity. The TEM micrographs yielded d-spacing values of 2.11 and 2.80 Å for the {310} and {211} crystallographic planes of Ni_2Mo_3N, respectively which were in good agreement with XRD results.

Using TEM for catalyst structural studies, Kojima and Aika (2001) observed amorphous structures for Co_3Mo_3N, Mo_2N, and Co metal in their study of the shapes of the catalyst. In a similar study, Hara et al. (2007) investigated the structures of W_2N samples using transmission electron microscope technique but did not observe any characteristic structures for W_2N samples like the usual structures normally observed for W_2S samples. Nagai (2007) proposed that their Mo_2N sample had a body centered structure based on results of their TEM studies. This was de-

duced from the fact that the structure was in conformance with the (0 0 1) and (1 1 1) indices. The surface structures were however different from the bulk structures.

2.3.10. Infrared Spectroscopy

Application of infrared spectroscopy in catalysis includes identification of adsorbed molecules on catalyst surfaces (Nagai et al., 2000a). IR spectroscopy is also used to monitor steps in catalyst preparation by identifying phases present in each stage. It is frequently used to study the type and number of active sites on catalysts by adsorbing gaseous molecules such as CO, NO or pyridine and NH_3. It is also used to study the nature of acidic sites on catalyst surfaces (Satterfield, 1980).

The strong C-O dipole makes it easy to study. Linearly adsorbed CO has frequencies between 2000 and 2130 cm^{-1}. Two-fold or bridge bonded CO and three-fold CO frequencies fall between 1880 and 2000 cm^{-1} and 1800 and 1880 cm^{-1}, respectively, while four-fold CO falls below 1800 cm^{-1}. The metal-carbon bond which falls between 200 and 450 cm^{-1} is, however, more difficult to measure. NO is also used in IR studies and has especially been used in studying sulfided hydrotreating catalysts (Topsoe and Topsoe, 1983). It is possible to distinguish between Co and Mo sites using NO adsorption. This is because NO adsorbs on Co and Mo with different frequencies (Topsoe and Topsoe, 1983). For frequencies below 1000 cm^{-1} like metal-oxide and metal-sulfide bonds, Raman spectroscopy is a better option than infrared spectroscopy.

Nagai et al. (2000a) measured infrared spectra of Mo_2/Al_2O_3 at a resolution of 4 cm^{-1} in 100 scans at room temperature with NH_3 and reported that the sample nitride at 900 °C was less acidic compared to the 500 °C nitride sample. Klaus et al. (2000) studied the FTIR of tungsten and tungsten nitride samples and assigned a band at 3450 cm^{-1} to N-H_2 stretching vibration. Another band at 1500 cm^{-1} was assigned to N-H_2 scissors modes. Two prominent spectral features observed at 3455 and 1610 cm^{-1} were assigned to molecular NH_3. Common IR bands that are relevant to nitride catalysts and the molecules responsible for the bands are shown in Table 2.4.

2.3.11. X-ray Absorption near Edge Structure (XANES)

XANES is a region of x-ray absorption spectrum within 50 eV of the absorption edge. XANES is element specific and can be used for very small concentrations. Information obtainable from XANES include oxidation state, chemical species identification and investigation of

Table 2.4: Common infrared bands relevant to nitride catalysts.

Band Range	Structure	Name	Ref
200–1000	AL-N		(Balasubramanian et al., 2006)
300-550	MN (NMN)	Bridged metal nitrogen bond (M-NH_3)	
500-550	MN	M-NH_2	
665-893	W-O-W	Bridge bonds stretching vibration	(Atanasova et al., 1997)
912-1007	W=O	Terminal bond stretching	(Atanasova et al., 1997)
900–1800	Al-O	Frequency range	
1264	NH_3	Chemisorbed Ammonia (Surface Lewis acid sites) Coordinated NH_3 species	(Nagai, 2007)
3000–3580	H_2O	Absorbed water on uncalcined Al_2O_3	
3000–4000	-OH	Hydroxyl stretching region	(Ferdous et al., 2004a)
3677	-OH	Acidic hydroxyl group	(Ferdous et al., 2004a)
3727-3762	-OH	Basic hydroxyl groups	
3395, 3335	NH_x		(Puurunen et al., 2003)
1450-1485	NH_4^+	Deformational mode of NH_4^+ formed by interaction of NH_3 with Brønsted acid sites	(Nagai et al. 2000a)

local coordination environment. X-rays which are required for XANES spectra can be obtained from K and L_{III} edges corresponding to 1s and 2p electrons, respectively. The choice of the type of edge, K or L_{III}, depends on the following factors:

1. overlap between accessible energy range of beamline and
2. binding energy of the 1s and 2p electrons

Generally, K edge is used for 3d and 4d metals while L_{III} is used for 5d metal spectra.

XANES can be used to determine oxidation states of species in catalyst. As the oxidation state of a molecule increases, an increase in the absorbing energy is observed. This is seen as a shift in the main absorbing edge of the species (Ferdous et al., 2005; Engemann et al., 1999). 11 eV shift in energy was observed in change in oxidation state from S^{2+} to S^{6+}. Absorption of energy in XANES mainly results in the following primary orbital electron transitions:

$s \rightarrow p$ for K (1s electron) and L_1 (2s core electron initial state) edges

$p \rightarrow d$ for L_2 ($2p_{1/2}$) and L_3 ($2p_{3/2}$) edges

There can also be transition from $s \rightarrow d$ when there are unoccupied d-orbitals and this results in pre-edge peaks (Sun et al., 2001; Okude et al., 1998; Hensen et al., 2007). Sigurdson et al. (2008) performed Al L-edge XANES experiments for Al_2O_3 supported p-doped NiMoW catalysts. They observed that even with increase in loading, the Al_2O_3 spectra was unaffected, suggesting that inclusion of P in the catalyst did not impact the bulk structure of the Al_2O_3.

2.4. Kinetic Analysis

Kinetic modeling in hydrotreating reactions is often studied using either Power Law or Langmuir-Hinshelwood models. The Power Law model is simple but it is unable to account for inhibition in the reaction process. The Langmuir-Hinshelwood model, on the other hand, is complex but has the advantage of accounting for inhibition in the reaction process. It also gives idea of the reaction mechanism and the active sites involved in the reaction. Power law model follows the form shown in Equation (2.9) where r is the rate of reaction, k is the rate constant,

$$-r = kC^n P^m \tag{2.9}$$

C is the concentration of the heteroatom, P is the hydrogen pressure and n and m are the reaction orders of concentration and pressure, respectively. Langmuir-Hinshelwood model follows the form shown in Equation (2.10) where the denominator is the inhibition term and K is the adsorption term. The rest of the parameters are as defined above.

$$-r = \frac{kC}{[1+KC]} \tag{2.10}$$

In heterogeneous catalytic reactions, reactions occur at the interface between the fluid and solid. This means that the reaction will be enhanced for large interfacial area. Porous catalysts are characterized by large surface areas obtained from pore structure distribution in the catalyst (Satterfield, 1980). Pores in a catalyst pellet are irregular network of randomly interconnected capillary channels with varying cross-section and length (Lee et al., 1991; Wood and Gladden, 2002; Rodriguez-Reinoso, 1998; Tsai and Chen, 1993). They can be classified into three main types as listed below (see also Figure 2.6):

1. Micropores (pore diameter $\leq$ 2 nm),
2. Mesopores (pore diameter 2 – 50 nm) and
3. Macropores (pore diameter $\geq$ 50 nm).

For a chemical reaction to take place in a porous catalyst, the following seven steps are required (see Figure 2.7):

1. Diffusion of reactants from the bulk fluid to the external surface of the catalyst pellet,
2. Diffusion of the reactant through the pores of the catalyst pellet,
3. Adsorption of the reactants onto the internal surfaces within the catalyst pores,
4. Surface reaction at the active sites of the catalyst pellet, Desorption of products from the active sites of the catalyst into the mainstream of the catalyst pores,
5. Diffusion of product from the pores to the external surface of the catalyst pellet and
6. Diffusion of products from the external surface of the catalyst pellet into the bulk fluid.

Steps 1, 2, 6 and 7 are mass transfer (diffusion) steps while steps 3, 4 and 5 are chemical reaction steps (Fogler, 2006). The seven steps occur in series, the slowest of which is the rate-limiting step. If diffusion to the active sites is slower than the chemical reaction step, the reaction is mass transfer-limiting and diffusion is considered restricted. For such reactions, concentration gradient within the catalyst pellet is significant. Only the outer portions of the catalyst pellet will be utilized for reaction (Chen and Tsai, 2005). On the other hand, if the diffusion steps are faster than the reaction steps, the overall reaction is surface reaction-limiting and the concentration within the pores and surrounding is uniform (Carberry and Varma, 1987).

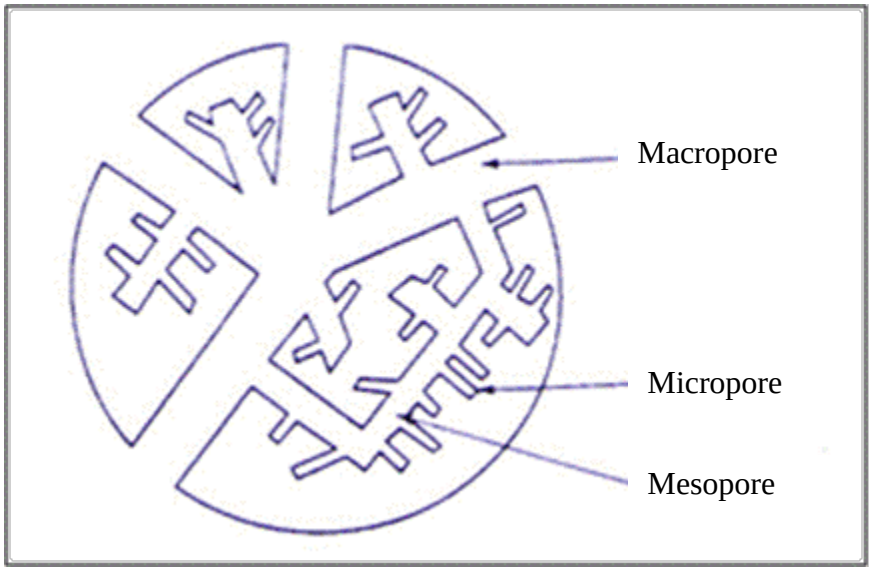

Figure 2.6: Schematic representation of the structure of activated carbon (Wood and Gladden, 2002).

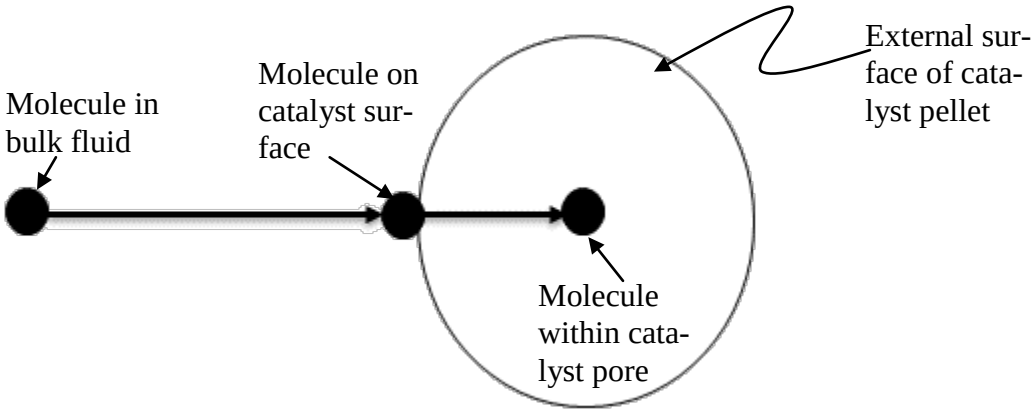

Figure 2.7: External and internal mass transfer of reactant molecule during reaction.

2.4.1. Limitations in Catalytic Reactions

Effective use of the catalyst is realized when the surface reaction step is rate-limiting, i.e. when the diffusion steps are faster than the surface reaction steps (low restrictive diffusion). Limitations are often observed that do not enhance effective use of the catalyst. They may be limitations relating to either diffusion or surface reaction. Causes of diffusion limitations include steric hindrance and change in catalyst pore structure.

2.4.1.1. Diffusion Limitations

For a chemical reaction to occur, the internal surfaces of the catalyst pellet containing the active sites must be accessible to the reactant molecule. This means the reactant must be able to diffuse through the pores of the catalyst to the surface. Depending on the size of the catalyst pore and the reactant molecular size, the diffusion process could be hindered. This is a common problem encountered in catalytic reactions. A number of studies have shown that effective diffusivity in catalyst pellets decrease with increase in reactant molecular size (Chen and Tsai, 2005; Philipopoulos and Papayannakos, 1988; Whitehurst et al., 1998). That is if the molecular size is larger than the pore diameter, the molecules will not be able to enter the catalyst pores and diffusion will be hindered.

Change in catalyst pore size is another common diffusion limitation. As reaction proceeds, changes occur in the catalyst pore structure due to deposition of particles in pores and sintering of catalyst pores from high reaction bed temperatures. Catalyst pores are constantly deposited with particles as reaction proceeds. In reactions involving especially, hydrocarbon molecules, carbonaceous particles (coke) are deposited in the pores of the catalyst pellet (Guin et al., 1986). This causes narrowing of the pores and reduces effective diffusivity of molecules to the active sites. Other particles that can cause reduction and blockage of catalyst pores are metallic deposits. Deposition of nickel and vanadium metals in catalyst pores during hydroprocessing of heavy petroleum fuel has been reported to decrease effective diffusivity (Shimura et al., 1086).

Sintering of catalyst pellets is a common cause of reduction in effective diffusivity. It is the agglomeration and alteration of catalyst pore structure at high temperatures. Although high reaction temperatures can increase the rate of reaction, excessive temperatures can cause a marked change in the morphology of the catalyst pores through agglomeration. This agglomeration narrows up the pores and reduces the effective diffusivity of reactant molecules through the

pores. Sintering could also be caused by the formation of hot spots within a catalyst bed (Marwaha and Luss, 2003).

2.4.1.2. Surface Reaction Limitation

Coverage of active sites by coke and metallic particles can reduce the effect of adsorption and hence, the reaction rate. Sintering and agglomeration do change the surface morphology of the active sites (Doraiswamy and Sharma, 1984). The activity of the catalyst largely depends on the morphology of the active sites. Any change in these sights could result in low activity. Formation of hot spots in catalyst beds and high reaction temperatures in the catalyst pellets can also cause sintering of the active sites which will eventually reduce the reaction rate.

Another cause of reaction rate reduction is poisoning of active sites. It is possible for a reactant or product to undergo secondary reaction (fouling) or inert molecules (poisoning) to be strongly adsorbed (chemisorption) unto the active sites without getting desorbed. Such a process poisons the active site in question and reduces the total number of active sites available for further reaction (Doraiswamy and Sharma, 1984).

2.4.2. Analyses of Catalyst Utilization

Factors used in the analysis of diffusion within catalyst pellets to determine effective utilization of the catalyst include the Thiele modulus, internal and overall effectiveness factors. For a catalyst pellet, the Thiele modulus is given by the expression in Equation (2.11)

$$\text{Thiele Modulus} = \frac{\text{surface reaction rate}}{\text{Diffusion rate}} \tag{2.11}$$

If Thiele Modulus is small, it means the diffusion rate is large and the reaction is not limited by diffusion or the reactants can diffuse through the catalyst pores to access the active sites. If Thiele Modulus is large (>1), it means the diffusion rate is smaller than the surface reaction rate and diffusion of reacting molecules through the catalyst pores to the active sites is hindered. Hence, the reaction is predominantly surface reaction and the catalyst is not fully utilized.

The effectiveness factor is a measure of the utilization of the catalyst pellet. For diffusion-limited reactions, a high concentration gradient exists in the catalyst pores. Only the outer pores of the catalyst would be utilized in such a case. The effectiveness factor is inversely proportional to Thiele Modulus and is defined as

$$\text{Effectiveness Factor} = \frac{\text{actual rate of reaction}}{\begin{array}{c}\text{rate of reaction that would result if entire}\\ \text{interior surface were exposed to the external}\\ \text{surface concentration and temperature}\end{array}} \tag{2.12}$$

For effective utilization of the catalyst in isothermal reactions, the effectiveness factor should approach 1. This can be achieved when the Thiele modulus is small. Factors that contribute to a decrease in the Thiele modulus are small pellet size and high reactant flow rate. For small pellet size, tortuosity (the path of travel for reactants to the active site) reduces, effective diffusivity increases and accessibility to active sites increases. High flow rates will generally increase diffusivity and hence, the effectiveness factor.

It is possible to obtain values of effectiveness factor greater than unity if the actual reaction rate is greater than the rate on the catalyst surface. This phenomenon occurs in some exothermic reactions where the temperature inside the catalyst pellet is greater than the temperature on the external surface of the catalyst pellet. Since temperature increases the rate of reaction (Satterfield, 1980; Fogler, 2006; Selley, 1971), higher reaction rate is observed inside the catalyst pellet compared to the rate outside. This results in effectiveness factor values greater than unity.

Catalyst effectiveness factor is normally evaluated in overall terms rather than just relative to the catalyst surface. This is because the surface concentration is not measurable. The overall effectiveness factor involves both external and internal mass transfer resistances and is related to the bulk fluid concentration which is measurable (see Figure 2.7). A small value of the overall effectiveness factor means both internal and external diffusion resistances are important and should be factored in the overall reaction analyses.

Another concern in fixed bed reactors is axial dispersion of reactant molecules in the reactor. The flow in a fixed bed reactor can deviate from ideality due to radial variation in turbulence in flow and mixing effects due to the presence of packing. Axial dispersion reduces concentration and temperature gradients in a fixed bed reactor and reduces the overall conversion in the reaction process (Froment and Bischoff, 1979). The axial dispersion term can be neglected compared to the bulk flow term (Fogler, 2006).

In general, for fixed bed reactors, high overall effectiveness factor will result in higher conversions. To achieve this, the internal effectiveness factor must be high, Thiele modulus should be low and effective diffusivity should be high. This could be obtained from small catalyst pellet sizes with large pore diameters and high flow rates. Reducing the catalyst particle size

means reducing the overall distance of the reacting molecule to the active sites. This makes the active sites more accessible and enhances activity. Steric hindrance is reduced for catalysts with larger pore diameters. This enhances accessibility to active sites through the catalyst pores. Increasing flow rate will enhance diffusion rate of molecules and hence, will increase catalyst activity.

2.4.3. HDS and HDN Kinetic

Hydrotreating kinetic expressions are developed based on power law and Langmuir-Hinshelwood models. Power law models are used to represent the overall rate law for the various reactions taking place in the hydrotreating process. On the other hand, Langmuir-Hinshelwood models are capable of accounting for inhibition in the reaction processes (Girgis and Gates, 1991). Most of the kinetic studies reported in the literature have been done using model compounds. Thiophenic compounds are commonly used for HDS kinetics while quinoline and pyridine compounds are commonly used for HDN kinetics (Kabe et al., 1999). The reason behind the use of these compounds is because they are the least reactive among the organosulfur compounds in petroleum.

2.4.3.1. Power Law Kinetic Modeling

Kinetic studies using model sulfur or nitrogen compounds have been reported to follow first-order (Speight, 2000; Callejas and Martinez, 1999; Ancheyta, et al., 2002). Narrow boiling cuts from gas oils also follow first order reaction kinetics (Sie, 1999). Real feedstock is composed of different complex compounds containing sulfur, nitrogen etc., each with its own reactivity and hydroprocessing kinetics (Ma et al., 1994a Callejas and Martinez, 1999). The complexity of the simultaneous reaction of the individual compounds makes it difficult to represent the overall hydroprocessing reaction with a single rate expression (Sie, 1999; Satterfield and Gultekin, 1981).

The rate of reaction is reported (Speight, 2000) to decline with molecular weight of feedstock. Compounds with simpler structures such as thiols (R-SH), sulfides (R-S-R$^{'}$) and amines (R-NH_2) react faster than the cyclic compounds such as thiophene and pyrrole. Kinetic expressions for petroleum feeds are sometimes expressed in two forms: one for the easy-to-hydrotreat compounds and the other to describe the difficult-to-hydrotreat compounds.

2.4.3.2. Langmuir-Hinshelwood Kinetic Modeling

In heterogeneous catalysis, the reactant (i) with an adsorption constant K_i must be adsorbed on to an active site of the catalyst for reaction to take place. Other reactants may be adsorbed on other sites or remain in the bulk solution. In the presence of other species, (*I*), there is competition for active sites and the concentration of the adsorbed reactant [i_{AD}] will be lower than when it is present alone. In other words, in the presence of other species, adsorption of i to the active sites is inhibited. Rate of conversion therefore depends on the fraction of adsorbed sites covered by the reactant (Θ_i) instead of the actual concentration of the reactant. Generally, the observed rate is given by:

$$\Theta_i = \frac{K_i[i]}{\left(1 + K_i[i] + K_I[I] + ...\right)} \tag{2.13}$$

where the degree of inhibition is given by

$$\frac{1}{\left(1 + K_i[i] + K_I[I] + ...\right)} \tag{2.14}$$

and varies between zero (complete inhibition) and 1 (no inhibition) (Whitehurst et al., 1998). Due to difficulty in analyzing adsorption and desorption of various sulfur and nitrogen compounds in real feedstock, various assumptions have been used to simplify the expressions obtained and to fit the experimental data to the expressions (Girgis and Gates, 1991). The final form of the Langmuir-Hinshelwood model is dependent on the type of assumptions made. Possible assumptions, which are based on the reaction mechanisms, include the following:

1. Same adsorption sites for all reactants (Leglise et al., 1996; Hanlon, 1987),
2. Different adsorption sites for reactants (Gates et al., 1979; Van Parijs and Froment, 1986),
3. One reactant adsorbing with the other remaining in the bulk fluid (Van Parijs and Froment, 1986),
4. Reactants such as hydrogen adsorbing molecularly (Leglise et al., 1996) and
5. Reactants (e.g. Hydrogen) adsorbing dissociatively (Van Parijs and Froment, 1986).

In the HDS of thiophene, for example, Gates et al. (1979) assumed that hydrogenation and hydrogenolysis occur on different sites as hydrogen sulfide affected rates of thiophene hy-

drogenolysis and olefin hydrogenation differently. In a related study, Van Parijs and Froment (1986) assumed two catalytic sites for reaction: one for hydrogenation and the other for hydrogenolysis. The assumption of dissociative adsorption of hydrogen on the catalyst (i.e. atomic adsorption of hydrogen instead of molecular adsorption) gave a good fit. Hydrogen sulfide was assumed to be formed from the reaction of gas phase hydrogen with adsorbed sulfur by an Eley-Rideal mechanism. A large difference between the adsorption equilibrium constants for hydrogen on the two sites confirmed the two-site assumption. Hiroshi et al. (2001) combined both power law and Langmuir-Hinshelwood models in their study of the inhibitory effects of hydrogen sulfide on HDS (see Equations (2.15) and (2.16))

$$k_S = \frac{1}{n-1}\left(\frac{1}{C_{Sp}^{n-1}} - \frac{1}{C_O^{n-1}}\right) LHSV \tag{2.15}$$

$$\frac{k_x}{k_o} = \frac{1}{1+\frac{K_{H2S}}{K_S P_S} P_{H2S}} = \frac{1}{1+ f_i x} \tag{2.16}$$

Zhang et al. (1997) maintained a constant hydrogen pressure in their models. The model was based on two different sites for hydrogenation and hydrogenolysis. Hydrogen sulfide produced from the HDS reaction was not factored in due to the low feed concentration and hence low conversion (<15%).

Most Langmuir-Hinshelwood rate equations have been derived with the hydrogenolysis of the C-S bond considered the rate-determining step. However, other steps have also been considered as rate-limiting in model development. Leglise et al. (1996) considered the dearomatization of thiophenes as rate limiting. They assumed the same site for both thiophene and hydrogen sulfide. They did not distinguish between dissociative and molecular hydrogen adsorption and evaluated their kinetic parameters by non-linear regression. Massoth and Zeuthen (1994) observed that the adsorption parameters for hydrogen sulfide and thiophene were about 3-orders greater than that of hydrogen.

Hanlon (1987) modeled the kinetics of pyridine assuming one site Langmuir-Hinshelwood rate expression. He obtained an adsorption equilibrium constant of 49.3 KPa^{-1} for ammonia. Satterfield (1984) assumed the presence of one-site in their kinetic studies of quinoline. In their kinetics of quinoline HDN studies, Yu et al. (1989) found the hydrogen and quinoline adsorption constants to be 2.5 and 78.9 MPa^{-1}, respectively. Yang and Satterfield (1984)

modeled the kinetics of quinoline using a one site model but suggested that better results could be obtained from a two-site model. On the other hand, Shih et al. (1997) assumed a two-site model but assumed all nitrogen-containing species had same adsorption parameters. They estimated the adsorption constants of hydrogen and nitrogen compounds to be 0.05 and 6.4 x 10^8 g-oil.mole^{-1}, respectively.

2.4.4. Solving Rate Equations and Evaluating Kinetic Parameters

The nth order Power Law rate equation as well as Langmuir-Hinshelwood equations and parameters can be evaluated using one or more of the following methods (Fogler, 2006):

1. Differential method
2. Integral method
3. Linear least square analysis and
4. Non-linear least square analysis

Description of how the methods are used to evaluate the equation parameters are in Appendix D.4

2.5. Knowledge Gaps

After comprehensive literature review it was discovered that although some work has been done on novel catalysts such as nitrides and carbides, there are still key areas that have not been investigated. The following points highlight some of the areas that have not been investigated which require intensive studies:

1. Most of the work done on nitride catalysts has been on monometallics in the form M-N (M is a metal). There is not much reported work on bimetallic nitride catalysts although there have been some reports on bimetallic oxynitrides (M_I-M_{II}-O-N). Ni has been reported to promote sulfide catalysts but there has not been much work on Ni-promoted nitride catalysts.
2. One of the catalysts that is commonly used in hydrotreating in place of alumina-supported Co(Ni)-Mo-S catalysts is Ni-W-S catalyst. It is reported to be active for hydrotreating processes, especially, aromatic saturation. However, in the literature, not much work has been done on nitrides of Ni-W. Work done on W has mostly been on W_2N catalysts.

3. The addition of phosphorus to conventional hydrotreating catalysts is reported to increase HDS and HDN activities. Commercial Ni-Mo/Al_2O_3 catalyst, for instance, does not only contain Ni and Mo but P as well. However, most of the reports on nitride catalysts in the literature have not included P in the synthesis.
4. Most of the work done on nitride catalysts has focused on model compounds. However, hydrotreating of model compounds are very different from that of real feed. The complexity of reactions in real feed due to the presence of various types of sulfur and nitrogen compounds as well as aromatic structures, makes hydrotreating of this feed more complex compared to model feeds. Also, the kinetics and catalyst stability with model feeds will be different from real feed. Work done on real feed using nitriding catalyst is very limited and there is virtually no data on real feed like bitumen-derived light gas oil from Athabasca.
5. A lot of work has been done on HDS and HDN hydrotreating kinetics for sulfide catalysts. There has not been any known report on HDS and HDN kinetics for nitride catalysts. Most of the work has been on activity test and characterization.

2.6. Hypothesis

Metal nitrides are known to have high hydrogenation properties. As a result, they are used for reactions such as hydrogenation of CO and unsaturated hydrocarbons. They are also used for NH_3 syntheses due to their high hydrogenation properties. Another use of nitride catalysts is in isomerisation reactions (Puurunen et al., 2003). The reason behind their high hydrogenation properties is that they are capable of adsorbing, activating and transferring active surface hydrogen to reactant molecules. These are the essential properties required in a hydrotreating catalyst. Since nitride catalyst possess all these properties they are likely to be good hydrotreating catalysts catalysts (Furimsky, 2003).

2.7. Research Objectives

2.7.1. Main Objective

The main objective of this work is to synthesize, characterize and test the activity of Ni-W(P)/γ-Al_2O_3 nitride catalyst for hydrodenitrogenation (HDN), hydrodesulfurization (HDS) and hydrodearomatization (HDA) of light gas oil (LGO) from Athabasca bitumen.

2.7.2. Sub-Objectives

1. Synthesize Ni-W(P)/γ-Al_2O_3 nitride catalysts at varying conditions of nickel (Ni), phosphorus (P), tungsten (W) loadings and nitriding temperature (T_N), and test their activities.
2. Use various characterization techniques to determine properties of the catalysts and active site on the catalyst surface.
3. Develop an optimized catalyst through HDS, HDN and HDA of Athabasca light gas oil (LGO) feed and to study its stability to deactivation and hydrogen sulfide.
4. Correlate the nitride catalysts surface properties to their activities
5. Perform kinetic analyses of HDS and HDN of LGO feed over the optimized nitride catalyst.

CHAPTER 3
EXPERIMENTAL

The experimental work covered in this chapter includes catalyst syntheses, catalysts characterization and catalyst activity studies. Experimental devices such as temperature controllers, metering pumps and mass flow controllers were calibrated prior to the experimental work. See Appendix A for results of the calibration work.

3.1 Catalyst Syntheses

This section gives an overview of the various groups of catalysts synthesized for the experimental work and also describes procedures for the catalyst synthesis.

3.1.1 Overview of Catalyst Synthesis Work

The catalyst synthesis procedure for this work consisted of calculation and measurements of required amounts of precursors and support, impregnation and equilibration, drying and calcination, and nitridation/sulfidation (see Figure 3.1). Three groups of catalysts were synthesized for the following studies (see Figure 3.2):

1. Catalyst activity screening,
2. Effect of H_2S on stability of nitride catalysts and
3. Detailed catalyst characterization.

The first group was synthesized based on statistical experimental design (this involved random variation of parameters) for catalyst screening. The statistical design was used to facilitate estimation of interaction and quadratic effects of parameters (in this case: Ni, P and T_N) as well as determine the shapes of the response surfaces of interest (hydrodenitrogenation, hydrodesulfurization and hydrodearomatization) during hydrotreating. Another reason for using statistical experimental design is because it provides quality predictions over the entire design space with minimum number of experiments. The Response Surface Method (RSM) of Central Composite Design (CCD) was chosen to enable parameter optimization for high catalyst activity. See Appendix B.1 for detailed description of CCD. Table 3.1 shows the design points of the catalysts synthesized for activity screening. Ni loading (0-8 wt%), P loading (0-5 wt%) and T_N

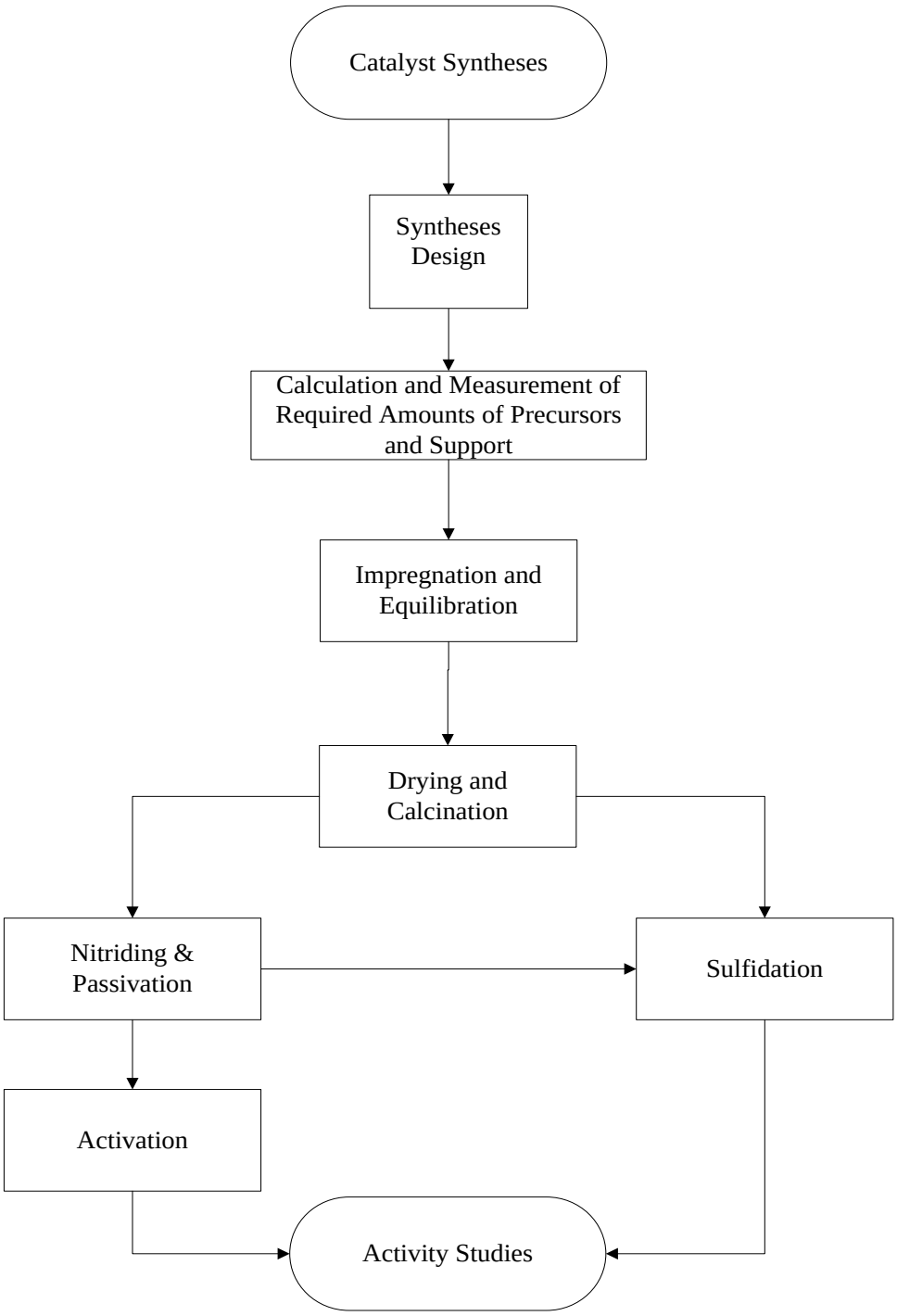

Figure 3.1: Overview of syntheses procedures for nitride and sulfide catalysts.

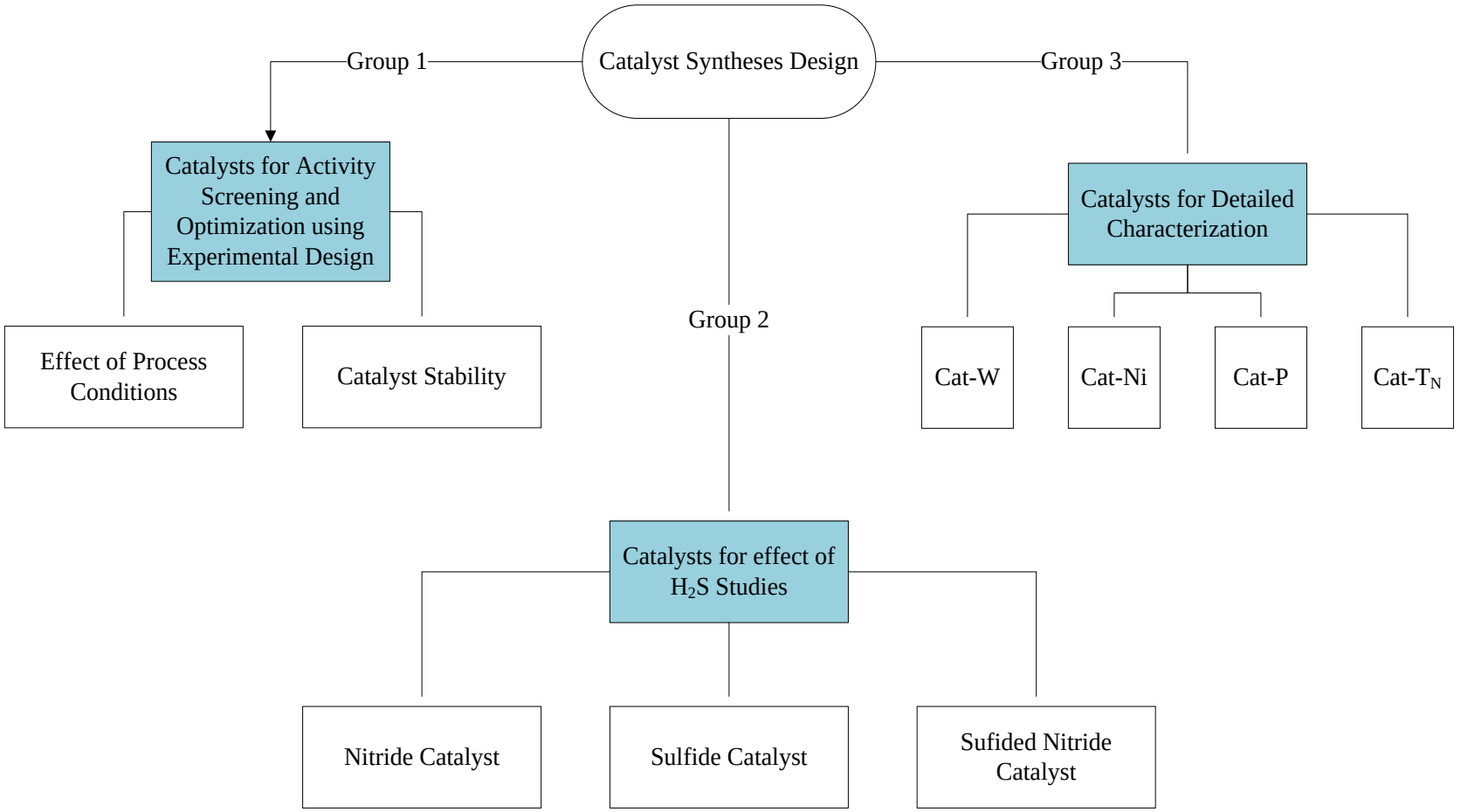

Figure 3.2: Different groups of catalysts prepared for various experimental work.

Table 3.1: Parameter values for nitride catalyst synthesis based on statistical experimental design; W loading, 15 wt%.

Catalyst Name	Ni Loading (wt %)	P Loading (wt %)	T_N (°C)
R-1	6.4 (0.6)	4.0 (-0.6)	561 (-0.6)
R-2	6.4 (0.6)	1.0 (0.6)	739 (0.6)
R-3	4.0 (0.0)*	2.5 (0.0)*	650 (0.0)*
R-4	1.6 (-0.6)	4.0 (-0.6)	739 (0.6)
R-5	1.6 (-0.6)	1.0 (0.6)	561 (-0.6)
R-6	4.0 (0.0)*	2.5 (0.0)*	650 (0.0)*
R-7	6.4 (0.6)	4.0 (-0.6)	739 (0.6)
R-8	1.6 (-0.6)	1.0 (0.6)	739 (0.6)
R-9	6.4 (0.6)	1.0 (0.6)	561 (-0.6)
R-10	4.0 (0.0)*	2.5 (0.0)*	650 (0.0)*
R-11	1.6 (-0.6)	4.0 (-0.6)	561 (-0.6)
R-12	4.0 (0.0)*	2.5 (0.0)*	650 (0.0)*
R-13	4.0 (0.0)*	2.5 (0.0)*	650 (0.0)*
R-14	0.0 (-1.0)	2.5 (0.0)	650 (0.0)
R-15	4.0 (0.0)	2.5 (0.0)	800 (1.0)
R-16	4.0 (0.0)	2.5 (0.0)	500 (-1.0)
R-17	8.0 (1.0)	2.5 (0.0)	650 (0.0)
R-18	4.0 (0.0)*	2.5 (0.0)*	650 (0.0)*
R-19	4.0 (0.0)	0.0 (-1.0)	650 (0.0)
R-20	4.0 (0.0)	5.0 (1.0)	650 (0.0)

*Centre points.

(500-800 °C) were varied while W loading was kept constant at 15 wt%. From the screening results, the catalyst synthesis parameters were optimized for further studies. Thus, nitride catalysts were synthesized based on the optimized conditions for studies on effects of process conditions on HDS, HDN and HDA, and nitride catalyst stability to deactivation.

The second group of catalysts was prepared to study the effect of H_2S on stability of nitride catalysts. Two catalysts, each with a different active phase, were synthesized for this work. The active phases were nitride and sulfided nitride. The sulfided nitride catalyst was obtained by subjecting a nitride catalyst to a sulfidation process. The catalysts were prepared at the following conditions: Ni loading, 2.5 wt%; P loading, 1 wt% and T_N, 560 °C and at two levels of W loading, 15 and 25 wt%.

The third group of catalysts was prepared with systematic variation in parameters (one at a time) for activity and detailed characterization studies. The range of parameters used were W loading (15-40 wt%), Ni loading (0-6 wt%), P loading (0-4 wt%) and T_N (500-900 °C). Table 3.2 shows the catalysts prepared and the parameter levels used. Cat-T_N is catalysts with varying nitriding temperature and Cat-X is catalyst with varying X loading (X is W, Ni or P).

3.1.2 Catalyst Impregnation and Calcination Processes

Ni-W(P)/γ-Al_2O_3 catalysts were prepared by co-impregnating calcined (500 °C) γ-Al_2O_3 support with an aqueous solution of the following catalyst precursors: {($Ni(NO_3)_2 \cdot 6H_2O$), ($(NH_4)_6W_{12}O_{39} \cdot xH_2O$) and ($H_3PO_4$)} by the incipient wetness method (drop-wise addition of precursor solution to the support until it was just wet). The amounts of precursors used were dependent on the compositions of the various catalysts. A sample of the required amounts of precursors evaluated for the synthesized catalysts is shown in Appendix C.1. The freshly impregnated catalyst was allowed to equilibrate for two hours and then dried for 12 h at 120 °C. The dried catalyst was then calcined in flowing air at 500 °C for 5 h to produce catalysts in the oxide state. The oxide catalysts obtained from the calcination process were either nitrided or sulfided to generate the catalyst active phase. Both methods of activation are described below.

3.1.3 Nitriding and Passivation Processes

Temperature programmed reaction (TPr) is the most commonly used method to synthesize nitride catalysts of high surface area (Aegerter et al., 1996; Liu et al., 2002; Korlann et al.,

Table 3.2: Elemental composition and nitriding temperature of synthesized nitride catalysts.

Name	W (wt%)	Ni (Wt%)	P(Wt%)	T_N (°C)	γ-Al_2O_3 (wt%)
Reference Samples					
γ-Al_2O_3	-	-	-	700	100
W/γ-Al_2O_3	30	-	-	700	70
Ni/γ-Al_2O_3	-	10	-	700	90
Cat-P Samples					
0%-P	30	4	-	700	66
1%-P	30	4	1	700	65
2%-P*	30	4	2	700	64
3%-P	30	4	3	700	63
4%-P	30	4	4	700	62
Cat-Ni Samples					
0%-Ni	30	-	2	700	68
1%-Ni	30	1	2	700	67
2%-Ni	30	2	2	700	66
4%-Ni*	30	4	2	700	64
6%-Ni	30	6	2	700	62
Cat-W Samples					
15%-W	15	4	2	700	79
20%-W	25	4	2	700	69
30%-W*	30	4	2	700	64
40%-W	40	4	2	700	54
Cat-T_N Samples					
500°-T_N	30	4	2	500	64
600°-T_N	30	4	2	600	64
700°-T_N	30	4	2	700	64
800°-T_N	30	4	2	800	64
900°-T_N	30	4	2	900	64

* Catalyst is common to all sets.

2002; Hada et al., 2002). Nitriding process is normally performed outside hydrotreating reactors due to high operating temperatures which are beyond the thermal capacities of most laboratory hydrotreating reactors. However, nitride catalysts are pyrophoric (react when exposed to air) hence, freshly prepared nitride catalysts must be passivated before exposure to air (Yuhong et al., 2001).

In this work Ni-W(P)/γ-Al_2O_3 nitride catalyst was synthesized from TPr of oxide precursors with ammonia as synthesis gas. The process consisted of loading 8 g of the oxide precursor in an inconel reactor (inner diameters 22 mm, outside diameter 25 mm, and a length of 870 mm) heated in a temperature-controlled furnace (see Figure A.5 for temperature and flow calibration results). The reaction involved a five-step process:

1. Temperature was increased at a rate of 1 °C /min from ambient temperature to 400 °C in a stream of helium flowing at a rate of 350 ml/min.
2. Ammonia gas was introduced at 400 °C at a rate of 200 ml/min while the temperature was increased further from 400 °C to the nitriding temperature (T_N) at a rate of 0.5 °C/min. The rate of increase in temperature was reduced (from 1.0 to 0.5 °C /min) in this stage to ensure a carefully controlled temperature ramp so as to avoid catalyst sintering and drastic decrease in the catalyst surface area (Wise and Markel, 1994).
3. The temperature was then held constant for 5 h to ensure complete reaction under ammonia flow.
4. After the 5 hour period, the reaction was quenched to room temperature under helium flow at 350 ml/min by disengaging the reactor from the furnace system.
5. In order to prevent reaction of the fresh catalyst with air on exposure, the surface was passivated under 1 vol % oxygen/helium flow for 4 h at ambient temperature before transferring to the hydrotreater for pretreatment and activity test.

3.1.4 Sulfide Catalyst Synthesis

The precursor for the sulfide catalyst was also an oxide catalyst except for the sulfided nitride catalyst where the precursor was a nitride catalyst. Sulfidation was performed over two days at 9.0 MPa, LHSV of 1 h^{-1}, hydrogen-to-oil ratio of 600 ml/ml and temperatures of 193 °C on day 1 and 243 °C on day two. Prior to introducing hydrogen, the catalyst bed was adequately wetted with the sulfiding solution (3 vol% butanethiol mixture in straight run gas oil) at 100 °C

and a helium flow of 50 ml/ml. This was to prevent the oxide catalyst from direct contact with hydrogen gas at high temperature as that may reduce the oxide catalyst. Once the catalyst bed was wetted, the gas flow was switched to hydrogen and the temperature increased at a rate of 10 °C/min to 193 °C. Sulfidation was performed for 24 h at 193 °C after which the temperature was increased to 243 °C for another 24 h. This was done to allow sufficient time for H_2S or sulfur breakthrough.

3.2 Catalyst Characterization

Characterization techniques employed in this study include N_2 sorption analyses (BET surface area, pore volume and pore diameter analyses), O_2 chemisorption, elemental analysis, TPO, TPD, TPR, XRD, SEM, energy dispersive x-ray spectroscopy (EDX), infrared spectroscopy (IR), transmission electron microscopy (TEM) and x-ray absorption near edge structure (XANES). All flow rates given here and in subsequent discussions are at standard temperature and pressure (STP).

3.2.1 Surface Area, Pore Diameter and Pore Volume Analyses

N_2 sorption analyses were performed in a Micromeritics ASAP 2000 instrument at -195 °C and vacuum pressure of 20 µmHg. Prior to analyses, the nitride catalyst sample (0.25 g) was degassed at 200 °C. N_2 sorption studies were done to determine the pore size distribution of the catalysts and to determine the available surface area for reaction. The method is commonly used to investigate properties of catalysts (Chu et al., 1999; Ozkan et al., 1997; Kojima and Aika, 2001). The catalyst pores must be large enough so as not to inhibit diffusion of reacting molecules to the active sites of the catalyst.

3.2.2 Catalyst Nitrogen and Sulfur Analyses

Catalyst nitrogen and sulfur contents were analyzed in an Elementar, Vario EL III analyzer to determine changes in the catalyst composition for the fresh and spent catalysts. The sample was wrapped in an aluminum foil and combusted in the analyzer. Any carbon, nitrogen or sulfur present was measured as CO_2, NO_2 and SO_2, respectively.

3.2.3 Temperature Programmed Techniques

TPD and TPR were carried out in a ChemBet 3000 instrument from ambient temperature to about 950 °C at 10 °C/min. In the TPD experiments, 0.25 g of the nitride catalyst sample, with pre-adsorbed NH_3, was heated in argon at 30 cm^3/min. A few selected samples were pre-reduced at 400 °C in 3 vol% H_2/N_2 gas (30 cm^3/min), followed by re-adsorption of NH_3 (0.1 vol% NH_3/N_2 gas) at ambient temperature for 30 min. In the TPR experiments, 0.25 g of sample was pretreated at 200 °C in argon (30 cm^3/min) for 1 hr and then cooled to ambient temperature. The reduction was done in 3 vol% H_2/N_2 gas at 30 cm^3/min. These techniques were critical to the thesis because they provide information on catalyst acidity and the presence of species that may be reduced during hydrotreating as hydrotreating is a hydrogenation reaction. Acidic sites do influence HDS and HDN activity and can also cause cracking of reacting petroleum molecules (Kwak et al., 1999; Sundaramurthy et al, 2008).

3.2.4 Temperature Programmed Oxidation (TPO)

TPO experiments were performed in a Pyris Diamond TG/DTA instrument (PerkinElmer) from 25 to 600 °C. About 30 mg of sample was heated at 10 °C/min in air (30 cm^3/min) and the change in weight measured. TPO was a means of determining how stable the catalyst was after exposure to air. Nitrides are known to react with air on exposure if not passivated with low concentration of oxygen gas.

3.2.5 X-ray Diffraction (XRD) Analyses

X-ray diffraction patterns were recorded in the 10 to 100 ° angle range in a Rotaflex RU-200 rotating anode x-ray diffractometer (Rigaku) using Cu Kα radiation (λ = 1.5405Å). A few milligrams of powdered nitride sample was mixed with methanol (to help the sample stick to the holder) and dried after which diffraction analysis was made. This work was done to determine the crystalline phases in the catalyst. By comparing the hydrotreating activity to the XRD results, it is possible to correlate the species on the catalyst surface to the activity.

3.2.6 Scanning Electron Microscopy (SEM)

SEM analysis was performed in an SEM-505 (Philips) instrument. Nitride catalyst samples were carbon-coated at 1 KV and 14 mA for 4 mins followed by sample analyses at 20 KV

and a magnification of 10,000. Information obtainable from SEM includes morphology of the catalyst and particle sizes. A catalyst with well dispersed metal particles often has high HDS and HDN activities. With such information, catalyst preparatory conditions can be adjusted to prevent particle agglomeration and to give better activity.

3.2.7 Transmission Electron Microscopy (TEM)

For transmission electron microscopy experiments, a small amount of the catalyst sample was ground and mixed with methanol to form slurry. A drop of the pre-ultrasonicated slurry was placed on carbon-coated nickel grid and experiments performed in a Hitachi H-7500 instrument at 100 kV. TEM can determine structure and size of active sites. Both structure and size of active sites are of importance during hydrotreating reaction. Small particle sizes and structures are often not accessible to large reacting molecules such as 4,6-dibenzothiophene due to steric hindrances and often reduce the overall activity.

3.2.8 Infrared Spectroscopy (IR)

Infrared spectroscopy was performed using a PerkinElmer Spectrum GX instrument equipped with DTGS detector and a KBr beam splitter. Pelletized samples were scanned 64 times at a resolution of 4 cm^{-1} in the region 400 to 4000 cm^{-1}. Infrared spectroscopy can be used to identify the type of molecules on a catalyst surface. Such information is useful and can be correlated to a catalyst's activity. IR can also be used to determine the types of acid sites present on a catalyst's surface.

3.2.9 X-ray Absorption near Edge Structure (XANES)

X-ray absorption near edge structure (XANES) studies were carried out in variable line spacing plane grating monochromator (VLS PGM) beamline at Canadian Light Source. Powder samples were pressed into a stainless steel holder and the spectra recorded near the L-edge of P between 130 and 155 eV with a step size of 0.1 eV. XANES is useful in that it enables one to identify the oxidation states and species present on the catalyst surface. This helps to correlate the catalyst activity to the catalyst surface properties.

3.3 Hydrotreating Experimental Setup and Activity Studies

The experimental setup included a 304 stainless steel, tubular, micro reactor and twin-furnace system (Vinci Technologies) with inner diameter of 10 mm and length of 285 mm, an Eldex metering pump, mass flow controller (Brooks Instrument) for the gas flow and temperature controller (Eurotherm Controls, model No. 2216e) to control the furnace temperature. A schematic diagram of the experimental set up for activity studies is shown in Figure 3.3. Prior to the hydrotreating runs, reactor preparations and catalyst pretreatment were performed which included reactor loading, reactor pressure testing, catalyst passive layer reduction for nitride catalysts and sulfidation for sulfide catalysts and catalyst activity stabilization.

3.3.1 Reactor Loading

The reactor loading process was preceded by thorough cleaning of the hydrotreating reactor with straight run gas oil to wash out residual gas oil from the reactor so as to prevent possible coke formation during catalyst pretreatment and hydrotreating processes. The lower end of the reactor was covered with 60 micron Swagelok, stainless steel ferule to hold the catalyst in place and then closed tight after applying Loctite nickel anti-seize gel around the threads. The reactor was then vertically suspended on a clamp for the catalyst loading process.

A complete catalyst loading comprised three main sections: the catalyst bed and two other sections of various sizes of silicon carbide (Ritchey Supply Ltd.) and glass beads (Fisher Scientific) above and below the catalyst bed. The catalyst bed length at each loading was maintained at approximately 10 cm in height in order to occupy the section of the reactor furnace with steady heating (see Figure A.1 for results of the temperature controller calibration). The bed consisted of 2.5 g of catalysts, loaded sequential but alternating with approximately 12 ml of 90 mesh silicon carbide particles. The silicon carbide particles were added to prevent channelling of fluids during hydrotreating and also to enhance liquid hold-up and catalyst wetting. Various particle sizes were loaded to increase liquid hold-up and to ensure reactants reach the reaction temperature prior to contacting the catalysts. Earlier studies on this particular reactor with such loading have led to the establishment of near trickle flow in the catalyst bed (Bej et al., 2001). Particles used in the loading were 16, 46 and 60 mesh silicon carbide particles, and 3 mm diameter glass beads. See a schematic diagram of a typical loaded reactor in Figure 3.4. The loading of the particles was done with intermittent vibration to ensure compact packing. Similar to the

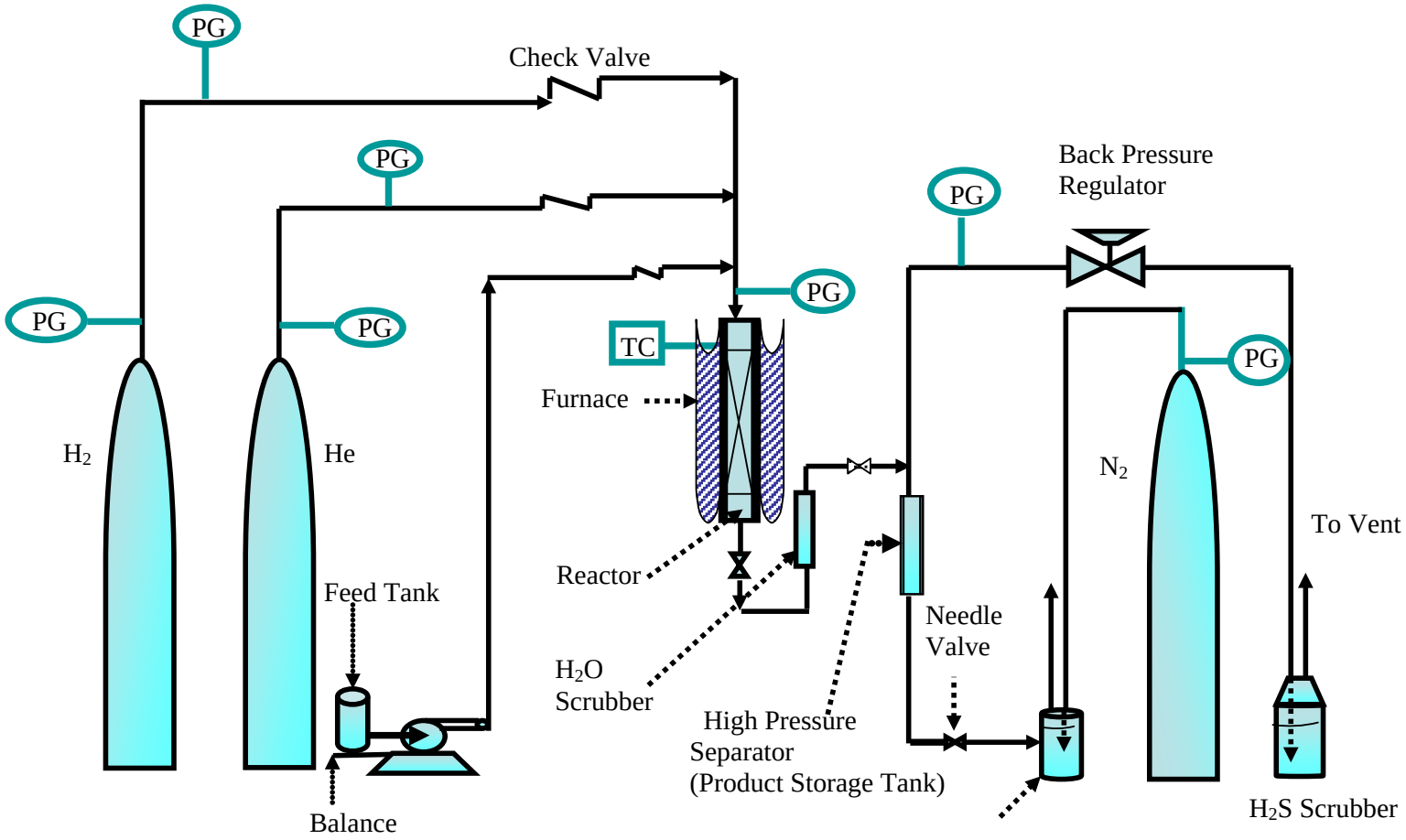

Figure 3.3: Schematic Diagram of Experimental Setup (TC: Temperature Controller, PG: Pressure gauge).

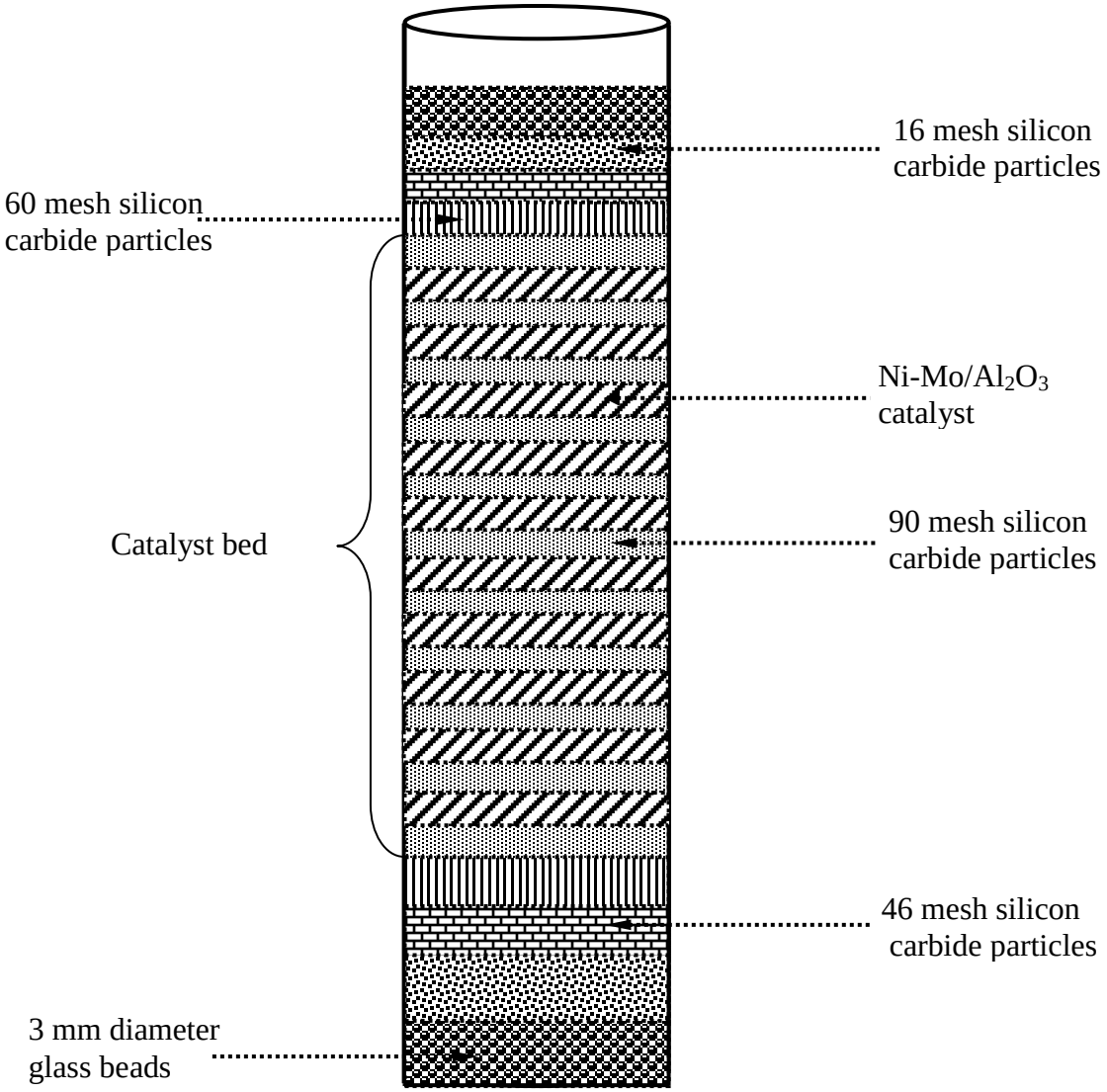

Figure 3.4: Schematic diagram of a loaded micro-reactor prior to hydrotreating.

lower end of the reactor, a 60 micron Swagelok, stainless steel ferule was placed at the top end of the reactor and closed after applying Loctite nickel anti-seize gel.

The oxide catalysts were dried at 200 °C for three hours in an oven and cooled in a desiccator prior to loading to remove adsorbed moisture. The nitride catalysts didn't need any such preheating because any adsorbed moisture was desorbed in the nitride catalyst activation process (see Section 3.3.3.1).

3.3.2 Reactor Pressure Testing

The reactor system and fittings were tested for leaks at pressures above the planned operating pressures to forestall any pressure leaks during the hydrotreating reactions. This is because pressure leaks would lead to errors in mass balances on the reactor as well as liquid hourly space velocity calculations.

About 50 ml of distilled water was pumped into the scrubber (see Figure 3.3) before pressurizing the system. The intent was to ensure any ammonium salts formed during denitrogenation reaction is absorbed to prevent blockage of downstream lines. The lines and reactor were pressurised in stages. This was achieved by letting in helium gas at very slow rates and simultaneously adjusting the back pressure regulator to stop the outflow of helium gas. Adjustment of the back pressure regulator continued until the required test pressure was reached then the helium valve was closed. The test pressure was always at least 0.7 MPa higher than the planned operating pressure.

A quick test was performed for major leaks by checking for drop in the pressure gauge within 10 min. Leaky fittings were identified with Swagelok liquid leak detector (Snoop solution) and tightened. Test for small leaks were performed by isolating portions of the reactor system having pressure gauges. Finally, the reactor was left to stand at the test pressure for a period of 12 h, with sections isolated. Any drop in pressure by way of leaks had to be fixed before the experiment could begin. Once the system had passed the test, the backpressure regulator was slowly released to reduce the system pressure to the planned operating pressure for catalyst pretreatment to begin.

3.3.3 Catalyst Pretreatment

Catalyst pretreatment consisted of catalyst activation process followed by stabilization of the initial activity. Prior to hydrotreating reaction, it was necessary to activate the catalysts in order to obtain the maximum possible activity. Two different activation processes were used; passive layer reduction for nitride catalyst and sulfidation for sulfide catalysts (see Section 3.1.4 for sulfidation process). The initial catalyst activity obtained after the activation process needed to be stabilized for consistent and steady results. The process employed for activity stabilization is referred to as precoking.

3.3.3.1 Passive layer Reduction

The passive layer reduction is an important step that removes the passive oxygen layer from the nitride catalyst surface and restores the original catalyst activity. It was stated in Section 3.1.3 that freshly prepared nitride catalysts had to be passivated to prevent bulk oxidation during transfer from the nitriding reactor to the hydrotreating reactor. After the reactor system pressure test, the pressure was reduced to atmospheric and the gas switched to hydrogen flow at 50 cm^3/min. The reactor temperature was increased to 350 °C at 10 °C/min and run for 3 h. Temperatures reported in the literature include 400 and 500 °C (Colling et al., 1996; Chu et al., 1999; Nagai et al., 2000a; Ozkan et al., 1997). After the activation process, the hydrogen flow was shut off and the reactor temperature reduced to 100 °C. Gas oil feed was then pumped at a high rate (25 ml/hr) to wet the catalyst bed. The wetted bed was then pressurized to 8.8 MPa to start the activity stabilization work.

3.3.4 Catalyst Activity Stabilization

The initial catalyst activity after activation was unstable and had to be stabilized prior to activity test (Speight, 2000) to ensure uniform catalyst activity across the catalyst surface. The stabilization process was carried out by running light gas oil (the feed for the hydrotreating studies) for a period of five days at 375 °C, 8.8 MPa, LHSV of 1 h^{-1} and hydrogen/oil ratio of 600 ml/ml. Products were withdrawn after every 24 h, stripped of hydrogen sulfide and analyzed for sulfur and nitrogen content. Activity test runs were performed once the catalyst activity was stabilized.

3.3.5 Catalyst Activity Test Runs

3.3.5.1 Reactor Operation

The feed used for the experimental work was bitumen-derived light gas oil (LGO) obtained from Athabasca and produced by Syncrude Canada. Table 3.3 shows properties of the gas oil feed. Temperature of the furnace was measured with a K-type stainless steel thermocouple inserted at the side of the furnace. Average temperature of the catalyst bed within the reactor was considered the operating temperature and this was obtained from calibration curves (see Appendix A.1 for the temperature calibration procedure and results). The reactor was operated in a down-flow concurrent mode with the flow of hydrogen controlled by a flow meter and mass flow controller (Brooks Instrument). See Figure A.3 for the hydrogen flow calibration curve.

The light gas oil feed was pumped down the reactor by a high pressure metering pump (Eldex Laboratories, Inc.; calibration curve can be found in Figure A.4). The flow was monitored continuously to forestall any fluctuations that may affect the results. The reactor design ensured a mixture of the feed and hydrogen gas before entering the reactor. Once in the reactor, the silicon carbide packing above the catalyst bed enable preheat and distribution of the mixture before contacting the catalyst bed. Any ammonia or ammonium sulfide produced from the reaction was absorbed in a 50 ml, 316 stainless steel scrubber filled with deionized water in order to prevent blockage of the downstream lines and connection joints (Landau et al., 1997). The water was replaced every other day to prevent contamination of products. The reaction products (a mixture of gas and liquid) were separated using a high-pressure separator. Hydrogen sulfide in the exit gas was absorbed in a sodium hydroxide solution and the liquid product collected in a product storage tank.

3.3.5.2 Product Sample Collection

The experiments were conducted at steady state, i.e. samples were withdrawn for analyses only after the process had reached steady state. To ensure only steady state samples were used for analyses, a transient period of at least 12 h was allowed after a change in process conditions. Samples taken within the initial 12 h were not analyzed.

The liquid sample products were collected every 12 h (24 h for LHSV of 1 h^{-1}) for 3 days. The second and the third day samples were the only ones used for analyses after they had been stripped (Section 3.3.5.4) of any trapped gases. The sample withdrawal was preceded by

Table 3.3: Properties of Light Gas Oil feed used for the experimental work.

Property	
Boiling Range (°C)	170-458
Density (g/cc)	0.89
Sulfur (wt%)	1.6
Nitrogen (ppm)	230
Aromatic Content (wt%)	32.7
Mono-	20.1
Di-	9.7
Poly-	2.9

stoppage of all flows and closure of downstream valves (reactor isolation) to prevent reactants and scrubber water from flowing into the product tank. One end of the sample tank was connected to the product storage tank (high pressure separator) and the other connected to a stock of sodium hydroxide solution to absorb any escaping hydrogen sulfide gas. Samples were withdrawn under pressure which resulted in decreased downstream line pressure. To keep the reactor system pressure from falling, the downstream line was backfilled with helium to the system pressure prior to restarting the run. The collected product was then transferred into sample bottles for stripping and analyses. At the end of each run, the reactor was shut down and prepared for the next run as described below.

3.3.5.3 Shut-Down Procedures

In the reactor shut down process, the pump and hydrogen flows were stopped. The reactor temperature was reduced to room temperature followed by reduction in reactor hydrogen pressure to zero. The reactor and pipelines were flushed with helium gas for five minutes after which the reactor was disengaged from the system and transferred into a glove box. Spent catalyst in the reactor was separated from the wet, inert material (SiC, glass beads and oil residue) and stored in a glove box (in argon atmosphere) to minimize exposure to air. The reactor was reconnected to the set up to enable the lines to be cleaned. After pumping 200 ml of straight run gas oil through the system and flushing with more helium, the reactor was again disengaged and cleaned for the next run's catalyst loading.

3.3.5.4 Sample Stripping and Analyses

The product was stripped of any trapped hydrogen sulfide gas to ensure no interference with sulfur content analyses. This was achieved by bubbling a steady flow of nitrogen gas at a pressure of 0.1 MPa through the product for at least 2 h (Ma et al., 1994b). The hydrogen sulfide-free product sample was then wrapped in cellophane wrapper to prevent contact with air and stored in a cold environment to prevent any further reaction prior to analyses.

Analyses were performed for both feed and product samples for sulfur, nitrogen and aromatic contents. Sulfur and total nitrogen analyses were done by combustion/fluorescence and combustion/chemiluminescence techniques, respectively, in an Antek 9000 NS analyzer (summary of the analytical procedure can be found in Appendix E). Aromatic content was determined by ^{13}C NMR spectroscopy using 500 MHz Bruker Avance NMR Spectrometer.

CHAPTER 4
CATALYST CHARACTERIZATION

The catalysts were characterized to study properties of the catalysts and how the properties are influenced by catalyst synthesis properties. In most cases, the characterization results were compared to those of reference samples (γ-Al_2O_3 support, and nitrides and oxides of W/γ-Al_2O_3 and Ni/γ-Al_2O_3) to determine changes in the properties as synthesis parameter levels were varied.

4.1 N_2 Sorption Studies

N_2 sorption studies were done to study the effect of the syntheses parameters on BET surface area, pore volume and pore diameter of Ni-W(P)/γ-Al_2O_3 catalysts. Experiments were performed for the various catalysts synthesized i.e. Cat-W, Cat-Ni, Cat-P and Cat-T_N. Observed results followed a similar pattern and are shown in Table 4.1. For better comparison, the surface area and pore volume were standardized to a unit weight of Al_2O_3. It should be noted that the oxide catalysts for the Cat-T_N samples came from the same batch that is why their surface areas, pore volumes and pore diameters are the same.

A surface area of 195 m^2/g was obtained for the γ-Al_2O_3 support which virtually did not change even after treating it with NH_3 at 700 °C. The error margin in surface area analyses was ±3.5%. There was not much difference in the pore volumes and diameters of the alumina samples (both NH_3-treated and untreated) suggesting that the high temperature NH_3 treatment did not affect the structure of the support. A similar observation was made for the W/γ-Al_2O_3 nitride samples as the surface area, pore volume and pore diameter of the nitride did not vary from the oxide. This suggests that the nitriding process did not cause any loss of W metals (volatilization) nor did it result in structural changes or migration of particles to cause agglomeration. In the case of the Ni/γ-Al_2O_3 (10 wt% Ni) oxide and nitride samples, the surface area decreased from 199 to 170 m^2/g while the pore diameter increased from 99 to 120 Å. The pore volume however remained the same. The results suggest that particle migration might have led to agglomeration and plugging of micropores causing an increase in average pore diameter and a decrease in surface area.

Generally, the surface areas (49.2%), pore volumes (32.7%) and pore diameters (15.0%)

Table 4.1: BET surface area, pore volume and pore diameter of Ni-W(P)/γ-Al_2O_3 nitride catalyst.

Catalyst Name	Surface Area (m^2/g Al_2O_3)		Pore Volume (cm^3/g Al_2O_3)		Pore Diameter (Å)	
	Oxide	Nitride	Oxide	Nitride	Oxide	Nitride
γ-Al_2O_3	195	193	0.55	0.55	111	113
W/γ-Al_2O_3	181	181	0.48	0.48	107	106
Ni/γ-Al_2O_3	199	170	0.49	0.51	99	120
			Cat-P			
0%-P	176	181	0.44	0.46	100	102
1%-P	166	174	0.39	0.47	94	109
2%-P	152	166	0.36	0.44	96	106
3%-P	149	163	0.36	0.45	97	110
4%-P	141	136	0.32	0.37	92	107
			Cat-Ni			
0%-Ni	154	159	0.39	0.45	102	114
1%-Ni	168	164	0.40	0.45	101	114
2%-Ni	163	165	0.41	0.44	100	107
4%-Ni	152	166	0.36	0.44	96	106
6%-Ni	174	167	0.36	0.45	87	108
			Cat-W			
15%-W	189	192	0.47	0.54	107	111
25%-W	165	172	0.42	0.46	101	106
30%-W	152	166	0.36	0.44	96	106
40%-W	131	149	0.30	0.42	92	111
			Cat-T_N			
500º-T_N	159	181	0.38	0.43	95	96
600º-T_N	159	172	0.38	0.46	95	107
700º-T_N	159	166	0.38	0.44	95	106
800º-T_N	159	149	0.38	0.44	95	118
900º-T_N	159	98	0.38	0.46	95	154

Error margin: surface area (± 3.5), pore volume (± 0.02), pore diameter (± 4.2).

deviated from those of the γ-Al_2O_3 support as metals were introduced and T_N changed. Addition of W to γ-Al_2O_3 (W/γ-Al_2O_3) caused a decrease of 6.4 % in both the surface area and pore diameter, and 12.3 % in the pore volume. With the addition of Ni (4 wt%) to the W/γ-Al_2O_3 sample (N-W/γ-Al_2O_3), no significant change was observed in the surface area with minor reductions observed in the pore volume (3.6 %) and pore diameter (3.9 %). This indicates that the Ni particles preferentially plugged the micropores but the effect on surface area was insignificant compared to that of W on γ-Al_2O_3. Addition of P to the N-W/γ-Al_2O_3 sample (N-W(P)/γ-Al_2O_3) caused a major decrease in the surface area (8.6 %), a moderate decrease in the pore volume (4.3) and a moderate increase in pore diameter (4.7). Addition of P might have decreased the metal-support interactions which caused migration of metal particles unto the surface of the catalyst. In summary, addition of Ni to the catalyst did not impact the textual properties of the catalyst. It should be noted that addition of P seems to have more effect on the catalyst textual properties than Ni. This might be because P modifies the structure of the alumina support. W had the most effect on the surface area of the catalysts.

4.1.1 Surface Area, Pore Volume and Pore Diameter of Cat-P Nitrides

At 0 wt% P loading (i.e. 0%-P or Ni-W/γ-Al_2O_3), deviations of surface area, pore volume and pore diameter from γ-Al_2O_3 were 6, 16 and 10 %, respectively. The surface area and pore volume continued to decrease as P was introduced to the catalyst. At the maximum P loading (4 wt%), the decrease in surface area and pore volume were 25 and 20 %, respectively, of the 0%-P sample. The pore diameter did not follow any specific trend with the introduction of P. Factors that generally affected surface area and pore volume reduction include agglomeration and sintering. Sintering is known to be caused by excessive temperature. Since the nitriding temperature is constant in this study, sintering cannot be the cause of the decreased properties with P loading. P addition is not expected to cause agglomeration of particles. This is because P is known to enhance dispersion of particles on the catalyst surface (Sundaramurthy et al., 2008; Eijsbouts et al, 1991a). SEM results (see Section 4.6) did not give any indication of sintering or agglomeration of the catalyst surface. The reduction in surface area and pore volume may therefore be due to the reduction in metal-support interaction and subsequent migration of particles unto the surface of the catalyst and pores.

4.1.2 Surface Area, Pore Volume and Pore Diameter of Cat-Ni Nitrides

At 0 wt% Ni loading, (i.e. 0%-Ni or W(P)/γ-Al_2O_3), the surface area (18 %) and pore volume (16 %) deviated from those of γ-Al_2O_3 with no significant change in the pore diameter. Ni loading at 1 wt% saw a minor change (3.5 % increase) in the surface area with no increase in the pore diameter nor pore volume. The small change, which is within the margin of error, can be attributed to particles of Ni plugging the small pores of the support (Kim et al., 1996). The small change can be attributed to the small amount of Ni used. As Ni loading increased, the surface area continued to increase while the pore diameter decreased but no major change was observed in the pore volume. The maximum changes observed were 5 % increase and 7 % decrease in surface area and pore diameter, respectively, at 6 wt% Ni loading (6%-Ni). The nitriding process (from oxide to nitride) did not show any trend in the surface area. However, it was clear that the pore diameters and volumes increased from the oxide state to the nitride state, a trend also observed by Neylon et al. (1999). The observation is confirmed by results of analysis of variance at 95% confidence. This suggests that the nitriding process caused structural changes in the catalyst. Although there was an observed trend in the surface area and pore diameter with increase in Ni loading, analysis of variance results showed that the increases were not significant.

4.1.3 Surface Area, Pore Volume and Pore Diameter of Cat-W Nitrides

BET surface area, pore volume and pore diameter results of catalysts with varying W loading are also shown in Table 4.1 above. At 15 wt% W loading, there was not much deviation (0.5%) in surface area from the γ-Al_2O_3 support. Similarly, there was no significant change in the pore volume (1.8%) and diameter (1.8%). As W loading increased, the surface area decreased. At 40 wt% W loading, the surface area decreased by 23 %. This is due to the metal particles plugging the pores of the support. Similar observations have been reported in the literature (Nagai et al., 1998; Kim et al., 1996; Cruz et al., 2002). The pore volume decreased by 24 % at 40 wt% W loading; a confirmation that metal particles plugged the pores of the support. There was no major change in the pore diameter suggesting that the metal particles entered both micropores and mesopores.

4.1.4 Surface Area, Pore Volume and Pore Diameter of Cat-T_N Nitrides

Increase in T_N also had a negative impact on the surface area of the catalysts. From 500 to 900 ºC T_N, the surface area reduced by 45 %. The decrease might be due to formation of large particles resulting from agglomeration. There was no corresponding change in the pore volume, though. This was expected as the number of metal particles was the same for all the Cat-T_N samples. The pore diameter, however, increased with increase in nitriding temperature (by 60 % from 500 to 900 ºC T_N). This might be due to change in structure of the catalyst which leads to increase in average pore diameter and decrease in the surface area. These results are contrary to preliminary surface area studies done for the screening catalysts where the surface area increased with increasing T_N (see Appendix D1). The different trends may be due to the different synthesis conditions used (15 wt% W for the screening catalyst while that for the detailed characterization was 30 wt%. Calcination temperature was the same in both instances at 500 °C.

4.2 Temperature Programmed Desorption (TPD)

TPD was conducted to investigate acidic properties of the catalysts and to ascertain the behaviour of species on the surface of the catalysts. It was also done to investigate the thermal stability of the nitride catalysts. Acidic catalysts enhance C-N bond breakage which is desirable in hydro-treating reactions (Sundaramurthy et al., 2008; Girgis and Gates, 1991). In nitrogen-containing hydrocarbon compounds, the nitrogen atom has two lone pair of electrons available for donation in reactions. In the presence of Lewis acids, donation of the lone pair of electrons is enhanced which facilitates breaking of the C-N bond. The higher the peak temperature of the TPD signal, the stronger the catalyst acidity. Peaks that fall below 200 °C are considered weak acid and those above 500 °C, strong acids. Any peak between 200 and 500 °C is considered to be of intermediate acid strength (Hada et al., 2000; Ferdous et al., 2007). From the observed results (Figure 4.1 to Figure 4.3) the weak acid sites are likely to be within the range 20 – 300 °C and would be considered as such.

The results generally exhibited an intense peak followed by two peaks over the range of temperatures studied, except for the Cat-T_N samples. The observed peaks can be assigned to desorbed NH_3 and decomposition of metal nitrides as discussed below. Figure 4.1 shows NH_3 TPD results for Ni/γ-Al_2O_3 nitride, W/γ-Al_2O_3 nitride and γ-Al_2O_3 support. Low temperature peaks (a) were observed for all three samples which can be attributed to weakly acidic sites on

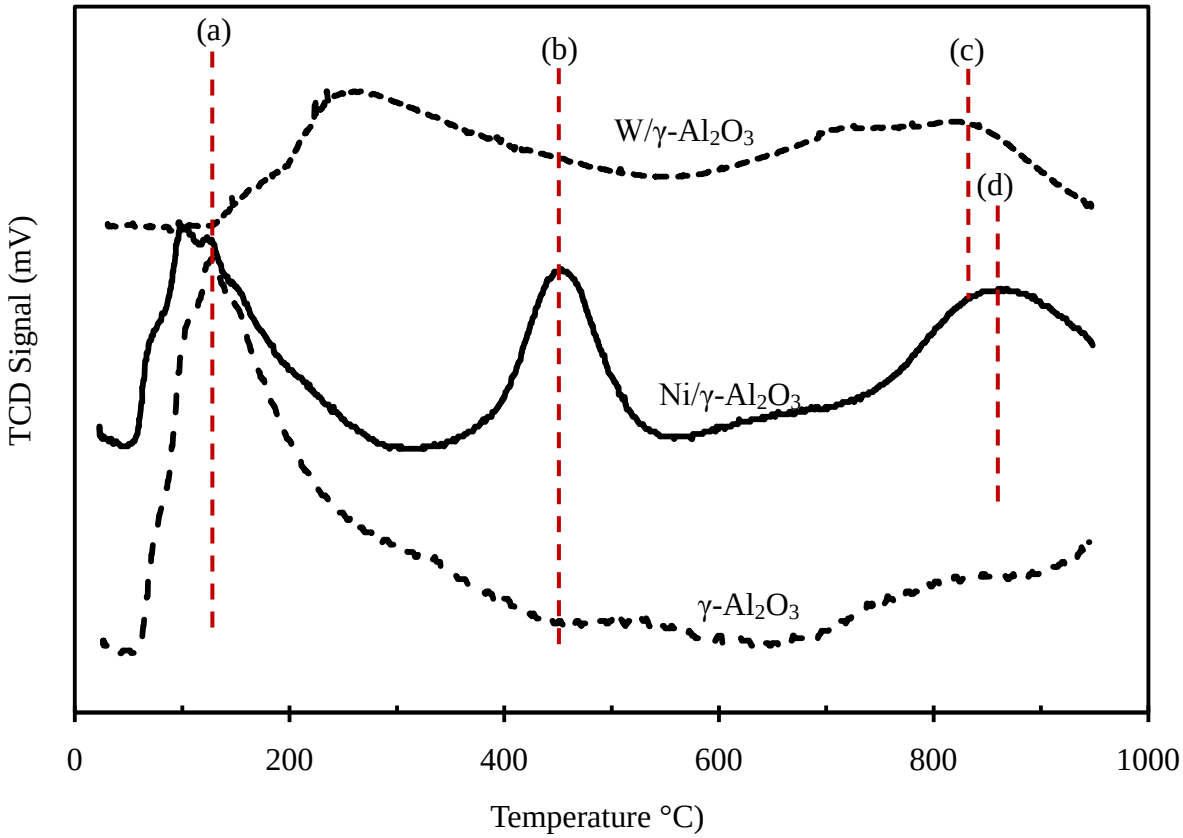

Figure 4.1: Temperature programmed desorption of NH_3 from reference nitride catalysts. Conditions: 30 wt% W, 10 wt% Ni, T_N of 700 °C and adsorption temperature of 30 °C.

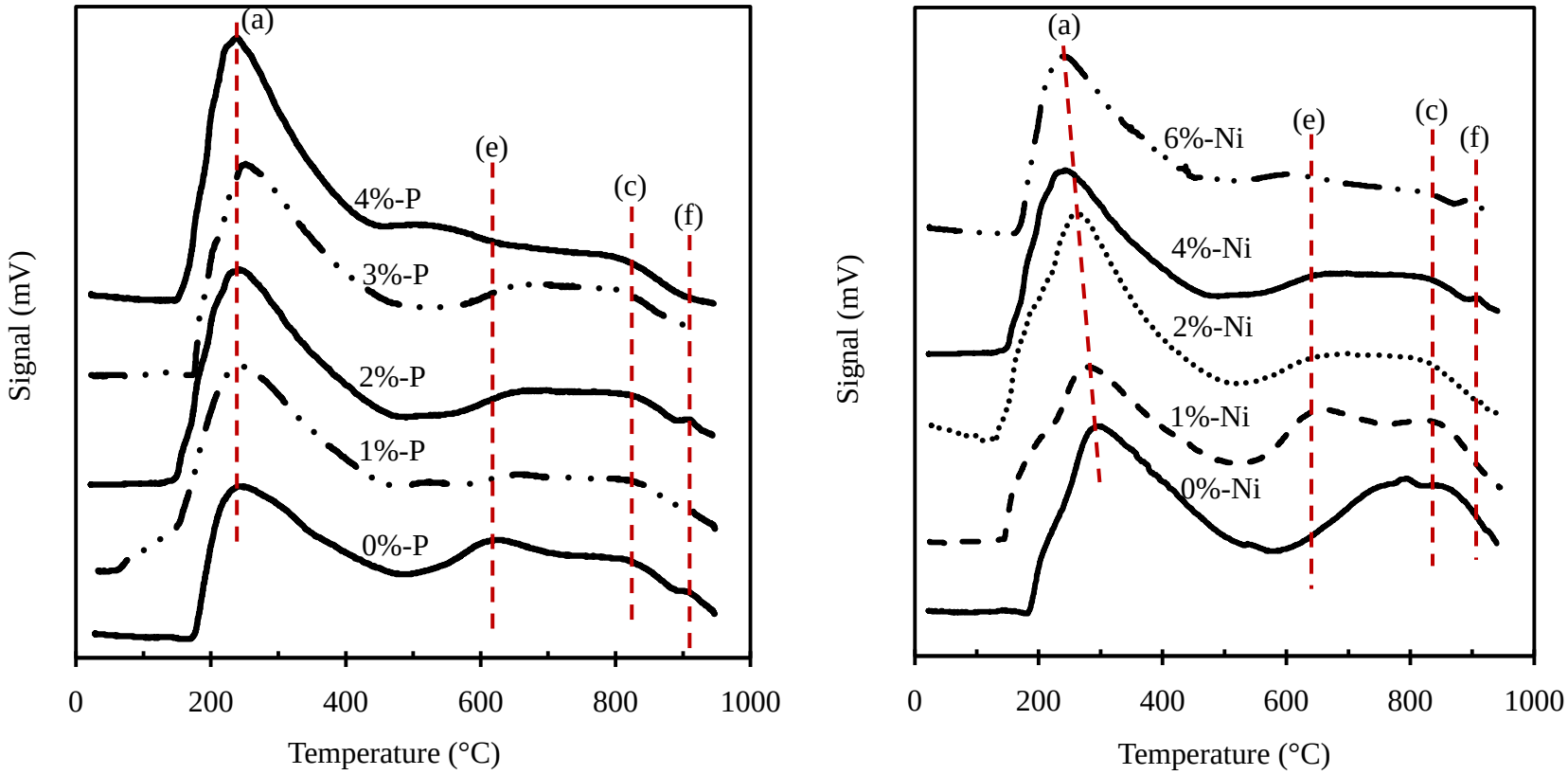

Figure 4.2: TPD profiles of NH_3 from (A) Cat-P and (B) Cat-Ni nitride samples. Conditions: 30 wt% W, T_N of 700 °C and adsorption temperature of 30 °C; (A) 4 wt% Ni; (B) 2 wt% P.

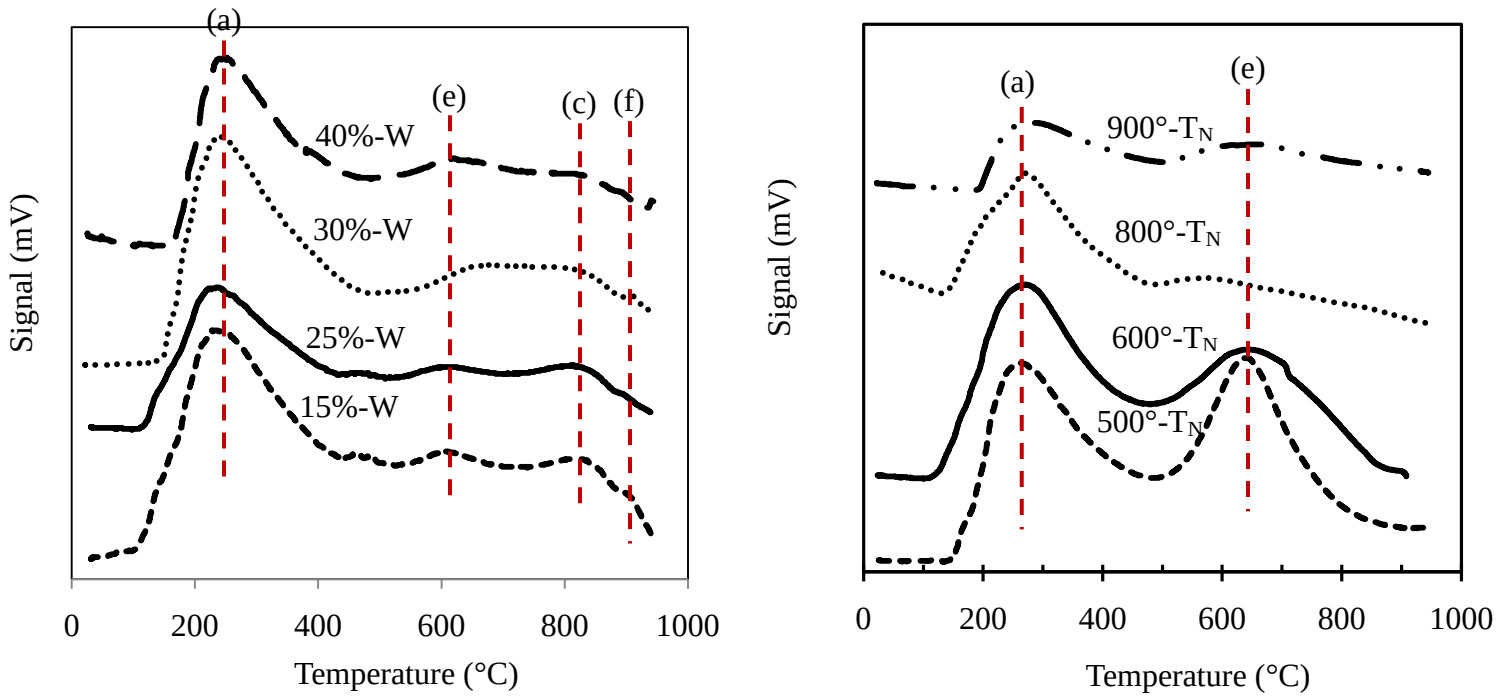

Figure 4.3: TPD profiles of (A) Cat-W and (B) Cat-T_N nitride samples. Conditions: 4 wt% Ni, 2 wt%, P and adsorption temperature of 30 °C; (A) T_N of 700 °C, (B) 30 wt% W.

the surface of the Al_2O_3 support. Peak (a) for W/γ-Al_2O_3 occurs at a higher temperature than that of the Ni/γ-Al_2O_3 suggesting that W influences the acid sites on γ-Al_2O_3 more than Ni. This might be due to the fact that the Lewis acid sites in W (empty 5d orbitals) are at higher energy than those in Ni (empty 3d orbitals). A medium temperature peak (b) is observed for Ni at 450 °C. This peak can be assigned to acid sites of intermediate strength on the catalyst surface. High temperature peaks are observed for both Ni (d) and W (c) nitrides. These peaks could be associated with the decomposition of nitride species as they were observed in the thermal analyses studies as well. They could also be associated with strongly adsorbed NH_3 species that decompose to give off N_2 gas (Shi et al., 2004).

4.2.1 Temperature Programmed Desorption of Cat-P Nitrides

Figure 4.2A shows the thermal desorption profiles of Cat-P samples with peaks labelled (a) to (f). Peaks (b) and (d) observed in the reference sample are not visible in the Cat-P samples. This may be because the amount of Ni (4 wt%) in the Cat-P samples is small compared to the reference Ni sample (10 wt%).

All catalysts studied exhibited weak acid sites, peak (a), due to the alumina support. The peak is attributed to desorption of weakly adsorbed NH_3 from the catalyst. The position of peak (a) did not change with P loading but the peak increased in intensity with increase in P loading suggesting that P increased the amount of weak acid sites on the catalyst surface (Herrera et al., 2005). Peak (e) was very broad and stretched from 400 (intermediate strength region) to about, 700 °C (strong acid region). Peak (e) was absent in γ-Al_2O_3 and W/γ-Al_2O_3 (see Figure 4 1) and may be attributed to desorption of NH_3 from coordinatively unsaturated sites or the release of nitrogen gas from decomposition of nickel nitrides. The observation is confirmed by literature reports (Colling et al., 1996; Nagai et al., 1998) that TPD of nitride species exhibits low and high temperature NH_3 peaks and nitrogen gas is released at such high temperatures (Nagai, 2007; Shi et al., 2004). Other authors (Colling et al., 1996; Perez-Romo et al., 2002) have reported that the nitrogen gas emanates from de-composition of desorbed ammonia gas into hydrogen and nitrogen at high temperatures. The two peaks above 800 °C, (c) and (f) were also absent in the γ-Al_2O_3 support but present in W/γ-Al_2O_3 (see Figure 4.1). These peaks can be assigned to decomposition of W_2N (Wei et al., 1997; Shi et al., 2004).

4.2.2 Temperature Programmed Desorption of Cat-Ni Nitrides

Figure 4.2B shows TPD profiles for Cat-Ni nitride catalyst. Similar to Figure 4.2A, TPD of Cat-Ni nitride samples exhibited four main peaks labelled (a), (c), (e) and (f). Peak (a) is assigned to the presence of weak acid sites on the catalyst. As Ni loading increased, the peak temperature shifted to lower temperature. This is an indication that as Ni loading increased the strength of the adsorbed NH_3 on the catalyst decreased. It was observed in Figure 4.1 that only W influences the weak acid sites on Al_2O_3. This means that Ni combines with available W to form N-W bimetallic species which reduces the amount of free W_2N available and hence, reduction in strength of adsorbed NH_3 on the catalyst surface. The peak intensity also decreased with Ni loading due to decrease in available W_2N on the catalyst surface. This means that increase in Ni loading decreased the amount of weak acid sites present on the catalyst surface. Peak (e) was not observed in the 0%-Ni sample but observed in all the other samples. The peak is assigned to strongly adsorbed NH_3 which may be related to the presence of bimetallic Ni-W species on the catalyst surface.

4.2.3 Temperature Programmed Desorption of Cat-W Nitrides

The thermal desorption profiles of Cat-W samples are shown in Figure 4.3A. All the profiles exhibited weak acid sites, strong acid sites and decomposition of metal nitrides. Peak (a) shifted to higher temperature with increase in W loading. This is because with increase in W loading, more W_2N species were formed. As seen in Figure 4.1 above, the strength of NH_3 adsorption on W/γ-Al_2O_3 is greater than that of NH_3 on γ-Al_2O_3, hence the shift in peak temperature. The peak intensity reduced with increase in W loading suggesting that increase in W loading reduces the weak acidity of the catalyst. Peak (e) which is associated with strong acid sites on the catalyst surface also shifts slightly to higher temperature with increase in W loading suggesting that W loading increases strong acid sites of the catalyst. Increase in W loading, however, did not affect the positions of peaks (c) and (f) as they are not directly related to adsorption of NH_3 on the catalyst surface.

4.2.4 Temperature Programmed Desorption of Cat-T_N Nitrides

The thermal desorption profiles for Cat-T_N samples are illustrated in Figure 4.3B. The intensity of peak (a) decreased with T_N indicating that the amount of adsorbed NH_3, which

corresponds to the number of weak acid sites, decreased with increase in T_N. Nagai et al. (2000a) also observed decrease in acidity of nitride catalysts with increase in T_N. The position of peak (a) shifted slightly to higher temperature with increase in the nitriding temperature. This means the strength of adsorbed NH_3 on the catalyst surface increases with nitriding temperature. Peak (e), occurring at 640 °C, is reported (Shi et al., 2004) to be due to decomposition of strongly adsorbed NH_x (x = 1-3) species on the catalyst surface to give N_2 and H_2. The peak intensity decreased with increase in T_N, meaning that the number of strong acid sites decreased with increase in T_N. It is possible that the 800 and 900 °C synthesis temperatures are so high that any NH_3 on the catalyst surface decomposes in the reaction process that is why no strongly adsorbed NH_3 was observed in the TPD studies.

In summary, TPD results show that P increases the amount of weak acid sites of nitride catalysts while increase in tungsten loading and nitriding temperature decrease the amount of weak acid sites. It should be noted that TPD measurements does not differentiate between Lewis and Bronsted acid sites. TPD measures total acid sites. The amount of strong acid sites also decreased with increase in nitriding temperature. Ni interacts with W thereby reducing the strength of weak acid sites. Metal nitrides decompose at temperatures above 800 °C to release N_2 gas.

4.3 Temperature Programmed Reduction (TPR)

Temperature programmed reduction was performed on the nitride samples to investigate the presence of reducible species on the surface of the catalyst. The surface species expected to be reduced during TPR included the oxygen passive layer and nitrides of Ni and W. It is reported (Yuhong et al., 2001) that reduction of the passive oxygen layer enhances the catalyst activity. Possible reduction equations are shown in Equations (4.1) to (4.3). It has been reported that the oxygen passive layer on the surface of the catalyst can be reduced at temperatures below 500 ˚C (Chu et al., 1999; Ozkan et al., 1997). To enable effective identification of peaks in the reduction profiles, TPR of reference catalysts were performed and the results are shown in Figure 4.4.

$$2Ni_3N + 3H_2 \rightarrow 6Ni + 2NH_3 \quad (4.1)$$

$$2W_2N + 3H_2 \rightarrow 4W + 2NH_3 \quad (4.2)$$

$$O_2 + 2H_2 \rightarrow 2H_2O \quad (4.3)$$

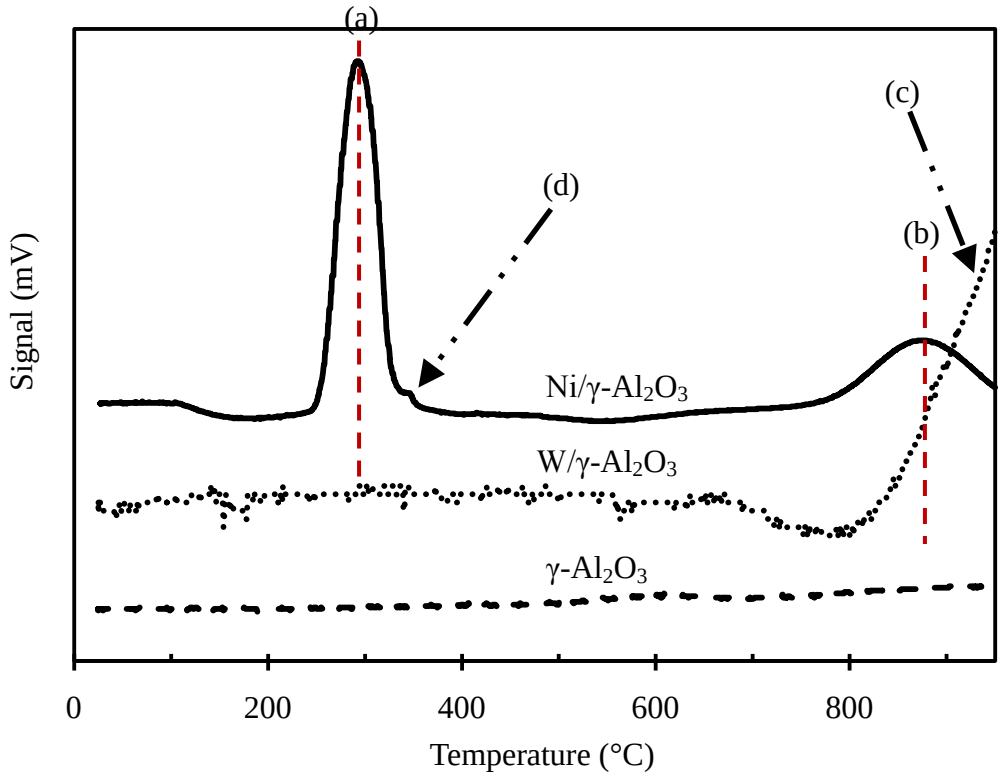

Figure 4.4: Temperature programmed reduction of reference nitride catalysts and γ-Al_2O_3. Conditions: 30 wt% W, 10 wt% Ni and T_N of 700 °C.

The TPR profile of Ni/γ-Al_2O_3 sample showed two main peaks; a lower temperature peak, (a) at about 300 °C and a higher temperature peak, (b), at about 875 °C. Peaks (a) and (b) were absent in the of W/γ-Al_2O_3 sample. The only peak present for W/γ-Al_2O_3 sample, peak (c), was incomplete because its maximum falls outside the range of temperatures studied. The γ-Al_2O_3 sample did not show any peak in its TPR profile. Peak (a) cannot be assigned to reduction of oxygen passive layer on the Ni/γ-Al_2O_3 catalyst as it was not observed in the TPR profile of the W/γ-Al_2O_3 sample. Based on the peak intensity and results of other studies (Figure 4.2B), peak (a) is assigned to reduction of Ni_3N species on the catalyst surface. The passive layer reduction may be the shoulder observed just after the Ni_3N reduction, peak (d). The oxide passive layer may not be stable at high temperatures on the surface of the W/γ-Al_2O_3 catalyst and may have desorbed in the degassing process prior to the reduction process as described in Section 3.2.3. Peak (b) is assigned to reduction of Ni metal to the hydride while peak (c) is associated with reduction of W_2N species.

4.3.1 Temperature Programmed Reduction of Cat-P Nitrides

Results of the TPR studies for Cat-P nitride samples are shown in Figure 4.5A. Three main reduction peaks, (a), (c) and (e), and a shoulder (b) were observed for the samples studied similar to the reference materials (see Figure 4.4). Peak (a) occurred below 400 °C for all samples but the position of the peak maximum temperature shifted to lower temperatures as P loading increased. Similarly, the peak intensity decreased with increase in P loading. Peak (a) is assigned to reduction of Ni_3N species on the catalyst surface. Literature (Eijsbouts et al, 1991a) shows that Ni tends to interact with Al_2O_3 to form $NiAl_2O_4$. As the P loading increased, P preferentially interacted with Al to form $AlPO_4$, thereby reducing the Ni-support interaction causing the formation of more readily reducible Ni_3N species. In catalysts containing both W and Ni, the Ni and W combine to form bimetallic $NiWO_4$ (precursor for bimetallic Ni-W nitride) which prevents the formation of free NiO (precursor for Ni_3N) (Eliche-Quesada et al., 2003). P is reported to promote the formation of $NiWO_4$ (Atanasova and Halachev, 1994). The decrease in peak intensity may therefore be due to formation of Ni-W bimetallic nitrides and reduction in free Ni_3N as P loading is increased.

Peak (c) which is a high temperature peak was observed above 700 °C. The peak was very intense but due to temperature limitations on the equipment, it could not be further

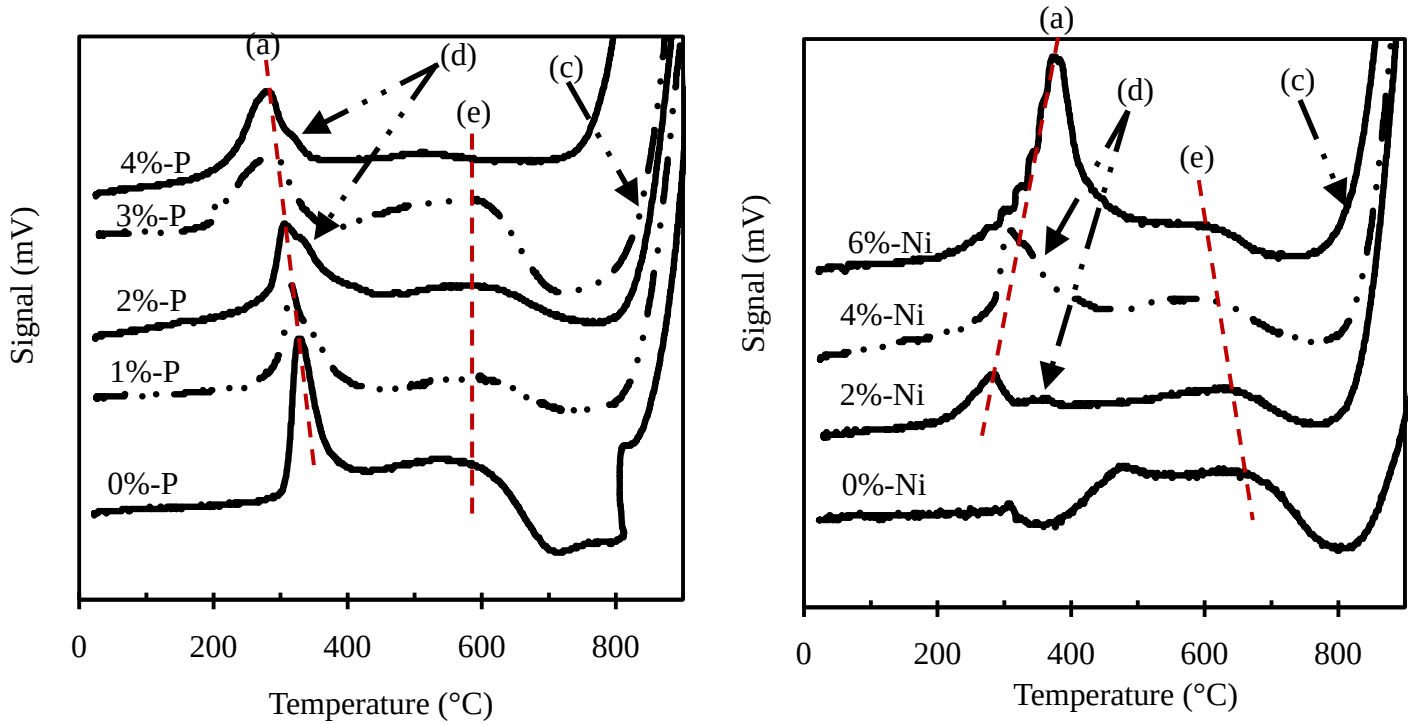

Figure 4.5: TPR profiles of (A) Cat-P and (B) Cat-Ni nitride samples. Conditions: 30 wt% W, T_N of 700 °C and (A) 4 wt% Ni; (B) 2 wt% P

explored. The peak was absent in the TPR profiles for Ni/γ-Al_2O_3 nitride and γ-Al_2O_3, meaning the peak could not be reduction of nickel nitride species. The peak must be reduction peak as it was not observed in the TPD studies (Section 4.2). The peak was observed in the TPD profile for W/γ-Al_2O_3 and in the profiles for all other catalysts, suggesting that the peak must be due to reduction of W_2N species on the surface of the catalyst. Shoulder (d) occurs during reduction of the Ni_3N species and is assigned to reduction of passive oxygen layer on the catalyst surface. Peak (e) is a broad peak with maximum at 600 °C. This peak is not present in any of the reference samples. It is similar to peak (e) in the temperature programmed desorption studies and may therefore be assigned to desorption of strongly adsorbed NH_3 on the catalyst surface (see Section 4.2).

4.3.2 Temperature Programmed Reduction of Cat-Ni Nitrides

Figure 4.5B shows results of the TPR studies for Cat-Ni nitride samples. Observed peaks were similar to those of the Cat-P samples with peak (a) maximum temperature falling below 400 °C. No peak (a) was observed in the 0%-Ni sample because it did not contain Ni_3N. As the Ni loading increased, the maximum peak temperature shifted to higher temperature. As Ni loading increased at constant P loading, the effect of P to reduce interaction of Ni with the support diminished. This made reduction more difficult, hence, the increase in the peak maximum temperature. The peak intensity increased with increase in Ni loading. This is because the increase in Ni loading promoted the formation of more NiN_3, hence, the increase in peak intensity. Peak (d) is a result of the reduction of passive oxygen layer on the catalyst surface. Figure 4.5B also shows an intense, broad, incomplete peak, (c), above 800 °C that can be assigned to reduction of W_2N species present on the surface of the catalyst. Peak (e), which is assigned to desorption of strongly adsorbed NH_3 from the catalyst surface, shifted to lower temperature with increase in Ni loading. This is because the addition of Ni promotes the formation of Ni-W bimetallic nitrides which reduces the effect of W on strongly adsorbed NH_3 on the catalyst.

4.3.3 Temperature Programmed Reduction of Cat-W Nitrides

Three peaks, labelled (a), (c), (e) and a shoulder (d) were observed for the profiles of the Cat-W nitride samples (see Figure 4.6A). Peak (a) occurred between 300 and 400 °C with (e) occurring at a higher temperature, ~ 600 °C. Peak (c) was observed at temperatures higher than

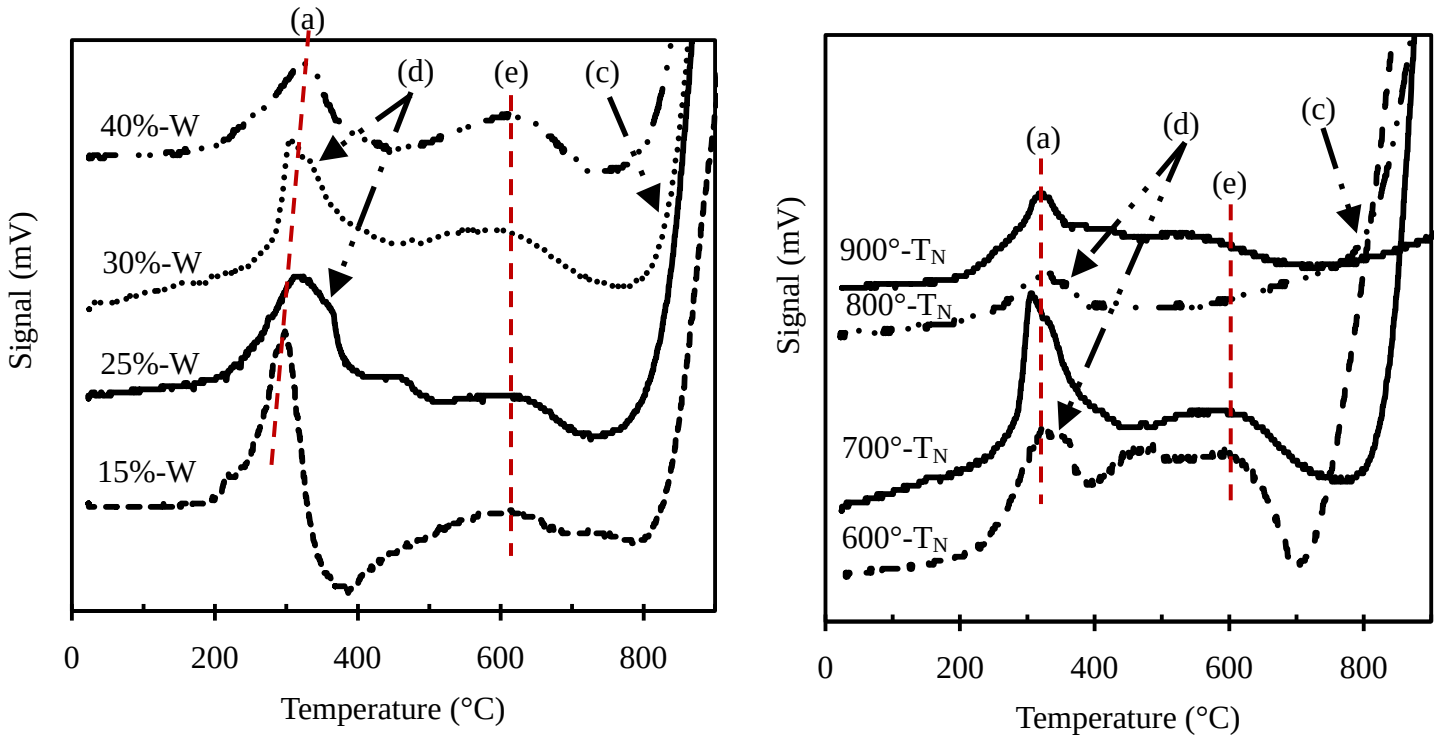

Figure 4.6: TPR profiles of (A) Cat-W and (B) Cat-T_N nitride samples. Conditions: 4 wt% Ni, 2 wt%, P (A) T_N of 700 °C and (B) 30 wt% W.

800 °C while shoulder (d) was observed between 350 and 400 °C. Peak (a) shifted slightly to higher temperature and reduced in intensity with increase in W loading. The peak shift to higher temperature is due to enhanced interaction between W metal and the Al_2O_3 support. As W loading increased at constant P loading, the effect of P to reduce interaction between W and the support diminished. This made reduction more difficult, hence, the increase in the peak maximum temperature. Reduction in peak intensity can be attributed to increased formation of bimetallic Ni-W nitride species with increase in W loading, reducing the amount of Ni_3N species available for reduction. As in previous discussions above, the high temperature peak, (c), can be attributed to reduction of W nitride species on the surface of the catalysts.

4.3.4 Temperature Programmed Reduction of Cat-T_N Nitrides

TPR studies of nitride catalysts synthesized at different nitriding temperatures also produced three peaks and a shoulder as seen in the previous sections. Peak (a) (see Figure 4.6B) was located at about 330 °C with no shift in temperature as T_N was increased. This is because T_N did not have any significant impact on the interaction of Ni metal with the support. Peak (e) reduced in intensity with increased T_N and is due to reduction in number of acid sites as T_N increased. Reduction in acid sites leads to reduction in adsorbed NH_3, hence, the reduction in peak intensity. Reduction of the passive oxygen layer appears as a shoulder (d). The high temperature peak is associated with reduction of W nitride species on the catalyst surface. Although reduction of the W nitride species is incomplete, Figure 4.6B shows that it was easier to reduce the W_2N species at lower nitriding temperatures. This is because the onset of the reduction peaks shift to higher temperature with increase in nitriding temperature. As T_N increased, particle dispersion reduced and agglomeration of the W_2N particles increased, making the particles less accessible and more difficult to reduce.

In summary, increase in P weakens metal-support interaction which eases the reduction of both Ni_3N and W_2N. Reduction of Ni_3N precedes or interferes with reduction of the passive layer of the catalyst. T_N did not affect the metal-support interaction.

4.4 Temperature Programmed Oxidation (TPO)

TPO of Cat-W, Cat-Ni, Cat-P and Cat-T_N was performed to see the effects varying parameters have on oxidation properties of Ni-W(P)/γ-Al_2O_3 nitride catalysts, the stability of the

catalysts to bulk oxidation after initial surface passivation and to characterize species on the surface of the catalyst based on their oxidizability. During oxidation, N atoms in the nitride are replaced by oxygen atoms as shown in Equations (4.4) and (4.5) below (Herle et al., 1998). This results in net weight increase of the catalyst as oxygen is heavier than nitrogen. Distinct

$$2Ni_3N + 3O_2 \rightarrow 6NiO + N_2 \quad (4.4)$$

$$2W_2N + 6O_2 \rightarrow 4WO_3 + N_2 \quad (4.5)$$

profiles were observed for Ni/γ-Al_2O_3, W/γ-Al_2O_3 nitrides and γ-Al_2O_3 as shown in Figure 4.7. The nitrides lost weight at temperatures < 200 °C due to loss of H_2O and/or NH_3. Ni/γ-Al_2O_3 nitride was oxidized over the temperature range 200 °C to 450 °C (peaks (a) and (c)) while that of W/γ-Al_2O_3 was over the range 300 °C to 480 °C (peaks (b) and (d)). No oxidation was observed for the γ-Al_2O_3 sample within the range of temperatures studied. The profile however changed with bimetallic Ni-W nitride catalysts as discussed below.

4.4.1 Temperature Programmed Oxidation of Cat-P Nitrides

TPO profiles of different levels of P in Ni-W/γ-Al_2O_3 nitrides are shown in Figure 4.8A. The TPO signals for 0%-P and phosphorus-containing samples looked similar but all looked different from those of the reference catalysts (see Figure 4.7). Generally, there was weight loss up to 300 °C due to loss of moisture and/or ammonia. Oxidation process set in after the temperature had reached 300 °C. As oxygen atoms replaced nitrogen atoms in the nitride catalysts, the catalyst weight increased. The process continued through the maximum temperature of ~580 °C. The oxidation profiles of the bimetallic catalysts suggest that there might be a species present on the bimetallic catalysts that is not present on the monometallics. The species is assigned to Ni_2W_3N (Herle et al., 1998) and it is responsible for the observed oxidation profile above 500 °C. In other words, complete oxidation of Ni_3N and W_2N ended at ~500 ˚C leaving Ni_2W_3N nitride for further oxidation above 500˚C. As P loading increased, the transition temperature between weight loss (loss of NH_3) and weight gain (oxidation), peak (e), slightly shifted to higher temperature. This is because P loading increased acidity of the catalyst leading to increased amounts of adsorbed NH_3 on the catalyst surface. It may also be that addition of P enhanced the formation of $NiWO_4$ (precursor for Ni-W bimetallic nitrides) (Atanasova and Halachev, 1994) and reduced the amount of NiO (precursor for Ni_3N species) formed. This is in agreement with

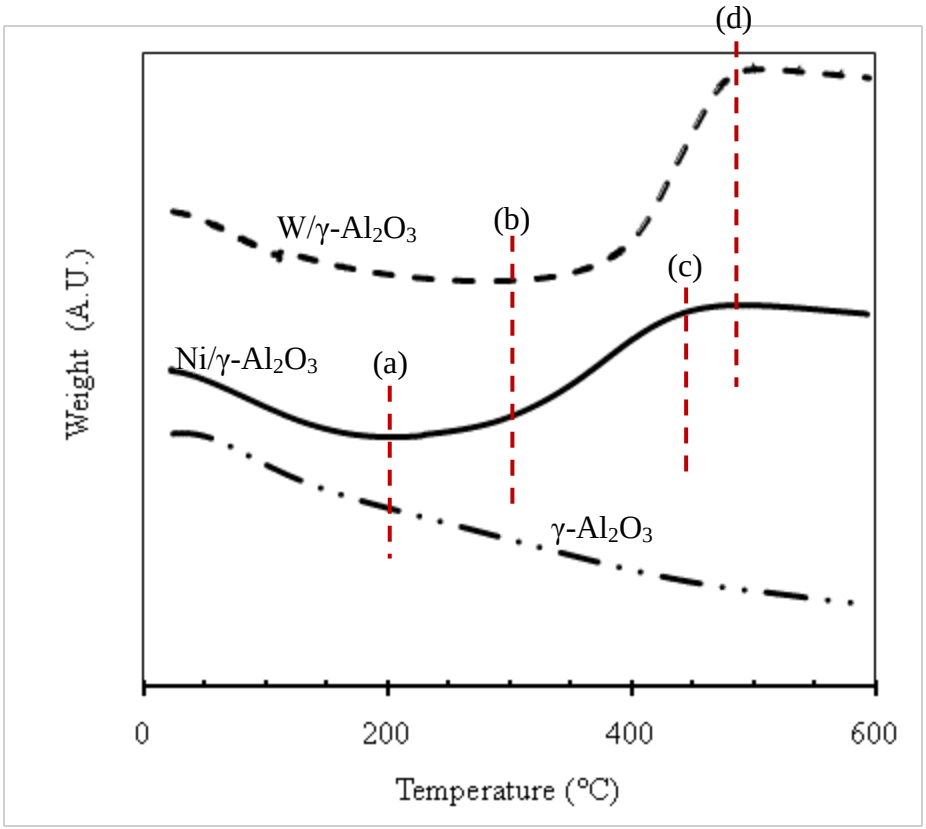

Figure 4.7: Temperature programmed oxidation of reference nitride catalysts and γ-Al_2O_3. Conditions: 30 wt% W, 10 wt% Ni and T_N of 700 °C.

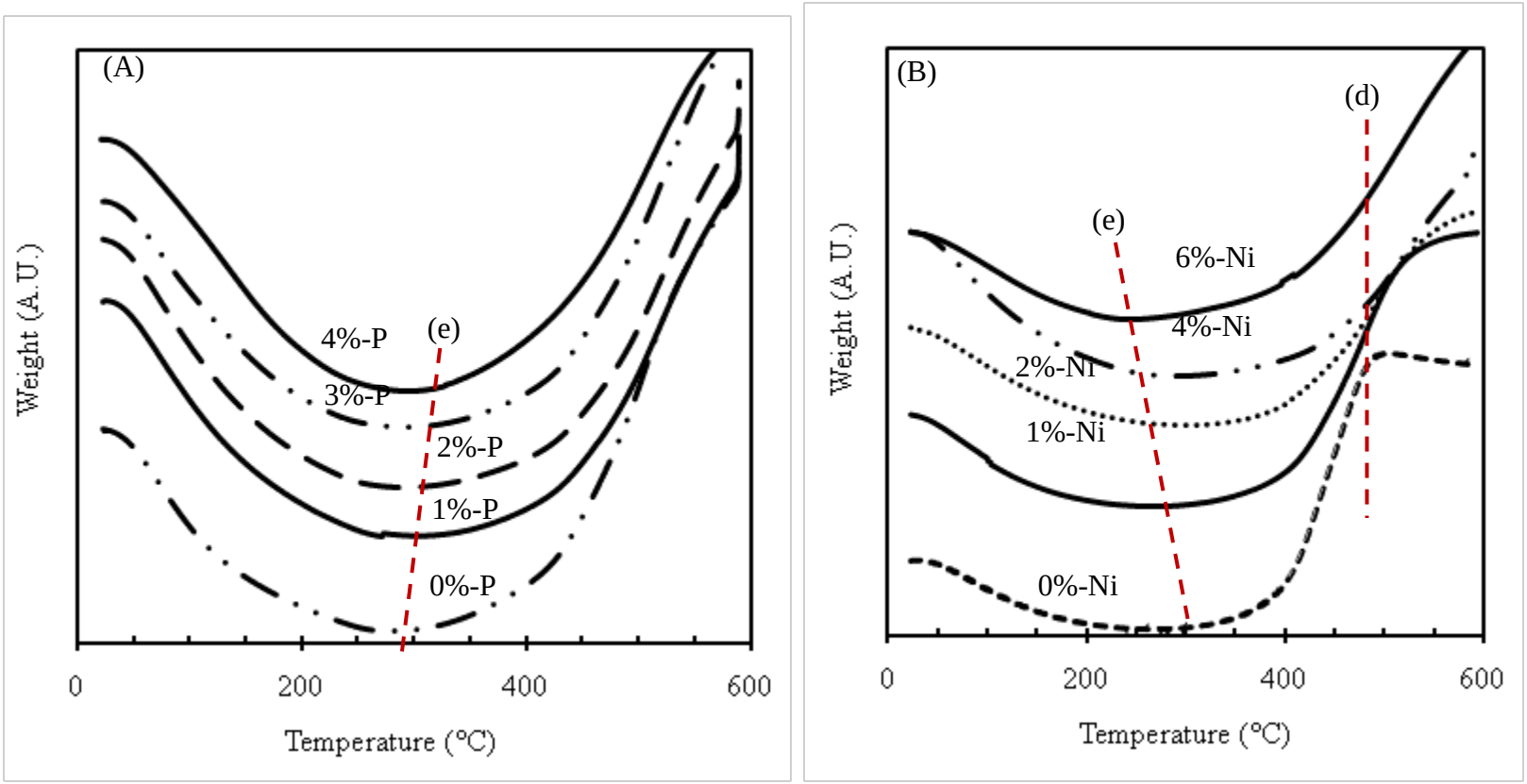

Figure 4.8: Temperature programmed oxidation profiles of (A) Cat-P and (B) Cat-Ni nitride samples. Conditions: 30 wt% W, T_N of 700 °C and (A) 4 wt% Ni; (B) 2 wt% P.

results of the TPD (see Figure 4.2A) where P loading increased the intensity of peak (a) and TPR results (see Figure 4.5A) where P loading decreased the intensity of peaks associated with reduction of Ni_3N species.

4.4.2 Temperature Programmed Oxidation of Cat-Ni Nitrides

Figure 4.8B shows the oxidation profiles for Cat-Ni nitride samples. Similar to the Profiles of Cat-P samples, there was initial weight loss due to loss of H_2O and/or NH_3. The Ni-free sample (0%-Ni) displayed a TPO profile similar to that of W/γ-Al_2O_3 (see peak (d) in Figure 4.7) and different from profiles of all the Cat-P samples (see Figure 4.8A). This is because the 0%-Ni did not form any bimetallic Ni-W species that would shift the oxidation process beyond 480 °C. It also suggests that the presence of P in the 0t%-Ni sample did not have any impact on the oxidation of W nitride in the catalyst. As Ni loading increased, the profile gradually changed to a profile similar to that of the bimetallic Ni-W/γ-Al_2O_3 nitride catalyst. The observations confirm that in the presence of Ni and W, bimetallic Ni-W nitrides are formed on the surface of the catalyst. The onset of oxidation also shifted to lower temperature as the Ni loading increased indicating the formation of more Ni_3N on the catalyst surface with increase in Ni loading.

4.4.3 Temperature Programmed Oxidation of Cat-W and Cat-T_N Nitrides

TPO results of the Cat-W nitride samples are shown in Figure 4.9A. All sample exhibited pro files similar to those of bimetallic Ni-W/γ-Al_2O_3 nitrides. As W loading increased, the intensity of the oxidation profiles increased, suggesting that more bimetallic Ni-W nitrides were formed. The extent of oxidation in the Cat-T_N samples (Figure 4.9B) increased with increase in T_N. Oxidation temperature for the 500°-T_N sample ranged from 300 to 500 °C, suggesting that the catalyst contained less amount of bimetallic Ni- W/γ-Al_2O_3. However, Figure 4.3B showed large NH_3 desorption amounts from the 500°-T_N sample at temperatures above 500 °C. The stunted weight gain in the TPO profile of the 500 °C T_N sample above 500 °C may therefore be due to weight loss from the desorbed NH_3.

Overall, the catalysts were stable to bulk oxidation after the initial passivation as oxidation only took place after the catalyst was heated to 200 °C. Secondly, combination of Ni and W leads to formation of bimetallic nitrides. More Ni3N is formed with increase in Ni loading and P wt%, another phase of Ni_2W_3N appeared at 40.3 °. Literature (Atanasova and Halachev, 1994)

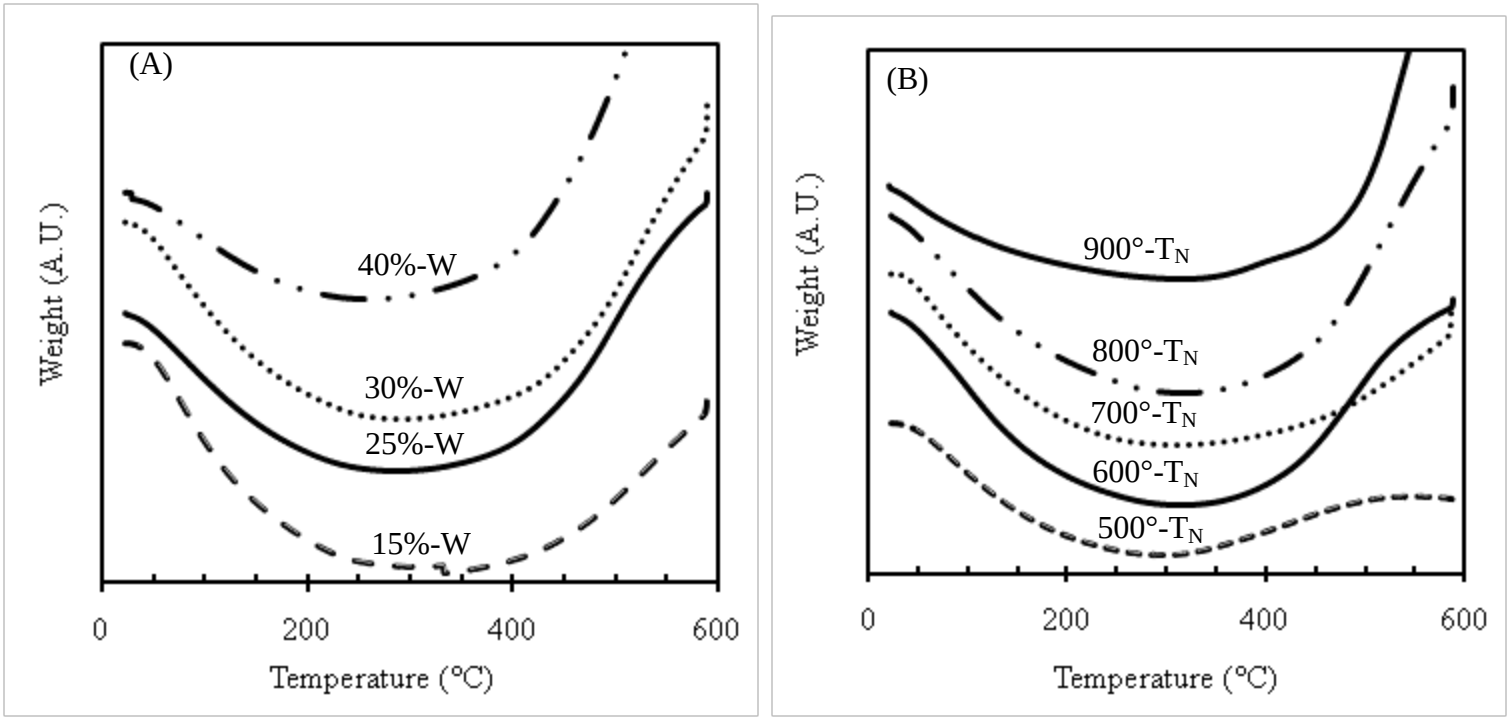

Figure 4.9: Temperature programmed oxidation profiles of (A) Cat-W and (B) Cat-T_N nitride samples. Conditions: 4 wt% Ni, 2 wt% P and (A) 700 °C T_N; (B) 30 wt% W.

enhances formation of bimetallic nitrides which shifts oxidation to higher temperatures.

4.5 X-Ray Diffraction (XRD)

XRD experiments were performed to determine crystalline phases in the catalysts and to investigate the impact of varying parameters such as W, Ni and P loading as well as T_N on catalyst activity. Reference samples used for this study included γ-Al_2O_3, nitrides of W/γ-Al_2O_3 and Ni/γ-Al_2O_3 and Ni-W(P)/γ-Al_2O_3 oxide. Results of the observed patterns for reference materials are shown in Figure 4.10. The XRD pattern of the oxidic phase of 30 wt% W, 4 wt% Ni and 2 wt% P sample did not show any crystalline phases apart from Al_2O_3 structures. This suggests that the oxide structures may be amorphous (Yuhong et al., 2001; Dezelah et al., 2004; Balasubramanian et al., 2006). Amorphous structures are not visible to XRD. Peaks of γ-Al_2O_3 (o) were observed at 37.2, 45.5 and 66.5 degrees. W_2N crystalline structures (+) were observed on the W/γ-Al_2O_3 nitride sample at 38, 43.5, 63.6 and 76 degrees (Shi et al., 2004) while those of Ni_3N (*) occurred at 44.5, 51.8, 76.2 and 92.6 degrees (Dezelah et al., 2004; Melo-Banda et al., 2001; Santillan-Vallejo et al., 2005).

4.5.1 X-ray Diffraction of Cat-P Nitrides

XRD for samples with varying P loading was conducted to determine the effect P has on the crystalline structures in the catalyst. The Ni_3N, W_2N and Al_2O_3 peaks identified in the reference material were also present in the patterns of the Cat-P nitride samples (see Figure 4.11A). New peaks (Δ) located at 25.9 and 60.5 degrees occur in all the samples (both P-containing and non P-containing) and so cannot be associated with the presence of P in the catalysts. The peaks can be assigned to the presence of Ni_2W_3N on the catalyst surface. As P loading increased to 4 wt%, another phase of Ni_2W_3N appeared at 40.3°. Literature (Atanasova and Halechev, 1994) shows that P promotes formation of $NiWO_4$ which is a precursor for Ni_2W_3N formation (Eliche-Quesada et al., 2003), hence appearance of the new phase. The peaks at 63.4 and 76.5 (W_2N) that appear in the 0 wt% and 2 wt% P samples are absent in the 4 wt% P sample. This shows that at high P loading, the surface of the catalyst is modified leading to the formation of new species. Generally, the peak intensities appeared to diminish slightly as P loading increased from 2 to 4 wt% which might be due to formation of smaller particles in the catalyst.

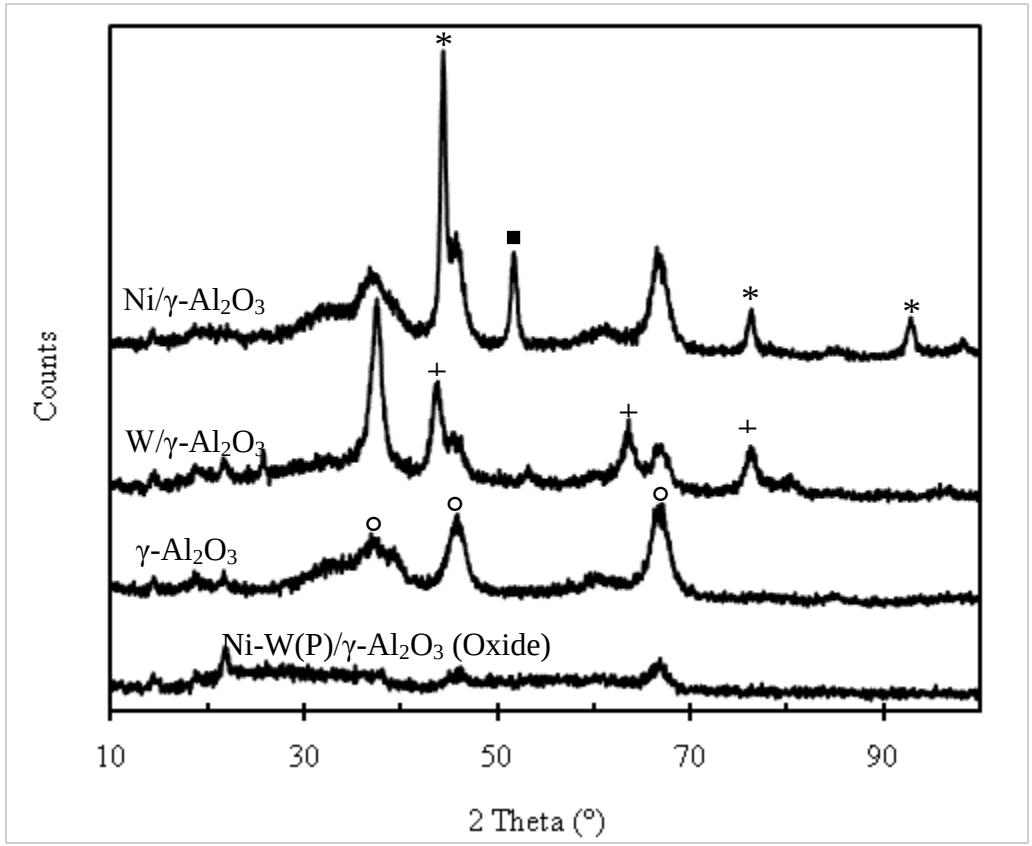

Figure 4.10: X-ray diffraction patterns of reference samples. (o) γ-Al_2O_3, (+) W_2N, (*) Ni_3N, (■) Ni metal. Conditions: 30 wt% W, 10 wt% Ni and T_N of 700 °C.

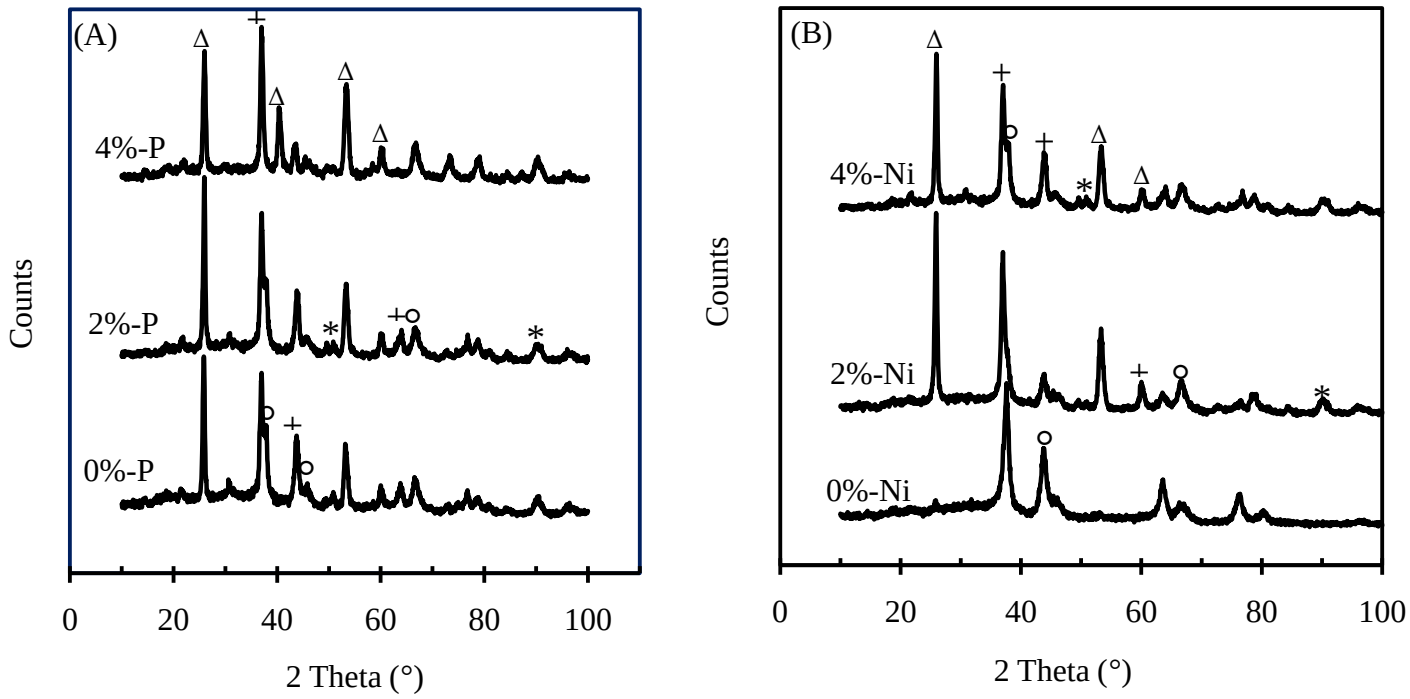

Figure 4.11: X-ray diffraction patterns of (A) Cat-P nitrides and (B) Cat-Ni nitrides. Peaks: - (o) γ-Al_2O_3; (+) W_2N; (*) Ni_3N; (Δ) Ni_2W_3N. Conditions: 30 wt% W, T_N, of 700 °C and (A) 4 wt% Ni; (B) 2 wt% P.

4.5.2 X-ray Diffraction of Cat-Ni Nitrides

The XRD patterns of the catalysts with varying Ni loading are shown in Figure 4.11B. The 0%-Ni catalyst showed mainly crystal structures of W_2N and Al_2O_3, in the XRD patterns. As Ni was introduced (at 2 and 4 wt%) most of the Ni_3N peaks (*) observed at 44.5 and 51.8 degrees in the reference material diminished with new peaks at 25.9, 53.2 and 60.5 degrees appearing. This is why an indication that Ni combined with W species to form bimetallic Ni_2W_3N catalyst species and confirms results of the TPO studies (Section 4.4).

4.5.3 X-ray Diffraction of Cat-W and Cat-T_N Nitrides

The XRD patterns for Cat-W samples are shown in Figure 4.12A with peaks at 37.2, 45.5, and 66.5 degrees attributed to γ-Al_2O_3 (◦). Peaks of W_2N and Ni_3N (∗) were also observed on the catalysts. The peaks at 25.9 and 53.2 degrees which are assigned to Ni_2W_3N species are absent from the XRD pattern of the 15%-W loading catalyst but present in the 30%-W and 40%-W catalysts. It is possible that the bimetallic Ni-W nitride species on the 15%-W sample are highly dispersed and so are not visible to XRD. SEM image for the 15%-W sample confirms high dispersion of species on the surface (see Figure 4.16). TPO profile of the 15%-W sample followed the bimetallic profile which suggests that Ni_2W_3N species is present on the catalyst surface. Increase in W loading increased intensity of the peaks in agreement with the W loading. which suggests that particle sizes increased with W-loading. This is also confirmed by SEM results.

The main Ni_3N and W_2N peaks observed in Figure 4.12A are also present in Figure 4.12B. The peaks at 19.3, 27, 28, 54.6 and 55.9 are only present in the pattern for the 900º-T_N catalyst. The peaks at 40.3 58.2, 73.4 and 86.9 degrees are present only in the patterns of the 800 and 900º-T_N nitride catalysts. The peaks at 25.9 38, 53.2 and 63.4, which were present on the 700 ºC T_N catalyst were absent in the 800 and/or 900 ºC T_N samples. The high T_N used may have resulted in decomposition, forming Ni and W metals on the catalyst surfaces (Shi et al., 2004; Herle et al., 1998). This is in agreement with TPD results which showed that nitride species decomposed to give off N_2 at temperatures greater than 800 °C. It also appears from Figure 4.12B that the bimetallic Ni_2W_3N decomposed easier than other species as the W_2N species were intact even at 900 °C.

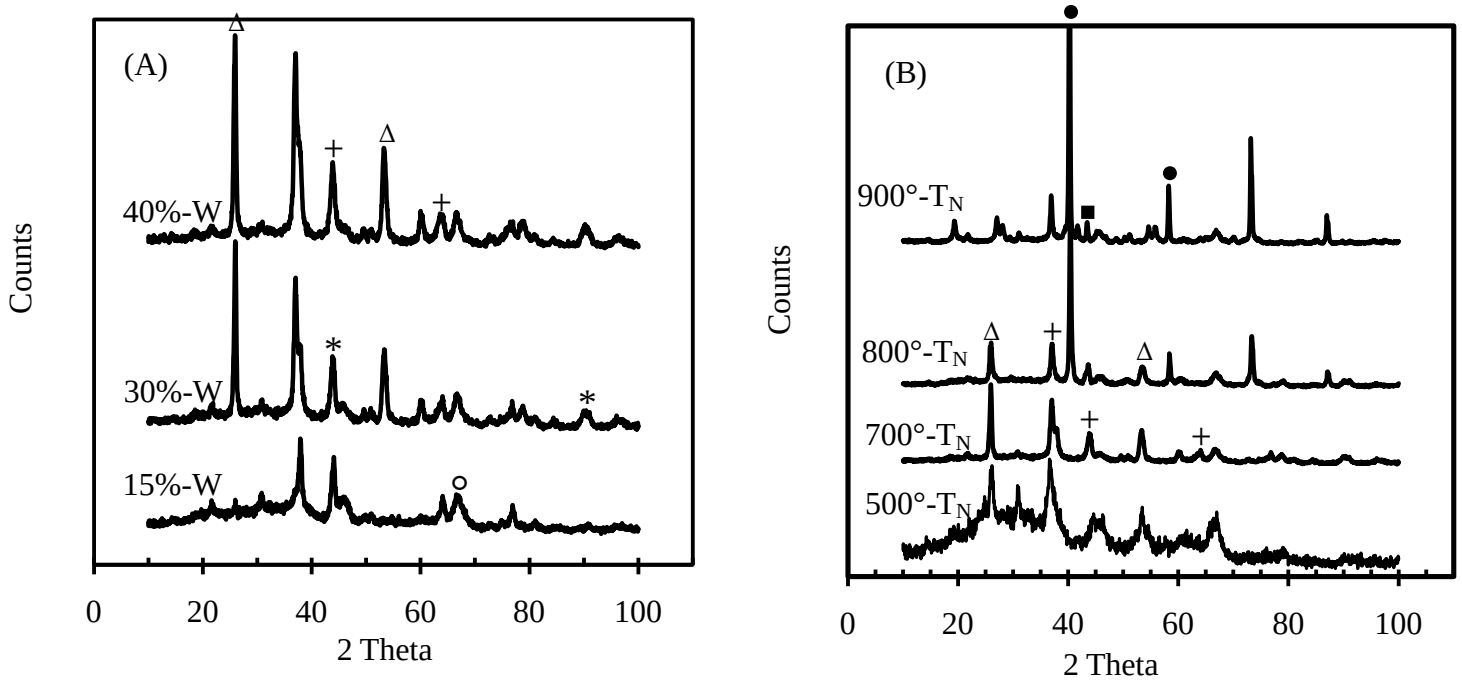

Figure 4.12: X-ray diffraction patterns of (A) Cat-W nitrides and (B) Cat-T_N nitrides. Peaks: - (o) γ-Al_2O_3; (+) W_2N; (*) Ni_3N; (Δ) Ni_2W_3N, (•) W metal, (▪) Ni metal. Conditions: 4 wt% Ni, 2 wt% P and (A) T_N of 700 °C; (B) 30 wt% W.

In summary, XRD results show that Ni_3N, W_2N and Ni_2W_3N are predominant species on the Ni-W(P)/γ-Al_2O_3 nitride catalysts. The species, especially Ni_2W_3N, decompose to metallic Ni and W at temperatures above 800 °C. Ni and W combine to form bimetallic Ni_2W_3N which is enhanced by addition of P.

4.6 SEM and EDX of Ni-W(P)/γ-Al_2O_3 Nitride Catalyst Samples

SEM, coupled with EDX, was used to study the shapes, sizes and compositions of particles on the surface of Ni-W(P)/γ-Al_2O_3 nitride catalysts. Work was done for catalysts of all groups i.e. catalysts with varying P, Ni, W loading and nitriding temperature. Most of the results are discussed in the following sections with additional results in Appendix F.2. EDX results confirmed the presence of W, Ni, P and Al in the catalysts samples. Results of the EDX analyses are also shown in Appendix F.2.

Micrographs of W/γ-Al_2O_3 are shown in Figure 4.13. Generally, the micrographs showed the presence of pores and metal particles on the surface of the catalyst. They also gave a measure of the sizes and distribution of the metal particles. Metal particles appeared well dispersed for all catalysts studied without much agglomeration or sintering. Metal particle sizes ranged from < 0.2 μm to ~ 1.3 μm. For the purpose of discussions, particle sizes will be classified as follows: particles ≤ 0.2μm will be classified 'small' particles while those > 0.2 μm will be 'large'.

4.6.1 Scanning Electron Microscopy of Cat-P Nitrides

Figure 4.13 shows a cluster of large particles and well distributed small particles. The large particles appeared cubic in shape with smooth edges. More exposed large particles were observed as P was added to W\γ-Al_2O_3 without Ni (see Figure 4.14B). This might be due to the preferential interaction of P with the support, causing metal particles to migrate to the surface (Ferdous et al., 2004a; Sundaramurthy et al., 2008; Atanasova et al., 1997). P did not have much effect on the shape of the large particles. When both Ni and P were added to W (see Figure 4.14C and D), two different particle sizes were observed. There were small, well distributed particles and a cluster of large particles. Comparing to XRD and TPO results, the cluster of large particles might be attributed to the formation of bimetallic Ni_2W_3N species which is formed in the presence of Ni and W species. As P loading increased, the amount of small particles

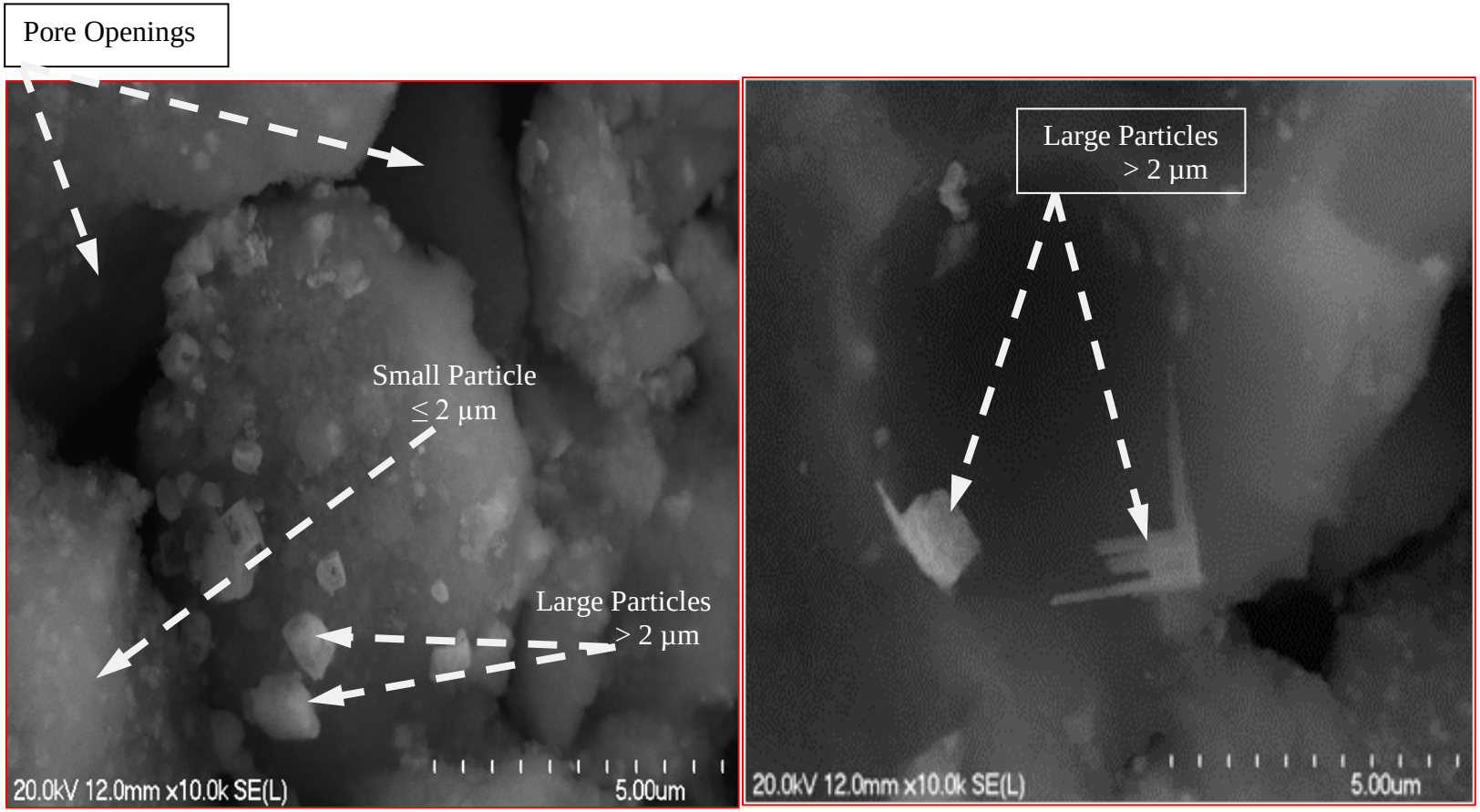

Figure 4.13: SEM micrographs of $W/\gamma Al_2O_3$ nitride catalysts. Conditions: 30 wt% Wand T_N of 700 °C.

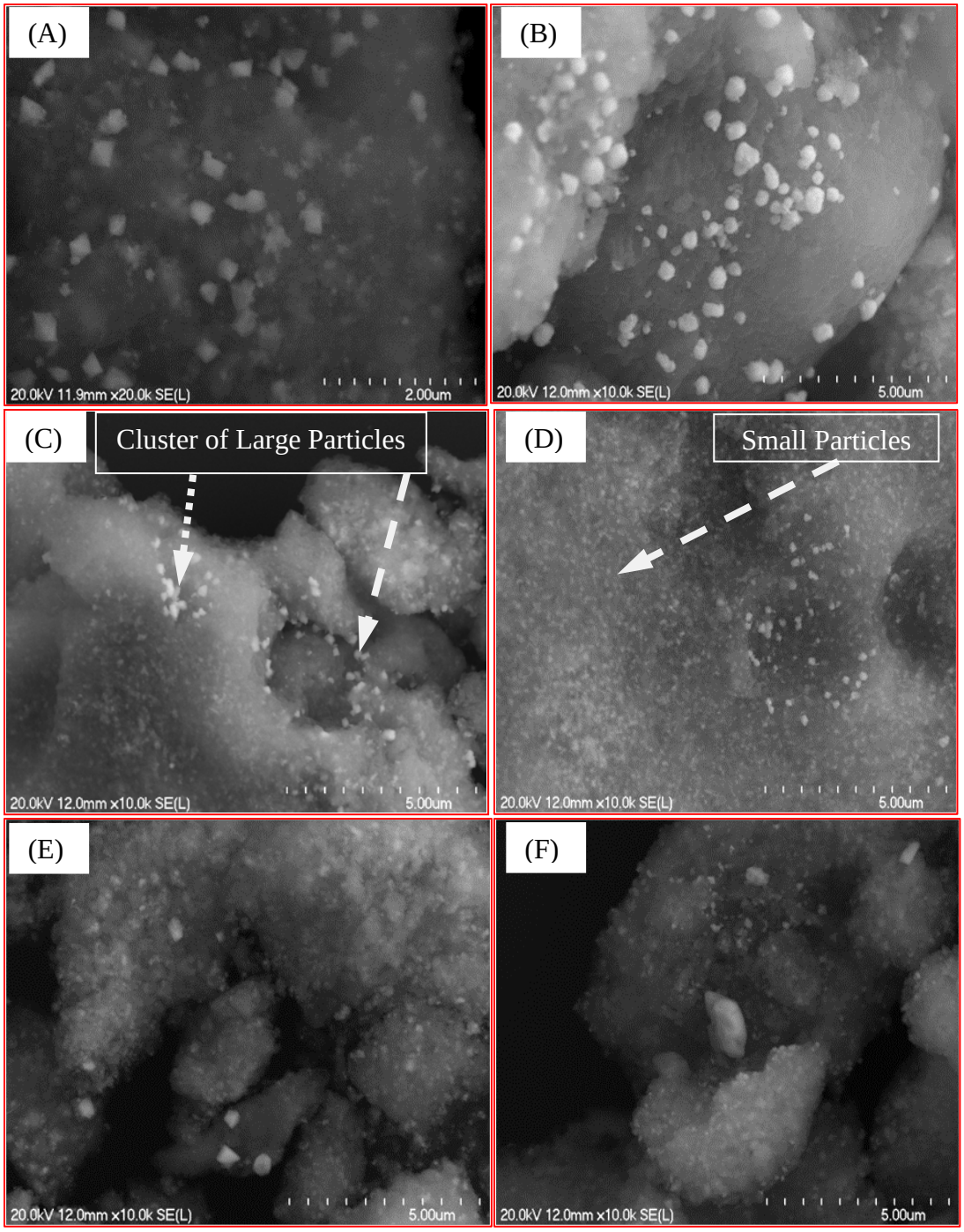

Figure 4.14: SEM micrographs of Cat-P nitride samples. (A) 0%-P; (B) W(P)/γAl_2O_3; (C, D) 2%-P; (E,F) 4%-P. Conditions: 30 wt% W, 4 wt% Ni and T_N of 700 °C.

increased relative to the large particles, increasing the dispersion of the catalyst.

4.6.2 Scanning Electron Microscopy of Cat-Ni Nitrides

On addition of Ni to W/γ-Al_2O_3 (without P addition), the most significant change observed was the shape of the large particles. The large particles appeared to have sharp, pointed edges (see Figure 4.15B) compared to the Ni-free samples (see Figure 4.15A). XRD results in Figure 4.11 revealed the formation of new crystalline phases on the bimetallic nitride catalysts that was not present on the monometallic nitrides. The different particle shapes may therefore be due to formation of either Ni_3N or Ni_2W_3N or both on the catalyst surface. Addition of nickel also reduced the average particle size of the large particles. This was evidenced in the XRD results with reduced intensity of the peaks. The largest particle size observed in Figure 4.13 was ~ 1.3 while that for Figure 4.15B was 0.4 μm. Increase in the Ni loading also led to a relative increase in the amount of small particles.

4.6.3 Scanning Electron Microscopy of Cat-W Nitrides

The 15%-W sample appeared well dispersed and comprised predominantly of small particles and scanty large particles (see Figure 4.16A and B). This resulted in highly dispersed active sites on the catalyst surface. The high dispersion and dominant small particles may be due to the relatively low W/Ni or W/P ratio in the catalyst as both Ni and P caused a reduction in the catalyst particle size. The high particle dispersion may also be the reason why XRD pattern of the 15%-W catalyst does not show bimetallic peaks (see Figure 4.12A). The 30%-W sample had a higher amount of large particles compared to the 15 wt% sample. There was a cluster of large particles with no sign of agglomeration. The 40%-W catalyst showed signs of agglomeration of large particles and had less number of small particles. The dispersion also appeared poor on the 40%-W catalyst sample.

4.6.4 Scanning Electron Microscopy of Cat-T_N Nitrides

Particles of the catalyst synthesized at T_N of 500 °C appeared well dispersed compared to other nitriding temperatures because it was made of small particles (Figure 4.17). This may be why its XRD pattern appeared amorphous compared to samples of other nitriding temperatures (Figure 4.12B). As nitriding temperature increased to 700 °C, the number of large particles increased but overall, there were more small particles than large. At 900 °C nitriding temperature,

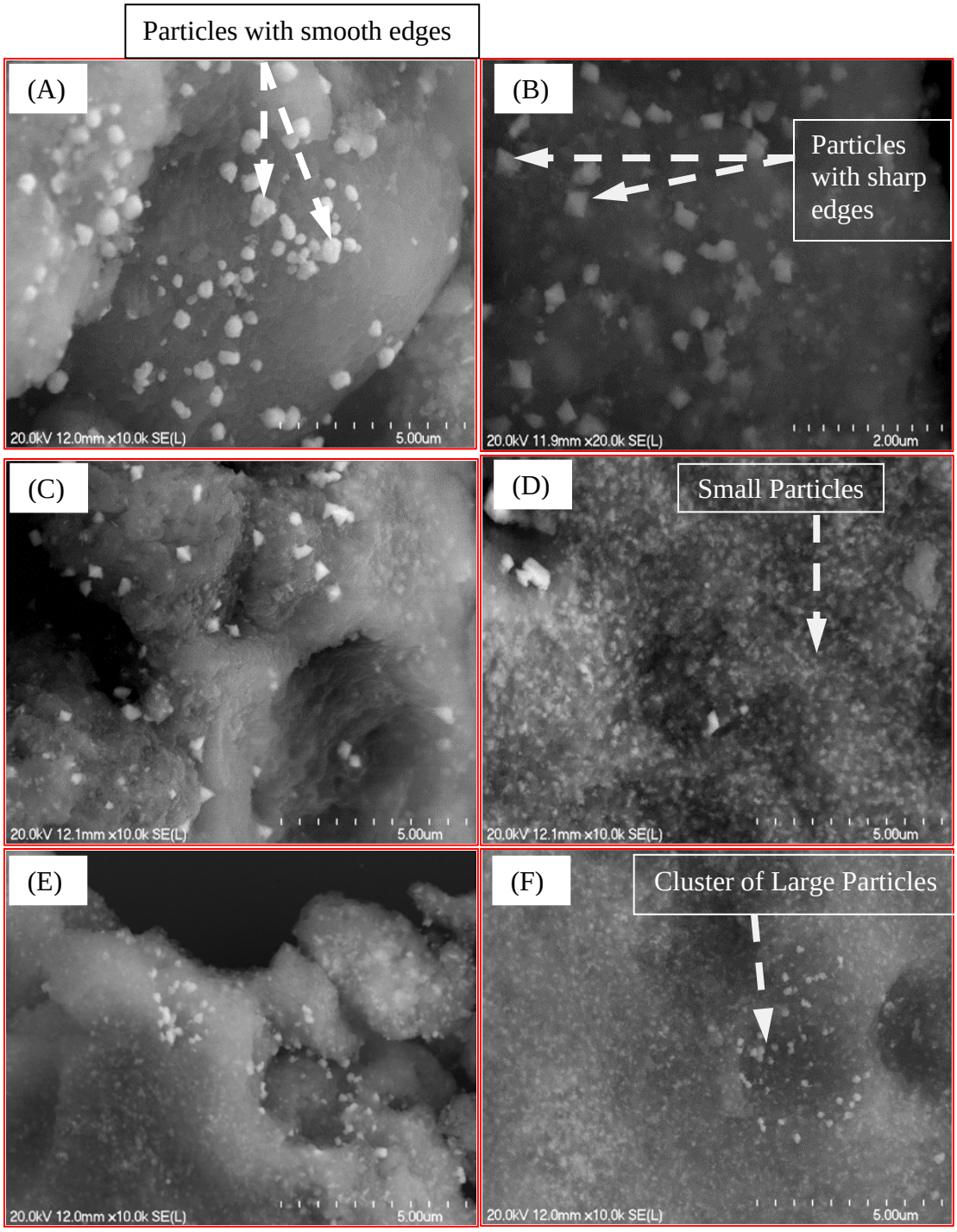

Figure 4.15: SEM micrographs of Cat-Ni nitride samples. (A) 0%-Ni; (B) Ni-W/γAl_2O_3; (C, D) 2%-Ni; (E, F) 4%-Ni. Conditions: 30 wt% W, 2 wt% P and T_N of 700 °C.

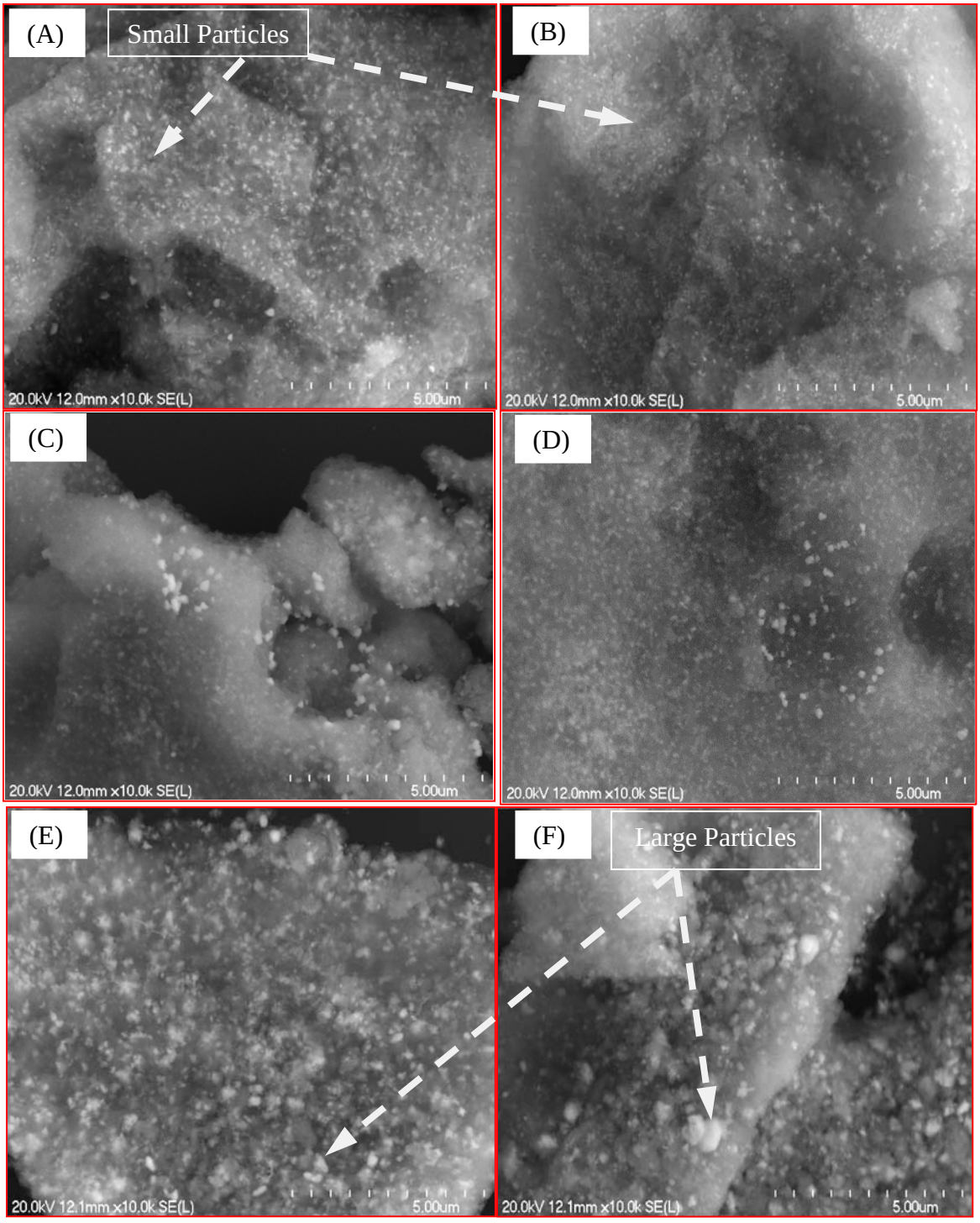

Figure 4.16: SEM micrographs of Cat-W nitride samples. (A, B) 15%-W; (C, D) 30%-W; (E F) 40%-W. Conditions: 4 wt% Ni, 2 wt% P and T_N of 700 °C.

.

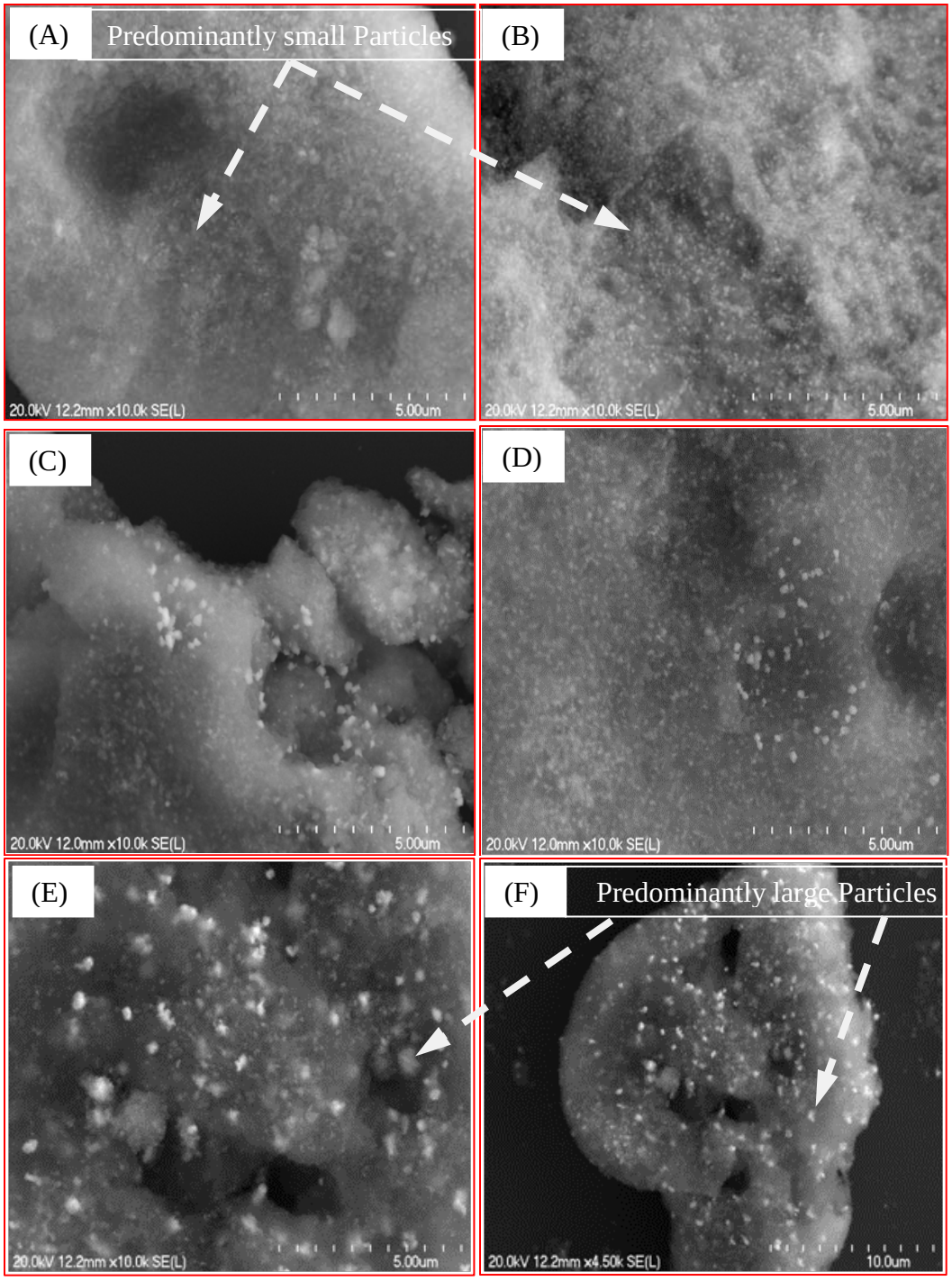

Figure 4.17: SEM micrographs of Cat-T_N nitride samples. (A, B) 500°-T_N; (C, D) 700°-T_N; (E, F) 900°-T_N. Conditions: 30 wt% W, 4 wt%, Ni and 2 wt% P.

more large particles were formed due to agglomeration of particles. The number of particles per unit area also increased. The micrograph of the 900°-T_N sample had a better contrast compared to the other images. In other words, the images appeared brighter. This is probably due to the more crystalline nature of the particles. TPD (Figure 4.2A) and XRD (Figure 4.12B) results showed that at high temperatures, the nitrides decompose to form metals. The presence of metals on the surface of the 900°-T_N sample may be the reason for the high contrast observed in the micrograph.

In summary, Ni promoted formation of smaller particle sizes when added to W-containing catalysts. P appeared to enhance migration of particles to the catalyst surface. Increasing W loading increased the size of catalyst particles while increase in nitriding temperature increased agglomeration of particles. The presence of Ni and W appeared to form a cluster of large particles with sharp edges that may be attributed to bimetallic Ni-W nitride species.

4.7 Energy Dispersive X-ray

EDX experiments were performed mainly to determine composition of the nitride catalysts. As indicated in Section 2.3.8, EDX does not give information on bulk composition. Only information on local composition can be obtained. Figure 4.18 shows the EDX spectra of 2%-P nitride catalyst (see Appendix F.2 for more EDX spectra). The peaks of the constituent metals in the catalysts as well as Al and O are present in the spectra which is a confirmation of the presence of the metals in the catalyst. Table 4.2 shows composition of selected catalysts and their metal to Ni and Al ratios. The results indicate irregular distribution of metals on the catalysts surface. For the Cat-P nitride catalysts, the compositions of both W (30wt%) and Ni (4wt%) were constant. Theoretically, the ratio of W to Ni should be about 7.5. The low ratios obtained from the EDX indicates that either the metal species are not uniformly distributed on the surface or that there is relatively more Ni on the surface than W metals. In other words, W might have interacted more with the support. The variation in the W:Ni ratio may also suggest that the metals are not evenly distributed on the catalyst surfaces.

4.8 Transmission Electron Microscopy (TEM)

TEM was performed for all groups of catalysts prepared. The images in Figure 4.19 to Figure 4.24 show particles of various sizes on the catalyst surface. The particles were mostly rod-like in shape, randomly dispersed on the support in terms of orientation and ranged between

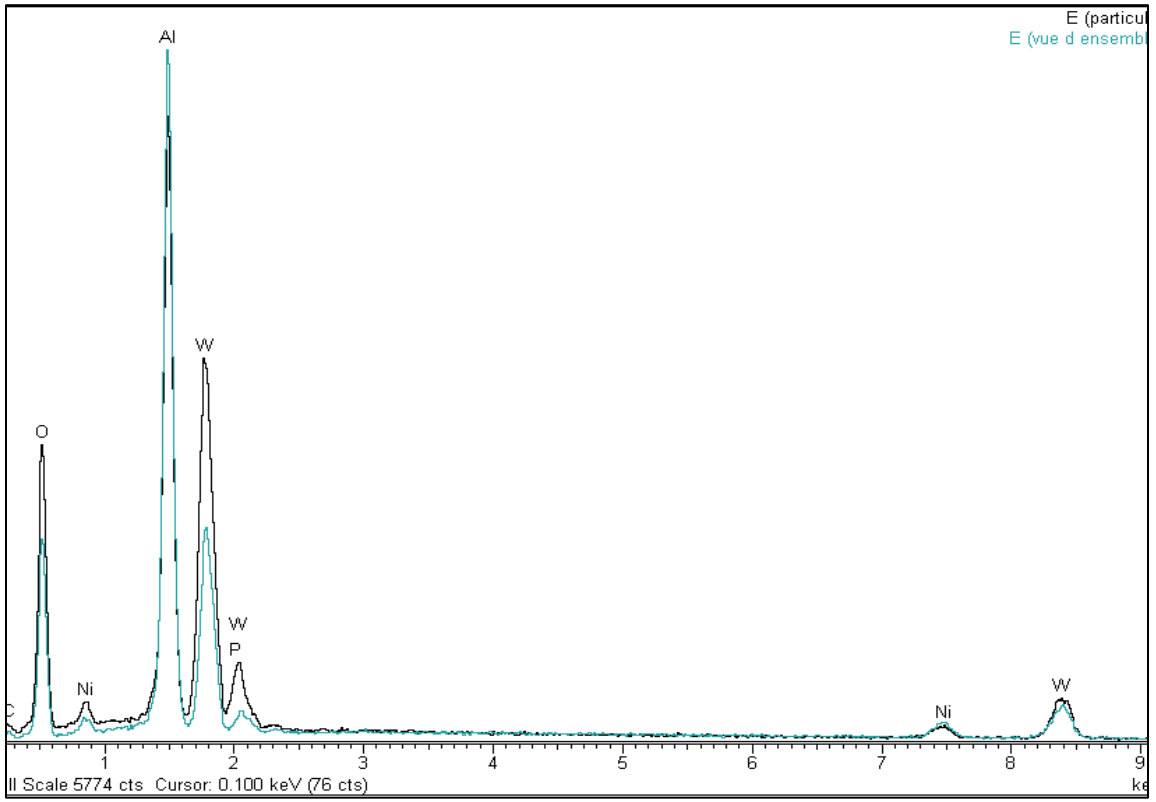

Figure 4.18: EDX spectra of 2%-P nitride catalyst. Conditions: 30 wt% W, 4 wt% Ni, 2 wt% P and T_N of 700 °C.

Table 4.2: Elemental composition from EDX analyses of Cat-P and Cat-W nitride samples.

Name	Composition (wt%)								Ratio				
	Theoretical				EDX								
	W	Ni	P	Al	W	Ni	P	Al	W	Ni	P	Al	
1%-P	30	4	1	17.2	8.61	2.94	1.29	13.12	2.93	1	0.44	4.46	Devisor is Ni
2%-P	30	4	2	16.9	10.17	3.09	2.34	14.47	3.29	1	0.76	4.68	
3%-P	30	4	3	16.7	12.83	3.19	1.78	15.13	4.02	1	0.56	4.74	
4%-P	30	4	4	16.4	13.44	3.84	7.45	13.14	3.50	1	1.94	3.42	
500°-T_N	30	4	2	16.9	14.12	4.08	1.76	13.95	1.01	0.29	0.13	1	Devisor is Al
700°-T_N	30	4	2	16.9	10.17	3.09	2.34	14.47	0.70	0.21	0.16	1	
800°-T_N	30	4	2	16.9	17.51	4.12	1.62	17.60	0.99	0.23	0.09	1	
900°-T_N	30	4	2	16.9	10.50	4.65	1.83	16.00	0.66	0.29	0.11	1	

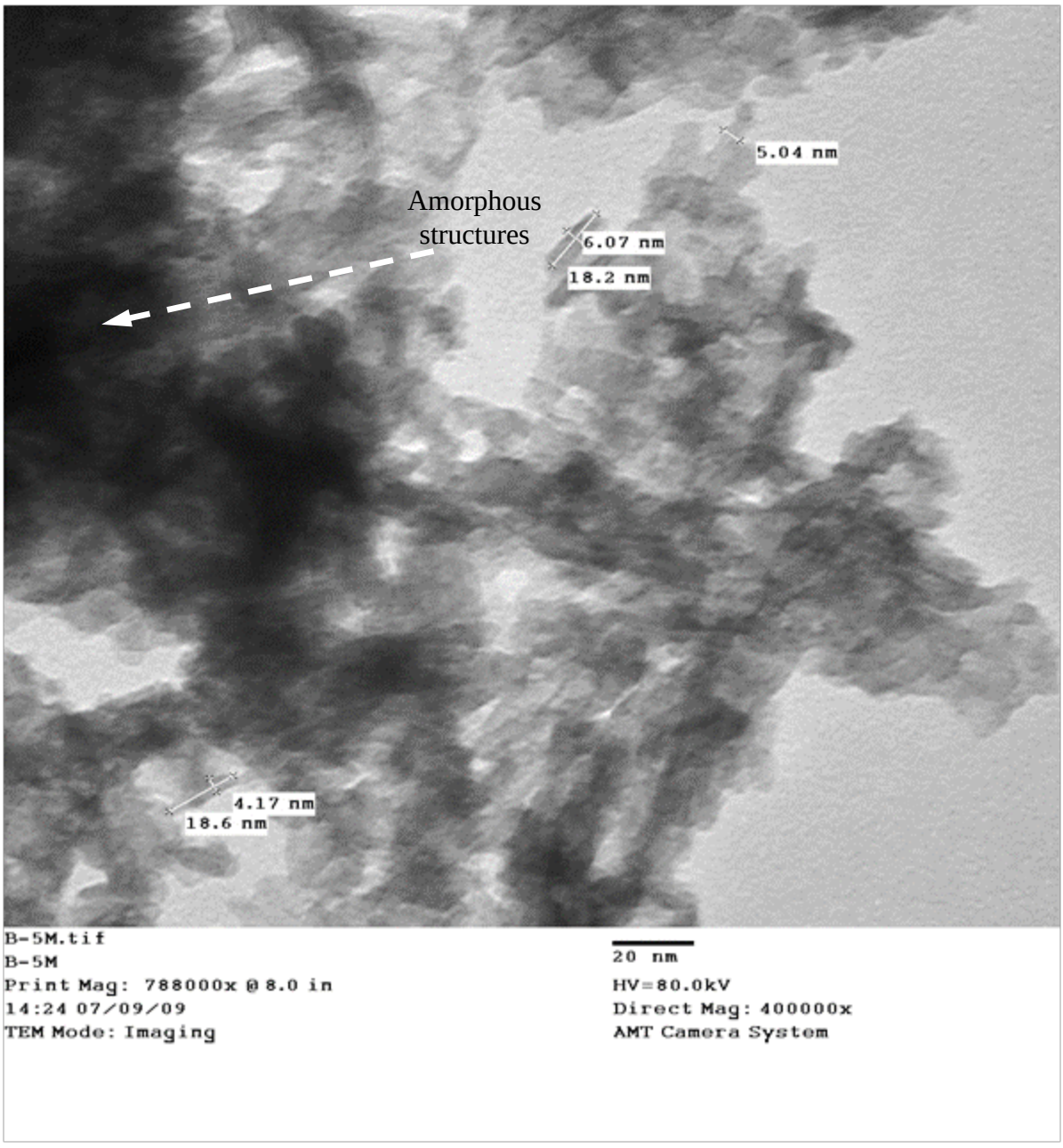

Figure 4.19: Transmission electron micrographs of Ni-W(P)/γ-Al_2O_3 oxide. Conditions: 30 wt% W, 4 wt% Ni and 2 wt% P.

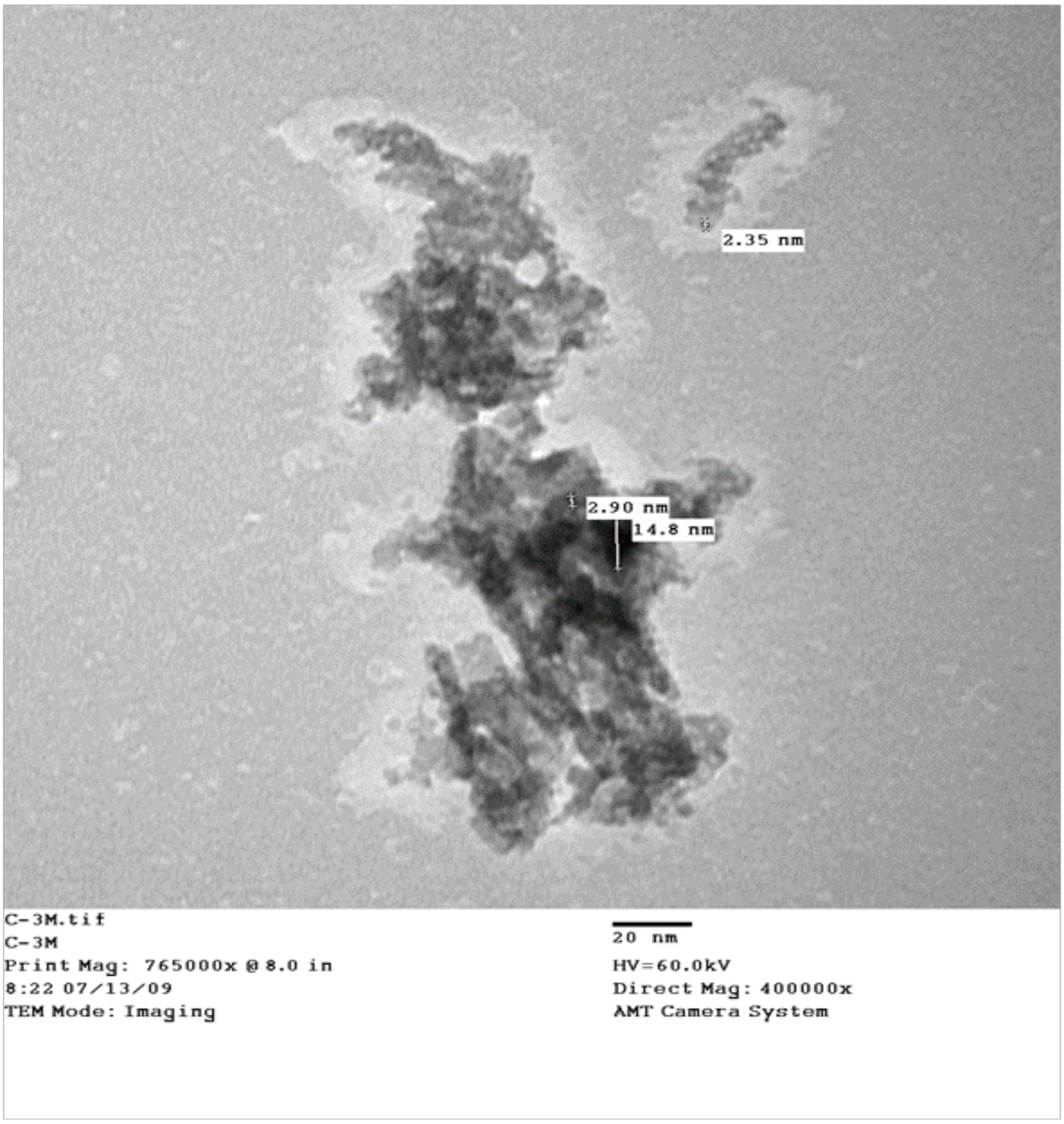

Figure 4.20: Transmission electron micrographs of W/γ-Al_2O_3 nitride. Conditions: 30 wt% W and T_N of 700 °C

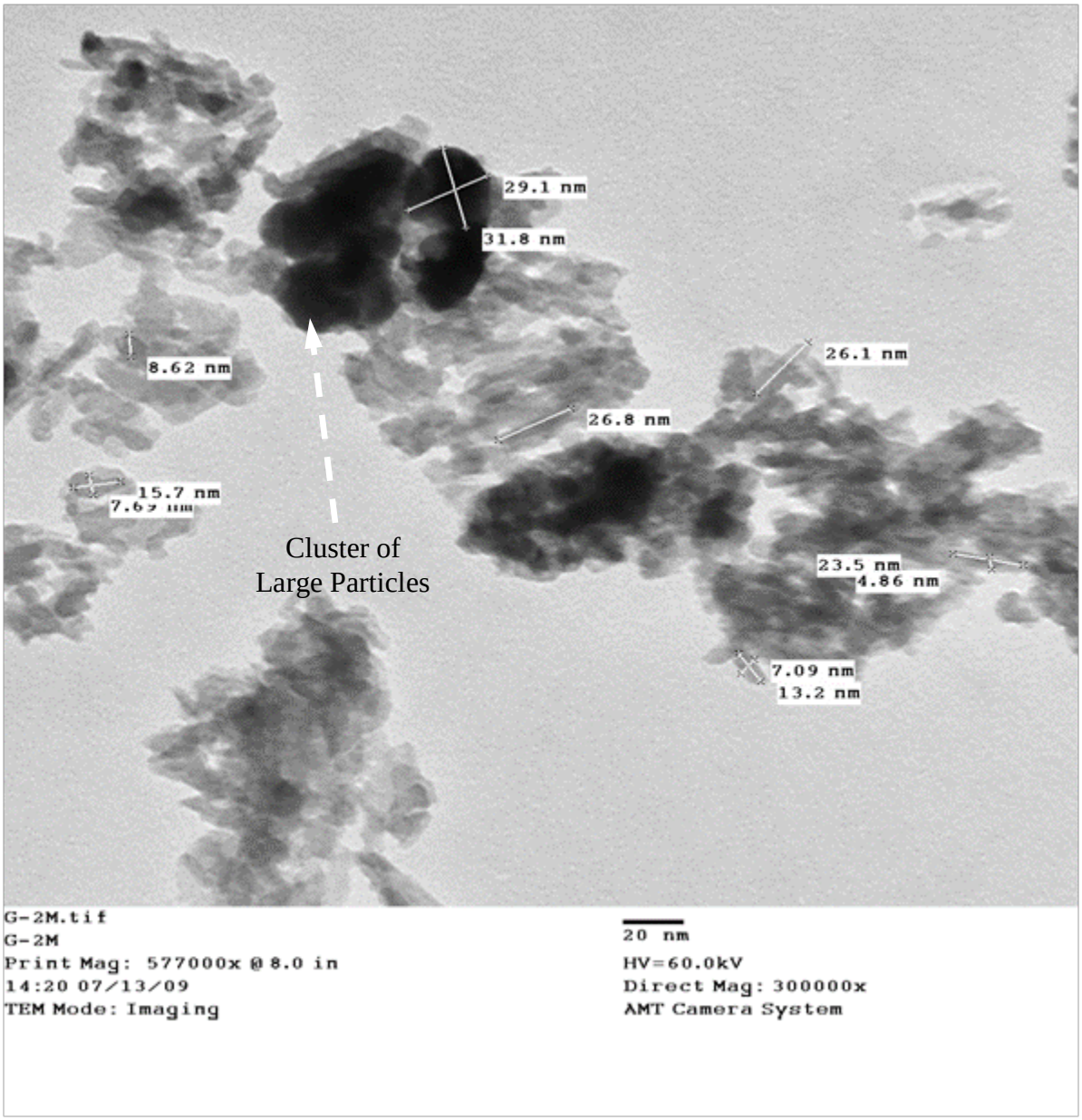

Figure 4.21: Transmission electron micrographs of W(P)/γ-Al_2O_3 nitride. Conditions: 30 wt% W, 2 wt% P and T_N of 700 °C

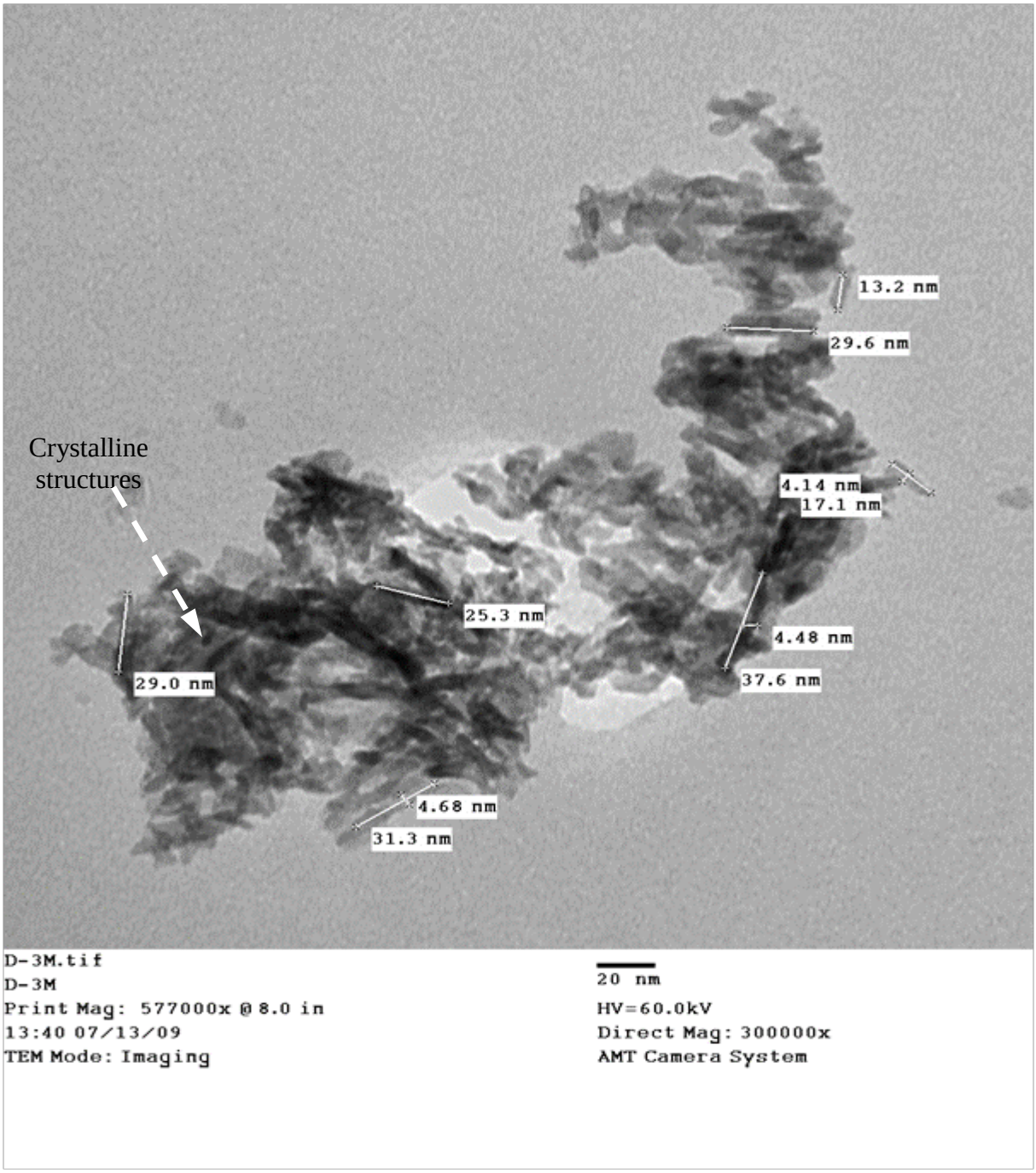

Figure 4.22: Transmission electron micrographs of Ni-W/γ-Al_2O_3 nitride. Conditions: 30 wt% W, 4 wt% Ni and T_N of 700 °C.

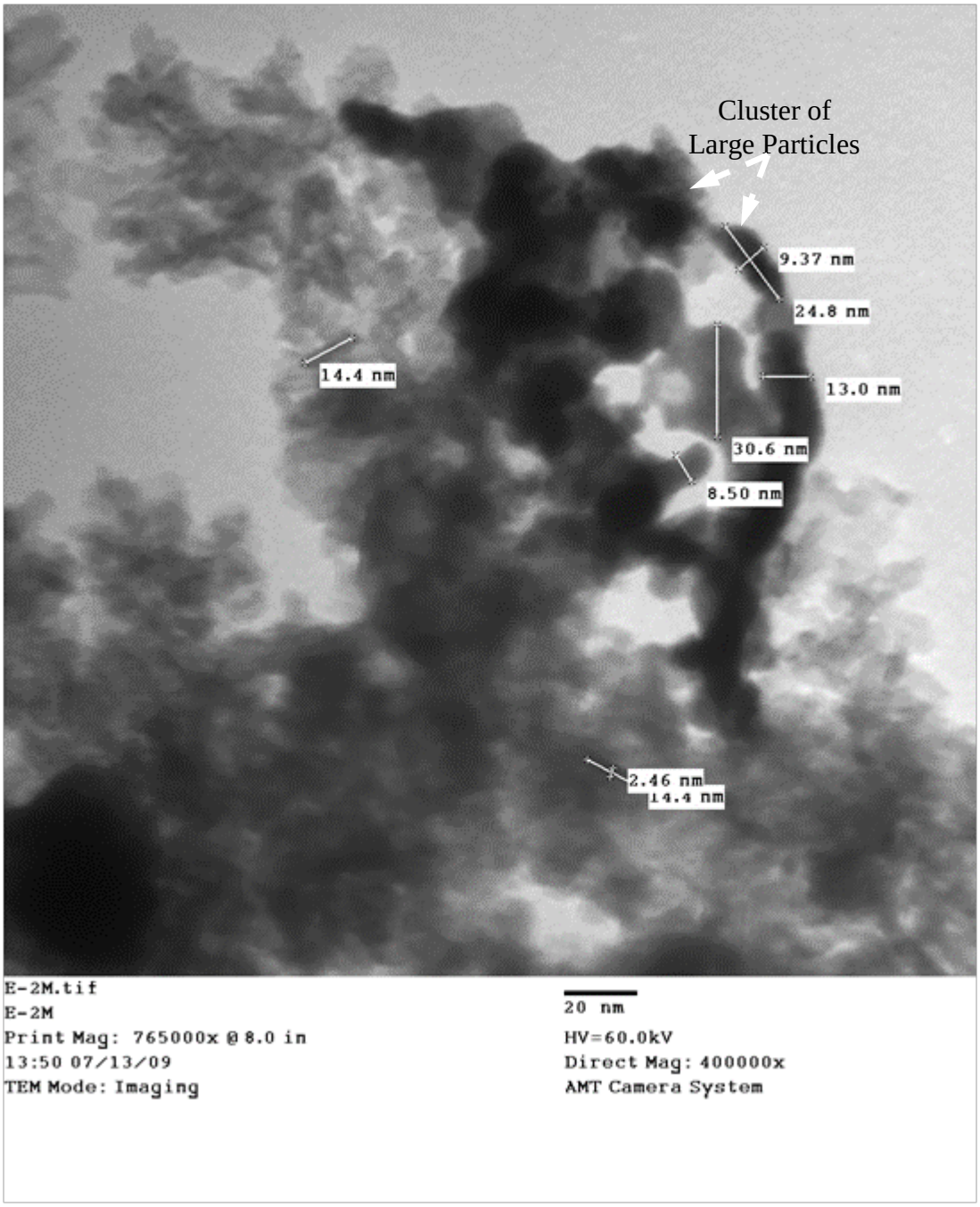

Figure 4.23: Transmission electron micrographs of Ni-W(P)/γ-Al_2O_3 nitride. Conditions: 30 wt% W, 4 wt% Ni, 2 wt% P and T_N of 700 °C.

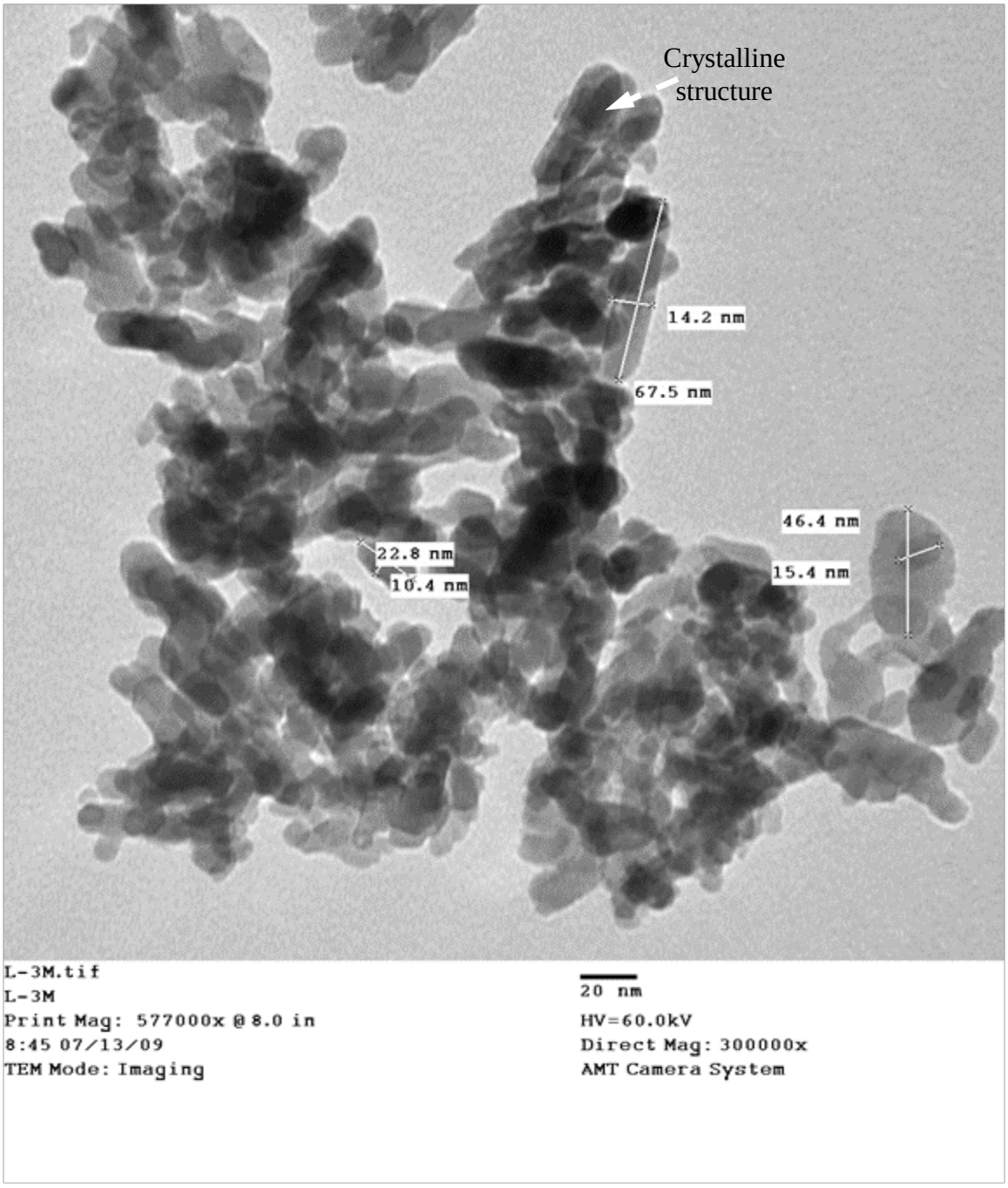

Figure 4.24: Transmission electron micrographs of Ni-W(P)/γ-Al_2O_3 nitride. Conditions: 30 wt% W, 4 wt% Ni, 2 wt% P and T_N of 900 °C.

2 – 21 nm in diameter and 5 – 72 nm in length. There were particles that looked spherical with diameters ranging between 2 – 32 nm.

The images did not display any characteristic structure, similar to reports in the literature (Hada et al., 2000; Hara et al., 2007; Weil, 2004). Amorphous structures were present in parts of the TEM images. The oxide catalyst, in particular (Figure 4.19), showed more amorphous structures in agreement with its corresponding XRD pattern (Figure 4.10). The images appeared more crystalline with Ni in the catalyst (see Figure 4.22). The non-Ni containing samples appeared spherical in shape and amorphous (see Figure 4.21). The clustering of large particles observed in the SEM micrographs can also be observed in the TEM images (see Figure 4.21 and Figure 4.23) and may also be due to formation of bimetallic Ni-W nitride species. The catalyst synthesized at 900 °C (Figure 4.24) was mostly rod-like, randomly dispersed and highly crystalline. The crystallinity was confirmed by XRD (Figure 4.12B) results. Other images from TEM analyses are shown in Appendix F.3.

4.9 Infrared Spectroscopy (IR)

IR was used to identify phases present in the supported nitride catalysts based on their IR absorption and vibration bands.

There was not much difference in the spectra for the various catalysts studied. The variation of Ni and W loading did not have any significant impact on the IR spectra. Similarly, variation of nitriding temperature did not show any noticeable differences in the spectra. The main difference observed was in the Cat-P samples. Figure 4.25A displays the IR spectra for reference materials and Cat-P samples with peaks labelled (a) to (d). The features in this figure were also observed in the Cat-Ni, Cat-W and Cat-T_N samples (see Figure F.11 and Figure F.12). Generally, a broad peak (a) with high intensity occurred at 3440 cm^{-1} in all the spectra. There was no apparent change in the peak intensity in all the catalysts studied. Hydroxyl stretching region is reported (Ferdous et al., 2004a) to be within the range 3000-4000 cm^{-1}. Possible hydroxyl groups that could be responsible for the observed peak are adsorbed H_2O, basic -OH groups (3727-3762 cm^{-1}) or acidic –OH groups (3672) (DeCanio and Weissman, 1995). Peak (a) stretches from 3310 to 3660 cm^{-1}. This means that the observed peak cannot be due to acidic or basic OH groups on the catalyst surface. In the study of chromium (III) supported on aluminum-nitride-surfaced alumina, Puurunen et al. (2003) observed a peak at 3395 and assigned it to N-H

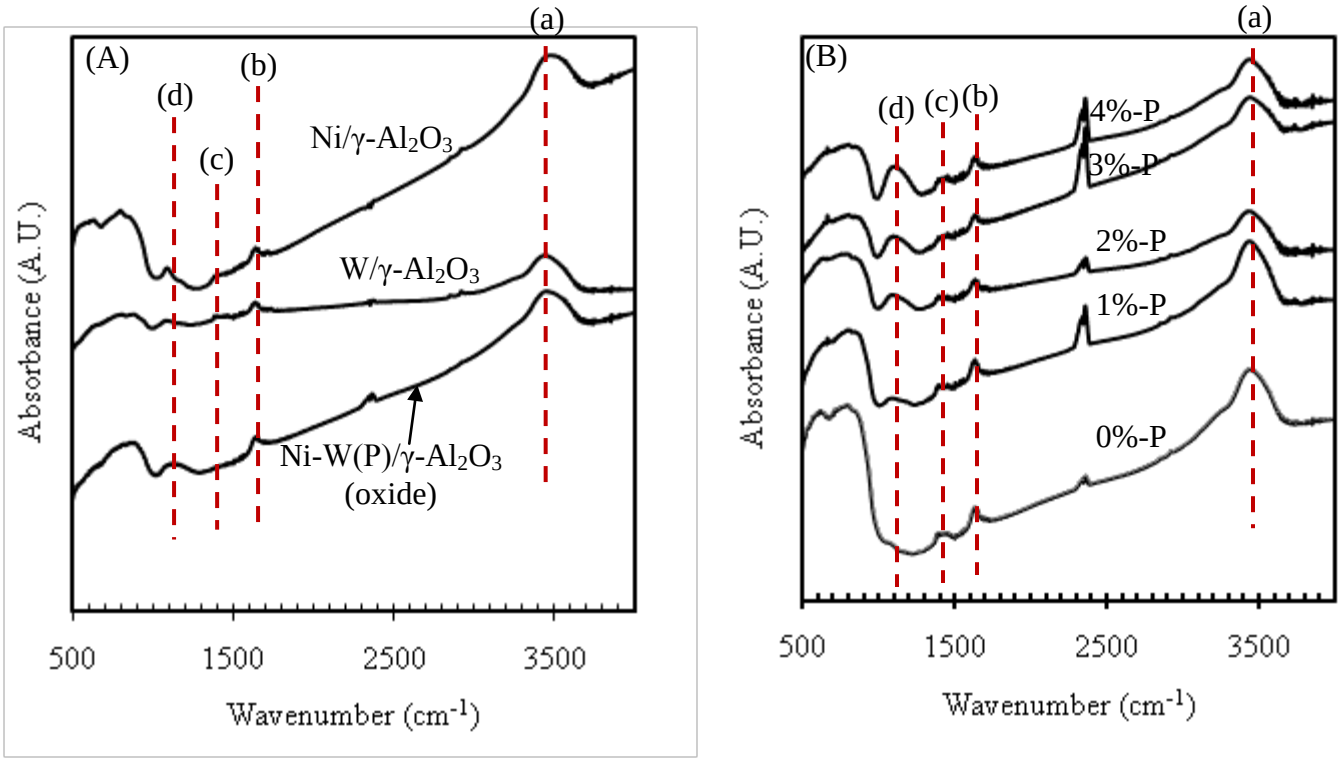

Figure 4.25: Infrared spectra of (A) reference oxide (P, 2 wt%) and nitrides (Ni, 10 wt%), and (B) Cat-P nitride samples in the 400-4000 cm^{-1} region. Conditions: 30 wt% W, 4 wt% Ni and T_N of 700 °C.

bond stretching. Considering that the spectra for an oxide catalyst (see Figure 4.25A) showed a similar peak, peak (a) cannot be attributed to N-H group stretch. The peak may therefore be due to the presence of adsorbed water on the surface of the catalyst (Ferdous et al., 2004a).

The peak at 1623 cm^{-1}, (b), was observed in all catalysts and is assigned to the Al-O bridge bond stretching. This is in agreement with reports in the literature (Ferdous et al., 2004a) that the frequency range for Al-O bond stretching is 900–1800 cm^{-1}. It has also been reported that adsorbed NH_3 on γ-Al_2O_3 gives infrared peaks at 1620, 1484 and 120 cm^{-1} (Chen et al., 2004). However, the peak at 1623 cm^{-1} was not assigned to adsorbed NH_3 on γ-Al_2O_3 because it was observed on the oxide catalyst as well. The peak at 1400 cm^{-1}, (c), was observed on all the nitride catalysts. Nagai et al. (2000a) assigned a peak at 1264 cm^{-1} to chemisorbed NH_3 on Lewis acid sites of Mo/Al_2O_3 nitride catalysts. They also reported that NH_3 can interact with Brønsted acid sites of Mo_2N to form NH_4^+ species giving peaks in the region 1450-1485 cm^{-1}. Peak (c) is therefore assigned to the presence of adsorbed NH_3 species interacting with acid sites on the catalyst surface seeing that it was absent in the oxide sample. The assignment is also in agreement with the report of Chen et al. (2004). In the Cat-P samples, the peak at 1090 cm^{-1}, (d), increased in intensity with increase in P loading. This must be due to the presence of $[PO_4]^{3-}$ on the surface of the catalysts. The phosphates are formed from interaction of H_3PO_4 with the Al_2O_3 support (Sigurdson et al., 2008; Atanasova and Halachev, 1994). As P loading increased, more $[PO_4]^{3-}$ were formed leading to increase in the peak intensity. Peak (d) can therefore be assigned to the presence of P-O-Ni and/or P-O-W bonds on the surface of the support. The peaks below 1000 cm^{-1} were observed in all the catalysts and may be due to vibration of Al-O bridge bonds and/or Ni-N, W-N bonds (Niemantsverdriet, 1993).

4.10 X-ray Absorption Near Edge Structure (XANES)

XANES experiments were performed to determine the oxidation state of P, the type of P species and how synthesis conditions affect the properties of P in the catalyst. All spectra were normalized to the intensity of the incident beam. The analysis is based on total electron yield which is a measure of surface properties. Figure 4.26 shows the L-edge XANES spectra of nitride catalyst samples with peaks labelled (a) to (c). Catalyst (I), and catalyst (II), all synthesized at 700 °C, exhibited peaks in the same position while that of catalyst (III), synthesized at 500 °C shifted to higher temperature. Peak (a) which was observed in all three catalysts, occurred at

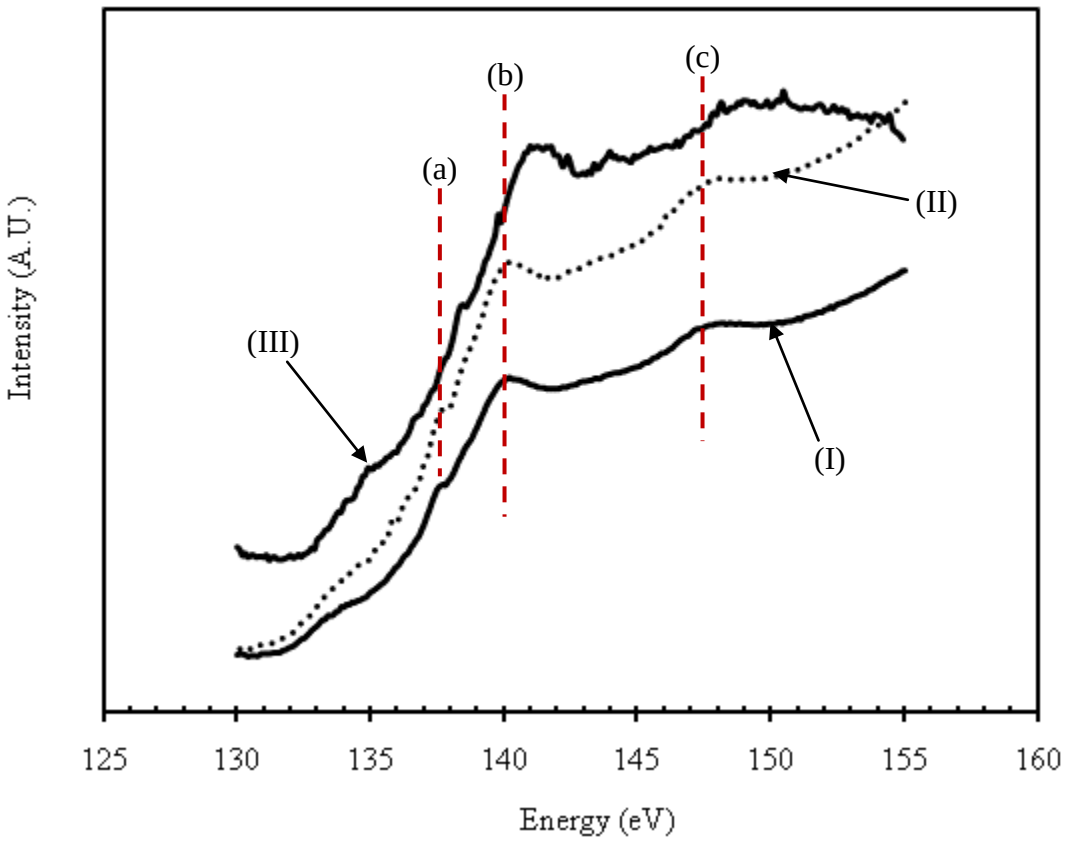

Figure 4.26: P L-edge XANES spectra of selected Cat-P nitride. Conditions: 30 wt% W, 4 wt% Ni, (I) 2 wt% P and T_N of 700 °C; (II) 4 wt% P and T_N of 700 °C; (III) 2 wt% P and T_N of 500 °C.

137.6 eV for the 700 °C synthesized catalyst and at 138.5 eV for the 500 °C synthesized catalyst Peak (b) also appeared in all samples. It occurred at 140.2 eV for the 700 °C T_N catalyst but shifted to 141.2 eV for the 500 °C T_N catalyst. Similarly, peak (c) occurred at 148 eV for the 700 °C T_N catalyst but shifted to 149.2 eV for the 500 °C T_N catalyst. In a study of the P $L_{2,3}$-edge XANES, Kruse et al. (2009) made similar observations for $AlPO_4$ and $AlPO_4{\cdot}H_2O$ samples. They observed that the peaks of $AlPO_4{\cdot}H_2O$ shifted to higher energy compared to those of $AlPO_4$. Kasrai et al. (1999) also made similar observation for $FePO_4$ and $Ca_3(PO_4)_2$. The peaks in Figure 4.26 can therefore be assigned to $[PO_4]^{3-}$ species on the catalyst surface. This is in agreement with results of the IR studies (Figure 4.25) where peak (d) was associated with the presence of P-O-Ni and P-O-W bonds. The shift in peak energy for the 500 °C T_N sample may be due to the presence of strongly adsorbed NH_3 on the catalyst. The NH_3 is absent from the 700 °C T_N catalysts (see Figure 4.3B) that is why their peaks occurred at lower energies

CHAPTER 5
HYDROTREATING OF GAS OIL OVER NITRIDE CATALYSTS

Hydrotreating experiments were performed in four phases as follows:

1. the effects of catalyst synthesis parameters (P, Ni, W and T_N) on catalyst activity,
2. catalyst stability to deactivation,
3. effects of process conditions (temperature, Pressure and LHSV) and
4. the effect of H_2S on catalyst stability.

Catalyst activity was measured in terms of hydrodesulfurization (HDS), hydrodenitrogenation (HDN) and hydrodearomatization (HDA). Under the effects of synthesis parameters, work was done in terms of catalyst screening to determine catalysts preparatory conditions that gave highest HDS, HDN and HDA activities. This was followed by investigating reaction conditions that gave the best activity and the effects of process conditions on optimized catalyst (optimized for P, Ni loading and nitriding temperature). Also investigated was stability of the optimized catalysts and kinetic analyses. The next stage was to investigate the effect of tungsten loading on the catalyst activity and the effect of H_2S on the nitride catalysts. This was done because in the previous work, tungsten loading was kept constant.

5.1 Catalyst Precoking

Precoking is the process where catalysts are exposed to the feed at reaction conditions to stabilize their activity prior to actual experimental runs. The precoking step is necessary because hydrotreating catalysts are known to undergo initial steep drop in activity on exposure to the feed due to deposition of coke on the catalysts. The activity of a good catalyst should stabilize for the duration of the reaction process after the initial drop.

Precoking for the experimental runs was carried out over six days. During this period, the catalyst was found to be stable for activity studies. Precoking was performed at the beginning of each experimental run with light gas oil feed at 375 °C, 9.0 MPa, LHSV of 1 h^{-1} and hydrogen-to-oil ratio of 600 (v/v). Figure 5.1 shows the precoking results for HDN of selected catalysts. The results show stable catalyst activity by the fifth and sixth days of precoking. It was observed for some of the catalysts that there was a steady rise in activity till stability was attained contrary to normal observation. The trend may be due to the mode of introduction of the

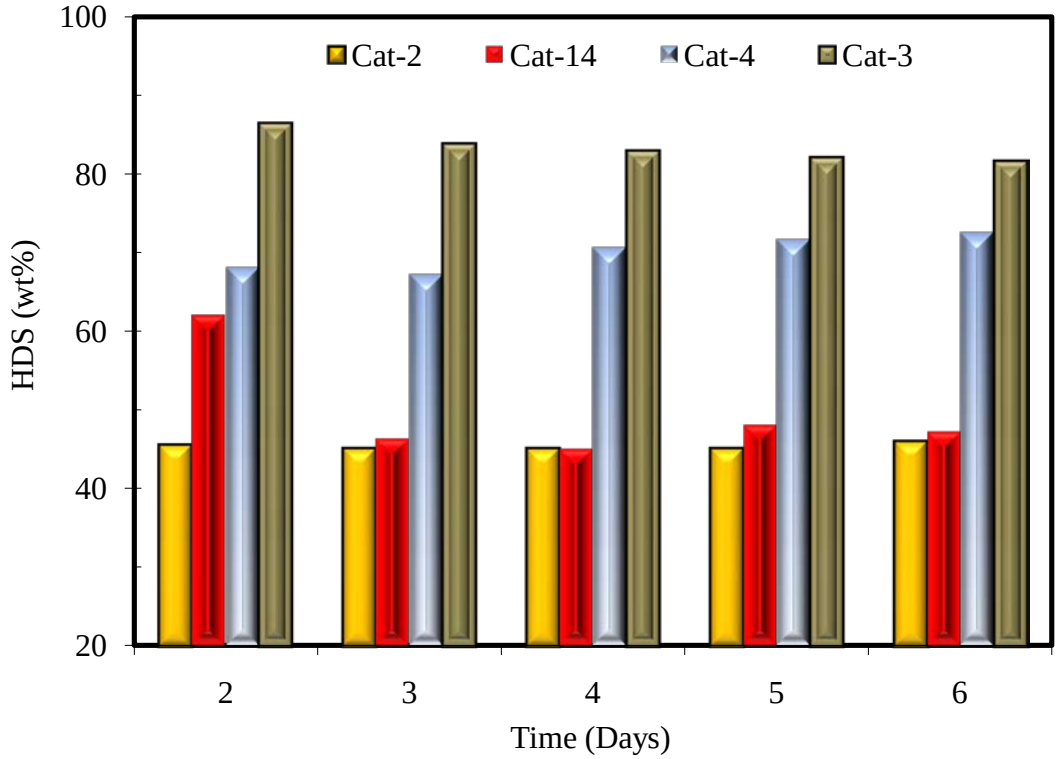

Figure 5.1: HDN activity for nitride catalyst precoking. Conditions: T, 375°C; P_H, 9.0 MPa; LHSV, 1 h^{-1} and H_2/oil: 600 ml/ml. 15 wt% W, (Cat-2) 6.4 wt% Ni, 1 wt% P and T_N of 739 °C; (Cat-3) 4 wt% Ni, 2.5 wt% P and T_N of 650 °C; (Cat-4) 1.6 wt% Ni, 4 wt% P and T_N of 739 °C; (Cat-14) 1.6 wt% Ni, 1 wt% P and T_N of 561 °C.

gas oil feed after the passive layer reduction. For conventional catalysts, the gas oil is preceded by a lighter feed (butanethiol in straight run gas oil) which is used in their activation. In the case of the nitride catalysts, no lighter feed was required prior to introduction of gas oil as the catalyst activation was done in the gaseous phase. To avoid the risk of completely deactivating the catalyst through coke formation on introduction of the gas oil, the reactor was run at 100 ºC immediately after passive layer reduction until the catalyst bed was wet and hydrogen gas had been introduced. This means the catalyst activity transitioned from less severe conditions (100 °C and He flow) to more severe conditions (375°C and H_2 flow) and that might be why the activity increased for some catalyst over the precoking period. Another reason for the increase in activity might be due to modification of the catalyst surface from the nitride to sulfide phase. There are conflicting reports in the literature regarding stability of nitride catalysts in H_2S environment. A study on this subject is discussed in Section 5.5. Another important observation from the precoking results was reproducibility of the experimental data. Precoking results for R-3 and R-6 show that the experimental data is reproducible. In general, the maximum error observed was ±3 wt%.

5.2 Effect of Catalyst Synthesis Parameters on HDS, HDN and HDA

Effect of synthesis parameters was studied in two stages. The first stage was to study the relationship between synthesis parameters and hydrotreating activity. This was done via statistical experimental design (Central Composite Circumscribe-Response Surface Method) in which 20 Ni-W(P)/γ-Al_2O_3 nitride catalysts were synthesized. The second stage (see Chapter 6) was designed to help correlate the catalyst hydrotreating activity to surface properties through detailed characterization. The catalysts were tested for HDS, HDN and HDA activities at the following conditions: temperature, 350 ºC; pressure, 9.0 MPa; LHSV, 2 h^{-1}; and hydrogen to oil ratio, 600 ml/ml.

Statistical modeling was used to analyze results of the catalyst screening work. Steps taken in the analyses of each response included model development (see Appendix B.2), generation of model graphs as well as model prediction of actual experimental data and parameter optimization. Model graphs for central composite design experiments are normally displayed as 3-D surfaces. However, such displays are often complicated and not easy to follow. To simplify the charts for discussion, they were converted to 2-D, i.e. for each response, two parameters were

kept constant while the other was varied. The horizontal axis was made dimensionless based on Equation (B.3) in order to fit all three parameters to a single chart.

Generally, catalyst synthesis properties such as Ni, P and W loading increased the hydrotreating activity of LGO. This is due to creation of more active sites on the catalyst. Excessive increase in Ni (8 wt%) and P (> 2.5 wt%) reduced the catalyst activity for HDS, HDN and HDA due to formation of less active species. The catalyst activity for all hydrotreating processes (HDS, HDN and HDA) were optimized at 2.5 wt% Ni, 1 wt% P, T_N of 560 °C and 15 wt% W but the optimization parameters may not hold for higher W loading as W loading was found to further enhance the catalyst activity.

5.2.1 Catalyst Screening: HDS

Figure 5.2A shows results of HDS of light gas oil over Ni-W(P)/γ-Al_2O_3 nitride catalyst at the reference conditions 4 wt% Ni, 2.5 wt% P and T_N of 650 °C (see Figure B.2A for a 3-D representation). The HDS response generally followed a quadratic trend with the maximum (84 wt% conversion) occurring at ~ 4 wt% Ni. Any further increase in Ni concentration resulted in a decrease in the catalyst HDS activity. This decreased activity may be due to formation of more HDS inactive sites relative to active sites on the catalyst surface. Similar trends have been reported in the literature (Escalona et al., 2007). Rangwala et al. (1990) found the most active ratio for Ni-Mo combination in the hydrogenation of quinoline to be 0.24. The results also show that increasing P concentration increased the HDS activity to a maximum (84 wt% at P loading of 2.5 wt%) and then decreased. Any further increase in P concentrations from the maximum condition resulted in decreased catalyst HDS activity due to loss of active sites (increased polymerization of tungsten leading to the formation of W_2N rather than bimetallic Ni-W nitride species). Similar observations were reported in the literature (Atanasova et al., 1997).

Within the range of conditions studied, HDS slowly increased to a maximum (86 wt% at 575 °C) and decreased sharply with further increase in nitriding temperature to a minimum of 78wt% at 740 °C. The reduction in HDS activity with T_N might be due to reduced dispersion and creation of less active sites on the catalyst surface. High nitriding temperature leads to metal particle agglomeration which leads to reduced dispersion. Agglomeration prevents accessibility of reacting molecules to the active sites of the catalyst, hence reduction in the activity. Figure 5.2B illustrates adequacy in prediction of the observed data with a minimum accuracy of

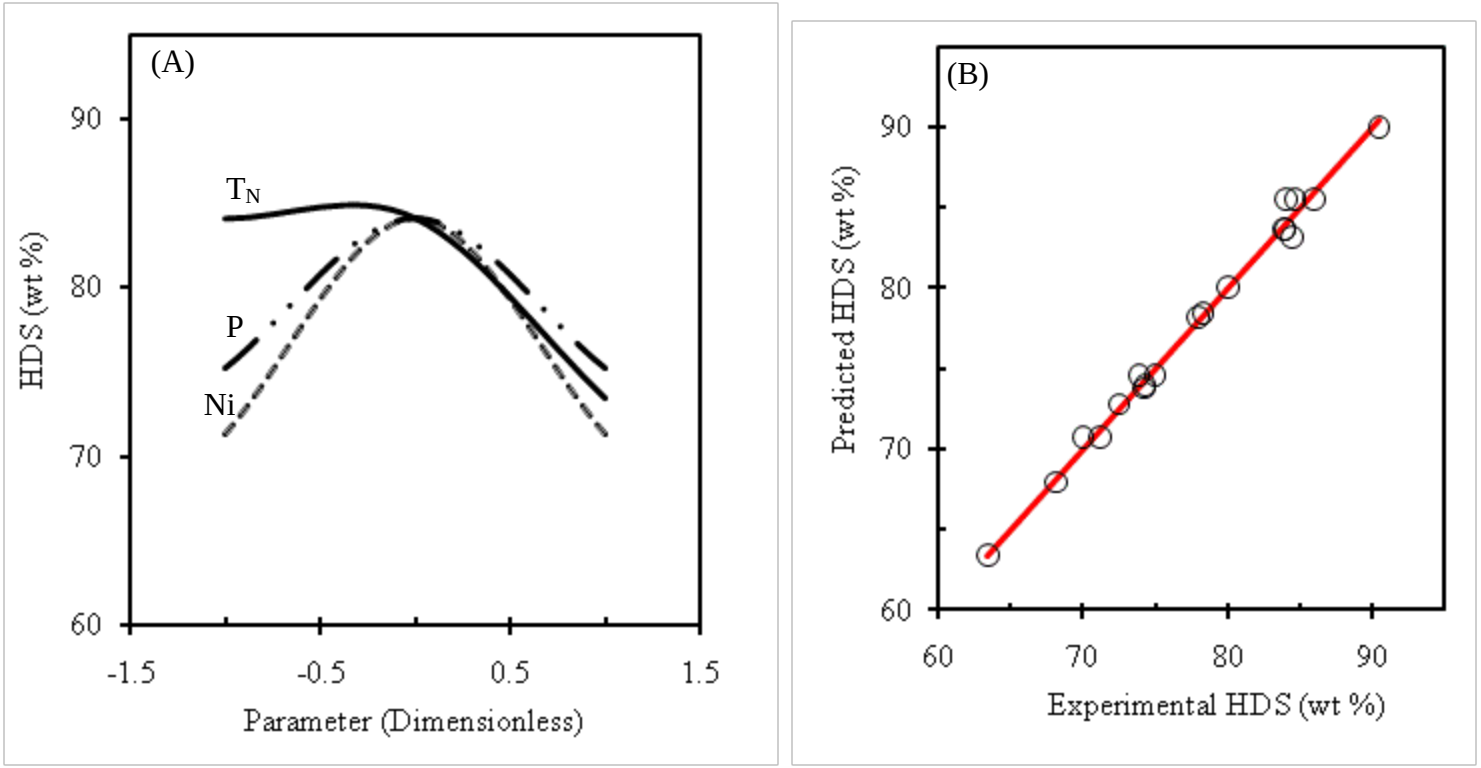

Figure 5.2: (A) Perturbation and (B) parity plots for Effects of synthesis parameters on HDS of LGO hydrotreated at 350 °C, 9.0 MPa, LHSV of 2 h^{-1} and H_2/Oil of 600 ml/ml. Reference Points: 4.0 wt% Ni, 2.5 wt% P and T_N of 650 °C.

98 wt%.

5.2.2 Catalyst Screening: HDA

Figure 5.3A shows the effects of synthesis parameters on HDA of light gas oil. Similar to the HDS activity, HDA activity also went through a maximum as the synthesis parameters (Ni loading, P loading and T_N) were increased. The maximum conversion observed was ~ 59 wt% and occurred at 4 wt% Ni, 2.5 wt% P and T_N of 650 ºC). The loss in activity as the synthesis conditions deviated from 4 wt% Ni, 2.5 wt% P and 650 ºC T_N can be attributed to loss in number of active sites or loss in dispersion of the catalyst. Figure 5.3B shows good agreements between model predicted and experimental values which confirms the significance and reliability of the model used.

5.2.3 Catalyst Screening: HDN

HDN of light gas oil over Ni-W(P)/γ-Al_2O_3 nitride catalyst (Figure 5.4) followed a near linear trend. The activities increased with Ni and P loading but decreased with T_N. The rate of increase in activity diminished with increase in Ni and P loadings which may be due to formation of more acidic sites which may preferentially crack rather than hydrotreat. It can also be attributed to the formation of less active species such as Ni_3N and Ni rather than bimetallic Ni_2W_3N on the catalyst surface (see Section 4.5.2). Generally, high nitriding temperatures were found to decrease the HDN activity. It has been reported (Colling et al., 1996; Furimsky, 2003; Guerrero-Ruiz et al., 1999) that the surface and the sub-surface of nitride catalyst particles are both utilized during catalytic reactions. At low surface area, which is attributed to the presence of large particle, the sub-surface of the catalyst particles is exposed, in addition to the surface particles, and accessible to reacting molecules which leads to higher activity (Choi et al., 1992).

In the catalyst screening studies, surface area analyses of the catalysts showed that the surface area reduced with decrease in nitriding temperature (see Appendix Figure F.1). This means that the low nitriding temperature samples formed large particles which exposed the sub-surface for enhanced activity. This might be why the HDN activity increased with decrease in nitriding temperature.

The optimized HDN conversion within the range of conditions studied was 60 wt% and occurred at 1.6 wt% Ni, 1 wt% P, and T_N of 560 ˚C. Figure 5.4B shows that the observed data

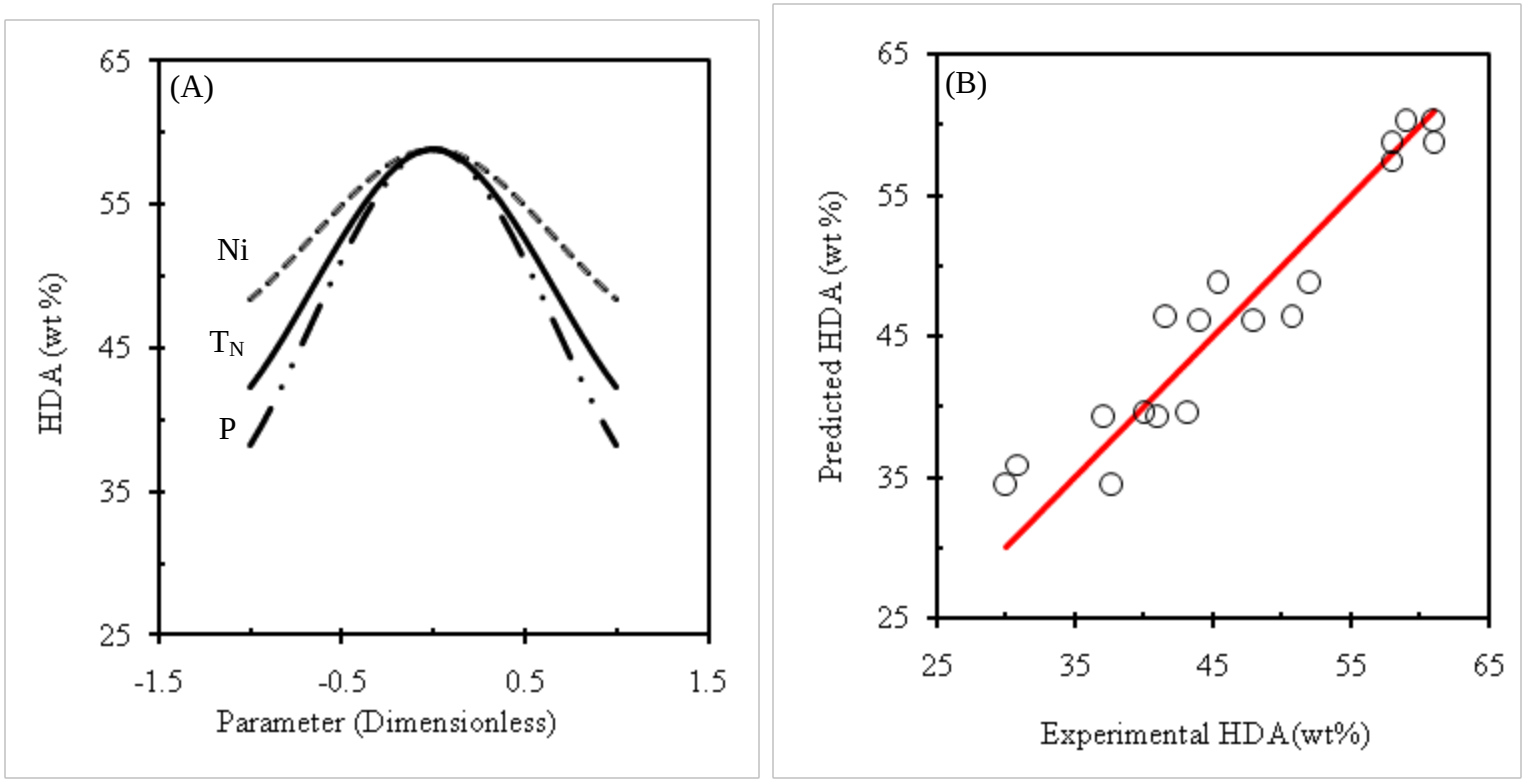

Figure 5.3: (A) Perturbation and (B) parity plots for Effects of synthesis parameters on HDA of LGO hydrotreated at 350 °C, 9.0 MPa, LHSV of 2 h^{-1} and H_2/Oil of 600 ml/ml. Reference Points: Ni = 4.0 wt%, P_H = 2.5 wt%, T_N = 650 °C.

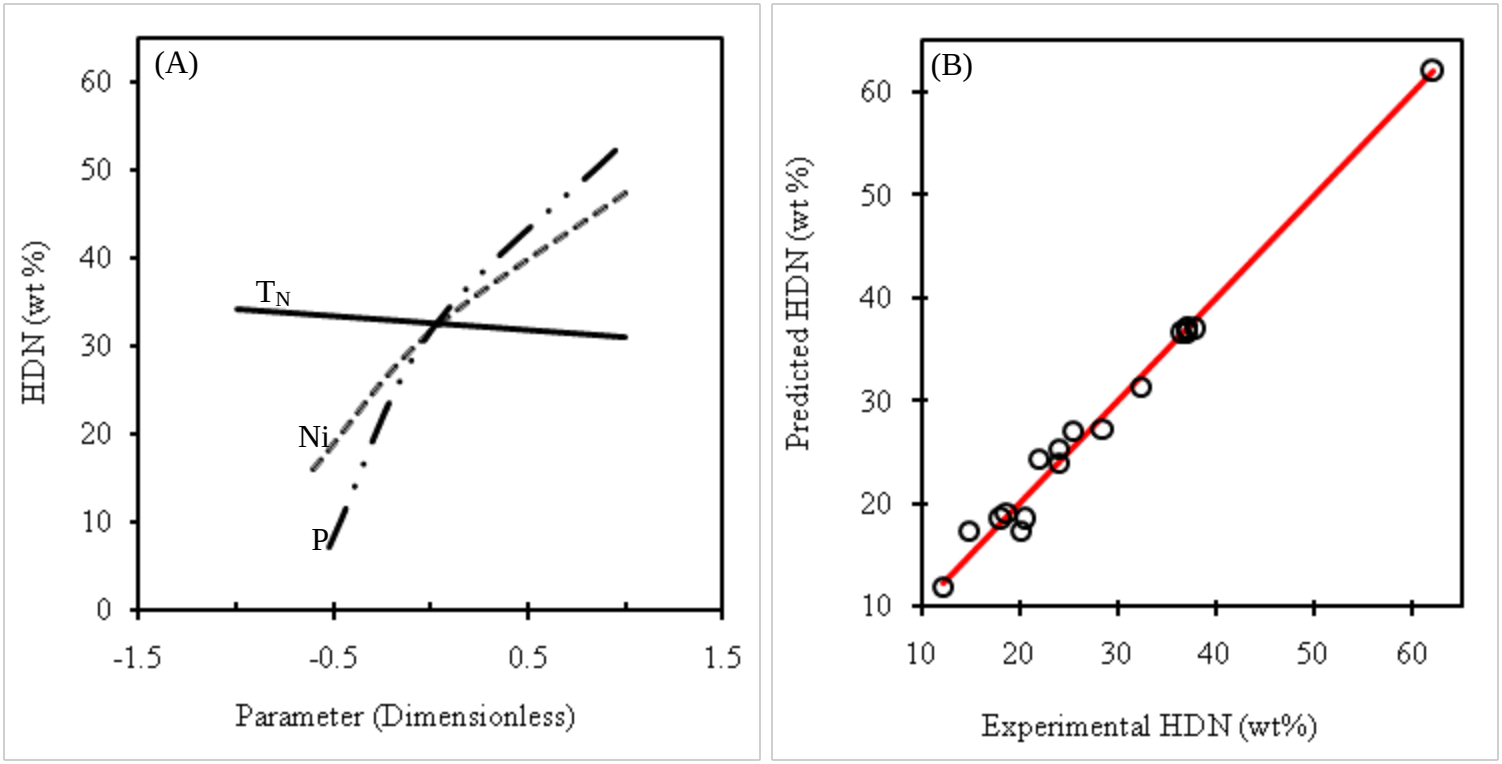

Figure 5.4: (A) Perturbation and (B) parity plots for Effects of synthesis parameters on HDN of LGO hydrotreated at 350 °C, 9.0 MPa, LHSV of 2 h^{-1} and H_2/Oil of 600 ml/ml. Reference Points: 4.0 wt% Ni, 2.5 wt% P and T_N of 650 °C.

could sufficiently be predicted by the model with maximum error of ±2.8 wt%. Overall optimization for all three activity studies (HDS, HDN and HDA) was performed with the objective of maximizing activity and minimizing Ni, P and T_N. The overall optimized catalyst composition was: 2.5 wt% Ni, 1 wt% P, 15 wt% W and T_N of 560 ˚C and had HDS, HDN and HDA conversions of 88, 59 and 47 wt%, respectively.

5.2.4 Catalyst Screening: Effect of Tungsten Loading

Previous work on catalyst syntheses and screening were done with constant W loading (15 wt %). In the present work, the focus was to study the effects tungsten loading has on HDS and HDN activities. Subsequently, tungsten nitride catalysts with tungsten loadings of 15, 20 and 25 wt% were prepared and tested for HDS and HDN activities. Hydrotreating temperature was varied (340, 350 and 360 ˚C) while pressure (9.0 MPa), LHSV (2 h^{-1}) and hydrogen to oil ratio (600 ml/ml) were kept constant. Figure 5.5 shows plots of the sulfur and nitrogen conversion at various catalyst tungsten loadings against temperature. Increase in tungsten loading increased both sulfur and nitrogen conversions at the conditions studied. Increase in the hydrotreating temperature increased both HDS and HDN without any sign of thermal equilibrium. For catalysts of the same tungsten loading, the HDS activity was higher than the HDN activity.

The increase in catalyst tungsten loading increased the number of active sites on the catalyst surface leading to increased activity. The trend is in agreement with results of BET surface area and oxygen chemisorption studies shown in Figure F.1. As the tungsten loading increased, so did the oxygen uptake of the catalysts. The amount of adsorbed gas in chemisorptions is a measure of the number of exposed metals or active sites on the catalyst surface (Satterfield, 1980; Yu et al., 1997). This means that the number of exposed metals and hence the active sites on the catalyst surface increased with increase in tungsten loading. On the other hand, the BET surface area decreased suggesting increased plugging of catalyst pores with increase in W loading. However, the effect of the decreased surface area was offset by increase in number of active sites as W loading increased. This phenomenon has been observed by other authors (Cruz et al., 2002). Results of nitrogen analyses of nitride catalysts with varying tungsten loading are also shown in Table 5.1. There was an increase in nitrogen content of the nitride catalysts with increase in tungsten loading. The increase in catalyst nitrogen content can be attributed to the formation of more nitride species and active sites on the catalyst surface leading to increased

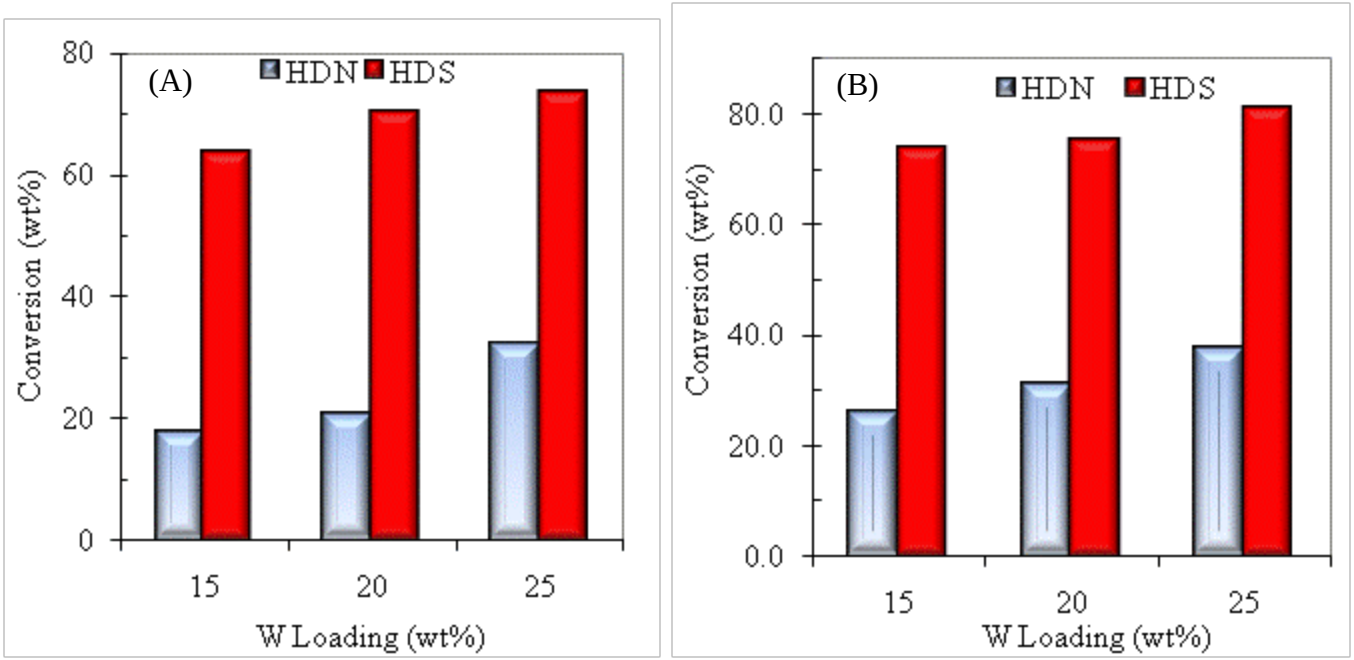

Figure 5.5: Effect of tungsten loading on HDS and HDN of LGO using Ni-W(P)/γ-Al_2O_3 nitride catalyst at (A) 350 °C and (B) 360 °C. Conditions: 2.5 wt% Ni, 1 wt% P and T_N of 560 ˚C. Process conditions: P_H = 9.0 MPa, LHSV= 2 h^{-1}, H_2/oil = 600 ml/ml.

Table 5.1 BET, chemisorption and nitrogen content of tungsten nitride catalysts

Tungsten Loading (wt%)	BET Surface Area (m^2/g)	Chemisorption ($\mu mole.g^{-1}$)	Nitrogen Content (wt %)
15	193	52.2	1.2
20	190	61.4	1.6
25	176	87.0	2.0

activity.

5.3 Effect of Process Conditions on HDS and HDN

The effect of process conditions on hydrotreating of light gas oil was studied using a nitride catalyst optimized for the synthesis conditions. The optimization studies were based on the catalyst screening work discussed in Section 5.2 above. The catalyst used was a nickel-phosphorus-promoted tungsten nitride on alumina support with composition of 2.5 wt% Ni, 1 wt% P, 15 wt% W and T_N of 560 °C. The process parameters of interest were temperature (340 to 385 ºC), pressure (6.2 to 9.0 MPa), and liquid hourly space velocity (1 to 3 h^{-1}). Hydrogen to oil ratio was constant at 600 ml/ml. The experiment was designed using Central Composite design (see Appendix B for description). Detailed design points as well as HDS and HDN results are shown in Table 5.2 (coded values in brackets).

5.3.1 Effect of Process Conditions on HDS

Figure 5.6A is a plot showing the effects the parameters have on HDS with deviation from reference point (0, 0, 0) i.e. (363 ºC, 7.6 MPa, 2 h^{-1}). While process temperature had a positive effect on HDS activity, liquid hourly space velocity had negative effect on HDS. Pressure had less significant effect on HDS within the conditions studied which suggests that direct desulfurization route may be the preferred method for sulfur removal on Ni-W(P)/γAl_2O_3 catalysts. There are reportedly (Ancheyta, et al., 2002) two possible routes for HDS reactions during hydrotreating. They are: 1, direct sulfur removal method and 2, hydrogenation prior to desulfurization. Section 2.1.1.1 provides illustration of the two different sulfur removal mechanisms in hydrotreating of gas oil). The preferred method is dependent on the operating conditions, the type of catalyst and/or the type of reactants. It is reported (Prins et al., 2006; Rabarihoela-Rakotovao et al., 2006) that while simple compounds like thiophene and benzothiophene prefer mechanism no. 1, substituted thiophenic compounds, especially with substitutions in 4, 6 positions, tend to prefer mechanism 2 during reaction. A pressure-influenced process will suggest preference for method two, i.e. hydrogenation prior to desulfurization (Girgis and Gates, 1991). Since the results were not significantly influenced by pressure, it can only suggest that the preferred method of reaction is direct desulfurization. Temperature had a parabolic effect on HDS while the effect of LHSV was linear. Temperature had the most significant effect on HDS. With

Table 5.2: Design factors, levels and conversions for HDS and HDN of light gas oil (coded values in brackets).

Run Number	Temperature (°C)	Pressure (MPa)	LHSV (h^{-1})	HDS (wt%)	HDN (wt%)
1	363 (0.0)	7.6 (0.0)	0.3 (-1.7)	78.4	79.6
2	363 (0.0)	7.6 (0.0)	3.7 (1.7)	98.3	96.8
3	325 (-1.7)	7.6 (0.0)	2.0 (0.0)	81.0	79.6
4	385 (1.0)	9.0 (1.0)	1.0 (-1.0)	94.8	96.8
5	340 (-1.0)	9.0 (1.0)	3.0 (1.0)	55.4	56.3
6	363 (0.0)	9.9 (-1.7)	2.0 (0.0)	83.8	90.7
7	363 (0.0)	7.6 (0.0)	2.0 (0.0)	96.0	90.7
8	385 (1.0)	9.0 (1.0)	3.0 (1.0)	53.2	53.1
9	385 (1.0)	6.2 (-1.0)	3.0 (1.0)	96.6	95.6
10	340 (-1.0)	9.0 (1.0)	1.0 (-1.0)	88.8	84.2
11	363 (0.0)	7.6 (0.0)	2.0 (0.0)	83.1	84.2
12	363 (0.0)	7.6 (0.0)	2.0 (0.0)	95.0	97.6
13	400 (1.7)	7.6 (0.0)	2.0 (0.0)	70.8	71.6
14	340 (-1.0)	6.2 (-1.0)	1.0 (-1.0)	83.0	84.2
15	363 (0.0)	5.3 (-1.7)	2.0 (0.0)	85.2	84.2
16	340 (-1.0)	6.2 (-1.0)	3.0 (1.0)	81.2	84.2
17	385 (1.0)	6.2 (-1.0)	1.0 (-1.0)	85.4	84.2
18	363 (0.0)	7.6 (0.0)	2.0 (0.0)	87.2	84.2
19	363 (0.0)	7.6 (0.0)	2.0 (0.0)	85.3	84.2
20	363 (0.0)	7.6 (0.0)	2.0 (0.0)	78.4	79.6

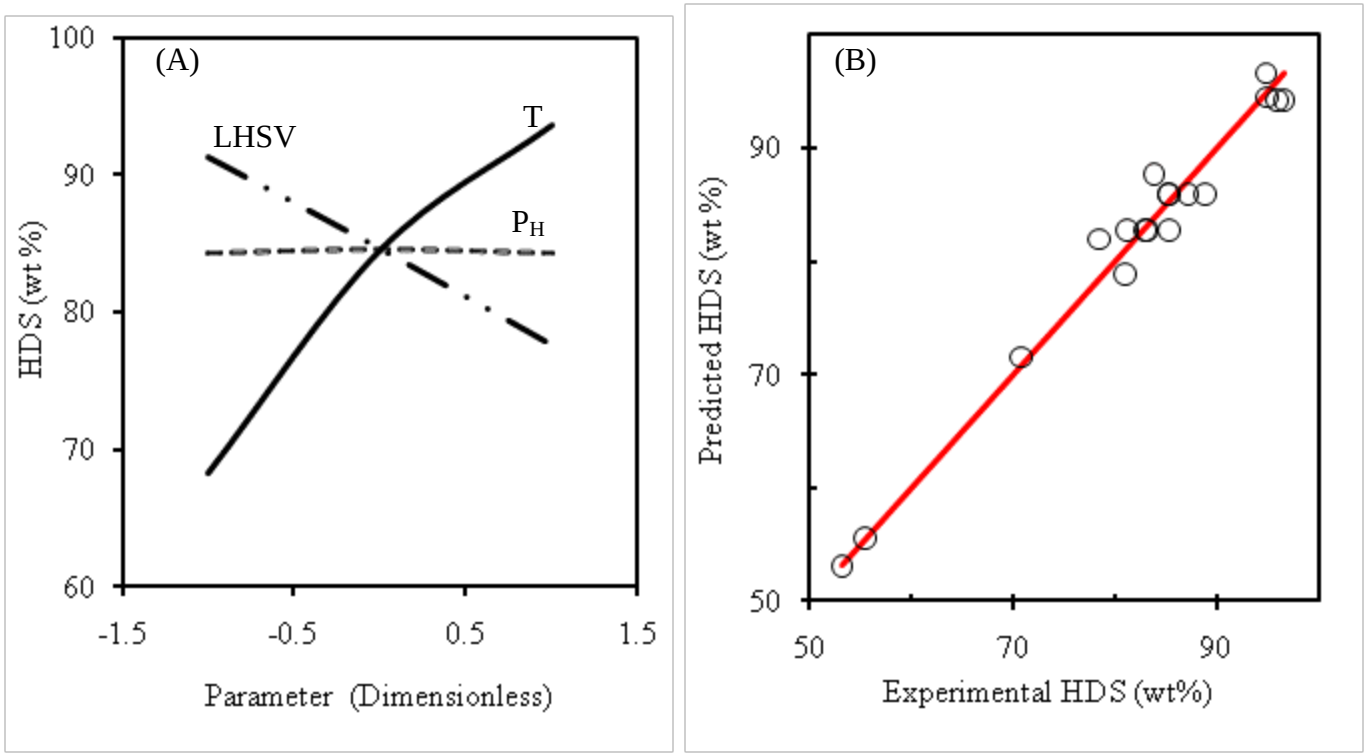

Figure 5.6: (A) Perturbation and (B) parity plots for effects of process conditions on HDS of LGO over Ni-W(P)/γ-Al_2O_3 nitride catalyst. Process conditions: 340 - 385 °C, 6.2 – 9.0 MPa, LHSV of 1 - 3 h^{-1} and hydrogen/oil of 600 ml/ml (STP). Catalyst conditions: 2.5 wt% Ni, 1 wt%, P and T_N of 560 °C.

all other parameters at their reference points, HDS changed by 26 wt% as temperature was varied from minimum to maximum value and may be the parameter of choice to influence the process. LHSV effect on HDS within the same range was 15 wt%. Although temperature had a parabolic effect on HDS, it can be inferred from Figure 5.6A that the catalyst activity did not reach a maximum (see Figure B.4). The highest HDS activity of 98.3 wt% occurred at 385 ºC and 1 h^{-1} LHSV. The maximum HDS activity of the catalyst may occur beyond 385 ºC. Figure 5.6B shows good agreement between experimental and model predicted data.

One reason for using experimental design for this work was to study interaction effects between parameters. The presence of interaction indicates dependence of parameter effect on each other and may also suggest likelihood of synergistic effects. Figure 5.7 shows interaction between temperature and LHSV for the HDS process. It shows that LHSV influences how temperature affects HDS. For instance, within the temperature range 340 to 385 ºC, the change in HDS at LHSV of 3 h^{-1} was 34.6 wt% while it was 17.2 wt% at LHSV of 1 h^{-1}. This means temperature impacts HDS more at high LHSV. Similarly, LHSV impacted HDS more at lower temperatures. The reason may be because at high temperatures, most of the sulfur compounds were already converted to hydrocarbon products that is why the added impact of LHSV was low.

5.3.2 Effect of Process Conditions on HDN

Unlike HDS, HDN was significantly affected by all three parameters. Figure 5.8 shows effects of the parameters on HDN with deviation from reference points (i.e. 0, 0, 0) or (363 ºC, 7.6 MPa, 2 h^{-1}). The associated model equation and statistics are shown in Table B.1. All parameters had almost linear effects on HDN. Temperature and pressure had positive effects on HDN while LHSV had negative effect. Similar to the HDS process, temperature had the most significant effect on the HDN process. Varying temperature, pressure and LHSV each separately and keeping the other two parameters at their reference points resulted in 47, 14 and 30 wt% changes in HDN for, respectively.

Effect of pressure was not as strong as the other parameters. It was about half the effect of LHSV and about a third the effect of temperature (see Figure 5.8). It's been reported (Girgis and Gates, 1991; Ho, 1988) that for conventional catalysts, HDN always goes through hydrogenation prior to denitrogenation. Despite its moderate impact, the positive effect of pressure on HDN suggests similar reactivity for the Ni-W(P)/γ-Al_2O_3 nitride catalyst. Nitride catalysts are

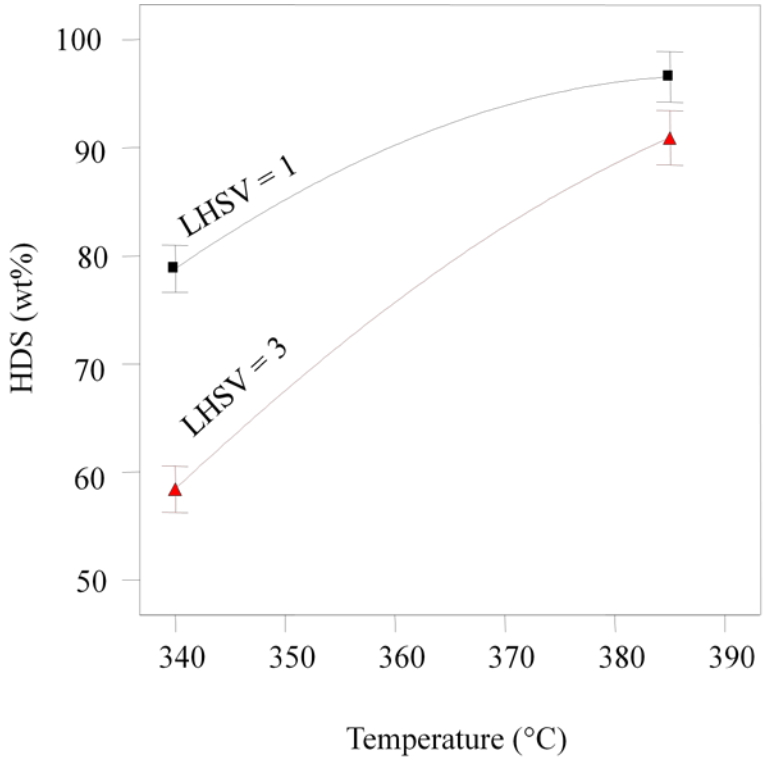

Figure 5.7: HDS Interaction effect between temperature and LHSV over Ni-W/γ-Al_2O_3 nitride using light gas oil. P_H, 7.6 MPa; Hydrogen/oil, 600 ml/ml (STP).

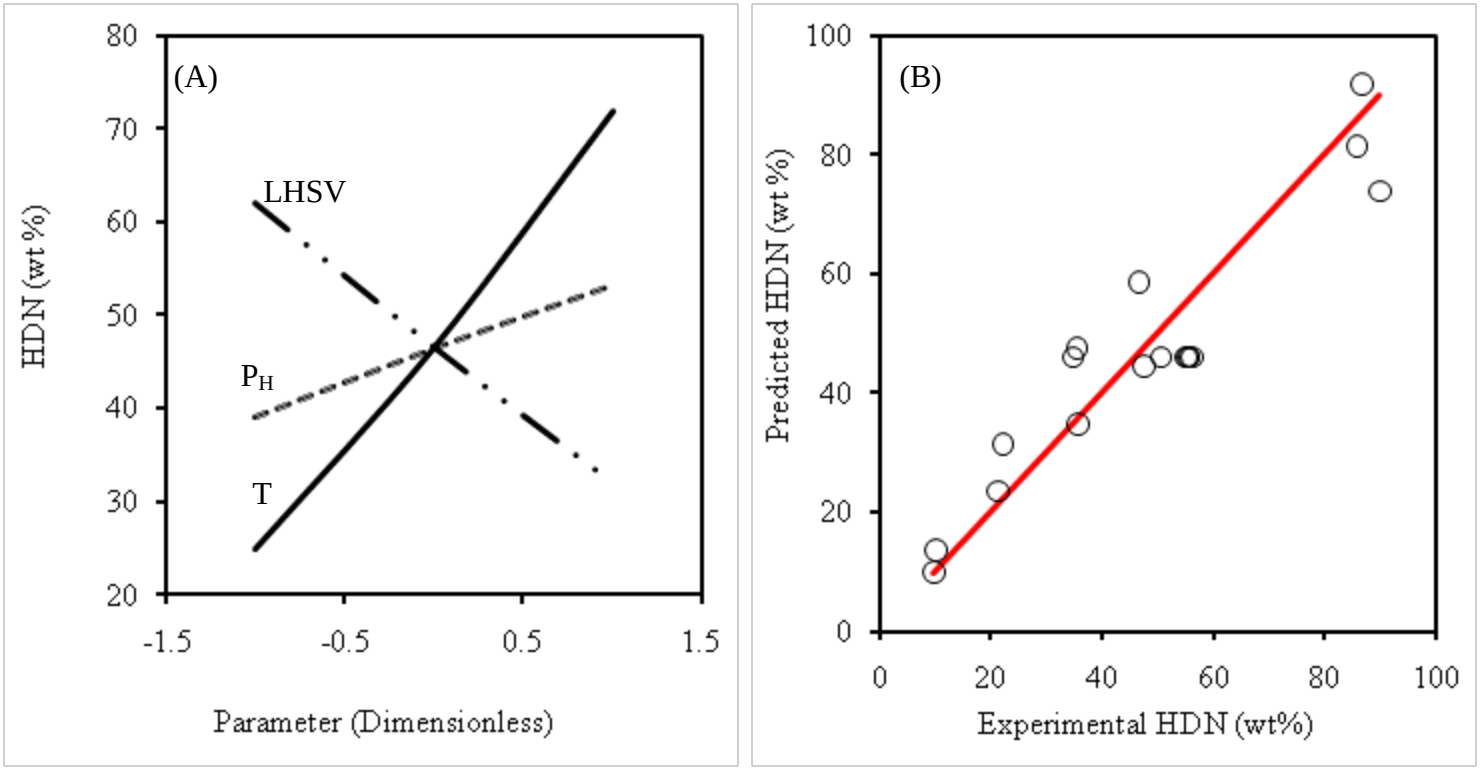

Figure 5.8: Perturbation plot for HDN of light gas oil using tungsten nitride catalyst. Reference conditions: 340 - 385 $^{\circ}$C, 6.2 - 9.0 MPa, LHSV of 1 - 3 h^{-1} and hydrogen/oil: 600 ml/ml (STP).

known for their strong hydrogenation properties. They are used in a number of hydrogenation processes such as hydrogenation of CO and unsaturated hydrocarbons (Da Costa et al., 2001; Ranhotra et al., 1987). Since nitride catalysts have good hydrogenation properties, at the high hydrogen pressures and flow rates (600 H_2/oil) used in the experiments, changes in pressure are not expected to make much difference in HDN activity. This is why the impact of pressure was not strong as shown in Figure 5.8A. There was no indication of thermodynamic equilibrium on the process within the conditions studied. Similarly, effect of interactions was not significant in the HDN process. This means the effect of any parameter can be considered almost independent of other parameters.

Although HDS activity was higher than that of HDN, generally, the effect of LHSV was greater on HDN than on HDS. This phenomenon may be related to the residence time of the reactants in the catalyst bed. As discussed above, one-step direct desulfurization was preferred for HDS while HDN went through a two-step process, i.e. prehydrogenation followed by denitrogenation. This means the residence time for denitrogenation would be much lower than that for HDS if the hydrogenation part of the reaction is the slowest step. Significant desulfurization occurred at both high and low LHSV (residence time) but there was only minimal HDN at high LHSV while significant HDN occurred at low LHSV. This is because at low LHSV, there was ample reaction time for both hydrogenation and denitrogenation to occur unlike at high LHSV. The hydrogenation step may therefore be rate limiting for HDN reaction on Ni-W(P)/γ-Al_2O_3 nitride catalyst.

5.4 Stability of Tungsten Nitride Catalysts to Deactivation

This phase of the Ni-W(P)/γ-Al_2O_3 catalyst studies was carried out to determine stability of the catalyst to deactivation over a long period of time. In the industry, catalysts are normally used for long periods (> 12 months) during hydrotreating before shut down. A good hydrotreating catalyst should be able to meet product specifications over the length of time the catalyst is loaded. It is of less importance to have an active hydrotreating catalyst with short-term stability. Stability of the Ni-W(P)/γ-Al_2O_3 nitride catalyst was investigated by keeping the catalyst with composition 2.5 wt% Ni, 1 wt% P and 15 wt % W, loaded for continuous hydrotreating experimental runs for a period of 51 days. The conditions were: reactor pressure of 9.0 MPa, LHSV of 2 h^{-1}, temperatures from 330 to 385 $^{\circ}$C and hydrogen to oil ratio of 600 ml/ml. The study was

divided into five stages. In Stage I (see Figure 5.9), the feed was introduced for 5 days in order to stabilize the initial catalyst activity. Stage II was to collect and analyze kinetic data just before Stage III which was the main focus of the stability study. Temperatures used in the kinetic studies were 340, 350, and 360 ºC. Stage III (run at 385 ºC for 30 days) was followed by Stage IV which was similar to Stage II but run after Stage III for comparison of kinetic data. The final stage of the stability study, Stages V, was included to compare activity to that of Stage I. This would give an idea of how much deactivation had occurred over the entire 51-day run. The catalyst activity in terms of HDS and HDN was quite stable with no significant deactivation over the entire period of study. Comparing results of Stages I and V, activity decreased by only 0.2 wt% for HDS and by 1.2 wt% for HDN which are well within the margin of error of ±1.6 wt%. Kinetic analyses of the results in Stages II and IV were based on kinetic models obtained for HDS and HDN (see Chapter 7). Table 5.3 lists the reaction rate constants of Stages II and IV for both HDS and HDN reactions. There is not much difference in the reaction rate constants at the two ends of the stability run i.e. for Stages II and IV. The maximum deviation in rate constant observed was 12% and occurred at 340 ºC for HDN. This is an indication of how stable the catalyst is to hydrotreating within the time frame and reaction conditions used. Thirdly, results in Stage III show steady activity of the catalyst both for HDS and HDN reactions. This means at 385 ºC, hydrotreating was more favoured than hydrocracking. Cracking simultaneously occurs with hydrotreating at high operating temperatures such as 385 ºC (Sambi et al., 1982). Cracking normally results in the deposition of carbon particles on the catalyst active sites and leads to deactivation. However, simulated distillation results in Table 5.4 show only minimal cracking at 385 °C.

5.5 Effect of H_2S on Hydrotreating

There are conflicting reports in the literature regarding stability of nitride catalysts during HDS reactions. While some reports (Ramanathan and Oyama, 1995) claim that nitride catalysts convert to sulfides during hydrotreating, others (Ozkan et al., 1997) suggest that nitrides are suitable for hydrotreating and are able to withstand sulfidation in hydrotreating environments. Theory seems to support the former view as per Equation (5.1) below (Furimsky, 2003). The Gibbs free energy, ΔG, for this reaction at 327 °C is -60.8 kcal/mol (327 °C is close to typical hydrotreating temperatures). This means that sulfur can adsorb and act as a sulfide on unsaturated

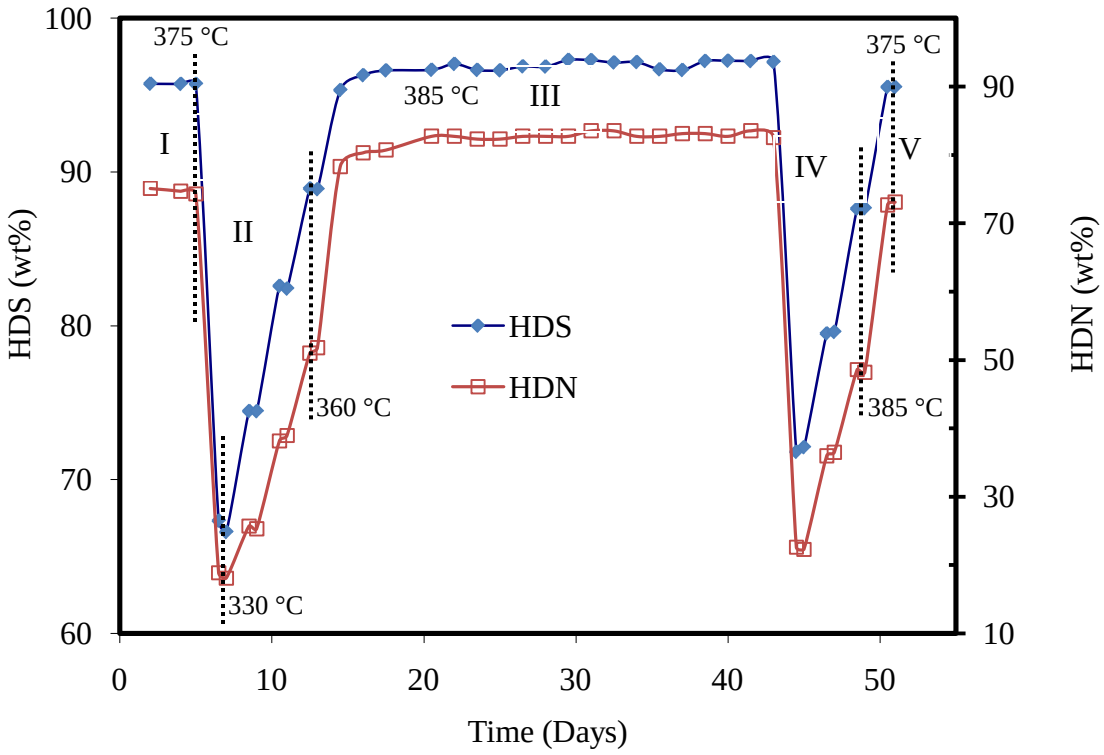

Figure 5.9: Ni-W(P)/γ-Al_2O_3 nitride catalyst stability to HDS and HDN reaction using light gas oil. Conditions: 330 to 385 °C, 9.0 MPa, LHSV of 2 h^{-1} and hydrogen/oil, 600 ml/ml (STP).

Table 5.3: HDS and HDN reaction rate constants for Stages II and IV of tungsten nitride catalyst stability studies.

Temperature (°C)	HDS		HDN	
	K_{II} ($s.Pa^{-1}$)	K_{IV} ($s.Pa^{-1}$)	K_{II} ($s.Pa^{-1}$)	K_{IV} ($s.Pa^{-1}$)
340	3.00E-05	2.91E-05	1.84E-07	1.61E-07
350	4.96E-05	4.79E-05	3.12E-07	2.91E-07
360	8.50E-05	8.37E-05	4.59E-07	4.23E-07
385	3.63E-04	3.69E-04	9.78E-07	1.03E-06

Table 5.4: Simulated distillation data for feed and sample hydrotreated at 385 ºC, 9.0 MPa and 2 h^{-1}.

	Gasoline (wt %)	Kerosene (wt %)	Light Gas Oil (wt %)	Heavy Gas Oil (wt %)	Total (wt %)
Product Sample	22.9	25.1	24.6	27.4	100
Feed	22.2	24.6	24.8	28.4	100

$$Mo_2N + 4H_2S \rightarrow 2MoS_2 + NH_3 + 2.5H_2 \quad (5.1)$$

sites of metal nitrides. It has also been reported that nitrides (mostly molybdenum nitrides) are more active than conventional sulfides (Ramanathan and Oyama, 1995; Aegerter et al., 1996). Since this work is about nitrides in H_2S environment, it was essential to investigate the effects of H_2S on the Ni-W(P)/γAl_2O_3 nitride catalysts and whether the nitride catalysts can withstand sulfidation during hydrotreating. Another study of interest was to compare activities of nitride and sulfide catalysts.

To carry out the investigation, two types of catalysts (nitride, and sulfided nitride) were synthesized at Ni and P loadings of 2.5 and 1 wt%, respectively. Each type of catalyst was synthesized at two levels of W loading (15 and 25 wt%) while the T_N and sulfidation temperatures were 560 °C and 243 °C, respectively. The sulfided nitride catalyst was obtained by subjecting a previously synthesized nitride catalyst to a sulfidation process (note that H_2S is generated in situ during the sulfidation process). Hydrotreating studies were performed at the following conditions: temperatures were 340, 350 and 360 °C, pressure was 9.0 MPa, LHSV was 2 h^{-1} and hydrogen-to-oil ratio was 600 ml/ml.

The activities increased with temperature (see Figure 5.10) with no significant difference between activities of the nitrides and sulfided nitrides. Although the sulfided nitride catalyst's activity appeared predominantly higher than that of the nitride catalyst, the difference was within the margin of error according to analysis of variance results. This suggests that the attempt to sulfide the nitride catalyst might not have been successful and the sulfided nitride catalyst may well have been in the nitride state during the reaction.

In a related study, the activities of nitrides and sulfided nitrides were compared to those of the corresponding sulfide (see Figure 5.11). Similar to results in Figure 5.10, no significant differences in activity were observed for the different catalysts suggesting that activities of the nitrides and sulfides were comparable. In elemental analyses studies performed, nitrogen content of the nitride catalysts increased with increase in tungsten loading, an indication that more tungsten nitrides were formed as tungsten loading was increased (see Table 5.5). For sulfur to replace nitrogen in the nitride catalyst, the sulfur content in the spent and sulfided nitrides catalyst would probably also increase with increase in tungsten loading similar to the nitrogen contents. However, the sulfur contents for both loadings were approximately the same. The measured sulfur in the spent and sulfided nitrides was therefore unlikely to be a result of replacement

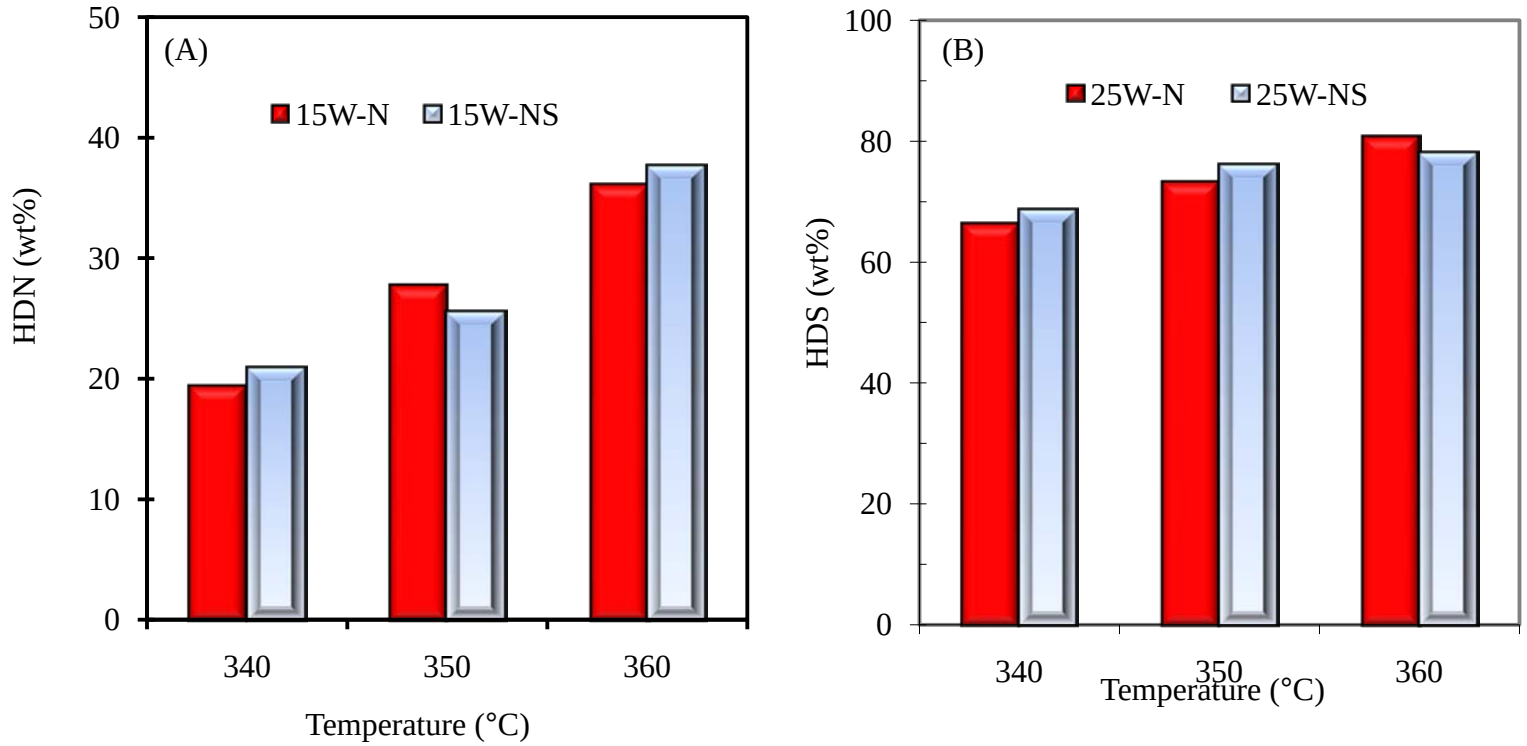

Figure 5.10: (A) HDN at 15 wt% W loading and (B) HDS at 25 wt% W loading of LGO using Ni-W(P)/γ-Al_2O_3 nitride catalyst. N = nitride; SN = sulfided nitride; P_H, 9.0 MPa; LHSV, 2 h^{-1}; H_2/oil, 600 ml/ml; Ni, 2.5 wt%; P, 1wt%; T_N, 560 °C.

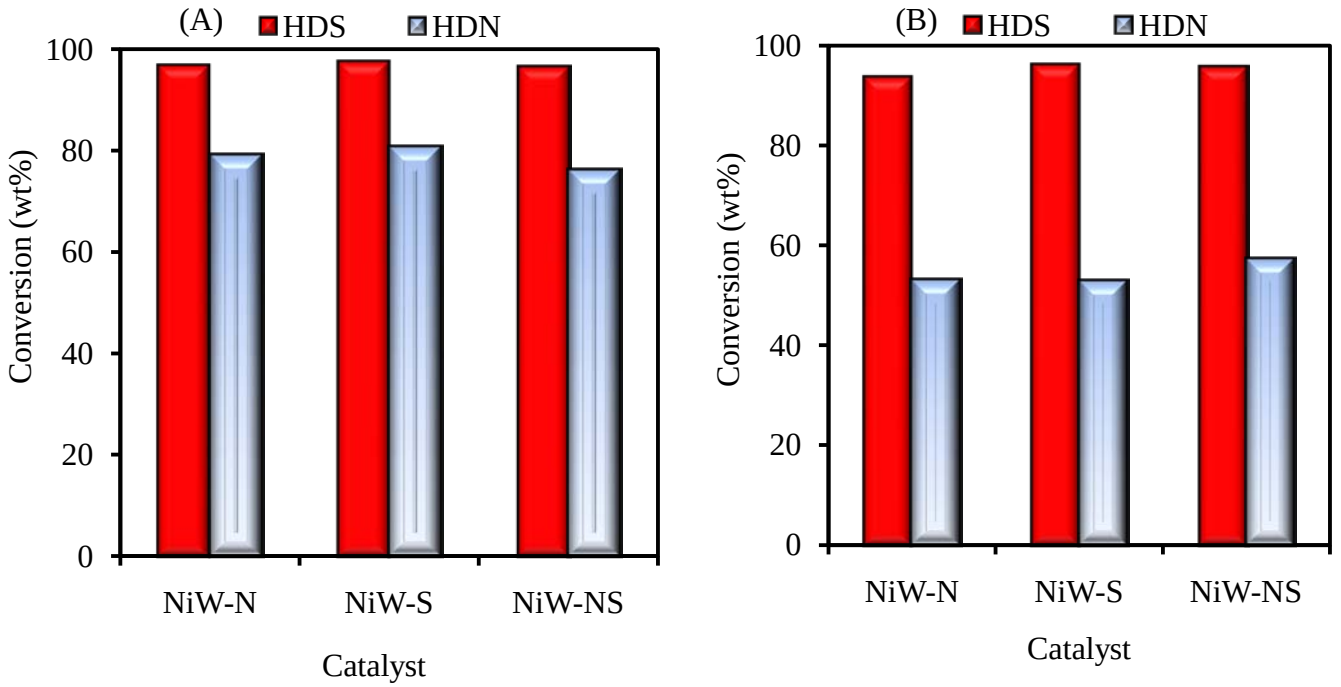

Figure 5.11: HDS and HDN of LGO using Ni-W(P)/γ-Al_2O_3 nitride catalyst at LHSV of (A) 1 h^{-1} and (B) 2 h^{-1}. N = nitride; NS = sulfided nitride; S = sulfide; P_H, 9.0 MPa; H_2/oil, 600 ml/ml; W, 15 wt%; Ni, 2.5 wt%; P, 1wt%; T_N, 560 °C.

Table 5.5: Nitrogen and sulfur content of nitride and sulfided nitride catalysts.

Tungsten Loading (wt%)	Fresh Nitride (wt%)	Spent Nitride (wt%)	Fresh Sulfided Nitride (wt%)
	Nitrogen Content		
15	1.20	0.40	0.40
25	2.00	1.00	1.02
	Sulfur Content		
15	0.07	3.42	2.67
25	0.07	3.61	2.41

of nitrogen in the catalyst. It might be due to liquid oil residue in the catalyst. Figure 5.12 shows FTIR spectra of nitride and sulfided nitride catalysts, each loaded with 25 wt% tungsten and sulphur L-edge XANES of fresh and spent nitride catalysts. The peaks for both fresh and sulfided nitride catalysts were identical which also supports the fact that the attempted sulfidation was not possible. Sulphur was not detected in the spent catalysts as shown by the XANES results. XRD patterns of the nitride and sulfided nitride catalysts (see Figure 5.13) did not show any difference between the catalysts. These observations confirm the activity results that the attempted sulfidation of nitride catalysts might have failed and that the nitride phase was intact during hydrotreating.

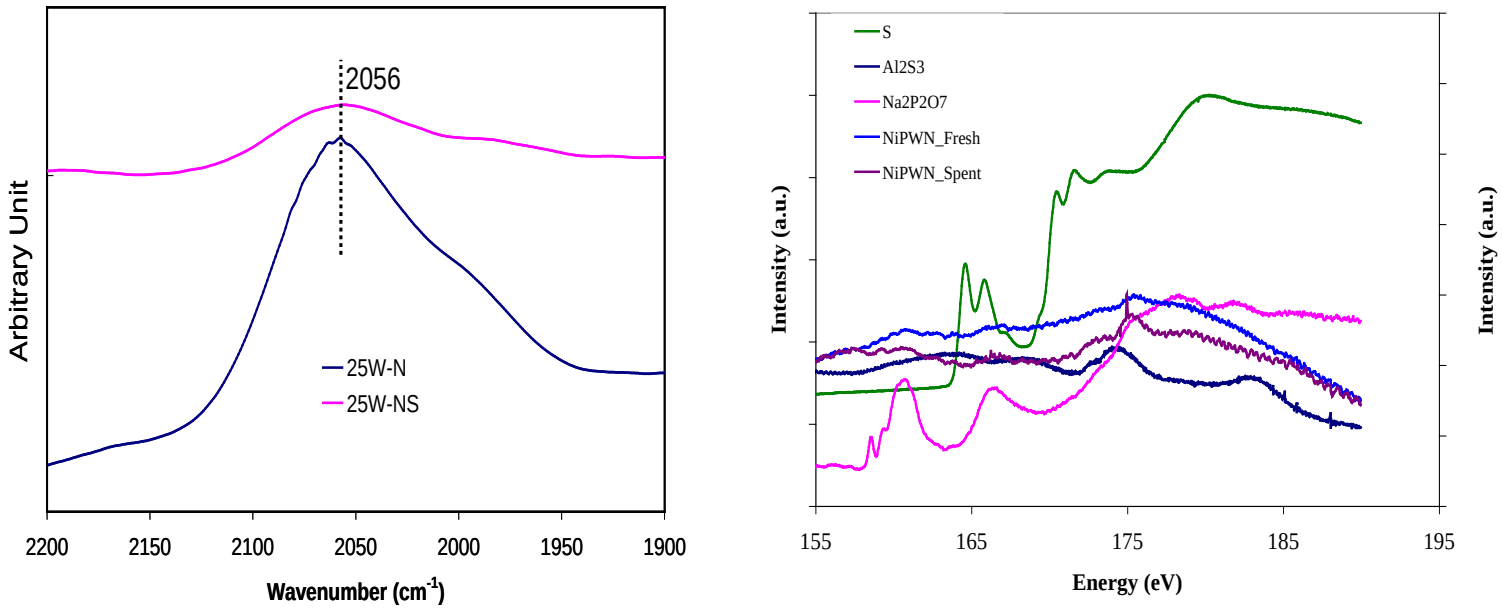

Figure 5.12: (A) FTIR spectroscopy of nitride and sulfided W(P)/γ-Al_2O_3 nitride catalyst and (B) sulphur L-edge XANES of fresh and spent nitride catalysts at 25 wt% W, 2.5 wt% Ni, 1 wt% P and T_N of 560 °C.

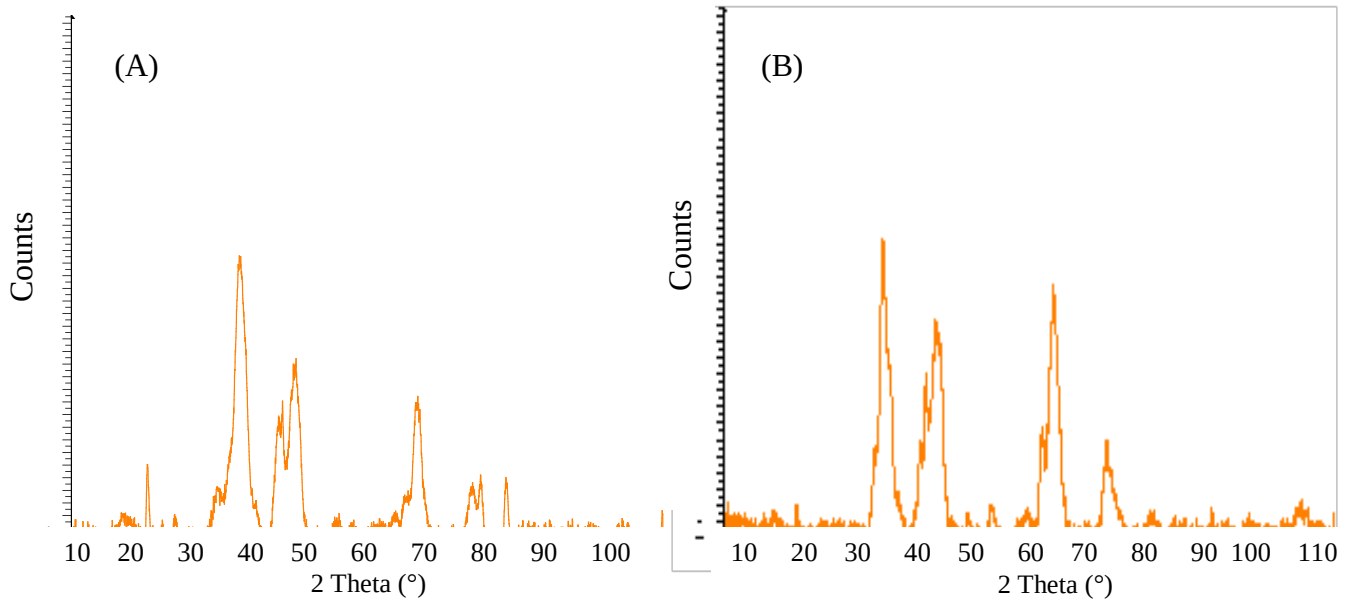

Figure 5.13: X-ray diffraction patterns of (A) sulfided nitride and (B) nitride catalysts. Conditions: 2.5 wt% Ni, 1 wt% P and,25 wt% W and T_N of 560 °C.

CHAPTER 6
CORRELATION OF ACTIVITY TO CATALYST PROPERTIES

In this chapter, properties of the catalyst have been correlated to the syntheses conditions and the HDS and HDN activities of the catalysts. Results of the characterization work used for the correlation are discussed in Chapter 4 while those of the activity work are in Chapter 5.

6.1 Correlation of Activity to Catalyst Properties: Effect of Phosphorus

The HDS and HDN results for Cat-P samples are shown in Figure 6.1A. Both HDS and HDN activities increased with P loading. The maximum P loading for HDS was about 3 wt%. Increase in activity with P loading is attributed to increased dispersion of active sites on the catalyst surface which was demonstrated by SEM results (see Figure 4.14), and the formation of phosphates on the support as seen in XANES results (see Figure 4.26). It is reported (Eijsbouts et al, 1991a) that P preferentially reacts with Al to form $AlPO_4$, which weakens metal-support interactions and increases the dispersion (Nava et al., 2006). IR results (see Figure 4.25) also showed the presence of P-O bonds and increase in P-O bonds with increase in P loading. Atanasova and Halachev (1994) reported that the presence of P promotes the formation of $NiWO_4$ species on the catalyst surface. $NiWO_4$ species lead to the formation of bimetallic Ni-W nitride species, hence the increase in catalyst activity. P also enhanced acidity of the catalyst (see Figure 4.2A) which is reported to promote C-N and C-S bond cleavage and enhance HDS (Sundaramurthy et al., 2008; Kwak et al., 1999). Although the catalyst acidity increased, cracking was not observed because acidity increased only moderately. A similar observation was. made by Kwak et al. (1999)

Figure 6.1B shows correlations of the amount of oxygen chemisorbed, surface area, catalyst nitrogen content and catalyst average particle size to the catalyst P loading as well as HDS and HDN activities (Figure 6.1A). The catalyst nitrogen content decreased with increase in P loading. This led to negative correlation between the catalyst nitrogen content and HDS and HDN activities. P is known to promote formation of Ni_2W_3N species rather than monometallic nitrides such as Ni_3N and W_2N. Equations for the formation of both monometallic and bimetallic nitrides are shown in Equations (6.1) to (6.3) below. The molar ratios of W and Ni to amounts of nitrogen in the nitride catalysts are 2:1, 3:1 and 3:1, respectively. This means the

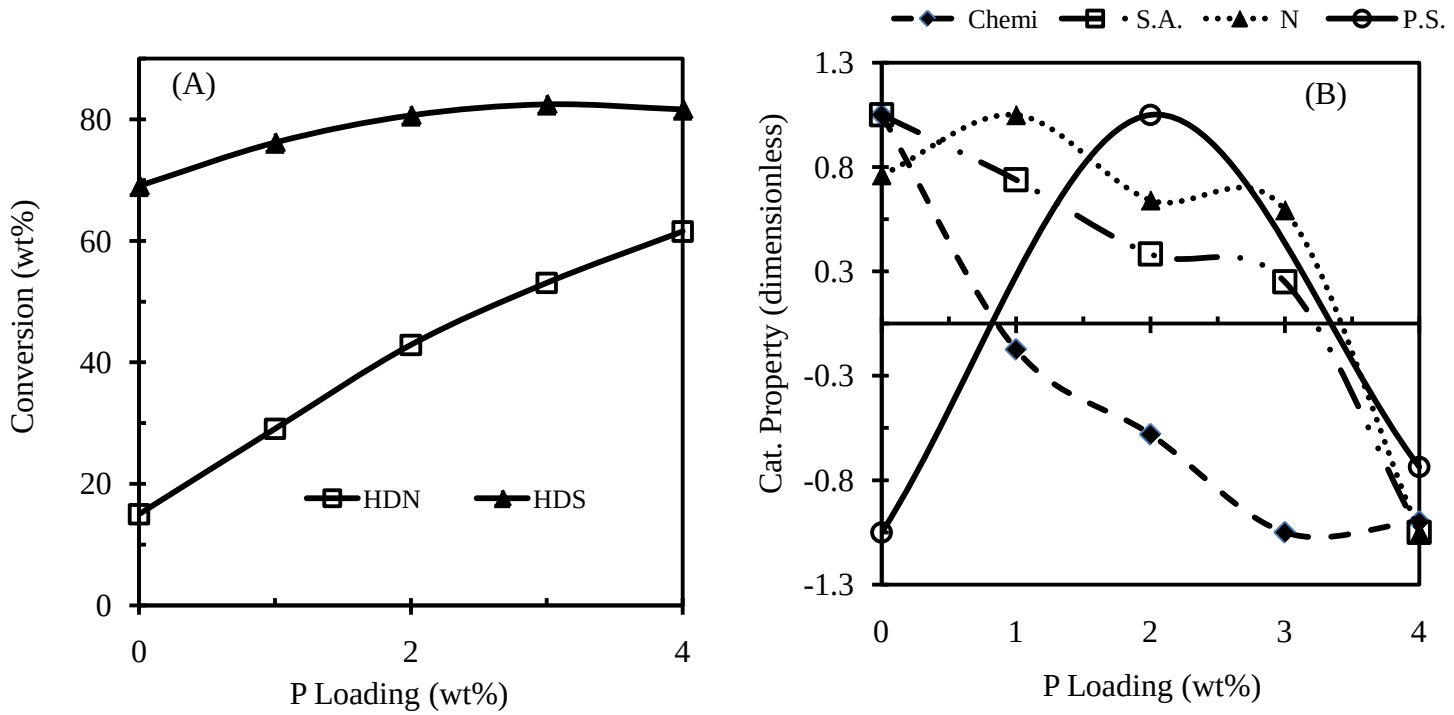

Figure 6.1: (A) Effect of P loading on HDS and HDN of light gas oil at 350 °C, 9.0 MPa, LHSV of 2 h^{-1} and H_2/oil of 600 ml/ml. (B) Correlation between amount of chemisorbed oxygen, surface area (S.A.), nitrogen content (N) and average particle size (P.S.) to catalyst P loading. Conditions: 30 wt% W, 4 wt% Ni and T_N of 700 °C.

$$4WO_3 + 8NH_3 \rightarrow 2W_2N + 12H_2O + 3N_2 \quad (6.1)$$

$$6NiO + 4NH_3 \rightarrow 2Ni_3N + 6H_2O + N_2 \quad (6.2)$$

$$6NiWO_4 + 16NH_3 \rightarrow 2Ni_2W_3N + 24H_2O + 2Ni + 7N_2 \quad (6.3)$$

catalyst nitrogen content in Ni_2W_3N is less than the amount of nitrogen formed in Ni_3N and W_2N combined. Since in the Cat-P samples, W and Ni loadings are constant and increase in P enhances formation of Ni-W bimetallic nitrides, the total amount of nitrogen in the catalyst is expected to reduce with increase in P loading. The increase in both HDS and HDN activities with decrease in catalyst nitrogen content suggests that the activity of Ni_2W_3N is greater than those of Ni_3N and W_2N combined. This is because, from Equations (6.1) to (6.3), if bimetallic Ni-W nitride were formed from oxides of tungsten and nickel, it would form less catalyst nitrogen compared to if monometallic N and W nitrides were formed (i.e. $12Ni_2W_3N + 7N_2 \equiv 8Ni_3N + 18W_2N$). The amount of chemisorbed oxygen also decreased with increase in P loading. As more Ni_2W_3N is formed, the total number of nitride species on the catalyst surface reduced compared to the number that would have formed from monometallic nitrides. In other words, the equivalent amount of monometallic nitrides that can be formed from six moles of Ni_2W_3N would be four moles of Ni_3N and nine moles of W_2N. Since amount of chemisorbed oxygen is associated with the number of exposed active sites, it is expected that the amount of chemisorbed oxygen will reduce with increase in P loading while the HDS and HDN activities increase. There was also negative correlation between the catalyst surface area and HDS and HDN activities. However, average particle size did not correlate well with the catalyst activities for HDS and HDN. The particle size (obtained from TEM analyses) went through a maximum at 2 wt% P loading and decreased, a trend that was not observed in the HDS and HDN activities.

6.2 Correlation of Activity to Catalyst Properties: Effect of Nickel

Figure 6.2A shows increase in HDS and HDN activities with increase in Ni loading. HDS increased to 4 wt% and then decreased. Similar observations were made by Chu et al. (1999), Yuhong et al. (2001) and Kim et al. (1996). At 0%-Ni, the W species in the catalyst predominantly formed monometallic W_2N after nitriding (see Equation(6.1)). Introduction of Ni, in the presence of W, led to formation of $NiWO_4$ and NiO species (Eliche-Quesada et al., 2003) which reacted with NH_3 to form bimetallic Ni_2W_3N and monometallic Ni_3N species as shown in

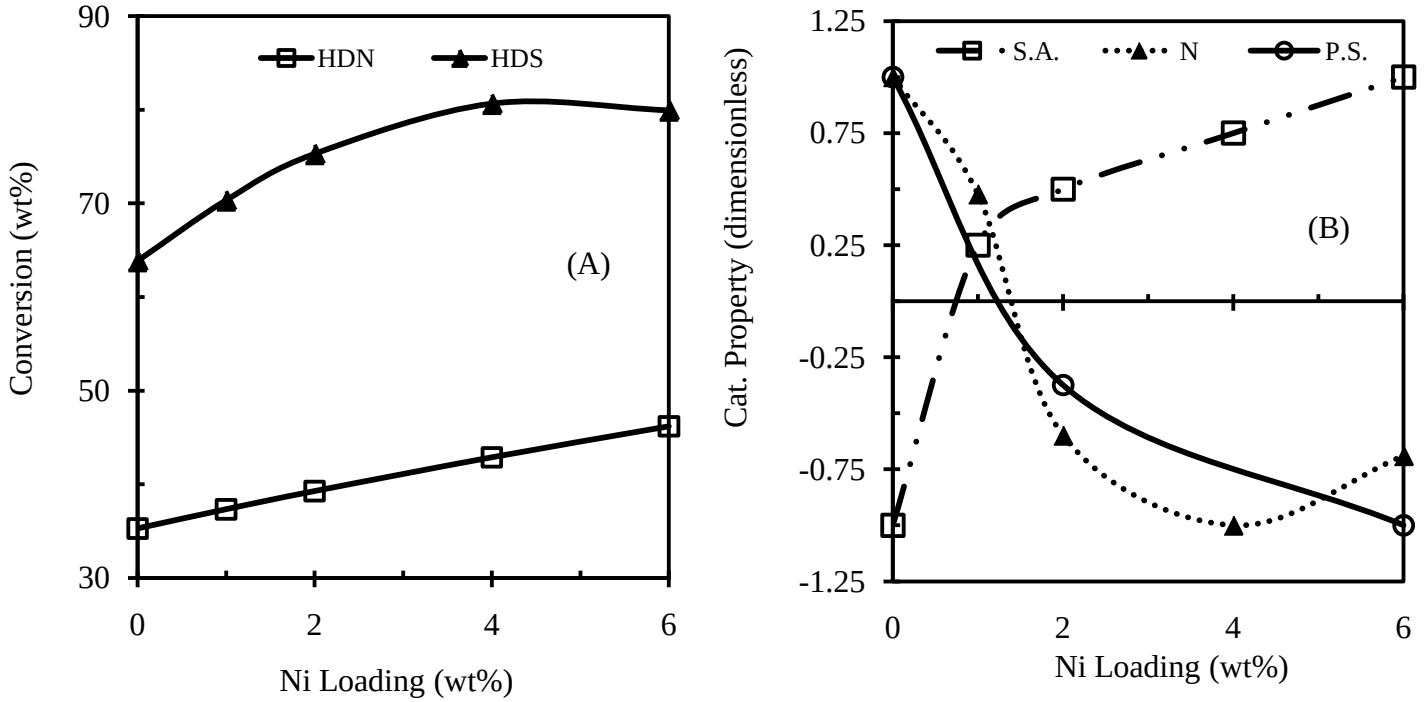

Figure 6.2: (A) Effect of Ni on HDS and HDN of light gas oil at T, 350 °C; P_H, 9.0 MPa; LHSV, 2 h^{-1}; H_2/oil, 600 ml/ml. (B) Correlation of surface area (S.A.), nitrogen content (N) and average TEM particle size (P.S.) to catalyst T_N. Conditions: 30 wt% W, 2 wt% P and T_N of 700 °C.

Equations (6.2)and (6.3) (Herle et al., 1998). TPO results in Figure 4.8 and XRD results in Figure 4.11 are in agreement with the above analysis. The 0%-Ni sample had the least HDS and HDN activities. The activities increased as Ni was added to the W-containing nitride catalysts. TPO and XRD results showed that addition of Ni to W-containing nitride catalysts caused the formation of the Ni_2W_3N nitride species. Since there is a net decrease in number of nitride species (see Section 6.1) and yet the activity increase, it suggests that the bimetallic Ni_2W_3N is more active for HDS and HDN than the monometallic W_2N. With W loading constant in the Cat-Ni samples, more Ni_2W_3N and Ni_3N (Figure 4.5B) are formed as a result of increase in Ni loading leading to increase in activities. Above 3 wt%-Ni, there is a slight dip in HDS activity which might be due to preferential formation of the less active Ni_3N and Ni metal.

Figure 6.2B shows that surface area for Cat-Ni nitride samples had positive correlation with HDS and HDN activities. The increase in surface area with increase in Ni loading might be due to decrease in catalyst particle sizes as shown by the SEM and TEM results. Cat-Ni nitride particle sizes decreased with Ni loading. Similar results were observed in the SEM studies (see Figure 4.15). Decrease in the catalyst particle sizes resulted in enhanced dispersion which increased the activity. There is a direct correlation between the catalyst surface area and the average particle size (from TEM analyses). As Ni loading increased, the catalyst surface area increased sharply and then slowly from 2 wt% Ni. Conversely, the particle size decreased sharply and then slowly from 2 wt% Ni. Nitrogen content had negative correlation with activity. The nitrogen content decreased as Ni loading increased up to ~ 4 wt% and then increased. The decrease can be attributed to the formation of more bimetallic Ni_2W_3N species as was observed in the Cat-P nitride samples. As Ni loading further increased at constant W loading, Ni_3N and Ni metal began to form rather than the bimetallic Ni_2W_3N. This resulted in increase in the catalyst nitrogen content and a corresponding decrease in the HDS activity. No decrease in HDN was observed, suggesting that bimetallic Ni_2W_3N species is more active for HDS than it is for HDN. Similarly, it can be inferred that Ni_3N is more active for HDN than for HDS.

6.3 Correlation of Activity to Catalyst Properties: Effect of Tungsten

In the activity studies for Cat-W nitride samples, it was observed that catalyst activity for HDS and HDN increased almost linearly with increase in tungsten loading (see Figure 6.3A). At all loadings HDS activity was higher than that of HDN. The increased activity with W loading

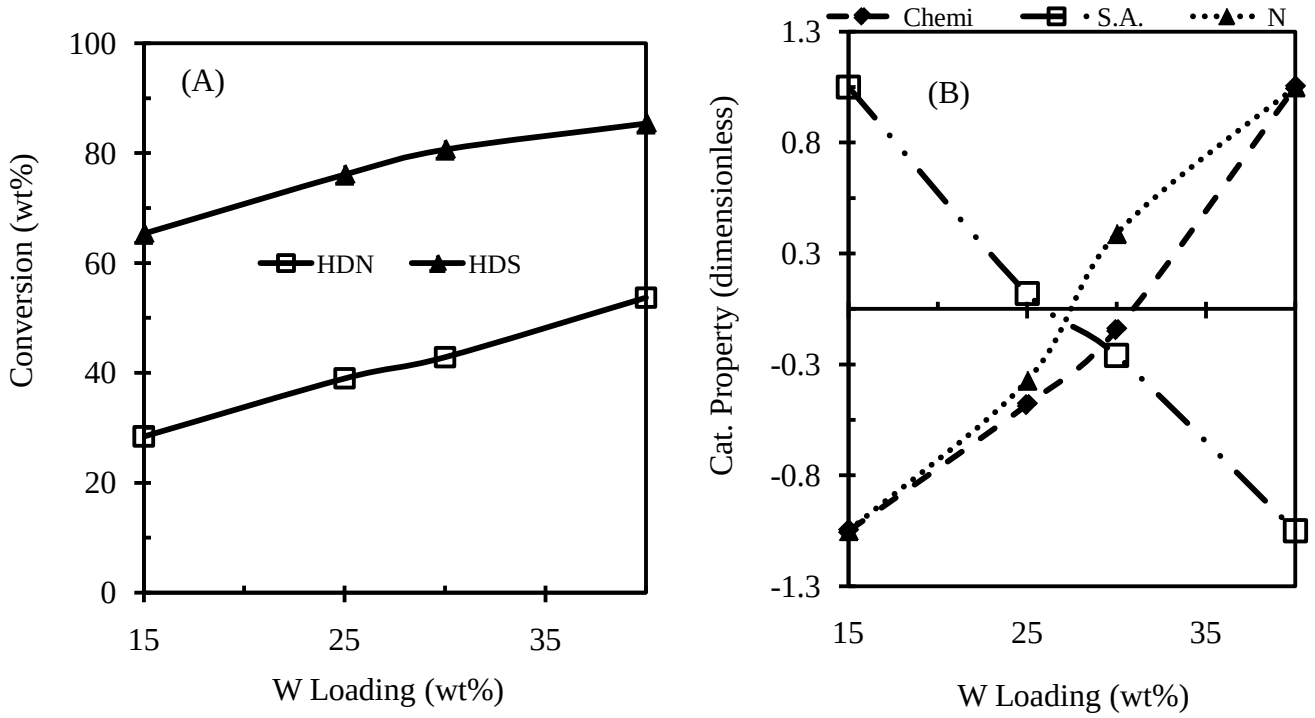

Figure 6.3: (A) Effect of W loading on HDS and HDN of light gas oil at T, 350 °C; P_H, 9.0 MPa; LHSV, 2 h^{-1}; H_2/oil, 600 ml/ml. (B) Correlation of amount of chemisorbed oxygen (chemi), surface area (S.A.), nitrogen content (N) and average particle size (P.S.) to catalyst W loading. Conditions: 2 wt% P, 4 wt% Ni and T_N of 700 °C.

can be attributed to formation of more active sites on the surface of the catalyst. Figure 6.3B shows that the amount of chemisorbed oxygen increased with increase in the tungsten loading. Since the chemisorbed oxygen volume is a measure of the number of exposed active sites, it confirms that the number of active sites increased with increase in tungsten loading. SEM results (Figure 4.16) of the 40%-W sample also showed an increased number of particles on the catalyst surface. Figure 6.3B shows positive correlation of catalyst nitrogen content with tungsten loading and with activity. Increase in the tungsten loading caused formation of more nitride species on the catalyst surface which improved the catalyst activity. Although the number of bimetallic nitride species increased with increase in tungsten loading, more monometallic W_2N species were formed with increase in the tungsten loading to compensate for any decrease in number of particles that may have resulted from formation of bimetallic species. Both surface area and catalyst particle size had negative correlations with tungsten loading and catalyst activity.

Figure 6.3B indicates that the number of exposed active sites increased with increase in W loading. This is seen in the chemisorptions results as the amount of chemisorbed oxygen increased with tungsten loading. The decrease in surface area observed can be associated with plugging of pores of the catalyst as the number of metal particles increased. The decrease in surface area was however, compensated for by increased number of active sites hence the increased HDS and HDN catalyst activities.

6.4 Correlation of Activity to Catalyst Properties: Effect of Nitriding Temperature

In Figure 6.4A, HDS and HDN activities decreased with increase in T_N. This is because as T_N increased, dispersion of metals on the catalyst surface decreased. SEM results showed increased dispersion of metal particles in the low T_N samples. The increased activity at low T_N might also be due to the increased acidity of the catalyst at low T_N as TPD results illustrated (see Figure 4.3B). Acidity of the catalysts facilitates C-N and C-S bond breakage and hence increases the overall hydrotreating activity (Sundaramurthy et al., 2008; Kwak et al., 1999). XRD results showed disappearance of the more active bimetallic Ni_2W_3N species at high T_N ($\geq$ 800 °C). The ratio of metals to Ni_2W_3N increased, hence, the decrease in HDS and HDN activities.

A similar trend is observed in the results of the surface area analyses (Figure 6.4B). Decrease in the surface area is attributed to loss of smaller pores. A sharp trend observed in the

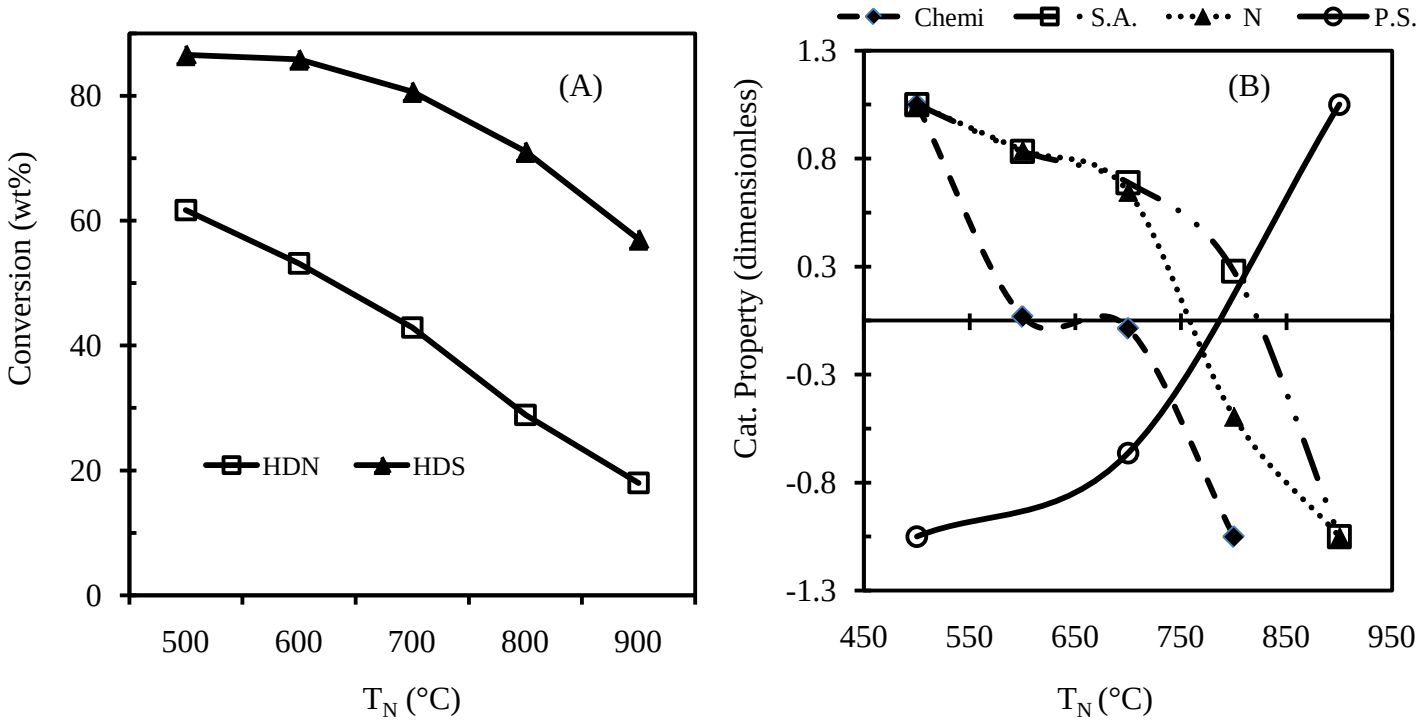

Figure 6.4: (A) Effect of T_N on HDS and HDN of light gas oil at T, 350 °C; P_H, 9.0 MPa; LHSV, 2 h^{-1}; H_2/oil, 600 ml/ml. (B) Correlation of amount of chemisorbed oxygen, surface area (S.A.), nitrogen content (N) and average particle size (P.S.) to catalyst T_N. Conditions: 30 wt% W, 2 wt% P and 4 wt% Ni.

surface area at $T_N \geq 800$ °C is similar to observation in the XRD results and explains why the HDS activity decreased sharply at corresponding T_N.

The amount of chemisorbed oxygen also correlated well with the nitriding temperature and the catalyst activities. As nitriding temperature increased, the number of exposed active sites decreased due to agglomeration of particles (see Figure 4.17). This led to decreased amount of chemisorbed oxygen as the amount of chemisorbed oxygen is a measure of the number of exposed active sites on the catalyst surface. The decrease in number of active sites is seen in corresponding decrease in both HDN and HDS with increase in T_N. Figure 6.4 also shows good correlation between the catalyst nitrogen content and the catalyst activity. The catalyst nitrogen content decreased with increase in nitriding temperature and increased with both HDS and HDN activities. As nitriding temperature increases, decomposition of the more active nitrides takes place to form less active metals. Decomposition of nitride catalysts was evidenced in the TPD study (Figure 4.2A). This reduced the catalyst nitrogen content and reduced the catalyst HDS and HDN activities. Another good correlation was seen in the average catalyst particle size. In this case, the correlation was positive with temperature and negative with activity. As the nitriding temperature increase, the average catalyst particle size from TEM analyses increased. This can be attributed to agglomeration of the catalyst particles as seen in the SEM results. Increase in the catalyst average particle size reduced the surface area of the catalyst. Dispersion decreased as a result and number of exposed active sites decreased. This resulted in HDS and HDN activity decrease.

In general, there were good correlations between surface area, amount of chemisorbed oxygen, catalyst nitrogen content and catalyst particle size. Catalyst activity increased with increase in nitrogen content but in the case of Cat-P nitride catalysts, the activity increased with decreased nitrogen content. This was due to enhanced formation of bimetallic Ni-W nitride species. Smaller particle sizes enhance catalyst activity while increased number of catalyst active sites increased the catalyst activity. Although surface area correlates with catalyst activity, it did not have a significant impact on the activity. This is because in the Cat-W samples the surface area decreased even with increase in activity. Ni_2W_3N is more active than Ni_3N and W_2N, Ni and W metals are less active for HDS and HDN compared to Ni_3N, W_2N and Ni_2W_3N.

CHAPTER 7
KINETIC ANALYSES

Kinetic analyses were done to study the active sites responsible for HDS and HDN reaction over Ni-W(P)/γ-Al_2O_3 nitride catalyst and to investigate the influence of mass transfer limitations on the reactions. As mentioned in Section 2.4, the methods employed in the kinetic studies included kinetic model considerations, kinetic parameter evaluation, model discrimination, implication of model results and mass transfer limitation. The following assumptions were made in the kinetic analyses:

1. A pseudo-homogeneous reaction system was assumed in order to lump the properties of all the different species of sulfur and nitrogen compounds in the feed and products (Chen and Ring, 2001).
2. Sulfur containing compounds in light gas oil were assumed to be equimolar amounts of thiophene, benzothiophene and dibenzothiophene and properties of the sulfur compounds were based on these.
3. In the case of nitrogen compounds, the chosen representative compounds were pyridine, quinoline and acridine.
4. No axial dispersion was considered as a result of the catalyst dilution used in the experimental work which led to liquid trickle flow. Earlier work with such dilution has confirmed the establishment of trickle flow in the bed (Bej et al., 2000). Particle Peclet number evaluation (0.006 – see Appendix C.2.3) from the set up satisfies the criterion proposed by Gierman (1988) for uniform radial concentration in a micro-trickle bed reactor. This observation is supported by van Herk et al. (2005).Using the criteria by Weisz-Prater and Mears (Fogler, 2006), it was shown that there were no internal nor external diffusion limitations in the experimental work (see Section 7.3).

7.1 Kinetic Model Considerations

Different kinetic models (Power Law and Langmuir-Hinshelwood) were evaluated to determine the model that best described the experimental data. The Langmuir-Hinshelwood models would also give information on the reaction mechanism and the active sites involved in the

reaction. Three of the models were of the Langmuir-Hinshelwood type and the other, a Power Law model. The models considered are as follows:

Model I: $$-r = \frac{k * C_i * P_H * L^n}{\left(1 + K_i * C_i\right)} \tag{7.1}$$

Model II $$-r = \frac{k * C_i * P_H * L^n}{\left(1 + K_i * C_i + K_H * P_H\right)} \tag{7.2}$$

Model III $$-r = \frac{k * C_i * P_H * L^n}{\left(1 + K_i * C_i\right) * \left(1 + K_H * P_H\right)} \tag{7.3}$$

Model IV $$-r = k * C^x * P^y * L^n \tag{7.4}$$

where $$k = k_o * e^{\left(-E/R_g * T\right)} \tag{7.5}$$

$$K_i = K_{oi} * e^{\left(Q_i/R_g * T\right)} \tag{7.6}$$

$$K_H = K_{oH} * e^{\left(Q_H/R_g * T\right)} \tag{7.7}$$

All the parameters are defined in the Nomenclature. The LHSV term was included because the experiments were conducted based on statistical model at varying LHSV (see Table 5.2). Model I can be interpreted as having identical sites involved in the reaction process with only species i adsorbing on the surface of the catalyst. The reaction is only inhibited by species i as it is the only adsorbing species. If, however, there were identical sites present and both species i and hydrogen were adsorbed, then model II would be the most appropriate model for the data. Model III illustrates a reaction where two unidentical sites are utilized in the reaction; one site for hydrogenation and the other for species i adsorption and both inhibit the reaction. The Power Law model, on the other hand, only considers reaction between species i and hydrogen as elementary reactions (reactions in which reactants form products in a single reaction step).

7.2 Evaluation of Parameters and Model Discrimination

All parameters were evaluated using non-linear least squares and the less suitable models eliminated from consideration. Factors considered in the model discrimination included: sum of squares, the 95% confidence value of the parameters, residual plot and the adjusted R^2. POLYMATH software package was used to solve the equations.

7.2.1 Analyses of HDS Kinetics

The output of the POLYMATH solutions for the HDS kinetic models is given in Table 7.1. On the basis of F-test discrimination, Models II and IV can be quickly eliminated from the list of consideration. In Model II, the average values of K_{oi} and K_{oH} were $7.58*10^4$ and $4.59*10^5$ while their 95 % confidence levels were $\pm 9.55*10^4$ and $\pm 5.09*10^5$, respectively. The confidence levels for these parameters were greater than the parameters themselves making the calculated parameter values and the model less reliable. Similarly in Model IV, the confidence level for parameter E was greater than the parameter value itself. Besides, considering the reaction in question, the value of E was too small to make any physical meaning. This leaves Models I and III to be considered. Out of the two models left, the one with the minimum sum of squares was Model III. It was two orders of magnitude smaller than that of Model I.

i.e.
$$\frac{\sigma_I^2}{\sigma_{III}^2} = \frac{1.04}{0.004} = 2.6*10^2$$

A look at the residual distribution for Model III also showed the data was fairly randomly distributed. The adjusted R^2 of 0.982 also indicated good fitting. Model I was superior to Model III in terms of random distribution of the error but the sum of squares was the more deciding factor. This made Model III, simplified in Equation (7.8), the most suitable for the data.

$$-r = \frac{0.5e^{\left(-66/R_gT\right)}C_iP_HL^2}{\left(1+5.7*10^7e^{\left(-61/R_gT\right)}C_i\right)\left(1+10^8e^{\left(-180/R_gT\right)}P_H\right)} \qquad (7.8)$$

The chosen model was then tested with a new set of data outside what was used in the model development. Figure 7.1 shows the parity plot of the experimental data against model- predicted data. The model was able to predict well the experimental data, confirming reliability

Table 7.1: Kinetic parameters for HDS of LGO using Ni-W(P)/γ-Al_2O_3 nitride catalyst

Parameter	Converged Value	95% Confidence	Model I
k_0 ($Pa^{-1}.h^{-(1+n)}$)	$3.84*10^{-4}$	$1.15*10^{-5}$	Sum of Squares = 0.104
E (kJ/mole)	41.40	0.16	Adjusted R^2 = 0.855
n	1.53	0.03	No of positive Residuals = 4
K_{oi} ($ppm^{-1}*10^4$)	$1.01*10^7$	$5.29*10^5$	No of negative Residuals = 4
Q_i (kJ/mole)	-78.49	0.28	
Parameter	Converged Value	95% Confidence	Model II
k_0 ($Pa^{-1}.h^{-(1+n)}$)	1.71	1.05	
E (kJ/mole)	68.14	3.22	Sum of Squares = 0.097
n	1.33	0.54	Adjusted R^2 = 0.600
K_{oi} ($ppm^{-1}*10^4$)	$7.58*10^4$	$9.55*10^4$	No of positive Residuals = 3
Q_i (kJ/mole)	-38.40	6.47	No of negative Residuals = 5
K_{oH} (Pa^{-1})	$4.59*10^5$	$5.09*10^5$	
Q_H (kJ/mole)	-134.59	5.92	
Parameter	Converged Value	95% Confidence	Model III
k_0 ($Pa^{-1}.h^{-(1+n)}$)	0.53	0.07	
E (kJ/mole)	65.95	0.66	Sum of Squares = 0.004
n	2.00	0.11	Adjusted R^2 = 0.982
K_{oi} ($ppm^{-1}*10^4$)	$5.66*10^6$	$7.55*10^5$	No of positive Residuals = 3
Q_i	-60.96	0.70	No of negative Residuals = 5
K_{oH} (Pa^{-1})	$1.01*10^8$	$2.33*10^7$	
Q_H (kJ/mole)	-179.76	1.23	
Parameter	Converged Value	95% Confidence	Model IV
k_0 $wt\%^{(1-x)}.Pa^{-y}.h^{-(1+n)}$	$1.59*10^{-8}$	$8.69*10^{-8}$	Sum of Squares = 0.051
E (kJ/mole	-19.25	26.74	Adjusted R^2 = 0.929
n	0.51	0.46	No of positive Residuals = 4
x	0.51	0.46	No of negative Residuals = 4
y	0.81	0.34	

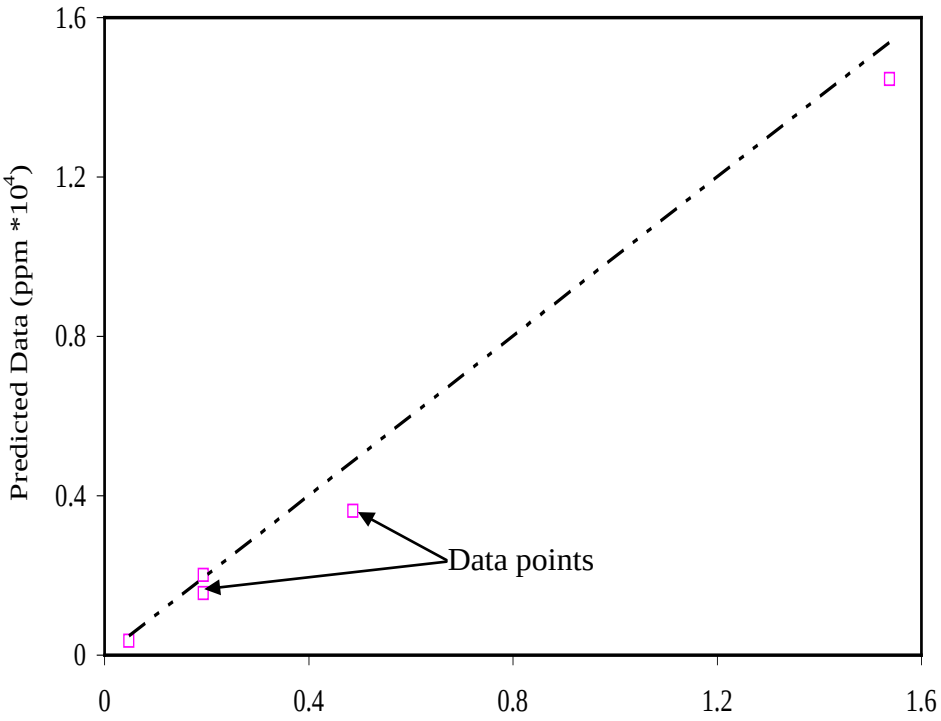

Figure 7.1: Parity plot for the experimental and model-predicted product sulfur concentrations of the HDS of light gas oil using Ni-W(P)/γ-Al_2O_3 catalyst. T, 340 to 385 ºC; P_H, 9.0 MPa; LHSV, 2 h^{-1}; H_2/oil, 600 ml/ml (STP); 15 wt% W, 2.5 wt% Ni, 1 wt% P and T_N, of 560 °C.

of the evaluated parameters. The results suggest that two main sites were involved in the HDS reaction: one for hydrogenation and the other for sulfur removal. This means that in the HDS reaction, the sulfur first adsorbs on the catalyst. The sulfur-carbon bond was then attacked by adsorbed hydrogen to break the bond and to hydrogenate the hydrocarbon. It should be noted that this step is different from the prior hydrogenation explained in Section 2.1.1.1 which requires hydrogenation of the sulfur-containing ring prior to sulfur removal. The next step in the reaction process is hydrogenation of the adsorbed sulfur atom by adsorbed hydrogen atoms to form the bi-product H_2S. So although HDS prefers direct sulfur extraction, it still requires a form of hydrogenation to break the sulfur-carbon bond. Both sulfur compounds and hydrogen pressure inhibited the rate of desulfurization.

7.2.2 Analyses of HDN Kinetics

The POLYMATH output for HDN kinetic analyses is shown in Table 7.2. A look at the results suggested that the Power Law model (Model IV) may be the most suitable model for the data. This is because it had the lowest sum of squares of 0.002, two orders of magnitude smaller than the other models. However, an F-test for the parameters of Model IV indicated otherwise. The activation energy obtained for the model was negative (-0.43). Secondly, the 95 % confidence level of the activation energy (±0.68) was greater than the value of the activation energy itself, making the value unreliable and ruling out the model as a suitable one. The next model with the lowest sum of squares was Model III (0.269). However, its residuals were not randomly distributed. Out of 8 data points used in the kinetic analyses, only two residuals were positive. This clearly suggested a trend in the data and did not make Model III suitable for the experimental data. Model II was the next with the lowest sum of squares (1.025). It had fairly randomly distributed residuals. However, the 95 % confidence for Q_H (13.40) was greater than the value of Q_H itself (-10.76) making the model less reliable.

The remaining model, Model I, had a sum of squares of 1.155. The residuals were fairly randomly distributed about the mean with 5 positive and 3 negative. F-test of the parameters confirmed reliability of the model. The results indicated that for all the models considered, Model I, simplified in Equation (7.9), was the most suitable for the HDN process.

Table 7.2: Kinetic parameters for HDN of light gas oil using Ni-W(P)/γ-Al_2O_3 nitride catalyst.

Parameter	Converged Value	95% Confidence	Model I
k_0 ($Pa^{-1}.h^{-(1+n)}$)	0.06	0.03	Sum of Squares = 1.155
E (kJ/mole)	31.87	2.26	Adjusted R^2 = 0.995
n	2.00	0.20	No of positive Residuals = 5
K_{oi} ($ppm^{-1}*10^4$)	9.12E+04	4.17E+04	No of negative Residuals = 3
Q_i (kJ/mole)	-26.86	2.36	
Parameter	Converged Value	95% Confidence	Model II
k_0 ($Pa^{-1}.h^{-(1+n)}$)	0.06	0.01	
E (kJ/mole)	27.97	0.53	Sum of Squares = 1.025
n	2.00	0.09	Adjusted R^2 = 0.987
K_{oi} ($ppm^{-1}*10^4$)	7.58E+04	7.97E+03	No of positive Residuals = 5
Q_i (kJ/mole)	-21.98	0.56	No of negative Residuals = 3
K_{oH} (Pa^{-1})	8.96E-07	2.21E-06	
Q_H (kJ/mole)	-10.76	13.40	
Parameter	Converged Value	95% Confidence	Model III
k_0 ($Pa^{-1}.h^{-(1+n)}$)	0.81	0.13	
E (kJ/mole)	31.17	0.82	Sum of Squares = 0.269
n	1.97	0.13	Adjusted R^2 = 0.997
K_{oi} ($ppm^{-1}*10^4$)	7.58E+04	1.18E+04	No of positive Residuals = 2
Q_i	-13.58	0.83	No of negative Residuals = 6
K_{oH} (Pa^{-1})	1.92E-03	9.01E-04	
Q_H (kJ/mole)	-55.48	2.53	
Parameter	Converged Value	95% Confidence	Model IV
k_0 $wt\%^{(1-x)}.Pa^{-y}.h^{-(1+n)}$	5.66E-05	1.37E-05	Sum of Squares = 0.002
E (kJ/mole	-0.43	0.68	Adjusted R^2 = 0.999
n	-0.001	0.006	No of positive Residuals = 3
x	-0.001	0.006	No of negative Residuals = 5
y	0.66	0.02	

$$-r = \frac{0.06e^{\left(-32/R_gT\right)}C_i P_H L^2}{1+91200e^{\left(-27/R_gT\right)}C_i} \tag{7.9}$$

Equation (7.9) was tested with data outside those used for the kinetic analyses and was able to predict well the fresh data as shown in Figure 7.2. This is a confirmation of the reliability of the HDN model. The implication of the results is that identical active sites were involved in the hydrodenitrogenation and the process was inhibited by only nitrogen compounds. This means that during HDN reactions, the nitrogen atom adsorbs on to an active site of the catalyst. However, unlike the HDS mechanism, due to the large energy of the C=N bond (see Table 2.1), the nitrogen-containing ring is hydrogenated by molecules of hydrogen. This reduces the bond energy between nitrogen and carbon. The C-N bond is then attached by hydrogen in the bulk fluid to break the bond and further hydrogenation leads to formation of NH_3. Hydrogen did not inhibit the HDN process.

7.3 Mass Transfer Considerations

Heterogeneous catalytic reactions have widely been applied in industry since the discovery of catalysts especially, in fixed-bed reactors (Froment and Bischoff, 1979). However, fixed-bed operations are beset with the problem of inter-particle and intra-particle mass transfer limitation among others. The impact of these diffusion limitations can be very pronounced and could affect the output of a fixed bed reactor. It was therefore important to study the role of mass transfer both within and between the catalyst pellets and their influence on reactions in the reactor. The evaluations in this work include both external and internal mass transfers.

7.3.1 External Mass Transfer Limitations

Various criteria have been proposed for the evaluation of external mass transfer limitations in the literature. To check if diffusion from the bulk of the fluids to the catalyst external surface was not a limiting step in the reaction steps, Mears' criterion, shown in Equation (7.10) was used.

$$C_m = \frac{-r_i' \rho_b Rn}{k_c C_{ib}} \prec 0.15 \tag{7.10}$$

(Fogler, 2006) where

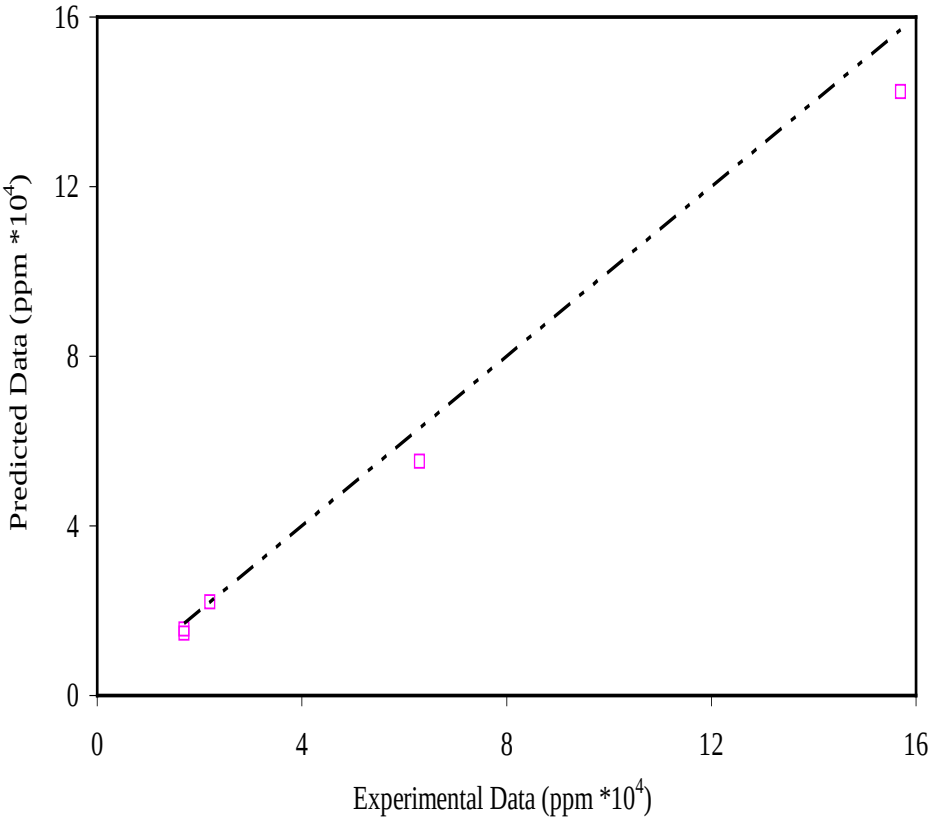

Figure 7.2: Parity plot for the experimental and model-predicted product nitrogen concentrations of the HDN of light gas oil using Ni-W(P)/γ-Al_2O_3 catalyst at 340 to 385 ºC, 9.0 MPa, LHSV of 2 h^{-1} and H_2/oil, 600 ml/ml (STP). Catalyst properties: 15 wt% W, 2.5 wt% Ni, 1 wt% P and T_N of 560 °C.

C_m = ratio of reaction rate to the external diffusion rate,

r' = reaction rate per unit mass of catalyst (kmol/kg-s)

ρ_b = bulk density of the catalyst bed (kg/m^3)

R = catalyst particle radius (m)

n = reaction order

k_c = mass transfer coefficient (m/s)

C_{ib} = bulk concentration (kmol/m^3)

A C_m value < 0.15 means external diffusion resistance is negligible. C_m was evaluated for both HDS and HDN at all the temperatures the kinetic studies were performed (330 - 380 °C). A sample calculation is shown in Appendix C.2.1. r'_A was evaluated from the final kinetic expressions for HDS Equation (7.8) and HDN(7.9) while generalized correlations were used to evaluate some of the parameters involved in the calculations. Results show that there was no external mass transfer limitation in the kinetic studies as the obtained C_m values (in the order of 10^{-6} for HDS and 10^{-3} for HDN) were far less than 0.15.

7.3.2 Internal Mass Transfer Limitations

In kinetic data analyses, it's important to eliminate any possible chance of internal mass transfer limitation. Any limitations due to internal mass transfer will reduce the effectiveness of the catalysts and will reduce the activity of the catalyst. In this study, the intra-particle mass transfer limitation was evaluated based on the Weisz-Prater criterion, Equation (7.11) (Fogler,

$$C_{WP} = \frac{-r_A \rho_c R^2}{D_e C_{As}} \tag{7.11}$$

2006) where

r_A = observed rate of reaction (kmol/kg-s)

ρ_c = catalyst pellet density (kg/m^3)

R = catalyst particle radius *(m)*

D_e = effective diffusivity (m^2/s)

C_{As} = catalyst surface concentration (kmol/m^3)

If C_{WP} << 1, internal diffusion does not limit the reaction rate. However, if C_{WP} >> 1, internal diffusion limitation exists and steps need to be taken to reduce the limitation. A sample internal mass transfer limitation calculation based on the Weisz-Prater criterion is shown in Appendix 0. Results show that the reactions (both HDS and HDN) were not limited by internal diffusion. Values of C_{WP} were in the order of 10^{-3} and lower for HDS and 10^{-5} and lower for HDN.

In summary, kinetic analyses results showed that Langmuir-Hinshelwood model was the most suitable for both HDS and HDN reactions. While HDS went through direct sulfur extraction, HDN had ring hydrogenation prior to denitrogenation. HDS employed two active sites in reaction while HDN used one. Activation energies of 66 and 32 kJ/mole/K were obtained for HDS and HDN reactions, respectively. The values from Mears and Weisz-Prater criteria for HDS and HDN (all in the order of 10^{-3} and below) indicated that there were no mass transfer limitations in the HDS and HDN reactions over Ni-W(P)/γ-Al_2O_3 nitride catalyst.

CHAPTER 8
CONCLUSIONS AND RECOMMENDATIONS

8.1 Conclusions

The main objective of this thesis was to synthesize, characterize and test the activity of Ni-W(P)/γ-Al_2O_3 nitride catalyst for hydrodenitrogenation (HDN), hydrodesulfurization (HDS) and hydrodearomatization (HDA) of light gas oil (LGO) from Athabasca bitumen. Other studies done were the stability of the nitride catalysts, the effects of process conditions on catalyst activity, kinetic analyses for HDS and HDN reactions and correlation of catalyst activities to their surface properties. A list of the conclusions drawn from the thesis is presented here in this section.

8.1.1 Nitride Catalyst Syntheses

1. The central composite design used in the experimental methods offers a better way of obtaining as much information as possible from a limited number of experiments.

2. The passivation step during temperature programmed reduction stabilizes nitride catalysts and prevents it from bulk oxidation at ambient conditions.

3. Active Ni-W(P)/γ-Al_2O_3 nitride catalysts can be successfully synthesized by the temperature programmed reaction process. Parameter ranges used for this work were: W loading (15-40 wt%), Ni loading (0-8 wt%), P loading (0-5 wt%) and T_N (500-900 °C).

8.1.2 Nitride Catalyst Characterization

1. Ni-W(P)/γ-Al_2O_3 nitride catalysts have both weak and strong acid sites on the surface. Increasing P loading increases the amount of weak acid sites while increasing T_N decreases the amount of strong acid sites.

2. At low temperatures (below 700 °C), adsorbed NH_3 desorbs from the surface of Ni-W(P)/γ-Al_2O_3 catalysts. At temperatures above 800 °C, nitride species decompose to give off nitrogen gas.

3. Ni_3N, W_2N, Ni_2W_3N, Ni and W are among the species on the surface of Ni-W(P)/γ-Al_2O_3 nitride catalysts

4. Ni_3N can be reduced at temperatures below 400 °C while W_2N is reduced at temperatures above 800 °C. It is difficult to reduce the passive oxide layer on the catalyst surface without reducing Ni_3N species.

5. The presence of Ni and W in the catalyst leads to formation of bimetallic Ni-W nitride species on the surface of the Ni-W(P)/γ-Al_2O_3 nitride catalysts.

6. Introduction of P in Ni-W(P)/γ-Al_2O_3 reduces the metal-support interaction and increases dispersion of active species on the catalyst surface. P also promotes formation of bi-metallic nitride species.

7. Active bimetallic Ni-W nitride catalysts decompose at temperatures above 800 °C to form less active Ni and W metals.

8. The presence of W in Ni-W(P)/γ-Al_2O_3 prompts the formation of Ni-W bimetallic nitride species and reduces the formation of Ni_3N species on the catalyst surface.

8.1.3 Hydrotreating of Gas oil

1. Ni-W(P)/γ-Al_2O_3 nitride catalyst exhibits a parabolic activity trend for HDS and HDA of LGO and a near linear trend for HDN with increase in the Ni, P and T_N and at W loading of 15 wt%. Increase in tungsten loading increases the number of active sites and increases HDS and HDN activities linearly. HDS and HDN increased by 23.5 and 47 wt% respectively, as W loading increased from 15 to 40 wt%.

2. Increase in Ni loading of Ni-W(P)/γ-Al_2O_3 increases the HDS and HDN activities of light gas oil. This is due to the enhanced formation of Ni-W bimetallic nitride species.

3. Increase in T_N decreases the HDS and HDN activities of LGO due to reduction in dispersion and loss of active bimetallic Ni-W nitride species and formation of less active Ni and W metals on the catalyst surface. BET and SEM results showed that increase in T_N results in decreased surface area and dispersion, respectively. XRD results showed loss of the active bimetallic Ni-W nitride species and formation of less active Ni and W metals on the catalyst surface.

4. HDS, HDN and HDA of LGO over Ni-W(P)/γ-Al_2O_3 nitride catalysts can be modeled statistically using analyses of variance (ANOVA). Significant models were developed for the hydrotreating reactions and they predicted well the experimental results.

5. At 15 wt% W loading, synthesis parameters (Ni, P and T_N) of Ni-W(P)/γ-Al_2O_3 nitride catalyst for high, HDS (88 wt%), HDN (59 wt%) and HDA (47 wt%) can be optimized at Ni = 2.5 wt%, P = 1 wt% and T_N = 560 °C).

6. Ni-W(P)/γ-Al_2O_3 nitride catalysts are stable to deactivation during hydrotreating of LGO at 385 ºC, 9.0 MPa and LHSV of 2 h^{-1}. After prolonged exposure (51 days on stream) to hydrotreating, the observed loss in HDS and HDN activities were < 3 wt%.

7. Ni-W(P)/γ-Al_2O_3 nitride catalysts are stable in the presence of sulfur compounds during hydrotreating. HDS and HDN activities for nitride and sulfide catalysts are comparable within the conditions studied.

8. Hydrogen pressure has more effect on HDN than on HDS of LGO within the process conditions studied. This indicates that HDS goes through one-step desulfurization process during hydrotreating of LGO. Temperature has the most significant effect on both HDS and HDN reactions.

8.1.4 Correlation of Catalyst Surface Properties to Activity

1. N_3N and W_2N as observed in XRD analyses, are among the active species on the catalyst surface. However, bimetallic Ni_2W_3N is the most active species for hydrotreating of LGO from Athabasca.
2. In terms of P loading, HDS and HDN of LGO have negative correlations with the number of exposed active sites, the amount of nitrogen in the catalyst and the available surface area for reaction. This means the number of exposed active sites (in the case of different active species) is not a direct measure of the strength of the active sites.
3. Catalyst particle size and surface area correlate positively with HDS and HDN of LGO but the nitrogen content of the catalyst has negative correlation. Increase in Ni loading reduces catalyst particle size and increases surface area. However, increase in Ni loading

at 30 wt% W promotes formation of bimetallic nitrides leading to decrease in N content but increase in catalyst activity.

4. The amount of chemisorbed oxygen and catalyst nitrogen content correlate positively with HDS and HDN reactions as W loading is varied. At 4 wt% Ni loading, optimum bimetallic nitride is already formed and further increase in W loading leads to formation of more W_2N which increases the number of exposed active sites and nitrogen content of the catalyst.
5. Increase in T_N increases catalyst particle size which reduces catalyst HDS and HDN activities. Increase in T_N leads to decomposition of nitrides and formation of less active metals. This decreases the amount of catalyst nitrogen content, the number of exposed active species and decreases the HDS and HDN activities. Increase in T_N leads to agglomeration of active sites which reduces catalyst surface area and decreases catalyst activity.

8.1.5 Kinetic Analyses

1. Langmuir-Hinshelwood kinetic model provides a better fit to HDS and HDN of LGO over Ni-W(P)/γ-Al_2O_3 nitride catalyst compared to Power law models.
2. HDS of LGO over Ni-W(P)/γ-Al_2O_3 uses two active sites during reaction while HDN reaction uses only one site.
3. HDS of LGO over Ni-W(P)/γ-Al_2O_3 is inhibited by sulfur and hydrogen compounds but HDN is inhibited by only nitrogen compounds.
4. Activation energies for HDS and HDN of LGO over Ni-W(P)/γ-Al_2O_3 nitride catalysts are 66 and 32 kJ/mol, respectively.

8.2 Recommendations

The following recommendations are made for further improvement in the activity of Ni-W(P)/γ-Al_2O_3 nitride catalysts

1. Ni-W(P)/γ-Al_2O_3 nitride catalysts were found active for HDS, HDN and HDA reactions, their HDS and HDN activities were only comparable to those of the corresponding sulfides. The activities of nitrides increase, especially, at high tungsten loadings and low nitriding temperatures. It is recommended to do further investigation at these conditions.

2. Passivation of nitride catalysts after synthesis only for it to be reduced prior to hydrotreating is not efficient for the hydrotreating process. TPR results showed that reduction of Ni_3N species occurs just around the same temperature reported in the literature for passive layer reduction. More investigations should be done to ensure that Ni_3N species are not reduced in the process of reducing the passive layer as this will reduce the overall activity of the catalyst. Options available include finding ways of synthesizing nitride catalysts in the hydrotreater (in-situ synthesis). This will make redundant the need to passivated the catalyst and maintain the original activity of the nitride catalyst.

REFERENCES

"*NIST/SEMATECH e-Handbook of Statistical Methods*," **2010** (2010).

Aegerter, P. A., W. W. C. Quigley, G. J. Simpson, D. D. Ziegler, J. W. Logan, K. R. McCrea, S. Glazier and M. E. Bussell, "Thiophene Hydrodesulfurization over Alumina-Supported Molybdenum Carbide and Nitride Catalysts: Adsorption Sites, Catalytic Activities, and nature of the Active Surface," Journal of Catalysis. **164**, 109-121 (1996).

Alboudwarej, H., J. Felix, S. Taylor, R. Badry, C. bremner, C. Skeates, A. baker, D. Palmer, K. Pattison, M. Beshry, G. Brown, R. Calvo, J.A.C. Triana, R. Hathcock, K. Koerner, T. Hughes, D. Kundu, J.L. Cardenas and C. West, "Highlighting Heavy Oil," **18**, 20 (2006).

Alonso, G., J. Espino, G. Berhault, L. Alvarez and J.L. Rico, "Activation of tetraalkylammonium thiotungstates for the preparation of Ni-promoted WS_2 catalysts," Applied Catalysis A: General. **266**, 29-40 (2004).

Ancheyta, J., M. J. Angeles, J. M. Macias, G. Marroquin and R. Morales, "Changes in Apparent Reaction Order and Activation Energy in the Hydrodesulfurization of Real Feedstocks," Energy and Fuels. **16**, 189-193 (2002).

Atanasova, P. and T. Halachev, "Phosphorus induced formation of a NiWO4 phase in the oxide form of P-Ni-W/Al_2O_3 catalysts," Applied Catalysis A: General. **108**, 123-139 (1994).

Atanasova, P., T. Tabakova, C. Vladov, T. Halachev and A. Lopez Agudo, "Effect of phosphorus concentration and method of preparation on the structure of the oxide form of phosphorus-nickel-tungsten/alumina hydrotreating catalysts," **161**, 105-119 (1997).

Bafrali, R. and A. T. Bell, "Interactions of H_2 and NH_3 with Mo(100) and Mo(100)-c(2 × 2) N surfaces," Surface Science. **278**, 353-363 (1992).

Balasubramanian, C., S. Bellucci, S. Cinque, A. Marcelli, M.C. Guidi, M. Piccinini, A. Popov and A. Soldatov, "Characterization of aluminium nitride nanostructures by XANES and FTIR spectroscopies with synchrotron radiation," J. Phys. : Condens. Matter. **18**, S2095-S2104 (2006).

Bej, S. K., A. K. Dalai and S. K. Maity, "Effect of Diluent Size on the Performance of a Micro-Scale Fixed Bed Multiphase Reactor in Up Flow and Down Flow Modes of Operation," Catal. Today. **64**, 333-345 (2001).

Bej, S. K., R. P. Debral, P. C. Gupta, K. K. Mittal, G.S. Sen, V. K. Kapoor and A. K. Dalai, "Studies on the Performance of a Micro Trickle Bed Reactor Using Different Sizes of Diluent," Energy and Fuels. **14**, 701-705 (2000).

Benitez, A., J. Ramfrez, J. L. G. Fierro and A. L. Agudo, "Effect of fluoride on the structure and activity of $NiW/A1_20_3$ catalysts for HDS of thiophene and HDN of pyridine," Applied Catalysis A: General. **144**, 343-364 (1996).

Botchwey, C., A. K. Dalai and J. Adjaye, "Product Distribution during Hydrotreating and Mild Hydrocracking of Bitumen-Derived Gas Oil," Energy and Fuels. **17**, 1372-1381 (2002).

Breysse, M., J. L. Portefaix and M. Vrinat, "Support effects on hydrotreating catalysts," Catalysis Today. **10**, 489-505 (1991).

Calafat, A., J. Laine, A. Lopez-Agudo and J. M. Palaciosy, "Effect of Surface Oxidation of the Support on the Thiophene Hydrodesulfurization Activity of Mo, Ni, and NiMo Catalysts Supported on Activated Carbon," Journal of Catalysis. **162**, 20-30 (1996).

Callejas, M. A. and M. T. Martinez, "Hydroprocessing of a Maya Residue. Intrinsic Kinetics of Sulfur-, Nitrogen-, Nickel-, and Vanadium-Removal Reactions," Energy and Fuels. **13**, 629-636 (1999).

Carberry, J. J. and A. Varma, "Diffusion-Reaction Interactions in Catalyst Pellets," in "Chemical Reaction and Reactor Engineering," Anonymous Marcel Dekker, Inc:, New York, (1987), pp 239-292.

Chen, J. and Z. Ring, "Modeling and Simulation of a Fixed-Bed Pilot-Plant Hydrotreater," Industrial and Engineering Chemistry Research. **40**, 3294-3300 (2001).

Chen, X., T. Zhang, M. Zheng, Z. Wu, W. Wu and C. Li, "The reaction route and active site of catalytic decomposition of hydrazine over molybdenum nitride catalyst," J. Catal. **224**, 473-478 (2004).

Chen, Y.–W. and M.-C. Tsai, "Highly Restrictive Diffusion under Hydrotreating Reactions of Heavy Residue Oils," Industrial and Engineering Chemistry Research., 898-905 (1995).

Cho, D.-., T.-. Chang and C.-. Shin, "Variations in the surface structure and composition of tungsten oxynitride catalyst caused by exposure to air," Catalysis Letters. **67**, 163-169 (2000).

Choi, J.–., J. R. Brenner, C. W. Colling, B. G. Demczyk, J. L. Dunning and L. T. Thompson, "Synthesis, Characterization and Molybdenum Nitride Hydrodenitrogenation Catalysts," Catalysis Today. **15**, 201-222 (1992).

Chu, Y., Z. Wei, S. Yang, C. Li, Q. Xin and E. Min, "NiMoNx/γ-Al_2O_3 Catalyst for HDN of Pyridine," Applied Catalysis A:General. **176**, 17-26 (1999).

Claridge, J. B., A. P. E. York, A. J. Brungs and M. L. H. Green, "Study of the Temperature-Programmed Reaction Synthesis of Early Transition Metal Carbide and Nitride Catalyst Materials from Oxide Precursors," Chem. Mater. **12**, 132-142 (2000).

Colling, C. W., J.–. Choi and L. T. Thompson, "Molybdenum Nitride Catalysts II. H_2 Temperature Programmed Reduction and NH_3 Temperature programmed Desorption," Journal of Catalysis. **160**, 35-42 (1996).

Cruz, J., M. Avalos-Borja, R. L. Cordero, M. A. Banares, J. L. G. Fierro, J. M. Palacios and A. L. Agudo, "Influence of pH of the impregnation solution on the phosphorus promotion in W/Al2O3 hydrotreating catalysts," Applied Catalysis A: General. **224**, 97-110 (2002).

Da Costa, P., J. L. Lemberton, C. Potvin, J.–. Manoli, G. Perot, M. Breysse and G. Djega-Mariadassou, "Tetralin Hydrogenation Catalyzed by Mo_2C/Al_2O_3 and WC/Al_2O_3 in the Presence of H_2S," Catalysis Today. **65**, 195-200 (2001).

Daly, F. P., "The use of binary oxides as catalyst supports for hydrodesulfurization and hydrodenitrogenation," Journal of Catalysis. **116**, 600-603 (1989).

DeCanio, E. C. and J. G. Weissman, "FT-IR analysis of borate-promoted Ni-Mo/Al_20_3 hydrotreating catalysts," Colloids and Surfaces A: Physicochemical and Engineering Aspects. **105**, 123-132 (1995).

Dezelah IV, C. L., O. M. El-Kadri, M. J. Heeg and C. H. Winter, "Preparation and Characterization of Molybdenum and Tungsten Nitride Nonoparticles Obtained by Thermolysis of Molecular Precursors," Preparation and Characterization of Molybdenum and Tungsten Nitride Nonoparticles obtained by Thermolysis of Molecular Precursors. **14**, 3167-3176 (2004).

Dolce, G. M., P. E. Savage and L. T. Thompson, "Hydrotreatment Activities of Supported Molybdenum Nitrides and Carbides," Energy and Fuels. **11**, 668-675 (1997).

Doraiswamy, L. K. and M. M. Sharma, "Estimation of Effective Transport Properties," in "Heterogeneous Reactions: Analysis, Examples, and Reactor Design," Anonymous John Wiley & Sons Inc, New York (1984), pp. 202-219.

Duchet, J. C., N. Gnofam, J. L. Lemberton, G. Perot, L. Bekakra, C. Moreau, J. Joffre, S. Kasztelan and J. Grimblot, "Catalytic properties of nickel molybdenum sulfides supported on nickel and magnesium aluminates " Catalysis Today. **10**, 612 (1991).

Eijsbouts, S., De Beer, V. H. J. and R. Prins, "Hydrodenitrogenation of quinoline over carbon-supported transition metal sulfides," Journal of Catalysis. **127**, 619-630 (1991).

Eijsbouts, S., J. N. M. Gestel, Van Veen, J. A. R., De Beer, V. H. J. and R. Prins, "Effect of phosphate on the hydrodenitrogenation activity and selectivity of alumina-supported sulfided molybdenum, nickel, and nickel-molybdenum catalysts," Journal of Catalysis. **131**, 412-32 (1991).

Eliche-Quesada, D., J. Merida-Robles, P. Maireles-Torres, E. Rodriguez-Castellon, G. Busca and E.J. Finocchio A., "Effects of preparation method and sulfur poisoning on the hydrogenation and

ring opening of tetralin on NiW/zirconium-doped mesoporous silica catalysts," Journal of Catalysis. **220**, 457-467 (2003).

Engemann, C., R. Franke, J. Hormes, C. Lauterbach, E. Hartmann, J. Clade and M. Jansen, "X-ray absorption near-edge spectroscopy XANES/ at the phosphorus K-edge of triorganophosphinechalcogenides," Chemical Physics. **243**, 61-75 (1999).

EnviroFuels, L. L. C., "Ultra-Low Sulfur Diesel: Operational Challenges Facing Engine Operators," 2007. **2010**, 4 (2007).

Escalona, N., J. Ojeda, J. M. Palacios, M. Yates and J. L.G. Fierro, "Promotion of Re/Al_2O_3 and Re/C catalysts by Ni sulfide in the HDS and HDN of gas oil: Effects of Ni loading and support," Applied Catalysis A: General. **319**, 218-229 (2007).

Ferdous, D., A. K. Dalai and J. Adjaye, "X-ray absorption near edge structure and X-ray photo electron spectroscopy analyses of $NiMo/Al_2O_3$ catalysts containing boron and phosphorus," Journal of Molecular Catalysis A: Chemical. **234**, 169-179 (2005).

Ferdous, D., A K. Dalai and J. Adjaye, "A series of $NiMo/Al_2O_3$ catalysts containing boron and phosphorus Part I. Synthesis and characterization," Applied Catalysis A: General. **260**, 137-151 (2004).

Ferdous, D., A K. Dalai and J. Adjaye, "A series of $NiMo/Al_2O_3$ catalysts containing boron and phosphorus Part II. Hydrodenitrogenation and hydrodesulfurization using heavy gas oil derived from Athabasca bitumen," Applied Catalysis A: General. **260**, 153-162 (2004).

Ferdous, D., N. N. Bakhshi, A. K. Dalai and J. Adjaye, "Synthesis, characterization and performance of NiMo catalysts supported on titania modified alumina for the hydroprocessing of different gas oils derived from Athabasca bitumen," Applied Catalysis B: Environmental. **72**, 118-128 (2007).

Fish, R. H., J. N. Michaels, R. S. Moore and H. Heinemann, "Gas-phase hydrodenitrogenation reactions of polynuclear heteroaromatic nitrogen compounds and selected intermediates with a

50% nickel oxide/alumina supported on silica-alumina catalyst," Journal of Catalysis. **123**, 74-85 (1990).

Fogler, H. S., "Diffusion and Reaction," in "Elements of Chemical Reaction Engineering," Anonymous Prentice Hall Professional Technical Reference, Upper Saddle River (2006).

Froment, G .F. and K. B. Bischoff, "Fixed-Bed Catalytic Reactors," in "Chemical Reactor Analysis and Design," Anonymous John Wiley & Sons Inc, New York (1979), pp. 462-491.

Frost, C. M. and H. B. Jensen, "Hydrodenitrification of Crude Shale Oil," American Chemical Society, Division of Petroleum Chemistry., 119-128 (1973).

Furimsky, E., "Metal carbides and nitrides as potential catalysts for hydroprocessing," Applied Catalysis A: General. **240**, 1-28 (2003).

Gates, B. C., J. R. Katzer and G. C.A . Schuit, "Chemistry of Catalytic Processes," McGraw-Hill, New York (1979).

Gierman, H., "Design of Laboratory Hydrotreating Reactors Scaling Down of Trickle-Flow Reactors," Applied Catalysis. **43**, 277-286 (1988).

Gioia, F. and V. Lee, "Effect of Hydrogen Pressure on Catalytic Hydrodenitrogenation of Quinoline," Industrial and Engineering Chemistry Process Design and Development. **25**, 918-925 (1986).

Girgis, M. J. and B. C. Gates, "Reactivities, Reaction Networks, and Kinetics in High-Pressure Catalytic Hydroprocessing," Industrial and Engineering Chemistry Research. **30**, 2021-2058 (1991).

Gray, M. R., P. Jokuty, H. Yeniova, L. Nazarewycz and S. E. Wnke, "The Relationship between Chemical Structure and Reactivity of Alberta Bitumens and Heavy Oils," Canadian Journal of Chemical Engineering. **69**, 834 (1994).

Guerrero-Ruiz, A., Q. Xin, Y. J. Zhang and A. Marote-Valiente, "Microcalorimetric Study of H_2 Adsorption on Molybdenum Nitride Catalysts," Langmuir. **15**, 4927-4929 (1999).

Guin, J. A., K. J. Tsal and W. Curtis, "Intra-particle Diffusivity Reduction during Hydrotreatment of Coal-Derived Liquids," Industrial and Engineering Chemistry Process Design and Development. **25**, 515-520 (1986).

Gupta, A., "Physical and Chemical Properties," in "Handbook of Chemical Engineering Calculations," N. P. Chopey, Ed. McGraw-Hill, New York (2004), pp. 1.1-1.28.

Hada, K., M. Nagai and S. Omi, "XPS and TPR Studies of Nitrided Molybdena-Alumina," Journal of Physical Chemistry. **104**, 2090-2098 (2000).

Hada, K., J. Tanabe, S. Omi and M. Nagai, "Characterization of Cobalt Molybdenum Nitrides for Thiophene HDS by XRD, TEM and XPS," Journal of Catalysis. **207**, 10-22 (2002).

Hanlon, R. T., "Effects of P_{H2S}, P_H and P_{H2S}/P_H on the Hydrodenitrogenation of Pyridine," Energy and Fuels. **1**, 424-430 (1987).

Hara, Y., N. Minami, H. Matsumoto and H. Itagaki, "New synthesis of tungsten carbide particles and the synergistic effect with Pt metal as a hydrogen oxidation catalyst for fuel cell applications," Applied Catalysis A: General. **332**, 289-296 (2007).

Hensen, E. J. M., Y. van der Meer, van Veen, J. A. R. and J. W. Niemantsverdriet, "Insight into the formation of the active phases in supported NiW hydrotreating catalysts," Applied Catalysis A: General. **322**, 16-32 (2007).

Herle, P. S., M. S. Hegde, K. Sooryanarayana, T. N. G. Row and G. N. Subbanna, "Synthesis, structure and properties of a new ternary interstitial nitride: Ni_2W_3N," Journal of Material Chemistry. **8**, 1435-1440 (1998).

Herrera, J. M., J. Reyes, P. Roquero and T. Klimova, "New hydrotreating NiMo catalysts supported on MCM-41 modified with phosphorus," Microporous and Mesoporous Materials. **83**, 283-291 (2005).

Hiroshi, K., T. Fujikawa, H. Tagami and K. Idei, "Effect of Hydrogen Sulfide on Hydrodesulfurization of Straight-Run Light Gas Oil," Division of Petroleum Chemistry, Inc., 335-337 (2001).

Ho, C. T., "Hydrogenation Catalysis " Catalysis Review Science and Engineering. **30**, 117-160 (1988).

Hunter, M. A., A. Gentry, S. Lee, L. Groeneveld, C. Oliver and D. Pappal, "MAKFining-Premium Distllates Technology The Future of Distillate Upgrading," NPRA 2000 Annual Meeting. (2000).

Incropera, F. P. and D. P. DeWitt, "Introduction to Conduction," in "Introduction to Heat Transfer," C. Robichaud, Ed. John Wiley & Sons Inc, New York (1985), pp. 43-72.

Kabe, T., A. Ishihara and W. Qian, "Hydrodesulfurization and hydrodenitrogenation," Wiley-VCH, New York (1999).

Kasrai, M., M. Vasiga, M. S. Fuller, G. M. Bancroft and K. Fyfe, "Study of the effects of Ca sulfonate on antiwear film formation by X-ray absorption spectroscopy using synchrotron radiation," Journal of Synchrotron Radiation. **6**, 719-721 (1999).

Katzer, J. R. and R. Sivasubramanian, "Process and Catalyst Needs for Hydrodenitrogenation," Catalysis Reviews Science and Engineering. **20**, 155-208 (1979).

Kim, C. H., W. L. Yoon and I. C. Lee, "The effect of Ni loading and the sulfidation temperature on the structure and catalytic activity of Ni-W hydrodesulfurization catalysts," Applied Catalysis A: General. **144**, 159-175 (1996).

Kim, J. H. and K. L. Kim, "A study of preparation of tungsten nitride catalysts with high surface area," Applied Catalysis A: General. **181**, 103-111 (1999).

Kim, S. I. and S. I. Woo, "Effect of modifying alumina with sulfate and phosphate on the catalytic properties of molybdenum/alumina in HDS reaction," Journal of Catalysis. **133**, 124-35 (1992).

Klaus, J. W., S. J. Ferro and S. M. George, "Atomically controlled growth of tungsten and tungsten nitride using sequential surface reactions," Applied Surface Science. **162-163**, 479-491 (2000).

Kojima, R. and K.-. Aika, "Molybdenum nitride and carbide catalysts for ammonia synthesis," Applied Catalysis A: General. **219**, 141-147 (2001).

Kordulis, C., A. A. Lappas, C. Fountzoula, K. Drakaki, A. Lycourghiotis and I. A. Vasalos, "NiW-γ-Al_2O_3 catalysts prepared by modified equilibrium deposition filtration (MEDF) and non-dry impregnation (NDI). Characterization and catalytic activity evaluation for the production of low sulfur gasoline in a HDS pilot plant," Applied Catalysis A: General. **209**, 85-95 (2001).

Korlann, C., B. Diaz and M. E. Bussell, "Synthesis of Bulk and Alumina-Supported Bimetallic Carbide and Nitride Catalysts," Chemistry of Materials. **14**, 4049-4058 (2002).

Kozai, S., H. Kabashima and H. Hattori, "Participation of acidic sites on catalyst in hydrodenitrogenation of quinoline," Fuel. **79**, 305-310 (2000).

Kruse, J., P. Leinweber, K.-. Eckhardt and F. Godlinski, "Phosphorus $L_{2,3}$-edge XANES: overview of reference compounds," Journal of Synchrotron Radiation. **16**, 247-259 (2009).

Kwak, C., M. Y. Kima, K. Choib and S. H. Moon, "Effect of phosphorus addition on the behaviour of CoMoS/Al_2O_3 catalyst in hydrodesulfurization of and 4,6-dimethyldibenzothiophene dibenzothiophene," Applied Catalysis A: General. **185**, 19-27 (1999).

Lacroix, M., N. Boutarfa, C. Guillard, M. Vrinat and M. Breysse, "Hydrogenating properties of unsupported transition metal sulfides," Journal of Catalysis. **120**, 473-477 (1989).

Landau, M. V., M. Herskowitz, D. Givoni, S. Laichter and D. Yitzhaki, "Medium Severity Hydrotreating of Israeli Shale Oil – II. Testing of Novel Catalyst Systems in a Trickle Bed Reactor," Fuel. **77**, 3-13 (1997).

Lee, J. S., S. T. Oyama and M. Boudart, "Molybdenum Carbide Catalysts: I. Synthesis of Unsupported Powders Journal of Catalysis, **106**, 125-13, (1987)." Journal of Catalysis. **106**, 125-13 (1987).

Lee, K. S., H. Abe, J. A. Reimer and A. T. Bell, "Hydrodenitrogenation of Quinoline over High-Surface-Area Mo_2N," Journal of Catalysis. **139**, 34-40 (1993).

Lee, S. L. and M. de Wind, "Catani Improvement of Diesel Fuels with Single and Dual Stage Hydrotreating," American Chemical Society, Division of Petroleum Chemistry. **37**, 718-728 (1992).

Lee, S. Y., J. D. Seader, C. H. Tsai and F. E. Massoth, "Restrictive Liquid-Phase Diffusion and Reaction in Bidispersed Catalysts," Industrial and Engineering Chemistry Research. **30**, 1683-1693 (1991).

Leglise, J., V. Gestel and J.–C. Duchet, "Evidence for H_2S as Active Species in the Mechanism of Thiophene Hydrodesulfurization," in "Hydrotreating Technology for Pollution Control," Anonymous Marcel Dekker, Inc., New York (1996), pp. 147-157.

Lewandowskia, M. and Z. Sarbak, "The effect of boron addition on hydrodesulfurization and hydrodenitrogenation activity of $NiMo/Al_2O_3$ catalysts," Fuel. **79**, 487-495 (2000).

Li, Y., Y. Zhang, R. Raval, C. Li, R. Zhai and Q. Xin, "The modification of molybdenum nitrides: the effect of the second metal component," Catalysis Letters. **48**, 239-245 (1997).

Liang, C., W. Li, Z. Wei, Q. Xin and C. Li, "Catalytic Decomposition of Ammonia over Nitrided $MoN_x/\alpha\text{-}Al_2O_3$ and $NiMoN_y/\alpha\text{-}Al_2O_3$ Catalyst," Industrial and Engineering Chemistry Research. **39**, 3694-3697 (2000).

Liu, Y., C. Liu and G. Que, "Hydrodesulfurization of Dibenzothiophene over Cobalt-Molybdenum Nitride Catalysts," Energy and Fuels. **16**, 531-535 (2002).

Ma, X., K. Sakanishi and I. Mochida, " Hydrodesulfurization Reactivities of Various Sulfur Compounds in diesel Fuel," Industrial and Engineering Chemistry Research. **33**, 218-222 (1994).

Ma, X., K. Sakanishi, T. Isoda and I. Mochida, "Comparison of Sulfided Co-Mo/Al_2O_3 and Ni-Mo/Al_2O_3 Catalysts in Deep Hydrodesulfurization of Gas oil Fractions," Preprint-Division for Petroleum Chemistry AIChE. **39**, 622-626 (1994).

Maezawa, A., M. Kitamura, K. Wakamoto, Y. Okamoto and T. Imanaka, "Preparation of sulfided molybdenum catalysts from molybdenum hexacarbonyl," Chemistry Express. **3**, 1-4 (1988).

Malkani, K., P. Magnoux and G. Perot, "Hydrodenitrogenation of 7,8-Benzoquinoline over Nickel Molybdenum Alumina," Applied Catalysis. **30**, 371-375 (1987).

Marwaha, B. and D. Luss, "Hot Zones Formation in Packed Bed Reactors," Chemical Engineering Science. **58**, 733-738 (2003).

Massoth, F. E. and P. Zeuthen, "Sulfur Exchange Studies on a Mo/Al_2O_3 catalysts," Journal of Catalysis. **145**, 216-222 (1994).

McGee, R. C. V., K. B. Shyamal and L. T. Thompson, "Basic properties of molybdenum and tungsten nitride catalysts," Applied Catalysis A: General. **284**, 139-146 (2005).

McKetta, J. J., "Petroleum Processing Handbook," Marcel Dekker Inc, New York (1992), pp. 108-633.

Melo-Banda, J. A., J. M. Dominguez and G. Sandoval-Robles, "Hydrotreating of heavy Vacuum gas oil (HVGO) on Molybdenum and Tungsten Nitride Catalytic Phases," Catalysis Today. **65**, 279-284 (2001).

Milbourn, C., "EPA Gives the Green Light on Diesel-Sulfur Rule, in Environmental News," **2002** (2001).

Nagai, M., "Transition-Metal Nitrides for hydrotreating Catalyst – Synthesis, Surface Properties, and Reactivities," Applied Catalysis A: General. **322**, 178-190 (2007).

Nagai, M., T. Masunaga and N. Hanaoka, "Hydrodenitrogenation of Carbazole on a Mo/Al_2O_3 Catalyst. Effects of Sulfiding and Sulfur Compounds," Energy and Fuels. **2**, 645-651 (1988).

Nagai, M., Y. Goto, A. Irisawa and S. Omi, "Catalytic Activity and Surface Properties of Ni-trided Molybdena–Alumina for Carbazole Hydrodenitrogenation," Journal of Catalysis. **191**, 128-137 (2000).

Nagai, M., Y. Goto, O. Uchino and S. Omi, "TPD and XRD studies of molybdenum nitride and its activity for hydrodenitrogenation of carbazole," Catalysis Today. **43**, 249-259 (1998).

Nagai, M., T. Suda, K. Oshikawa, N. Hirano and S. Omi, "CVD preparation of alumina-supported tungsten nitride and its activity for thiophene hydrodesulfurization," Catalysis Today. **50**, 29-37 (1999).

Nava, H., J. Espina, G. Berhault and G. Alonso-Nun, "Effect of phosphorus addition on unsupported Ni–Mo–W sulfide catalysts prepared by the in situ activation of nickel/ tetramethylammonium thiomolybdotungstate," Applied Catalysis A: General. **302**, 177-184 (2006).

Neylon, M. K., S. Choi, H. Kwon, K. E. Curry and L. T. Thompson, "Catalytic properties of early transition metal nitrides and carbides: *n*-butane hydrogenolysis, dehydrogenation and isomerization," Applied Catalysis A: General. **183**, 253-263 (1999).

Niemantsverdriet, J. W., "Microscopy and Related Techniques:" in "Spectroscopy in catalysis," Anonymous Weinheim, New York (1993), pp. 193-218.

Okude, N., H. Noro, M. Nagoshi, H. Yamamoto, Y. Baba and T. A. Sasaki, "Electronic structures of phosphates studied by TEY-XANES and resonant AES," Journal of Electron Spectroscopy and Related Phenomena. **88-91**, 467-471 (1998).

Olguin, E., M. Vrinat, L. Cedeno, J. Ramirez, M. Borque and A. Lopez-Agudo, "Ti-Al The use of TiO_2-Al_2O_3 binary oxides as supports for Mo-based catalysts in hydrodesulfurization of thiophene and dibenzothiophene," Applied Catalysis A: General. **165**, 1-13 (1997).

Ozkan, U. S., L. Zhang and P. A. Clark, "Performance and Post reaction Characterization of γ-Mo2N Catalysts in Simultaneous Hydrodesulfurization and Hydrodenitrogenation Reactions," Journal of Catalysis. **172**, 294-306 (1997).

Pecoraro, T. A. and R. R. Chianelli, " Hydrodesulfurization catalysis by transition metal sulfides," Journal of Catalysis. **67**, 430-445 (1981).

Perez-Romo, P., C. Potvin, J.-. Manoli and G. Djega-Mariadassou, "Phosphorus-Doped Tungsten Oxynitrides: Synthesis, Characterization, and Catalytic Behaviour in Propene Hydrogenation and n-Heptane Isomerization," J. Catal. **205**, 191-198 (2002).

Philipopoulos, C. and N. Papayannakos, "Intra-particle Diffusion Effects and Kinetics of Desulfurization Reactions and Asphaltenes Cracking during Catalytic Hydrotreatment of a Residue," Industrial and Engineering Chemistry Research. **27**, 415-420 (1988).

Pille, R. C. and G. F. F. Yu, "Kinetic Study of Hydrogen Sulfide in the Conversion of Thiophene on Supported Co-Mo catalyst," Journal of Molecular Catalysis. **94**, 364-387 (1994).

Prins, R., de Beer, V. H. J. and G. A. Somorjai, "Structure and Function of the Catalyst and the Promoter Co-M- Hydrodesulfurization Catalyst," Catalysis Review-Science and Engineering. **31**, 1-41 (1989).

Prins, R., M. Egorova, A. Rothlisberger, Y. Zhao, N. Sivasankar and P. Kukula, "Mechanisms of hydrodesulfurization and hydrodenitrogenation," Catal. Today. **111**, 84-93 (2006).

Puurunen, R. L., S. M. K. Airaksinen and A. O. I. Krause, "Chromium(III) supported on aluminum-nitride-surfaced alumina: characteristics and dehydrogenation activity," Journal of Catalysis. **213**, 281-290 (2003).

Rabarihoela-Rakotovao, V., S. Brunet, G. Perot and F. Diehl, "Effect of H_2S partial pressure on the HDS of dibenzothiophene and 4,6-dimethyldibenzothiophene over sulfided $NiMoP/Al_2O_3$ and $CoMoP/Al_2O_3$ catalysts," Applied Catalysis A: General. **306**, 34-44 (2006).

Ramanathan, S. and S.T. Oyama, "New Catalysts for Hydroprocessing: Transition Metal Carbides and Nitrides," Journal of Physical Chemistry. **99**, 16365-16372 (1995).

Ramanathan, S., C. C. Yu and S. T. Oyama, "New Catalysts for Hydroprocessing: Bimetallic Oxynitrides, II. Reactivity Studies," Journal of Catalysis. **173**, 10-16 (1998).

Ramirez, J., J. Cuevas, L. Gasque, M. Vrinat and M. Breysse, "Promoting effect of fluorine on cobalt-molybdenum/titania hydrodesulfurization catalysts," Applied Catalysis. **71**, 351-361 (1991).

Rangwala, H.A., I.G. Dalla Lana, F.D. Otto, H. Yeniova and K. Al-Nuaimi, "Influence of Catalyst Properties and Operating Conditions on Hydrodenitrogenation of Quinoline," Energy and Fuels. **4**, 599-604 (1990).

Ranhotra, G. S., A. T. Bell and J. A. Reimer, "Cent. Adv. Mater Catalysis over molybdenum carbides and nitrides II. Studies of carbon monoxide hydrogenation and ethane hydrogenolysis," Journal of Catalysis. **108**, 40-49 (1987).

Reyes, J. C., M. Avalos-Borja, R. L. Cordero and A. L. Agudo, "Influence of phosphorus on the structure and the hydrodesulphurization and hydrodenitrogenation activity of W/Al_2O_3 catalysts," Applied Catalysis A: General. **120**, 147-162 (1994).

Rodriguez-Reinoso, F., "The Role of Carbon Materials in Heterogeneous Catalysis," Carbon. **36**, 159-175 (1998).

Sambi, I. S., K. C. Khulbe and R. S. Mann, "Catalytic Hydrotreatment of Heavy Gas Oil," Industrial and Engineering Chemistry Product Research and Development. **21**, 575-580 (1982).

Santillan-Vallejo, L. A., J. A. Melo-Banda, Reyes de la Torre, A. I., G. Sandoval-Robles, J. M. Domınguez, A. Montesinos-Castellanos and de los Reyes-Heredia, J. A., "Supported (NiMo,CoMo)-carbide, -nitride phases: Effect of atomic ratios and phosphorus concentration on the HDS of thiophene and dibenzothiophene," Catalysis Today. **109**, 33-41 (2005).

Satterfield, C. N., "Physical Characterization and Examination," McGraw-Hill, New York (1980), pp. 128.

Satterfield, C. N. and S. H. Yang, "Catalytic Hydrogenation of Quinoline in a Trickle-Bed reactor: Comparison with Vapour Phase Reaction, **23**, 11-19, (1984)." Industrial and Engineering Chemistry Process Design and Development. **23**, 11-19 (1984).

Satterfield, C. N. and J. F. Cocchetto, "Reaction network and kinetics of the vapour-phase catalytic hydrodenitrogenation of quinoline," Industrial and Engineering Chemistry Product Research and Development. **20**, 53-62 (1981).

Satterfield, C. N. and S. Gultekin, “Effect of Hydrogen Sulfide on the Catalytic Hydrogenation of Quinoline”, Industrial and Engineering Chemistry Process Design and Development, **20**, 62-68, (1981).

Seader, J. D. and E. J. Henley, "Membrane Separations," in "Separation Process Principles," Anonymous John Wiley & Sons Inc, New York (1998), pp. 713-777.

Selley, N. J., "Reaction Rate," in "Chemical Energetics," Anonymous William Clowes & Sons Ltd, London (1971), pp. 73-88.

Shi, C., X. F. Yang, A. M. Zhu and C. T. Au, "Catalytic activities of Tungsten Nitride for No dissociation and Reduction with Hydrogen," Catalysis Today. **93–95**, 819-826 (2004).

Shih, S.S., K.N. Mathur, J.R. Katzer, H. Kwart and A.B. Stiles, "Quinoline Hydrodenitrogenation: Reaction Network and Kinetics Preprint," American Chemical Society, Division of Petroleum Chemistry. **22**, 919-940 (1977).

Shimada, H., T. Sato, Y. Yoshimura, J. Hiraishi and A. Nishijima, "Support effect on the catalytic activity and properties of sulfided molybdenum catalysts," Journal of Catalysis. **110**, 275-284 (1988).

Shimura, M., Y. Shiroto and C. Takeuchi, "Effect of Catalyst Pore Structure on Hydrotreating of Heavy Oil," Industrial and Engineering Chemistry Research. **25**, 330-337 (1986).

Sie, S.T., "Reaction Order and Role of Hydrogen Sulfide in Deep Hydrodesulfurization of Gas Oils: Consequences for Industrial Reactor Configuration," Fuel Processing Technology. **61**, 149-171 (1999).

Siewe, C. N. and F. T. T. Ng, "Hydrodesulfurization of Cold Lake Diesel Fraction Using Dispersed Catalysts: Influence of Hydroprocessing Medium and Sources of H_2," Energy & Fuels. **12**, 598-606 (1998).

Sigurdson, S., V. Sundaramurthy, A.K. Dalai and J. Adjaye, "Phosphorus promoted trimetallic NiMoW/Al_2O_3 sulfide catalysts in gas oil hydrotreating," Journal of Molecular Catalysis A: Chemical. **291**, 30-37 (2008).

Singhal, G.H., R.L. Espino and J.E. Sobel, "Hydrodesulfurization of Sulfur Heterocyclic Compounds, Reaction Mechanisms," Journal of Catalysis. **67**, 446-456 (1981).

Speight, J. G., "The Desulfurization of Heavy Oils and Residua," Marcel Dekker Inc., New York (1981).

Speight, J. G., "The Desulfurization of Heavy Oils and Residua," Marcel Dekker, New York (2000).

Stanislaus, A. and B. H. Cooper, "Aromatic Hydrogenation Catalysis: A Review," Catalysis Reviews - Science and Engineering. **38**, 76-123 (1996).

Sun, M., T. Burgi, R. Cattaneo, D. van Langeveld and P. Prins, "TPS, XPS, QEXAFS, and XANES Investigation of the Sulfidation of NiW/Al_2O_3–F Catalysts," Journal of Catalysis. **201**, 258-269 (2001).

Sundaramurthy, V., A.K. Dalai and J. Adjaye, "The effect of phosphorus on hydrotreating property of NiMo/g-Al_2O_3 nitride catalyst," Applied Catalysis A: General. **335**, 204-210 (2008).

Suvanto, M., J. Raty and T.A. Pakkanen, "Catalytic activity of carbonyl precursor based W/Al_2O_3 and CoW/Al_2O_3 catalysts in hydrodesulfurization of thiophene," Applied Catalysis A: General. **181**, 189-199 (1999).

Tanaka, H., M. Boulinguiez and M. Vrinat, "Hydrodesulfurization of thiophene, dibenzothiophene and gas oil on various Co-Mo/TiO_2-Al_2O_3 catalyst**s**," Catalysis Today. **29**, 209-213 (1996).

Tatsumi, T., M. Taniguchi, S. Yasuda, Y. Ishii, T. Murata and M. Hidai, "Zeolite-supported hydrodesulfurization catalysts prepared by ion exchange with Mo and Mo-Ni sulfide clusters," Applied Catalysis A: General. **139** (1996).

Toolbox., T. E., "Density of fluids - changing pressure and temperature," The Engineering Toolbox. **2010**, 4 (2005).

Trawczynski, J., "Effect of synthesis conditions on the molybdenum nitride catalytic activity," Catalysis Today. **65**, 343-348 (2001).

Tsai M. –C. and Y.–W. Chen, "Restrictive Diffusion under Hydrotreating Reactions of Heavy Residue Oils in a Trickle Bed Reactor," Industrial and Engineering Chemistry Research. **32**, 1603-1609 (1993).

Tsai, M.-., F.E. Massoth, S.Y. Lee and J.D. Seader, "Effects of Solvent and Solute Configuration on Restrictive Diffusion in Hydrotreating," Industrial and Engineering Chemistry Research. **30**, 22-28 (1991).

van Herk, D., M.T. Kreutzer, M. Makkee and J.A. Moulijn, "Scaling down trickle bed reactors," Catalysis Today. **106**, 227-232 (2005).

Van Parijs, I.A. and G.F. Froment, "Kinetics of hydrodesulfurization on a Co-Mo/γ-AL_2O_3 Catalyst. 2. Kinetics of the Hydrogenolysis of Benzothiophene " Industrial and Engineering Chemistry Product Research and Development. **25**, 437-443 (1986).

Vishwakarma, S.K., "Sonochemical and Impregnated Co-W/γ-Al_2O_3 Catalysts: Performances and Kinetic Studies on Hydrotreatment of Light Gas Oil," 1-160, (2007).

Volpe, L. and M. Boudart, "Compounds of Molybdenum and Tungsten with High Specific Surface Area. I. Nitrides," Journal of Solid State Chemistry. **59**, 332-347 (1985).

Vrinat, M., D. Hamon, M. Breysse, B. Durand and T. des Courieres, "Zirconia- and alumina-supported molybdenum-based catalysts: a comparative study in hydrodesulfurization and hydrogenation reactions," Catalysis Today. **20**, 273-282 (1994).

Vrinat, M., M. Lacroix, M. Breysse, L. Mosoni and M. Roubin, "Catalytic properties in hydrogenation and hydrodesulfurization reactions of ruthenium sulfide solid solutions containing iron, cobalt, or nickel," Catalysis Letters. **3**, 405-412 (1989).

Wang, J., Y. Wang, J. Wena, M. Shen and W. Wang, "Effect of phosphorus introduction strategy on the surface texture and structure of modified alumina," Microporous and Mesoporous Materials. **121**, 208-218 (2009).

Wei, Z., Q. Xin, P. Grange and B. Delmony, "TPD and TPR Studies of Molybdenum Nitride," Journal of Catalysis. **168**, 176-182 (1997).

Weil, K. S., "The chromium tungsten nitride system: evidence of a disorder–order phase transformation," Journal of Solid State Chemistry. **177**, 1976-1986 (2004).

Whitehurst, D.D., I. Takaaki and I. Mochida, "Present State of the Art and Future Challenges in the Hydrodesulfurization of Polyaromatic Sulfur Compounds " Advances in Catalysis. **42**, 344-368 (1998).

Wikipedia, "Ultra-low sulfur diesel," **2010**, 7 (2010).

Wise, R.S. and E.J. Markel, "Synthesis of High Surface Area Molybdenum Nitride in Mixtures of Nitrogen and Hydrogen," Journal of Catalysis. **145**, 344-355 (1994).

Wood, J. and L.F. Gladden, "Modeling diffusion and reaction accompanied by capillary condensation using three-dimensional pore networks. Part 1. Fickian diffusion and pseudo-first-order reaction kinetics," Chemical Engineering Science. **57**, 3033-3045 (2002).

Yang, S. and L.M. Stock, "Molecular Catalytic Hydrogenation of Aromatic Hydrocarbons and the Hydrotreating of Coal Liquids," DE-AC22-91PC91056, 1-124 (1996).

Yang, S.H. and C.N. Satterfield, "Catalytic Hydrodenitrogenation of Quinoline in a Trickle-Bed Reactor," Industrial and Engineering Chemistry Process Design and Development. **23**, 20-25 (1984).

Yu, C.C., S. Ramanathan and S.T. Oyama, "New Catalysts for Hydroprocessing: Bimetallic M_I-M_{II}-O-N (M_I, M_{II} = Mo, W, V, Nb, Cr, Mn and Co)," Journal of Catalysis. **173**, 1-9 (1998).

Yu, C.C., S. Ramanathan, B. Dhanpani, J.G. Chen and S.T. Oyama, "Bimetallic Nb-Mo Carbide Hydroprocessing Catalysts: Synthesis, Characterization and Activity Studies," Journal of Physical Chemistry. **101**, 512-518 (1997).

Yu, C.Y., S.J. Hatcher and J.W. Bertsch, "Hydrodenitrogenation of Quinoline with Y-type Zeolite," Industrial and Engineering Chemistry Research. **28**, 13-20 (1989).

Yuhong, W., L. Wei, Z. Minghui, G. Naijia and T. Keyi, "Characterization and catalytic properties of supported nickel molybdenum nitrides for hydrodenitrogenation," Applied Catalysis A: General. **215**, 39-45 (2001).

Yui, S.M. and E.C. Sanford, "Kinetics of Hydrogenation of Aromatics Determined byCarbon-13 NMR for Athabasca Bitumen-Derived Middle Distillates," Preprints-American Chemical Society, Division of Petroleum Chemistry. **32**, 315-320 (1987).

Zhang, Q., W. Qian, A. Ishihara and T. Kabe, "Effect of H_2S on Hydrodesulfurization of Dibenzothiophene and 4,6-Dimethyldibenzothiophene," Sekiyu Gakkaishi. **40**, 185-191 (1997).

Zhao, D.-S., F.-T. Li, E.-P. Zhou and Z.M. Sun, "Kinetics and Mechanism of the Photooxidation of Thiophene by O_2 Adsorbed on Molecular Sieves," Chemical Research in Chinese Universities. **24**, 96-100 (2008).

APPENDICES

APPENDIX A
EXPERIMENTAL CALIBRATIONS

All equipment and instruments that were used in the catalyst nitriding process and hydrotreating reactions were calibrated. This included temperature controllers, mass flow controllers and a metering pump. The procedures and results are discussed below.

A.1 Reactor Temperature Controller Calibration

The reactor temperature controller was calibrated at the same reaction conditions as planned experimental runs. 2.5 g of spent catalyst was loaded together with silicon carbide and glass beads. Liquid hourly space velocity (LHSV) was 1 h^{-1} and hydrogen/oil was 600 ml/ml. Calibration temperature was varied from 340 to 420 °C. The catalyst temperature was measured from a thermowell that run down the length of the reactor through the bed. At each temperature set point, a thermocouple in the thermowell was moved along the length of the reactor within the range of the furnace at 1 cm intervals and the stable temperature recorded. The catalyst bed temperature profiles as measured from the thermowell at various temperature controller set points are shown in Figure A.1. These profiles show temperature variation along the heating range of the furnace. The average reactor temperature used for the experiment was evaluated over a range of steady temperatures from the calibration results, i.e. 2 cm from the bottom of the furnace to 12 cm up the furnace. Figure A.2 shows the average reactor temperature calibrated against the temperature controller set point.

A.2 Mass Flow Meter Calibration

The mass flow meter was calibrated for hydrogen gas flow at normal operating conditions i.e. temperature of 375 °C, pressure of 8.8 MPa and LHSV of 1 h^{-1}. The flow rate of the outlet hydrogen gas was calibrated against the mass flow controller set points using a bubble flow meter connected to the outlet of the backpressure regulator. Flow rates recorded were standardized using the operating atmospheric pressure and room temperature. For a particular flow rate, the corresponding standard volumetric flow rate was evaluated using Equation (A.1) where subscript “a”, denotes the actual operating conditions and “o”, the standard conditions.

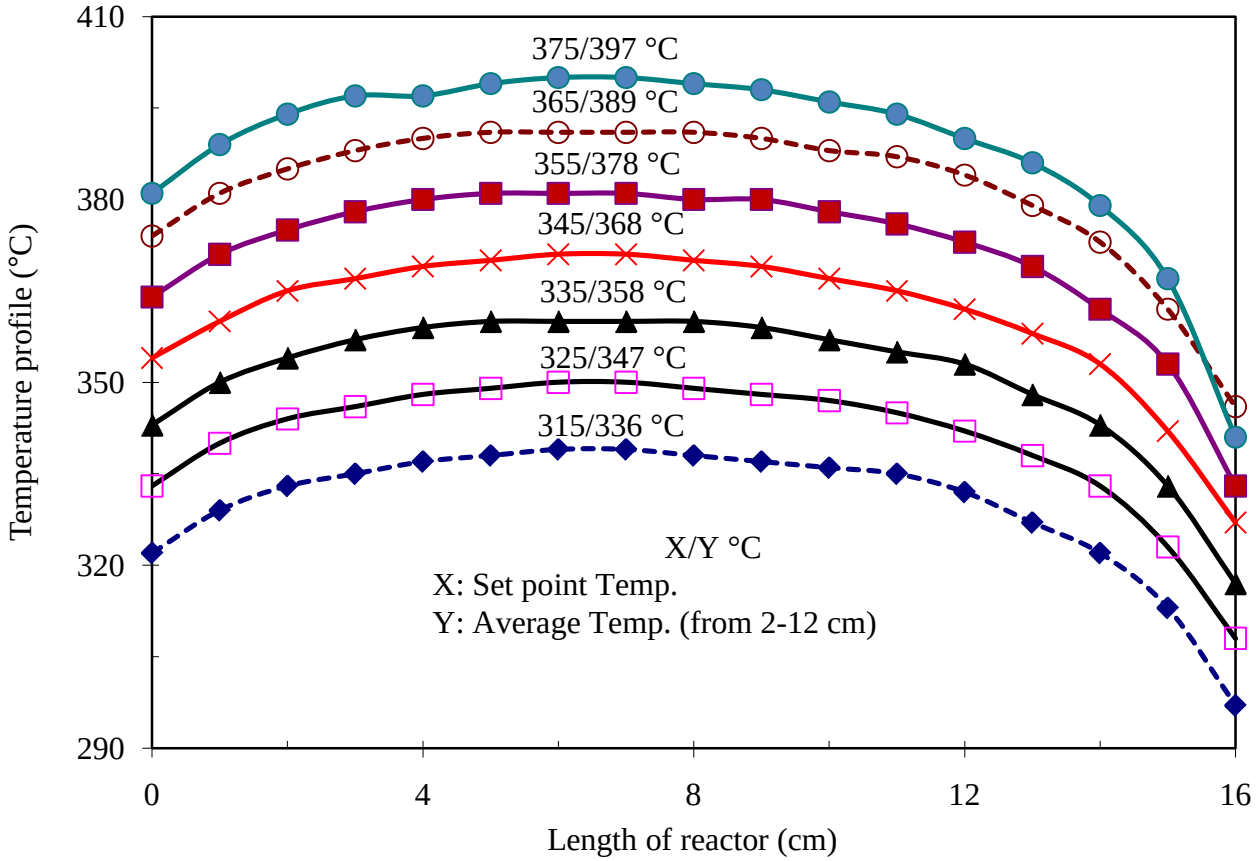

Figure A.1: Temperature pattern along the length of the reactor.

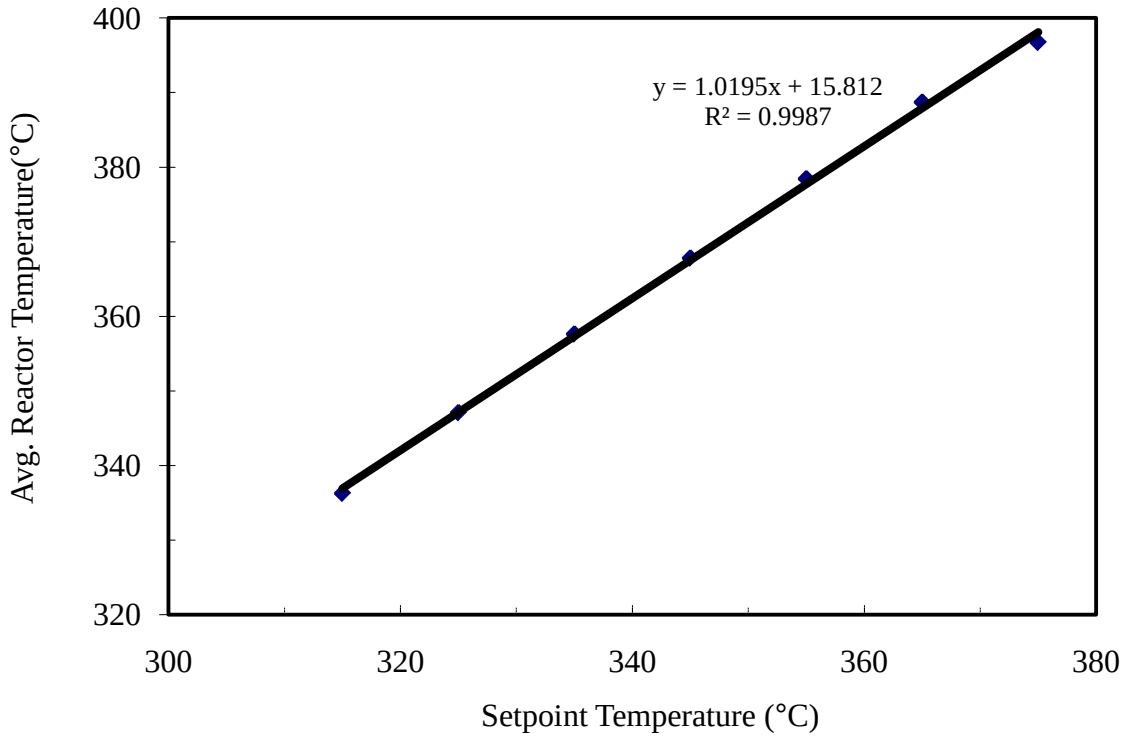

Figure A.2: Reactor average temperature curve.

$$V^o = \left(\frac{P_a}{P^o}\right)\left(\frac{T^o}{T_a}\right)V_a \qquad \text{(A.1)}$$

A plot of the standard volumetric flow rate against the mass flow controller set point as shown in Figure A.3 gave the readings necessary for the experimental hydrogen flow settings.

A.3 Pump Calibration

The Eldex metering pump was calibrated at the conditions used for precoking runs, i.e. 375 °C temperature and 8.8 MPa pressure. The mass flow rate of feed oil was measured at various set points from which a graph of mass and volumetric flow rate against pump set point was plotted (Figure A.4). The LHSV was calculated as

$$LHSV = \frac{\rho_c M_f}{\rho_f M_c}$$

where ρ_f , ρ_c are the feed oil and catalyst densities, respectively, and M_f, and M_c are the oil mass flow rate and mass of catalyst, respectively.

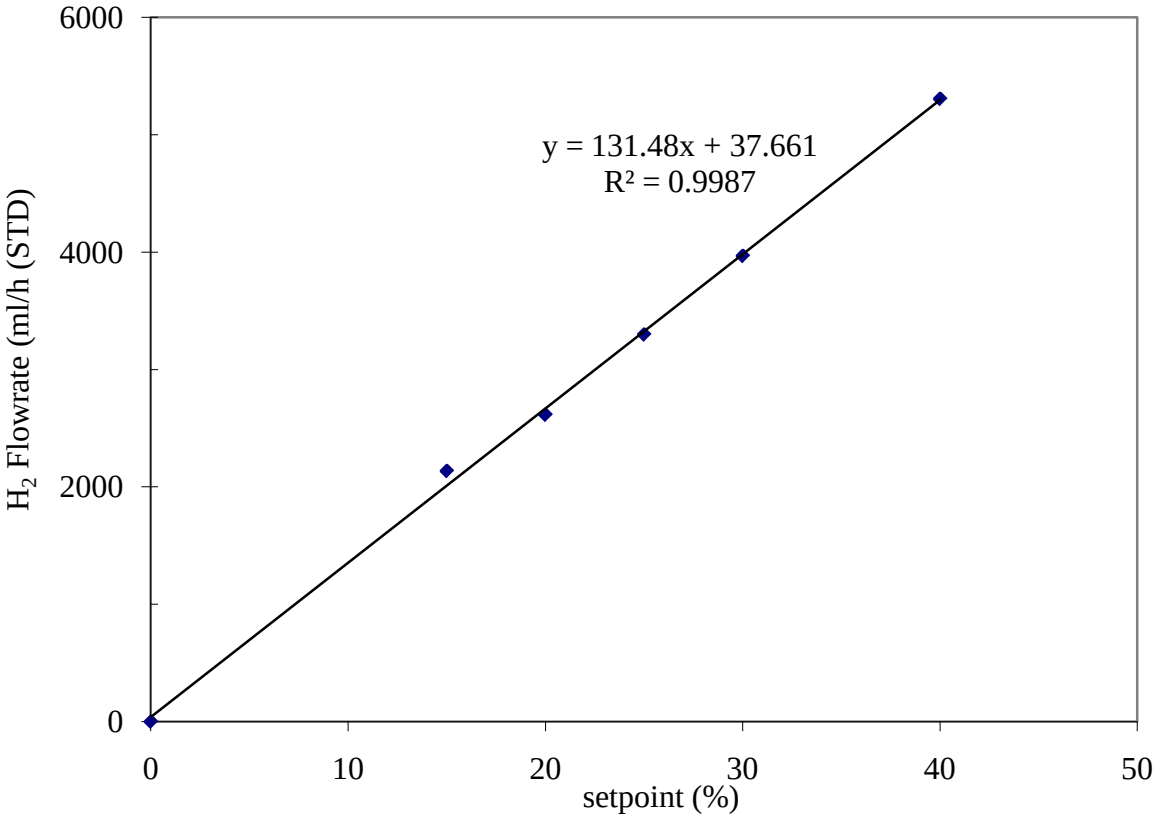

Figure A.3: Calibration curve for hydrogen mass flow controller.

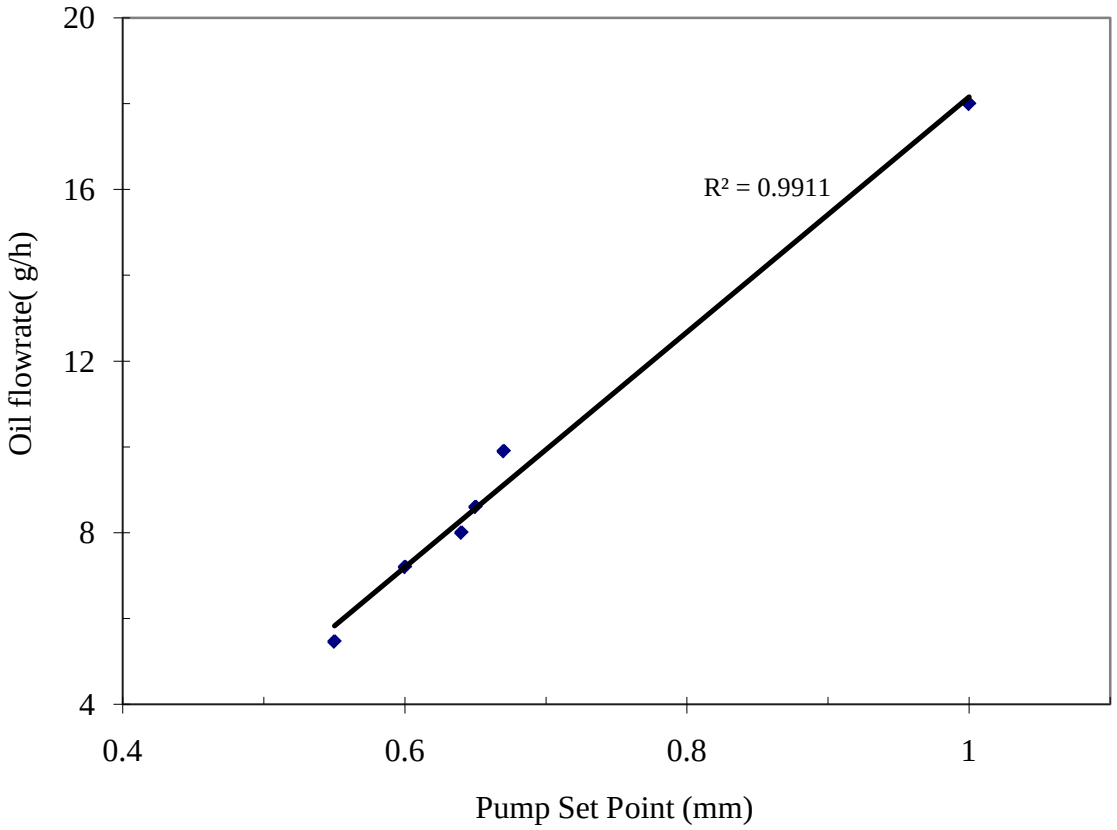

Figure A.4: Pump calibration curve.

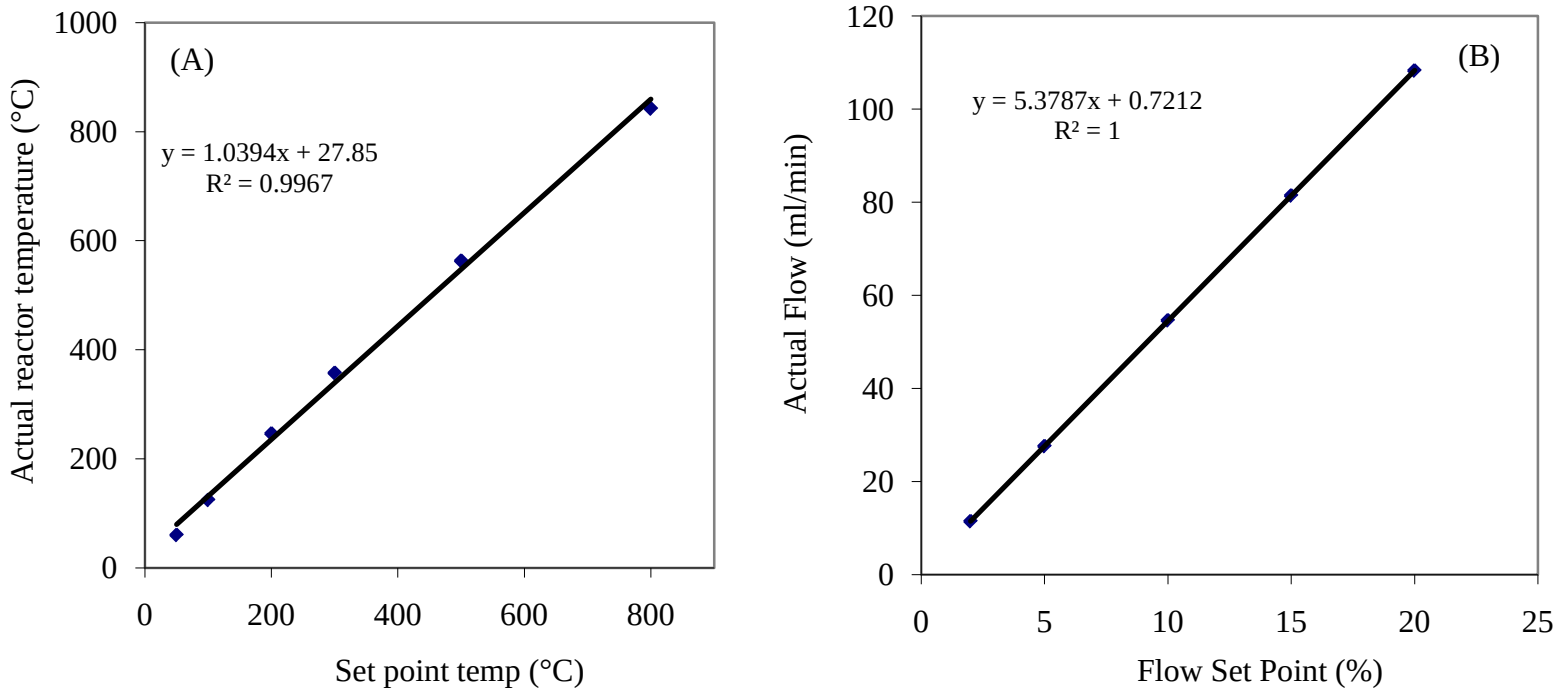

Figure A.5: (A) Temperature and (B) mass flow controller calibrations for temperature programmed nitriding set up.

APPENDIX B

STATISTICAL EXPERIMENTAL DESIGN

B.1 Central Composite Design

A central composite design is a statistical experimental design imbedded with 'factorial design points', 'center points' and 'star (axial) points'. The number of experiments to be performed depends on the number of factors under study. Figure B.1 shows the design structure for a three- factor CCD design. The total number of experimental runs (N) recommended by the

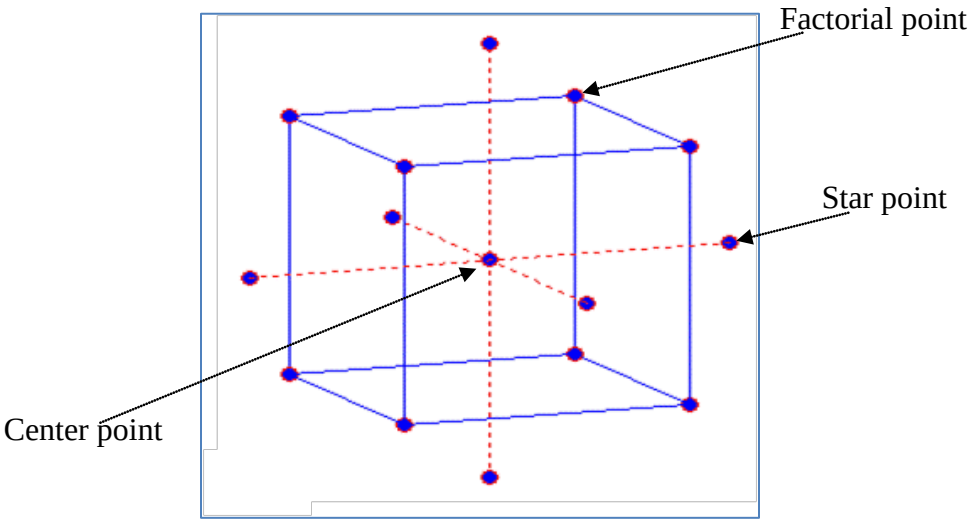

Figure B.1: Structure of central composite design.

design is given in Equations (B.1) and (B.2) where F is the number of factors (parameters) and

$$N_o = (\text{Factorial Points}) + (\text{Star Points}) + (\text{Center Points}) \quad \text{(B.1)}$$

i.e.

$$N_o = 2^F + 2F + n_C \quad \text{(B.2)}$$

n_C the number of center points (i.e. one center point with $n_C - 1$ replicates). The factorial points are the maxima and minima of each parameter and are coded -1 (for minima) and +1 (for maxima). The relation between the coded and actual parameter values is given by Equation (B.3) where CPV

$$CPV = -1 + \frac{(APV - APV_{\min})}{\frac{1}{2} * [APV_{\max} - APV_{\min}]} \quad \text{(B.3)}$$

is the coded parameter value and APV is the actual parameter value. The star points (α) are used to analyze curvature in the response and their values can be determined from the relation,

$$\alpha = (\text{Number of Factorial Points})^{1/4}$$

i.e. $$\alpha = 2^{F/4} \qquad \text{(B.4)}$$

to allow estimation of curvature. If the distance from the center of the design space to a factorial point is ±1 unit for each factor, the distance from the center of the design space to a star point is ± α with |α| > 1. For designs where the parameter minimum value was zero, all design points were divided by |α| to avoid having to work with negative parameter values. Center point is the midpoint between the maxima and minima. They are usually repeated 4-6 times to get a good estimate of experimental error (pure error) and inherent variability. The error is obtained from the expression $\bar{x} - x$ where $\bar{x}$ is the mean of the center point responses and x is a response of the center point.

B.2 Statistical Model Development

The regression model for each response was developed by sequentially adding terms such as linear, interaction and quadratic terms to a mean value (the constant of an equation) until the model became significant. A probability less than 0.05 indicated a significant model. This meant with 95% level of confidence, the observed experimental data could be adequately explained by the model. Other tests were also necessary to confirm the significance of the model. These were the lack of fit test and model statistic. A good model is one that fits well the observed data. For a model to well fit the data, the “model fit” should be “significant”. In other words or in statistical terms, the “lack of fit” should be, “not significant”. Model statistics are other indicators for adjudging a good model. Statistics such as the adjusted R-Squared and Predicted R-Squared must be in reasonable agreement and should be as close to unity as possible. "Adeq Precision" (adequate precision) is another statistic that measures the signal to noise ratio. A ratio greater than 4 is desirable.

The second step in the data analyses was to look at the diagnostics to see if all the assumptions made in the model development were obeyed. One that was of much importance was the parity plot between model prediction and observed data. The maximum error in the prediction gave an idea of how good the prediction was. Under model graphs, the effect of the various

factors (parameters) on the responses will be discussed. The significance of the trends in the graphs will also be discussed. The final section under analyses would be the optimization of the catalyst for the various responses. A measure of the optimization is the desirability factor. A desirability factor close to unity is an indication of how good the optimization was.

B.2.1 Modeling of Catalyst Screening Results: HDS

The model that appropriately described the HDS data from statistical analysis was a reduced quadratic. It is reduced because it did not contain all the terms found in a full quadratic model. Terms that did not significantly contribute to the prediction of HDS were removed from the full model. As a result, the model was in coded form and actual parameter values have to be codified before they are used in the model. The coded reduced HDS model can be written in the form,

$$HDS = \left[\begin{pmatrix} 141.30 + 13.14 * T' - 19.61 * Ni'^{2} + 12.46 * P'^{2} + 7.85 * T'^{2} + \\ 6.56 * Ni' * P' - 23.48 * Ni' * T' - 23.04 * P' * T' \end{pmatrix} * 10^{-6} \right]^{-1/2} \quad \text{(B.5)}$$

where Ni', P' and T' are the coded factors (parameters) of Ni loading, P loading and nitriding temperature. The coded factors Ni', P' and T' can be evaluated from the relations,

$$Ni' = -1 + \frac{(Ni - 1.62)}{2.38} \qquad P' = -1 + \frac{(P - 1.01)}{1.49} \qquad T = -1 + \frac{(T - 560.81)}{89.2} \quad \text{(B.6)}$$

where Ni, P and T are the actual parameter values for Ni loading (0 to 8 wt %), P loading (0 to 5 wt %) and nitriding temperature (500 to 800 ºC), respectively. The model was highly significant in that there was less than 0.01% chance the chosen model was due to noise. For a good model fit, the probability associated with the lack of fit test should be greater than 0.1. In the HDS model lack of fit test, the probability was 0.28 indicating that the model fit was good. At "Adjusted R-Squared" of 0.99 and "Predicted R-Squared" of 0.95, a good agreement existed between the model summary statistics confirming the goodness of the fit. Figure 5.2 illustrates adequacy in prediction of the observed data with a minimum accuracy of 98 wt%. A response surface for HDS is shown in Figure B.2.

B.2.2 Modeling of Catalyst Screening Results: HDA

As in the case of HDS, HDA was also described by a reduced quadratic model and can be represented in coded factors as,

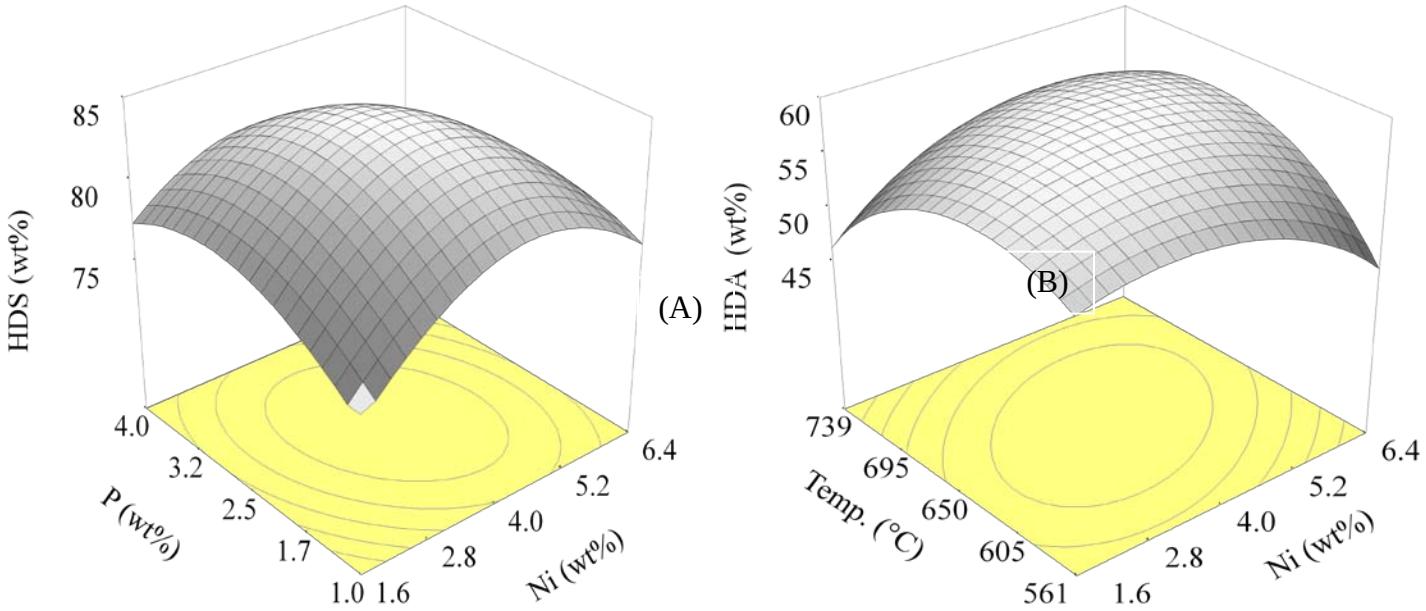

Figure B.2: (A) HDS and (B) HDA of LGO over Ni-W(P)/γ-Al_2O_3 nitride catalysts. Conditions: 30 wt% W, (A) T_N of 650 °C and (B) 2.5 wt% P.

$$HDA = \left[\left(20.41 - 3.21 * Ni'^2 - 5.25 * P'^2 - 4.55 * T'^2 + 2.7 * Ni' * T'\right) * 10^4\right]^{1/3} \quad \text{(B.7)}$$

Equation (B.6) is still applicable in Equation (B.7) in the conversion of Ni, P and T to the coded form. The model was significant with only 0.01% chance of it being due to noise. The model fit was equally good with a probability of 0.33 (it should not be < 0.1). The model summary statistics showed reasonable agreement between the Adjusted R-Squared (0.9025) and Predicted R-Squared (0.8198) confirming the fit of the model. The maximum error in data prediction was ±5.0 wt%. Adequate precision of 13.9 suggests that the model can effectively be used to navigate through the design space. The associated HDA response surface is shown in Figure B.2B.

B.2.3 Modeling of Catalyst Screening Results: HDN

The final model obtained for HDN after twenty experimental runs and data processing is shown in Equation B.8 where Ni is the nickel loading, P is the phosphorus loading and T the nitriding

$$HDN = \left[\begin{array}{l} 25219.6 - 2981.4 * Ni - 5.472.8 * P - 34.3 * T + 189.6 * Ni * P + \\ 3.8 * Ni * T + 7.4 * P * T \end{array}\right]^{1/2} \quad \text{(B.8)}$$

temperature. At 95% confidence level, analysis of variance (ANOVA) results showed that the model was significant with only 0.01% chance of the significance being due to noise. The lack of fit test also showed that the fit was significant (i.e. lack of fit – insignificant) with a probability of 0.56 (it should not be less than 0.1). There was good agreement between the "Adjusted R-Squared" (0.99) and "Predicted R-Squared" (0.95) (Table B.1) confirming goodness of the fit. Results of HDN activities in 3-D is shown in Figure B.3

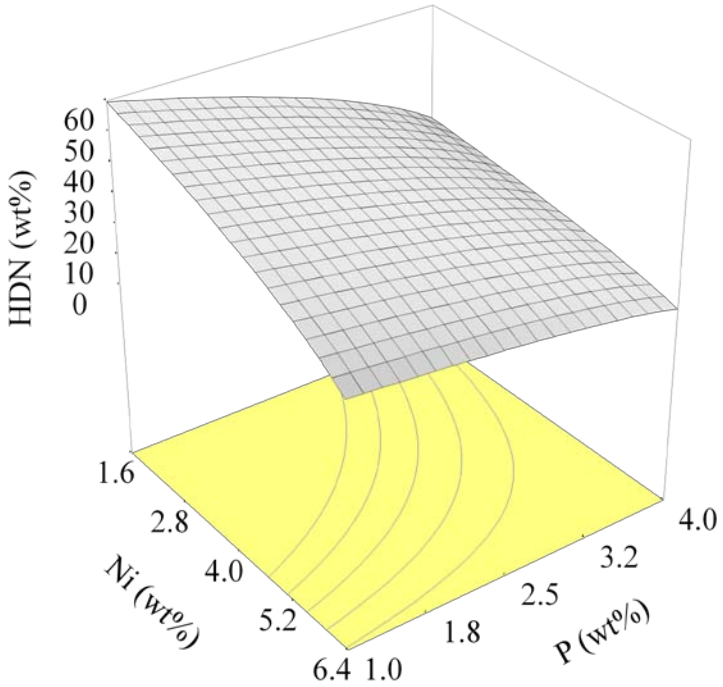

Figure B.3: HDN of LGO over Ni-W(P)/γ-Al_2O_3 nitride catalysts at T_N of 560 ^oC.

B.2.4 Effect of Process Conditions on HDS of LGO

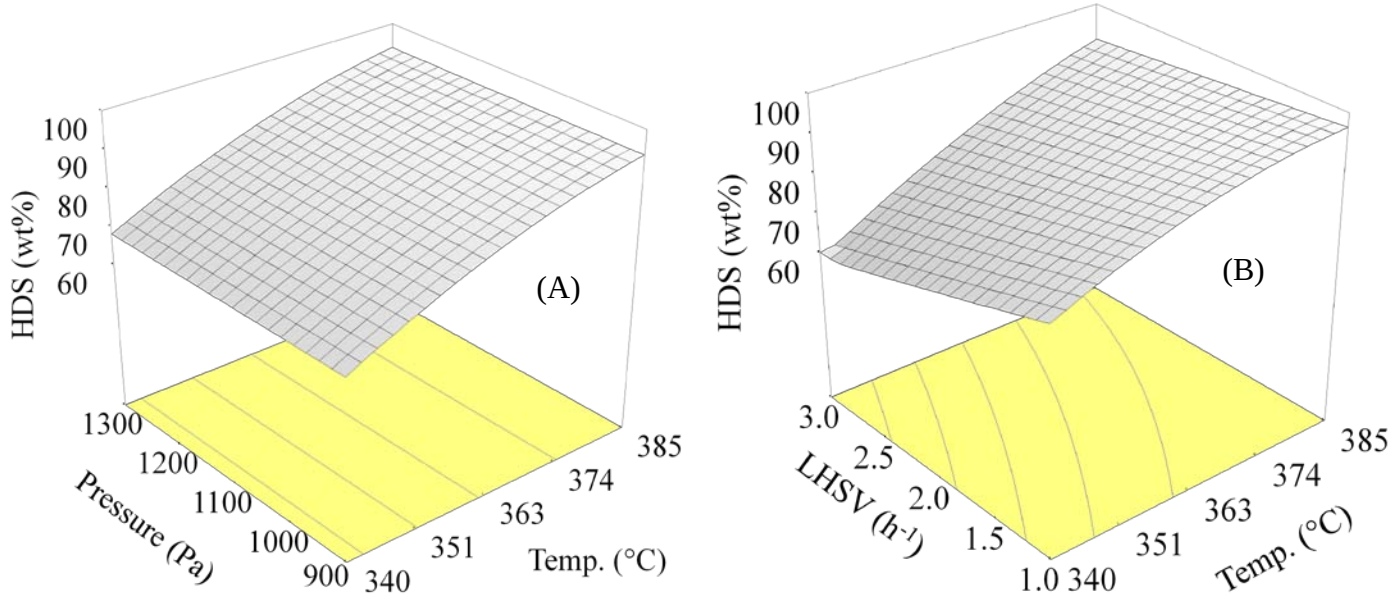

Figure B.4: Effect of process conditions on HDS of LGO over Ni-W(P)/γ-Al_2O_3 nitride catalyst. H_2/oil, 600 ml/ml (STP); (A) LHSV = 2 h^{-1}; (B) P_H = 7.6 MPa. Catalyst conditions: Ni = 2.5 wt%, P_H = 1 wt%, T_N = 560 °C.

Table B.1: Modeling statistics for effects of process conditions on HDS and HDN.

Statistic	HDS	HDN
Model Significance	Significant	Significant
Lack of fit	Not significant	Not significant
Adjusted R-Squared	0.955	0.826
Predicted R-Squared	0.914	0.756
Adequate Precision	29.35	18.45
Model Equation	$HDS = (-123 + 8*10^{-1}*T - 11*L - 10^{-3}*T^2 + 3*10^{-2}*T*L)^{1.56}$	$HDN = (-43 + 10^{-1}*T + 5*10^{-3}*P_H - 2*L)^{1.64}$

APPENDIX C

SAMPLE CALCULATIONS

C.1 Calculation for Amounts of Precursors in Catalyst Synthesis

For a given catalyst composition X (wt%), the amount of precursor Y (wt) required for synthesis is given by the relation

$$Y = \frac{X * M_c * MM * Z}{M_A * 100} \qquad \text{(C.1)}$$

where M_c is the total amount of catalyst to be synthesized, MM is the molecular weight (or equivalent) of the precursor, Z is the purity of the precursor and M_A is the atomic weight (or equivalent). For instance, 4 g of catalyst with the following composition is required: W = 15 wt%; Ni = 4 wt %; P = 2 wt%; and Al_2O_3 = 79 wt%. The precursors used in the catalyst syntheses and their corresponding molecular weights (or equivalent) are shown in Table C.1.

The amount of precursors required for 4 g of catalyst at the compositions above are given by Equation (C.1)) as follows:

1. For Ni, $$\mathrm{Ni(NO_3)_2} = \frac{4 * 4 * 290.81 * 0.999}{58.69 * 100} = 0.792g$$

2. For W, information provided by the manufacturer indicated that 100 g of the precursor contained 68.4 g of W, meaning the amount of ammonium metatungstate that will give 15 wt% catalyst W composition will be given by a modified Equation (C.1) as

$$\mathrm{(NH_4)_6W_{12}O_{39}xH_2O} = \frac{15 * 4 * 100 * 1}{68.4 * 100} = 0.877g$$

3. For P, the weight of phosphoric acid was divided by the specific gravity to obtain the volume (acid was in liquid form) required as

$$\mathrm{H_3PO_4} = \frac{2 * 4 * 98 * 0.85}{30.97 * 100 * 1.69} = 0.127cm^3$$

4. The amount Al_2O_3 required is given as,

   Composition (%) x Weight of Catalyst Required.

   i.e. Amount of Al_2O_3 = 0.79 * 4 = 3.16 g

Table C.1: Precursors used for catalyst syntheses and their molecular weights.

Element	Precursor	Molecular Weight (g)	Atomic Wt in Precursor (g)	Percentage Purity (%)
W	$(NH_4)_6W_{12}O_{39}{\cdot}xH_2O$	3226.51	2206.08	--
Ni	$Ni(NO_3)_2$	290.81	58.69	99.99
P	H_3PO_4	98	30.97	0.85

5. The approximate amount of water required for impregnation is a measure of the alumina pore volume and was given by the relation,

   1.4 x Weight of Al_2O_3 x Pore Volume

   = 1.4 * 3.16 * 0.55 = 2.43 cm^3

C.2 Mass Transfer Calculations

C.2.1 External Mass Transfer Limitations

Mears' criterion, defined in Section 7.3.1, is given by the expression

$$C_m = \frac{-r_i' \rho_b Rn}{k_c C_{Ab}} \prec 0.15 \qquad \text{(C.2)}$$

Evaluation of Observed Rate of Reaction (r_i')

r' was evaluated from the developed kinetic expressions for HDS – Equation (7.8) and HDN – Equation (7.9). For HDS,

$$-r'_s = \frac{0.5e^{\left(-66000/R_gT\right)} C_s P_H L^2}{\left(1+5.7*10^7 e^{\left(-61000/R_gT\right)} C_s\right)\left(1+10^8 e^{\left(-180000/R_gT\right)} P_H\right)} \qquad \text{(C.3)}$$

where

T = 598 K (325 °C)

R_g = 8.314 $Jmol^{-1}K^{-1}$

P_H = 7580000 Pa (1100 psi)

L = 5.6 *10^{-4} s^{-1} (2 h^{-1})

C_s = 0.73553 wt% (7355.3 ppm, i.e. mg/l)

This gives:

$$-r'_s = \frac{0.5e^{\left(-66*10^3/8.314*598\right)} * 0.73553 * 7.58*10^6 * 2^2}{\left(1+5.7*10^7 e^{\left(-61*10^3/8.314*598\right)} 0.73553\right)\left(1+10^8 e^{\left(-180*10^3/8.314*598\right)} 7.58*10^6\right)} * 10^4 = 967\, ppm.h^{-1}$$

Unit Conversion for $r_s^{'}$

The unit of $r_s^{'}$ in Equation (C.3) is in ppm.h^{-1} and need to be changed to kmol/kg.s. This is achieved as shown below:

$$-r'_s = \left[\frac{967\,ppm}{h}\right] * \left[\frac{10^{-3}\,Kg}{m^3}\right] * \left[\frac{h}{3600s}\right] * \left[\frac{LHSV}{134201.6kg}\right] / \rho_p = 1.75 * 10^{-15}\,kmol / kg_{cat}.s$$

where LHSV is the liquid hourly space velocity used to convert the units from volume of liquid sample to volume of catalyst (in this case, 5.56*10^{-4} S^{-1}) and ρ_p is the density of the catalyst (636 kg/m^3). Light gas oil contains various mixtures of sulfur compounds of which thiophenic monologs are the least reacting. As a result, the molecular weight of sulfur compounds (134.2016 g/mol), for the purpose of these calculations, was taken as the average of the molecular weights for thiophene (84.1418 g/mol), benzothiophene (134.2016 g/mol) and dibenzothiophene (184.2615 g/mol).

Evaluation of Mass Transfer Coefficient (k_c)

The mass transfer coefficient was evaluated from the dimensionless Sherwood parameter based on the Theones-Kramers correlation (Fogler, 2006)

i.e. $$k_c = \frac{Sh^{'} * D_e}{d_c} \qquad \text{(C.4)}$$

where

d_c = catalyst particle diameter (m)

D_e = effective diffusivity (m^2.s^{-1})

k_c = the mass transfer coefficient (m.s^{-1}) and

$$Sh^{'} = \left(\mathrm{Re}^{'}\right)^{1/2} \left(Sc\right)^{1/3} \qquad \text{(C.5)}$$

where $Sh^{'}$ and $\mathrm{Re}^{'}$ are modified Sherwood and Reynolds numbers while Sc is the Schmidt number, respectively.

Evaluation of Re′

$\mathrm{Re}^{'}$ is given by $$\mathrm{Re}^{'} = \frac{\rho_f U d_c}{\left(1-\varepsilon_b\right)\mu\psi} \qquad \text{(C.6)}$$

where ρ_f is the fluid density (kg/m^3), U is superficial velocity = 2.78*10^{-5} m/s, d_c is the catalyst particle diameter (equivalent diameter of sphere of the same volume) = 4.46*10^{-2} m, ε_b is the void fraction of the catalyst bed (assumed as 0.3 considering the 90-mesh SiC particles used for dilution during catalyst loading), μ is dynamic viscosity (kg/m.s) and ψ is shape factor (external surface area divided by $\pi(d_c)^2$. Density of the oil at operating temperature and pressure can be evaluated using Equation (C.7) (Engineering Toolbox, 2005)

$$\rho_1 = \frac{\rho_0}{1+\beta_v(T_1-T_0)} \Big/ \frac{1-(P_1-P_0)}{El} \qquad \text{(C.7)}$$

where

ρ_1 = final density (kg/m^3)

ρ_0 = initial density = 871 kg/m^3,

β_v = volumetric temperature expansion coefficient = 0.00095 (m^3/m^3 °C)

T_0 = initial temperature =15.6 °C

T_1 = final temperature = 325 °C

El = bulk modulus fluid elasticity = 1.5 *10^9 N/m^2 (The Engineering Toolbox)

P_1 = final pressure = 7580000 N/m^2

P_0 = initial pressure = 101 325.01 N/m^2

This gives a density of

$$\rho_1 = \frac{871}{\{1+0.00095(598-288.6)\}} \Big/ \frac{\{1-(7580000-101325.01)\}}{1.5*10^9} = 676.516 kg/m^3$$

Glasso's correlation, Equation (C.8) (Vishwakarma, 2007), was used to calculate viscosity of the gas oil at the operating conditions.

$$\mu = 3.141*10^{10}*(T-460)^{-3.444}*(\log^o API)^a \qquad \text{(C.8)}$$

where

$$a = 10.313\log\left(T - 460\right) - 36.447$$

T = operating temperature = 1076.4 °R and

$$^{o}API = \frac{141.5}{SG} - 131.5$$

Evaluating the equivalent density of water (945 kg/m^3) and S.G. (specific gravity) of LGO (0.716) at operating conditions gave °API of = 66.13. This implies

$$a = -7.675 \text{ and}$$

$$\mu = 3.141*10^{10} * \left(1076.4 - 460\right)^{-3.444} * \left(\log 66.13\right)^{-7.675}$$

$$= \underline{0.078 \text{ cp}} = \underline{7.8*10^{-5} \text{ kg/m.s}}$$

With all values in Equation(C.6), known Re' can be evaluated as

$$\text{Re}' = \frac{676.516*2.78*10^{-5}*1.5*10^{-3}}{\left(1-0.3\right)*7.8*10^{-5}*5.65*10^{-3}} = 2720$$

Evaluation of Sc

Sc is given by

$$Sc = \frac{\mu}{\rho_f D_b} \qquad \text{(C.9)}$$

Sc is as defined in Equation (C.5). D_b = bulk diffusivity (m^2/s) and μ and ρ_f are as defined in Equation (C.6).

Evaluation of fluid bulk diffusivity (D_b)

The fluid bulk diffusivity was evaluated from Equation (C.10) (Vishwakarma, 2007)

$$D_b = 8.93*10^{-8}\frac{\upsilon_L^{0.267} * T}{\upsilon_s^{0.433} * \mu} \qquad \text{(C.10)}$$

where

T = the operating temperature = 598 K

μ = as defined above =7.8*10^{-5} kg/m.s

υ_s = molar volume of sulfur compounds at normal boiling conditions (cm^3/mol)

υ_L = molar volume of gas oil at normal boiling conditions (cm^3/mol)

The molar volume of gas oil is given by the expression

$$\upsilon = 0.285 \upsilon_c^{1.048} \tag{C.11}$$

where the specific critical volume of gas oil v_c (cm^3/mol) is given by Equation (C.12)

$$\upsilon_c = 0.4695 * T_{M_x}^{0.2896} SG_{15.6}^{-0.7666} * M \tag{C.12}$$

T_{Mx} = Mean average boiling point = 1022.4 °R, (the mid boiling point of gas oil).

M = 134.20 g/mol = (see evaluation of observed rate of reaction above)

$SG_{15.6}$ = specific gravity at 15.6 °C

Evaluating Equation (C.12) gave

$$\upsilon_c = 0.4695 * 1022.4^{0.2896} * 0.871^{-0.7666} * 134.20 \ = \ 521 \text{ cm}^3 / \text{mol}$$

This implies molar volume of gas oil is

$$\upsilon_L = 0.285 * 521^{1.048}$$

$$\upsilon_L = 200.5 \text{ cm}^3/\text{mol}$$

The specific molar volume of sulfur compounds was evaluated from critical properties of the compounds (data obtained from ChemDraw) using Equation (C.13) (Gupta, 2004)

$$\upsilon_x = \sum_{i=1}^{m} x_i \upsilon_{si} \tag{C.13}$$

where x_i is mole fraction of sulfur compound, υ_{si} is the molar critical volume of the i^{th} sulphur compound. Equal moles were assumed for the sulfur compounds. The molar volume of sulphur compounds at normal boiling point (υ_{si}) was evaluated from Equation (C.14) (Gupta, 2004)

$$\upsilon_{si} = V_c Z_c^{(1-T_b/T_c)^{(0.2857)}} \tag{C.14}$$

where V_c is molar critical volume (cm^3), Z_c is compressibility factor, T_c is critical temperature (K) and T_b is boiling point (K). Data for the calculations are shown in Table C.2. After using Equations (C.13) and (C.14), and the data in Table C.2, the average molar volume of sulfur compounds at normal boiling points obtained was v_s = 134.78 cm^3/mol (see Table C.3). Equation (C.10) can now be evaluated as follows

$$D_b = 8.93 * 10^{-8} \frac{200.5^{0.267} * 598}{134.78^{0.433} * 7.8 * 10^{-5}}$$

Table C.2: Thermodynamic properties of three sulfur-containing compounds in petroleum (Data from ChemDraw)

Name of Compound.	Molar Mass (g)	Boiling Pt. (K)	Critical Pressure (atm)	Critical Vol. (cm3/mol)	Critical T (K)
Thiophene	84.1418	387.11	56.384	219.5	628.13
Benzothiophene	134.2016	513.79	45.239	365.5	784.94
Dibenzothiophene	184.2615	606.72	37.100	511.5	880.86

Table C.3: Evaluated results of specific molar volume for three sulfur-containing compounds in petroleum

Name of Compound	Molar Volume (cm^3/mol)	Mole Ratio (g/g)	Avg. Molar Vol. (cm^3/mol)
Thiophene	74.1615	0.33	134.7800
Benzothiophene	133.9640	0.33	
Dibenzothiophene	196.2142	0.33	

$= \underline{3.37 * 10^{-1}\ cm^2/s} \quad = \underline{3.37*10^{-5}\ m^2/s}$

Substituting evaluated values into Equation (C.9) gives Sc as

$$Sc = \frac{7.8*10^{-5}}{676.516*3.37*10^{-5}} \qquad = \underline{3.42*\ 10^{-3}}$$

Evaluation of Sh'

With Re and Sc known, Sh can be evaluated from Equation (C.5) as follows:

$$Sh' = (2720)^{1/2}\left(3.42*10^{-3}\right)^{1/3} = 7.85$$

k_c is evaluated from Equation (C.15) and gives $k_c = 6.32*10^{-5} m/s$.

$$k_c = \frac{(1-\varepsilon_b)\psi D_b Sh'}{\varepsilon_b d_c} \qquad \text{(C.15)}$$

Using Equation (C.2), $\underline{\mathbf{C_m = 2.05*10^{-7}}}$

C.2.2 Internal Mass Transfer Limitations

Evaluation of internal mass transfer limitation for this study was based on the Weisz-Prater criterion as shown in Equation (C.16) below.

$$C_{WP} = \frac{-r_A \rho_p R'^2}{D_e C_{As}} \qquad \text{(C.16)}$$

where

$-r_A$ = observed rate of reaction = 1.75 *10^{-15} kmol/kg-s (from Section C.2.1)

ρ_p = density of the catalyst pellet (kg/m^3)

R' = catalyst particle radius (equivalent to radius of a sphere) = 2.23*10^{-2} m

D_e = effective diffusivity (m^2/s)

C_{As} = concentration on the surface of the catalyst = 5.481*10^{-05} kmol/m^3 (assumed same as final concentration)

C.2.2.1 Evaluation of Parameters

Effective Diffusivity Calculation:

$$D_e = \frac{D_b \varepsilon_p \vartheta}{\tau} \qquad \text{(C.17)}$$

(Seader and Henley, 1998) where

D_e = effective diffusivity of gas oil in the catalyst pores (m^2/s)

D_b = bulk diffusivity of gas oil $3.37*10^{-5}$ m^2/s (from Section C.2.1)

ε_p = catalyst pellet porosity

ϑ = restrictive factor

τ = tortuosity

The restrictive factor is given by

$$\vartheta = \left[1 - \frac{d_m}{d_p}\right]^4 \tag{C.18}$$

(Seader and Henley, 1998) where

d_m = molecular diameter (cm) and

d_p = pore diameter (cm)

Taking d_m = 0.55 nm (Zhao et al., 2008), and d_p = 9.2 nm (the minimum average pore diameter from the BET analyses- see Table 4.1) and substituting into Equation(C.18), gives:

$$\vartheta = 0.78$$

The ratio of ε_p / τ in Equation (C.17) was evaluated using the relation

$$\frac{\varepsilon_p}{\tau} = e^{\left(m(1 - 1/\varepsilon_p)\right)} \tag{C.19}$$

(Vishwakarma, 2007) where m ranges from 1.4 – 2.2. 1.8 was chosen for this study and ε_p ranges between 0.35 and 0.7. For this work, the worst case of 0.35 is chosen.

Evaluation of Equation (C.19) gives:

$$\varepsilon_p / \tau = 0.0353$$

Substituting all the values into Equation (C.17) gives

$$D_e = 3.37*10^{-5}*0.0353*0.78$$

$$D_e = \underline{9.29 * 10^{-9}}\ \underline{m^2/s}$$

The average density of the catalyst pellet can be estimated from the expression

$$\rho_p = \varepsilon_p \Big/ V_p \qquad \text{(C.20)}$$

(Seader and Henley, 1998) where

V_p *is* the catalyst specific pore volume = $5.5*10^{-4}$ m^3/kg (taken as the BET measured specific volume of γ-Al_2O_3). ρ_p and ε_p are as defined above.

Substituting the values of ε_p and V_p into Equation (C.20) gives

$$\rho_p = 0.35 \Big/ 5.5*10^{-4}$$

$$= \underline{636.36}\ kg/m^3$$

To check the initial assumption of 0.35 for ε_p, another relation was used which involved the measured specific surface area as given in Equation (C.21) (Seader and Henley, 1998)

$$\varepsilon_p = \frac{\rho_p * d_p * S_g}{4} \qquad \text{(C.21)}$$

where

S_p is the catalyst specific surface area = 193000 m^2/kg (taken as the BET measured specific surface area of γ-Al_2O_3). The rest of the parameters in Equation (C.21) are defined above.

Substituting values and evaluating gives

$$\varepsilon_p = \frac{636.36*0.0015*193000}{4}$$

And ε_p = $\underline{0.347}$ which is close to the original assumption of 0.35

Substituting all values into Equation (C.16) gives

$$C_{WP} = \frac{1.75*10^{-15}*636.36*\left(2.23*10^{-2}\right)^2}{9.29*10^{-7}*5.48*10^{-5}}$$

And C_{WP} = **$\underline{\underline{2.12 * 10^{-4}}}$ $\underline{\underline{<< 1}}$**

It must be noted that the sulphur concentrations used in the calculations are reactor outlet sulphur concentrations and are less than or equal to the catalyst surface concentration term in Equation (C.16). At worst, it should have pushed the results towards a value greater > 1 but that was not observed.

To evaluate the difference in temperature between the center and surface of the catalyst during reaction, Equation (C.22) (Fogler, 2006) was used.

$$\beta = \frac{C_{As}\left(-\Delta H_R\right)D_e}{k_t Ts} \tag{C.22}$$

where

k_t = effective thermal conductivity (J/s.cm.°C)

β = a parameter representing difference in temperature between surface and center of catalyst (°C)

ΔH_R = heat of reaction

T_s = catalyst surface temperature (°C).

C_{As} and D_e are already defined above.

To evaluate Equation(C.22), the thermal conductivity of the catalyst bed must first be estimated

Estimation of Thermal Conductivity

There are two main ways in which the catalyst conducts heat:

1. Conduction of heat from the furnace through the reactor wall (Static) and
2. Conduction of heat by way of fluid flow in the reactor (dynamic - consists of radial and axial components).

The total heat conducted is given as

$$k_t = k_{ec}^{'o} + k_{er}^{'d} + k_{el}^{'} \tag{C.23}$$

(Doraiswamy and Sharma, 1984) where/

k_t = overall effective thermal conductivity (J/s.cm.°C)

$k_{ec}^{'o}$ = static catalyst bed thermal conductivity (cal/s.cm.°C)

$k_{er}^{'d}$ = dynamic catalyst bed radial thermal conductivity (cal/s.cm.°C)

$k_{el}^{'}$ = dynamic catalyst bed axial thermal conductivity (cal/s.cm.°C)

Static catalyst bed thermal conductivity Estimation

$k_{ec}^{'o}$ is given by Equation (C.24) (Doraiswamy and Sharma, 1984)

$$\frac{k_{ec}^{'o}}{k_f^{'}} = f_B + (1+ f_B)\left[\frac{\beta^{''}}{\delta + 2/3(k_f^{'}/k_s^{'}}\right] \qquad \text{(C.24)}$$

where

$\beta^{''}$ = 0.895 (empirical constant)

f_B = 0.1 (empirical constant)

$k_f^{'}$ = thermal conductivity of fluid in the reactor (cal/s.cm.°C.)

$k_s^{'}$ = thermal conductivity of solids (SiC + Al_2O_3) in the reactor (cal/s.cm.°C.)

δ = constant from Fig. 10.3 of Doraiswamy and Sharma, (1984) based on the ratio $\frac{k_f^{'}}{k_s^{'}} = 0.18$

The solid part of the bed is a combination of SiC packing and catalyst pellet (Al_2O_3 chosen for simplicity). For SiC: Al_2O_3 reactor packing ratio of 4:1,

$k_s^{'}$ = Sum of thermal conductivities for SiC and Al_2O_3 and

$k_s^{'}$ = 0.8*0.61 + 0.2*0.1 = 0.508 cal/s.cm.°C (Incropera and DeWitt, 1985).

Thermal conductivity of the fluid, $k_f^{'}$ = 0.1768 W/m.K = 4.226*10-4 cal/s.cm. °C. Therefore

$$\frac{k_s^{'}}{k_f^{'}} = \frac{4.226*10^{-4}}{0.508} = 8.319*10^{-4} cal/s.cm.^oC .$$

Substituting all values obtained into Equation (C.24) gives

$$k_{ec}^{'o} = 1.928*10^{-3} cal/s.cm.^oC$$

Dynamic Catalyst Bed Thermal Conductivity Estimation

The dynamic bed thermal conductivity consists of radial and axial thermal conductions. The radial contribution can be estimated from Equation (C.25) (Doraiswamy and Sharma, 1984)

$$k_{er}^{'d} = \frac{0.0025}{1+46(d_p/d_t)^2}\text{Re} \qquad \text{(C.25)}$$

where d_t *is the* diameter of the reactor = 1 cm. The rest of the parameters are already defined. Substituting all values into Equation (C.25) gives

$$k_{er}^{'d} = \frac{0.0025}{1+46(0.15/1)^2} * 1.17 = 2.58 * 10^{-4} \, cal/s.cm.^oC$$

Effective Axial Thermal Conductivity Estimation

The axial thermal conductivity was estimated from Equation (C.26) (Doraiswamy and Sharma, 1984)

$$\frac{1}{P_e} = \frac{k_{el}^{'o} \diagup k_f^{'}}{\mathrm{Re}^* \mathrm{Pr}} + \frac{14.5}{\left(1 + \frac{C}{\mathrm{Re}^* \mathrm{Pr}}\right) d_p} \qquad \text{(C.26)}$$

where P_e is the Peclet number, $k_{el}^{'o}$ is the effective axial thermal conductivity, Pr is the Prandtl number and C is empirical constant = 0.5 (Doraiswamy and Sharma, 1984). Using heat capacities of thiophene (72.946 J/mol.K), benzothiophene (123.77 J/mol.K) and dibenzothiphene (174.59, J/mol.K), the average heat capacity can be evaluated as follows:

$$\mathrm{Cp}_{avg} = 1/3\left(72.946 + 123.77 + 174.59\right) = 123.77 \, \mathrm{J/mol.K} = 0.9223 \, \mathrm{J/g.K}$$

$$\mathrm{Pr} = \frac{C_{p_{avg}} * \mu}{k_s} = \frac{0.9223 * 8 * 10^{-5}}{212.55} = 3.47 * 10^{-7}$$

$$\mathrm{P}e = \mathrm{Re}^* \mathrm{Pr} = 1.7 * 3.47 * 10^{-7} = 5.899 * 10^{-7}$$

Substituting all values into Equation (C.26), gives

$$k_{el}^{'o} = 4.23 * 10^{-4} \, \mathrm{cal/s.cm.°C} \text{ to give}$$

The effective thermal conductivity will therefore be

$$k_t = 1.928 * 10^{-3} + 2.58 * 10^{-4} + 4.23 * 10^{-4} = 2.61 * 10^{-3} \, \mathrm{cal/s.cm.°C}$$

$$k_t = 1.09 \, \mathrm{J/s.m.°C}$$

Estimation of Heat of Reaction

Heat of reaction of the sulphur compounds at reaction conditions was estimated from reactions of thiophene, benzothiophene, and dibenzothiophene with hydrogen to form hydrocarbon products. Because HDS prefers direct desulfurization reactions, it was assumed that the reactants react to give a sulfur-free product without prior hydrogenation of the ring containing the sulfur compound. For example, in Equations (C.27) to (C.29), two moles each of hydrogen are required to form H_2S and simultaneously hydrogenate the sulfur-containing compound.

$$C_4H_4S + 2H_2 \rightarrow C_4H_6 + H_2S \quad \text{(C.27)}$$

$$C_8H_6S + 2H_2 \rightarrow C_8H_8 + H_2S \quad \text{(C.28)}$$

$$C_{12}H_8S + 2H_2 \rightarrow C_{12}H_{10} + H_2S \quad \text{(C.29)}$$

The heat of reaction can be evaluated from the expression

$$\Delta H_T = \Delta H^o_{298} + (T - 298) * \sum_p^n Cp_p - \sum_r^n Cp_r \quad \text{(C.30)}$$

(Gupta, 2004) where

ΔH_T = heat of reaction

ΔH^o_{298} = standard heat of reaction at 298 K

Cp_p = heat capacity of products

Cp_r = heat capacity of reactants

T = temperature

ΔH^o_{298} is obtained from the heats of formation of the reactants and products as

$$\Delta H^o_{298} = \sum \left(\Delta H_f\right)_p - \sum \left(\Delta H_f\right)_r \quad \text{(C.31)}$$

$\left(\Delta H_f\right)_p$ and $\left(\Delta H_f\right)_r$ are the heats of formation of products and reactants at 298 K. The thermodynamic properties of all reactants and products involved in Equations (C.27) to (C.29) are shown in Table C.4. Summing Equations (C.27) to (C.29) up gives Equation (C.32).

$$C_4H_4S + C_8H_6S + C_{12}H_8S + 6H_2 \rightarrow C_4H_6 + C_8H_8 + C_{12}H_{10} + 3H_2S \quad \text{(C.32)}$$

Using Equations (C.30) to (C.32), the standard heat of formation at 298 can be evaluated a

$$\Delta H^o_{298} = \left[\left(124.97 + 153.51 + 182.05 + 3 * 50.96\right) - \left(115.75 + 212.79 + 309.83 + 6 * 68.29\right)\right] * 10^3$$

and ΔH^o_{298} = <u>-434700 J/mol</u>

Now the heat of reaction at operating temperature is given as

$$\Delta H_{598} = -434700 + (598 - 298) * \left[\begin{array}{l}\left(76.42 + 118.81 + 161.20 + 3 * 21.80\right) - \\ \left(72.95 + 123.77 + 174.59 - 6 * 4.62\right)\end{array}\right]$$

$$\Delta H_{598} = \underline{\underline{-443436 \text{ J/mole}}}$$

Evaluation of Difference in Bulk Fluid and Catalyst Surface Temperatures

Mears Criterion in Equation (C.33) was used to estimate the difference in temperatures between the bulk fluid and the catalyst surface.

Table C.4: Thermodynamic properties of reactants and products of hydrodesulfurization reaction (all data – at 298.15 K and 1 atm – obtained from ChemDraw)

Name	Formula	ΔH (KJ/mol)	Cp (J/mol.K)
Thiophene	C_4H_4S	115.75	72.95
Benzothiophene	C_8H_6S	212.79	123.77
Dibenzothiophene	$C_{12}H_8S$	309.83	174.59
Hydrogen	H_2	68.29	-4.62
1,3-Butadiene	C_4H_6	124.97	76.42
Styrene	C_8H_8	153.51	118.81
Biphenyl	$C_{12}H_{10}$	182.05	161.20
Hydrogen sulfide	H_2S	50.96	21.80

$$\frac{-\Delta H_R\left(-r'_A\right)\rho_b RE}{h_h T^2 R_g} < 0.15 \qquad \text{(C.33)}$$

All the parameters in Equation (C.33) have been earlier defined except the heat transfer coefficient (h) which can be estimated from Equation (C.34) (Doraiswamy and Sharma, 1984).

$$h_h = \frac{20k_e^{'o}}{d_t} + 0.0115*\left(\frac{d_t}{d_p}\right)*\mathrm{Re} \qquad \text{(C.34)}$$

where h_h is wall heat transfer coefficient. Values of all the parameters in Equation (C.34) are known and h can be evaluated as

$$h_h = \frac{20*1.928*10^{-3}}{1} + 0.0115*\left(\frac{1}{0.15}\right)*1.17 \qquad \text{(C.35)}$$

and h_h = 0.12826 cal/s. cm.°C = 53.66 J/s.m.°C

Equation (C.33) can now be evaluated and this gives;

$$\frac{415386*6.29*10^{-9}*416*1.17}{53.66*598^2*8.314}$$

$$= 7.97*10^{-9} << 0.15$$

This means that the bulk fluid temperature T, is virtually the same as the catalyst surface temperature. Going back to Equation (C.22), β can be evaluated as shown below:

$$\beta = \frac{5.481*10^{-2}*\text{-}443436*4.763*10^{-8}}{1.09*598}$$

And β = 1.78E-06

The small value for β shows that there was no temperature difference between the center of the catalyst and its surface.

C.2.3 Particle Peclet Number Calculations

The Peclet number is given by Equation (C.36)

$$Pe = \frac{LU}{De} \qquad \text{(C.36)}$$

where Pe is the Peclet number, L (0.1 m) is the catalyst bed length, U (2.78 *10^{-5} m/s) is the superficial velocity and De (4.93 *10^{-5} m^2/s) the catalyst bed diffusivity. Substituting the values into Equation (C.36) gives

$$Pe = \frac{0.01 * 2.78 * 10^{-5}}{4.93 * 10^{-5}} = 0.006$$

APPENDIX D

THERETICAL ANALYSES OF ANALYTICAL TECHNIQUES AND KINETICS

D.1 Electron Microscopy

Electron microscopy is a technique that helps to determine size, shape, composition and structure of a supported catalyst. It can be operated at a magnification of about a million times and can reveal details to a resolution of 0.1 nm. In electron microscopy, the interaction of electrons of wavelength less than Agstrom with samples, lead to a number of signals which help in seeing atomic details. The electrons can be transmitted through the sample without energy loss depending on the thickness of the sample. Electrons could also be diffracted depending on the orientation of the particles in the sample. Another signal that could be obtained is backscattered electrons. In this case, electrons collide with particles in the sample and are elastically scattered. Auger electrons and x-rays could also be formed in electron microscopy. However, many of the electrons lose energy due to inelastic collision with particles. Common hydrotreating characterization techniques based on electron microscopy are scanning electron microscopy (SEM), energy dispersive x-ray (EDX) and transmission electron microscopy (TEM). The schematics of TEM and SEM are shown in Figure D.1 (Niemanstverdriet, 1993).

D.2 Vibrational Spectroscopies

Vibrational spectroscopies involve infrared spectroscopy (IR), laser Raman spectroscopy, (LR) and electron energy loss spectroscopy (EELS). The principle involves the excitation of vibrations in molecules or in solid lattices by the absorption of photons (infrared spectroscopy) or scattering of photons (Raman spectroscopy). There are different types of vibrations which include stretch vibrations, bending vibrations in one plane, bending vibrations out of plane and torsion vibrations. In this thesis, only IR will be discussed because the use of LR and EELS in hydrotreating catalysis is not very common.

The modes of operation are shown in Figure D.2 It is commonly operated in transmission mode where 10-100 mg sample size is pelletized into thickness of 1 cm^2 and used. This is particularly suitable in oxide supported metal catalysts where the oxide support absorbs weakly with wave numbers above 1000 cm^{-1}. In such cases, the support particles should also be smaller than the IR radiation to minimize scattering losses. Another mode of operation is the diffuse

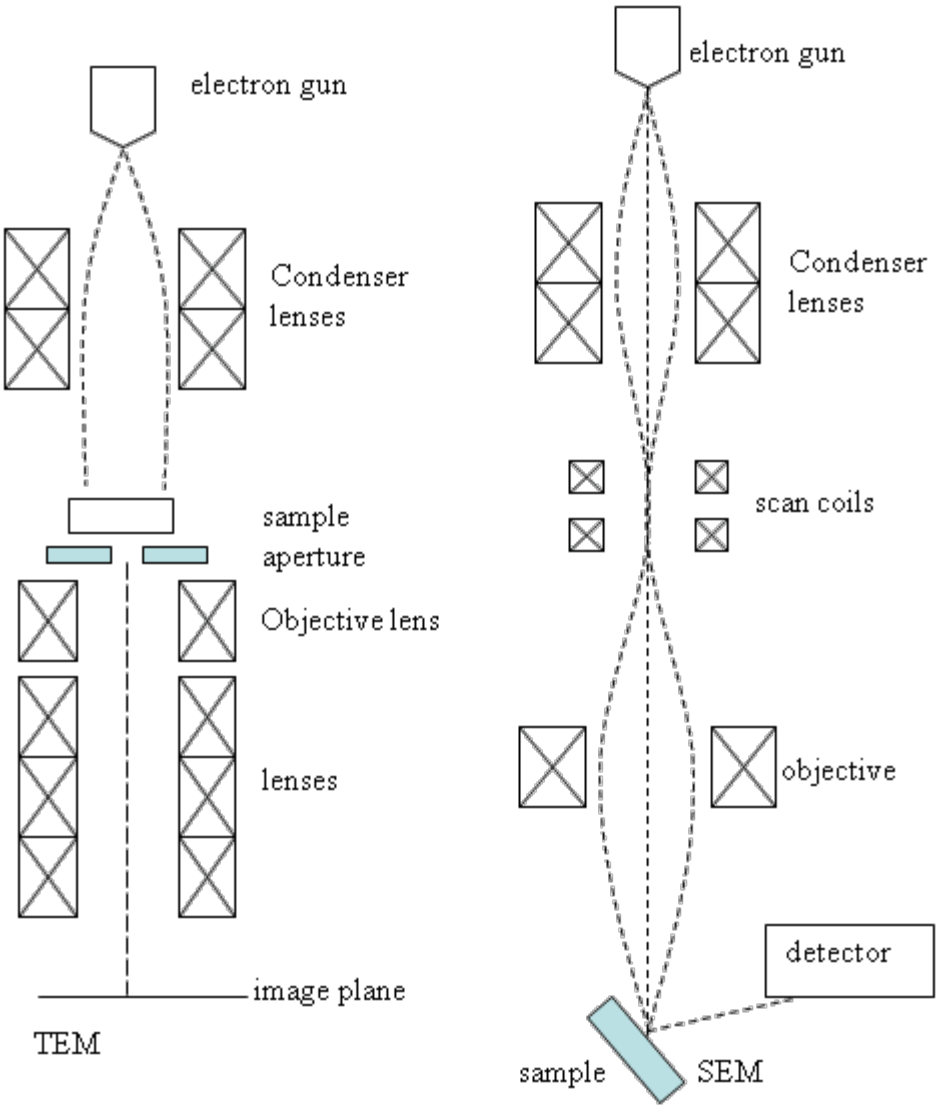

Figure D.1: Schematic set ups of TEM and SEM (Niemantsverdriet, 1993)

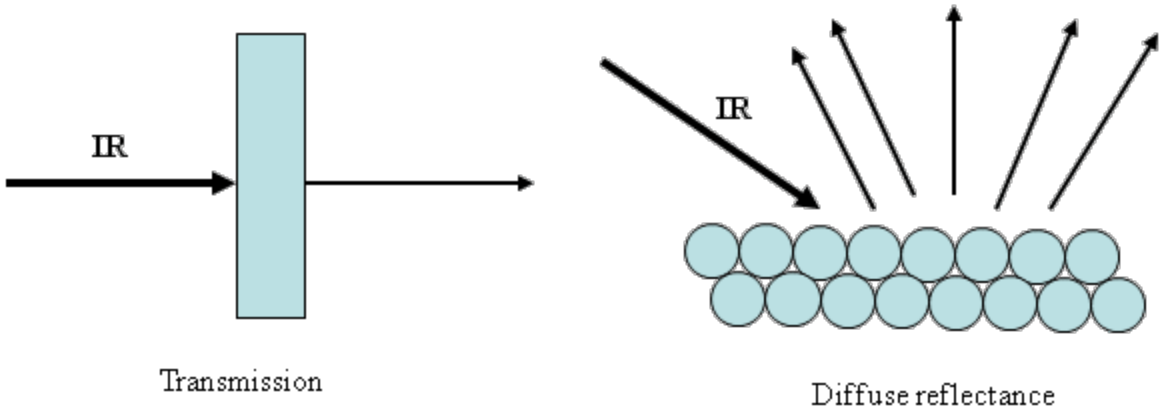

Figure D.2: Different forms of infrared spectroscopy: transmission infrared and diffuse reflectance infrared spectroscopy.

reflectance in which samples are usually in the powdered form. One advantage is that it avoids diffusion limitations associated with pelletized samples. It is also the choice for strongly absorbing or scattering samples. The scattered radiation is refocused by a mirror on to a detector for the spectrum which is described by the Kubelka-Munk function given by Equation (D.1)

$$\frac{K_{k-m}}{S_{k-m}} = \frac{\left(1-R_{\infty}\right)^2}{\left(2-R_{\infty}\right)} \tag{D.1}$$

where K_{k-m} is the absorption coefficient, S_{k-m} is the scattering coefficient and R_{∞} is the reflectivity of a sample of infinite thickness.

D.3 Developing Langmuir-Hinshelwood Kinetic Models

For a generic reaction (Equation (D.2)) with both reactants *A* and H_2 adsorbing on identical active sites , with adsorption constants K_A and K_{H_2}, reaction takes place between the

$$A \quad + \quad H_2 \rightarrow D + Z \tag{D.2}$$

adsorbed reactants to form products. The product formed desorbs from the active site back into the bulk solution to complete the reaction cycle. The different stages in the reaction process are always in equilibrium with each other (Marwaha and Luss, 2003; Tsai et al., 1991; Froment and Bischoff, 1979). The rate of adsorption of A to the active sites is proportional to the concentration of A and the fraction of unoccupied sites. This is given by the relation

$$r_A^{ads} = k_A\left(1-\sum\Theta\right)C_A$$

where $$\sum\Theta = \Theta_A + \Theta_{H_2} + \Theta_D + \Theta_Z$$

The rate of desorption of A from the active sites is

$$r_A^{des} = k_A'\Theta_A$$

At equilibrium, $$r_A^{ads} = r_A^{des}$$

and $$k_A'\Theta_A = k_A\left(1-\sum\Theta\right)C_A$$

Hence $$\Theta_A = K_A C_A\left(1-\sum\Theta\right) \tag{D.3}$$

where $K_A = \frac{k_A}{k'_A}$

For hydrogen (assuming molecular adsorption) the rate of adsorption will be

$$r_{H_2}^{ads} = k_{H_2}\left(1-\sum\Theta\right)P_{H_2}$$

Rate of desorption is $r_{H_2}^{des} = k'_{H_2}\Theta_{H_2}$

At equilibrium, $r_{H_2}^{ads} = r_{H_2}^{des}$

and $$\Theta_{H_2} = K_{H_2}P_{H_2}\left(1-\sum\Theta\right) \qquad \text{(D.4)}$$

From equations (D.3) and (D.4), generally,

$$\Theta_i = K_i P_i\left(1-\sum\Theta\right) \qquad \text{(D.5)}$$

The rate of reaction is proportional to the fraction of molecules adsorbed, i.e.

$$-r_{rxn} \quad = \quad k\Theta_A\Theta_{H_2} \quad = \quad K_A K_{H_2} C_A P_{H_2}\left(1-\sum\Theta\right)^2 \qquad \text{(D.6)}$$

From equations (D.3), (D.4) and (D.5),

$$\sum\Theta = \left(1-\sum\Theta\right)\left[K_A C_A + K_{H_2}P_{H_2} + K_D P_D + K_Z C_Z\right]$$

which gives $$\left(1-\sum\Theta\right) = \frac{1}{\left[1+K_A C_A + K_{H_2}P_{H_2} + K_D P_D + K_Z C_Z\right]} \qquad \text{(D.7)}$$

Combining equations (D.6) and (D.7), the rate of reaction becomes

$$-r_{rxn} = \frac{kK_A K_{H_2} C_A P_{H_2}}{\left[1+K_A C_A + K_{H_2}P_{H_2} + K_D P_D + K_Z C_Z\right]^2} \qquad \text{(D.8)}$$

D.4 Evaluation of Kinetic Parameters

D.4.1 Differential Method

This method can be applied in rate expressions that can be linearized, e.g. the kinetics of the HDS and HDN processes. A rate expression in the form

$$-r_A = -\frac{dC_A}{dt} = k_A C_A^n \qquad \text{(D.9)}$$

Can then be linearized to give

$$\ln\left(-\frac{dC_A}{dt}\right) = \ln k_A + n\ln\left(C_A\right) \tag{D.10}$$

Finite difference analog could be written for $\frac{dC_A}{dt}$ (e.g. $\frac{dC_A}{dt} = \frac{\Delta C}{\Delta t} = \frac{C_A - C_{A_0}}{t-0}$). Reactions can then be performed at various reaction times (e.g. t_1 to t_5) and the corresponding concentrations (e.g. C_{A_1} to C_{A_5}) measured. A plot of $\ln\left(-\frac{dC_A}{dt}\right)$ against $\ln\left(C_A\right)$ will give a slope of n and an intercept of $\ln\left(k_A\right)$ from which k_A can be evaluated.

D.4.2 Integral Method

The integral method is used for rate expressions that are integrable and can be linearized. This method can be applied to HDS and HDN kinetics expressions if they meet the above conditions. The rate expressions for the HDS and HDN processes can be represented generally as

$$-r_A = -\frac{dC_A}{dt} = k_A C_A^n \tag{D.11}$$

with n known (n = 1 for HDN and 1.5 for HDS), its value can be substituted into the rate expression and the whole expression integrated. For HDN, n = 1, and the solution equation becomes

$$\frac{C_A}{C_{A_0}} = e^{(-k_A/LHSV)} \tag{D.12}$$

Equation (D.12) can be linearized to give

$$\ln C_A = \ln C_{A_0} - k_A/LHSV \tag{D.13}$$

Varying the flow rate of the feed oil at constant temperature, various $LHSV$ (e.g. $LHSV_1$ to $LHSV_5$) and the corresponding C_A (e.g. C_{A_1} to C_{A_5}) can be measured. A plot of $\ln\left(C_A\right)$ on the ordinate axis and $\frac{1}{LHSV}$ on the abscissa will give a slope of $-k_A$ from which k_A can be obtained. To obtain the activation energy for the reaction, the procedure outlined in Section D.4.4 can be followed.

For $n \neq 1$ the solution equation becomes

$$\frac{1}{C_A^{n-1}} - \frac{1}{C_{A_O}^{n-1}} = (n-1)\frac{k_A}{LHSV} \tag{D.14}$$

By varying the flow rate of the feed oil at constant temperature, various $LHSV$ (e.g. $LHSV_1$ to $LHSV_5$) and their corresponding C_A (e.g. C_{A_1} to C_{A_5}) can be measured. A plot of $\frac{1}{C_A^{n-1}}$ on the ordinate axis and $\frac{1}{LHSV}$ on the abscissa will give a slope of $(n-1)k_A$ from which k_A can be evaluated. To obtain the activation energy for the reaction, the procedure outlined in Section D.4.4 is followed.

D.4.3 Non-linear Least Squares Analysis

If the kinetic expression obtained cannot be linearized, e.g. some Langmuir-Hinshelwood models, the kinetic expressions could be evaluated by non-linear least-squares analyses. The non-linear least-squares technique involves minimization of error, i.e. the sum of squares of the difference between experimental data and calculated values as shown below.

$$\Phi^2 = \sum_j^{\pi} \frac{\left[\left(-r_j\right)_{Exp} - \left(-r_j\right)_{Cal}\right]^2}{\pi - \delta} \tag{D.15}$$

where Φ is the error term, $\left(-r_j\right)_{Exp}$ is the experimental rate for run j, $\left(-r_j\right)_{Cal}$ is the calculated rate obtained from the kinetic expression for run j, π is the total number of experimental runs and δ is the number of parameters to be determined. For a constant operating temperature, estimates can be made for the parameter values in the kinetic expressions to calculate $\left(-r_j\right)_{Cal}$. For example, in Equation (D.16), parameter estimates are made for k, K_A, K_{H_2}, K_D and K_Z

$$-r_{rxn} = \frac{kC_A P_{H_2}}{\left[1 + K_A C_A + K_{H_2} P_{H_2} + K_D P_D + K_Z C_Z\right]^2} \tag{D.16}$$

to calculate $\left(-r_{rxn}\right)_{Cal}$ for π different experimental runs. The number of parameters to be determined, δ, is 5. Different sets of parameters are used for each Φ^2 calculated (e.g. $[k, K_A, K_{H_2}, K_D, K_Z]_1$ for $[\Phi^2]_1$, $[k, K_A, K_{H_2}, K_D, K_Z]_2$ for $[\Phi^2]_2$). The set of parameter values

that minimizes Φ^2 is chosen to be the correct set of parameters from which the activation energies, heat of adsorptions and pre-exponential factors are evaluated (discussed in Section D.4.4). The initial parameter estimates can be selected from literature (Girgis and Gates, 1991).

D.4.4 Evaluation of Activation Energy and Heat of Adsorption

The activation energy, heat of adsorption and pre-exponential factors can be evaluated through linear least squares and linear regression techniques. The least squares technique will, however, not be discussed.

For both HDS and HDN, the Arrhenius and van't Hoff expressions for the specific rate and adsorption constants are, respectively;

$$k = k_0 e^{-\left(E/R_g T\right)} \tag{D.17}$$

and

$$K = K_0 e^{\left(Q/R_g T\right)} \tag{D.18}$$

Linearizing Equations (D.17) and (D.18) gives

$$\ln(k) = \ln(k_O) - \frac{E}{R_g T} \tag{D.19}$$

$$\ln(K) = \ln(K_O) + \frac{Q}{R_g T} \tag{D.20}$$

Plots of $\ln(k)$ and $\ln(K)$ against $1/T$ give E and Q as slopes, respectively. The intercepts give $\ln(k_O)$ and $\ln(K_O)$, respectively from which k_0 and K_O are obtained.

APPENDIX E
FEED AND PRODUCT ANALYSES

The light gas oil feed and hydrotreated products were analyzed for sulfur, total nitrogen and basic nitrogen. Sulfur content was analyzed by combustion/fluorescence technique following ASTM D5453 procedure. Nitrogen content of the oil was measured by combustion/chemiluminesence technique following ASTM D4629.

E.1 Sulfur Analysis

The feed/product sample was injected directly into a sample boat and swept by a stream of inert gas (helium or argon) into a high temperature combustion tube. The sulfur present in the sample is oxidized to sulfur dioxide (SO_2) in an oxygen rich atmosphere. Any water generated from the combustion is removed after which the combustion gases are exposed to ultraviolet (UV) light. The SO_2 absorbs energy from the UV light which converts it into excited SO_2*. As the excited SO_2* returns to the stable SO_2 state, fluorescence is emitted which is detected by a photomultiplier tube. The signal observed is a measure of the sulfur content of the sample. The sulfur content of the test sample, W_S , is calculated in ppm as:

$$W_S = \frac{J - Y}{S * M * K_g} \tag{E.1}$$

where J is the average of integrated detector response for test specimen solution, counts, K_g is the gravimetric dilution factor, mass of test specimen/mass of test specimen and solvent, g/g, M is the mass of test specimen solution injected, S is the slope of standard curve, counts/μg and Y is the y-intercept of standard curve, counts.

E.2 Nitrogen Analysis

A feed/product sample is directly injected into a sample boat where it is carried by a stream of inert gas (helium or argon) into a high-temperature combustion tube. The nitrogen in the sample is then oxidized to nitric oxide (NO) in an oxygen atmosphere. The NO is converted to excited nitrogen dioxide (NO_2) as it contacts ozone. As the excited NO_2 decays, light is emitted which is detected by a photomultiplier tube giving a signal which is a measure of the nitrogen

content of the sample. The nitrogen content, W_N, in parts per million is then evaluated using Equation (E.2) as:

$$W_N = \frac{J - Y}{S * M * K_g} \tag{E.2}$$

where J is the average of integrated detector response for test specimen solution, counts, K_g is the gravimetric dilution factor, mass of test specimen/mass of test specimen and solvent, g/g, M is the mass of test specimen solution injected, S is the slope of standard curve, counts/ng and Y is the y-intercept of standard curve, counts.

E.3 Aromatic Hydrocarbon Analysis

Aromaticity is the per cent of carbon in a sample that is present as part of an aromatic ring structure. Feed and product aromaticity were measured directly from carbon-13 nuclear magnetic resonance (13C –NMR) spectroscopy operating at a frequency of 500 MHz. Other operating conditions were: pulse delay of 4 s, sweep width of 28 kHz and inverse gated proton coupling and 2000 scans. Each sample was diluted with deuterated chloroform, $CDCl_3$, prior to mounting in the setup for analyses. HDA is obtained by integrating the intensities over the aromatic hydrocarbon range (120-150 ppm) and saturated hydrocarbons range (0-50 ppm) and applying Equation (E.3)

$$HDA = \frac{I_{sat_f} - I_{sat_o}}{I_{^{13}C_0}} * 100 \tag{E.3}$$

Where I_{sat_f} is the total product saturated hydrocarbons, I_{sat_o} is the feed saturated hydrocarbons and $I_{^{13}C_0}$ is amount of aromatics in the feed.

APPENDIX F

EXPERIMENTAL RESULTS

F.1 Preliminary Characterization Results

F.1.1 BET Surface Area Analyses

BET surface area was performed for all twenty nitride catalysts. Surface area varied from 202 m^2/g at Ni loading of 1.8 wt%, 1.0 wt% P and 739 nitriding temperature, to 162 m^2/g at Ni loading of 6.3 wt%, P loading of 4 wt % and nitriding temperature of 561 ºC.

As illustrated in Figure F.1, surface area generally increased with increasing temperature but decreasing Ni and P loading. Temperature however had the most impact on the surface area. Hada et al. (2002) also reported increase in surface area with increasing nitriding temperature up to about 950 K. The pioneering work of Volpe and Boudart (1985) in nitride catalyst synthesis also showed increase in surface area with increasing nitriding temperature for Mo_2N samples. Increase in nitriding temperature must be responsible for decreasing the crystallite sizes of active sites and the subsequent increase in surface area. Colling (1996) observed that increase in surface area can be attributed to a decrease in catalyst crystallite sizes. As shown in Figure F.1, decreasing Ni and P loading may also be responsible for forming smaller crystallite sizes leading to higher surface areas.

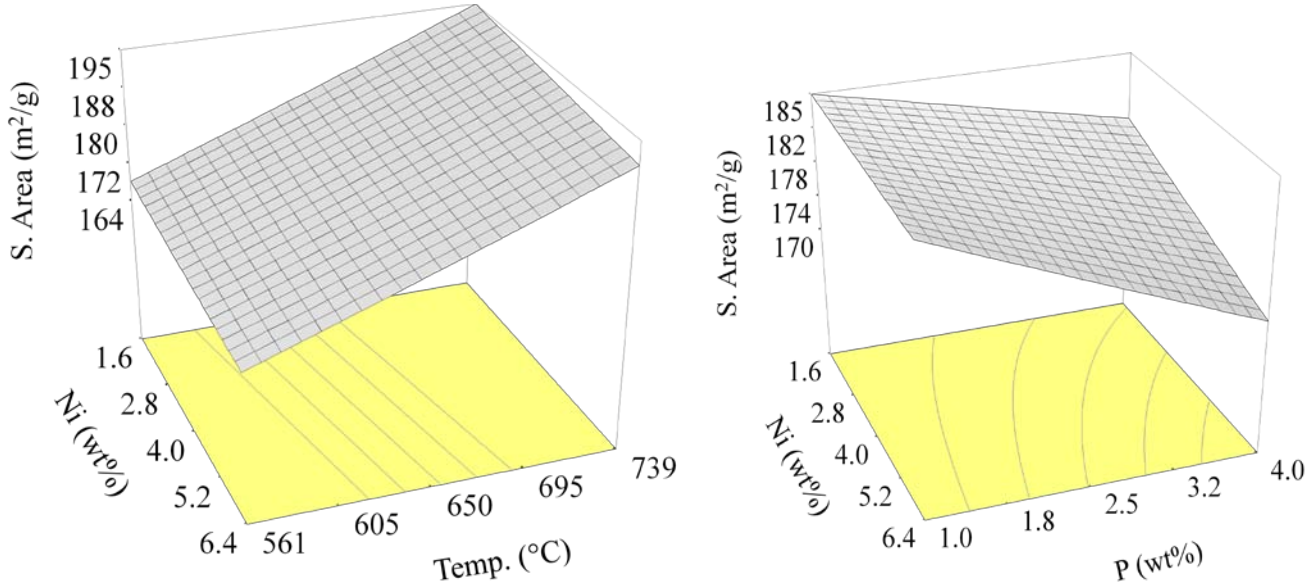

Figure F.1: BET surface area of Ni-W(P)/γ-Al_2O_3 nitride catalyst at varying T_N, Ni and P loadings. Conditions: 15 wt% W, (A) 2.5 wt% P and (B) 4 wt% Ni.

F.2 SEM and EDX Results

F.2.1 Reference Samples

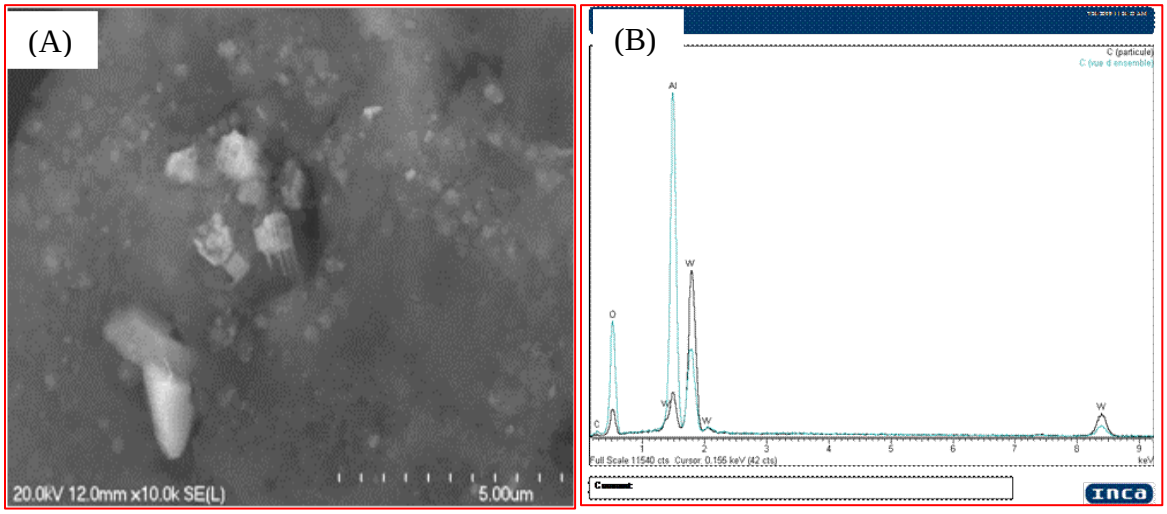

Figure F.2: (A) SEM micrograph and (B) EDX of W/γ-Al_2O_3 nitride catalyst. Conditions: 30 wt% W, 4 wt% Ni, 2 wt% P and T_N of 700 °C.

F.2.2 SEM and EDX of Cat-P Samples

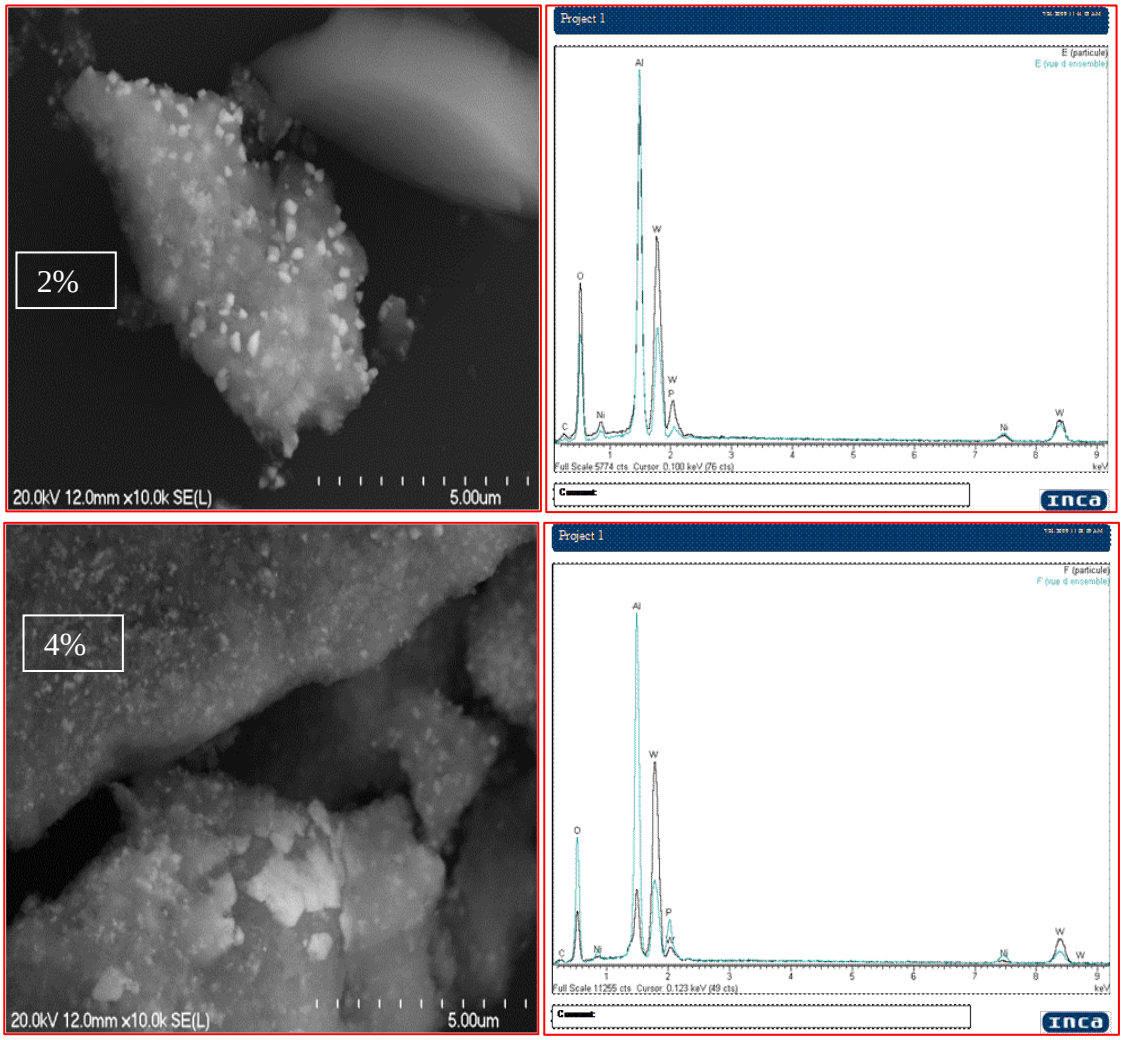

Figure F.3: (A) SEM micrograph and (B) EDX of W/γ-Al_2O_3 nitride catalyst. Conditions: W, 30 wt%; Ni, 4 wt%; P, 2 wt%; 700 °C

.

F.2.3 SEM and EDX of Cat-Ni Samples

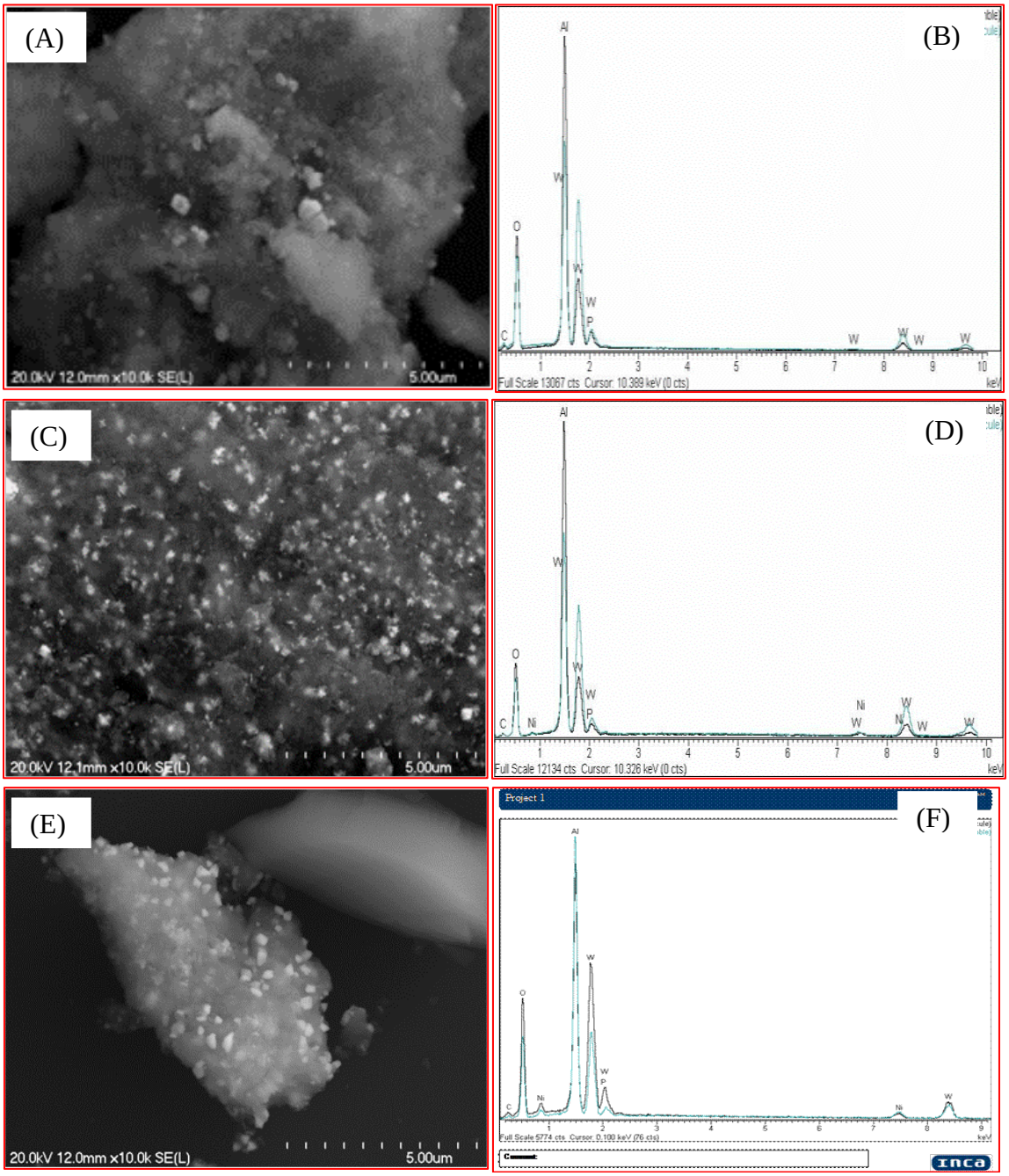

Figure F.4: SEM micrographs and EDX spectra of Cat-Ni nitride samples. (A, B) 0%-Ni; (C, D) 2%-Ni; (E,F) 4%-Ni. Conditions: 30 wt% W, 2 wt% P and T_N of 700 °C.

F.2.4 SEM and EDX of Cat-W Samples

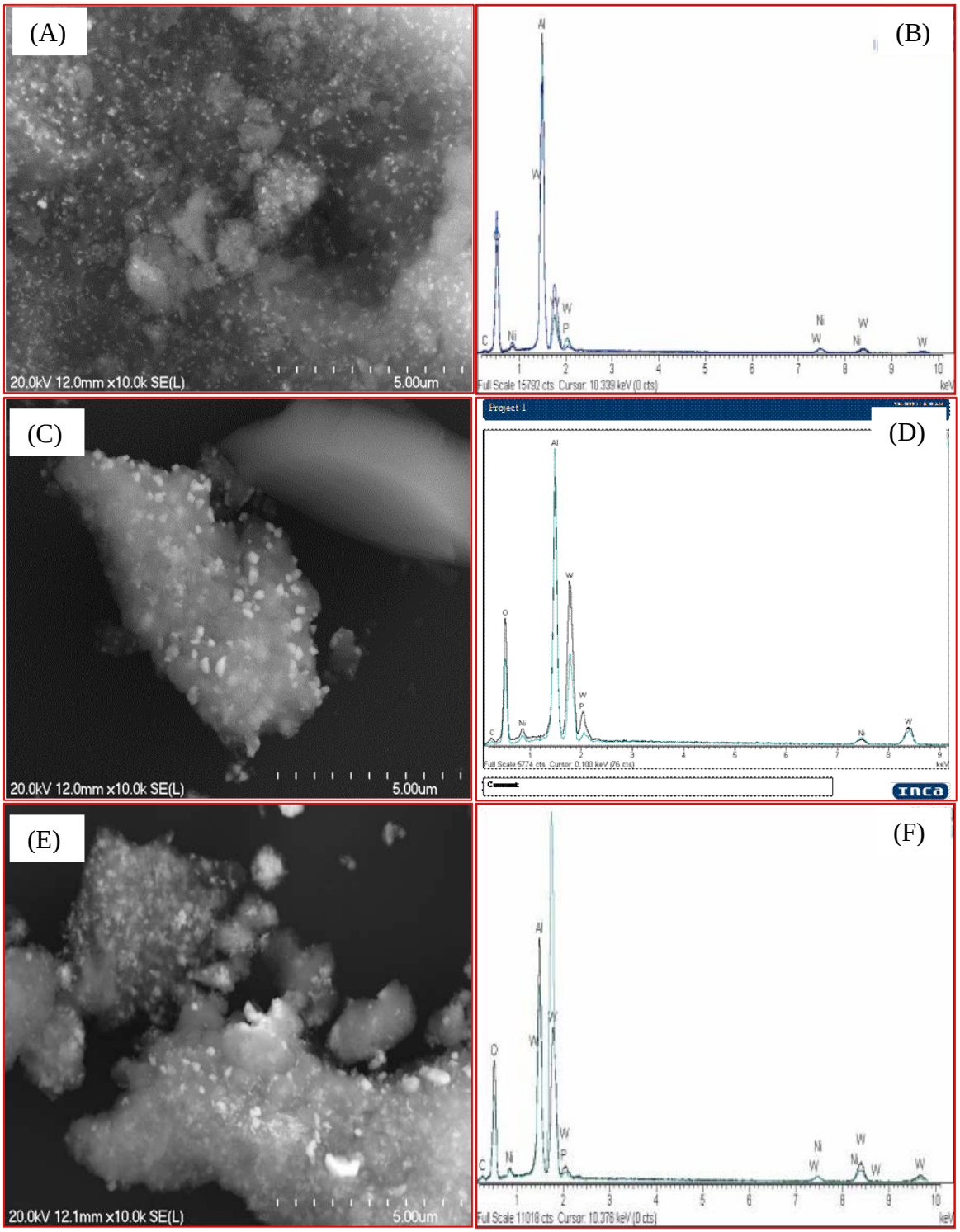

Figure F.5: SEM micrographs and EDX spectra of Cat-W nitride samples. (A, B) 15%-W; (C, D) 30%-W; (E, F) 40%-W. Conditions: 4 wt% Ni, 2 wt% P and T_N of 700 °C.

F.2.5 SEM and EDX of Cat-T_N Samples

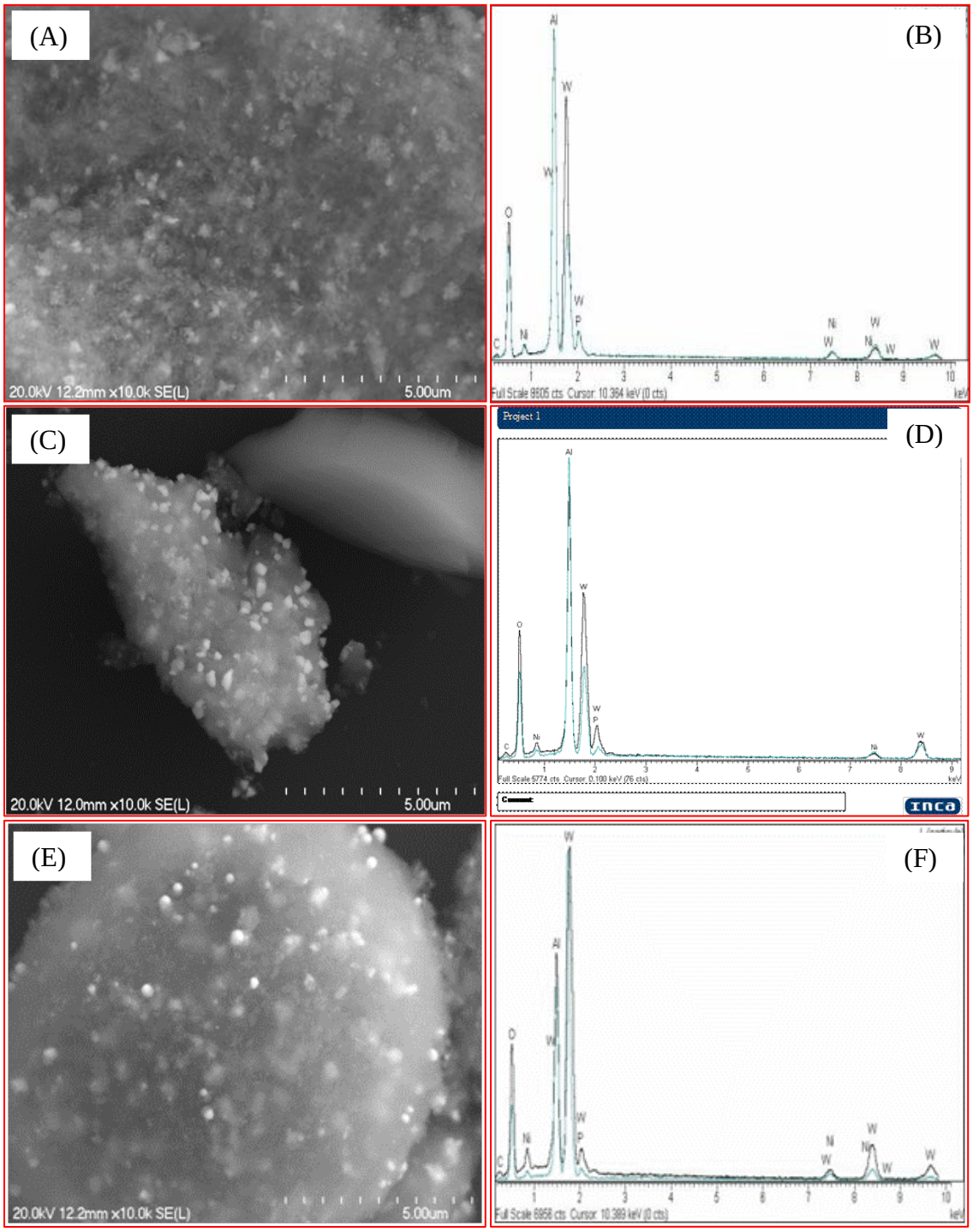

Figure F.6: SEM micrographs and EDX spectra of Cat-T_N nitride samples. (A, B) 500°-T_N; (C, D) 700°-T_N; (E, F) 900°-T_N. Conditions: 30 wt% W, 4 wt% Ni and 2 wt% P.

F.3 Transmission Electron Microscopy Results

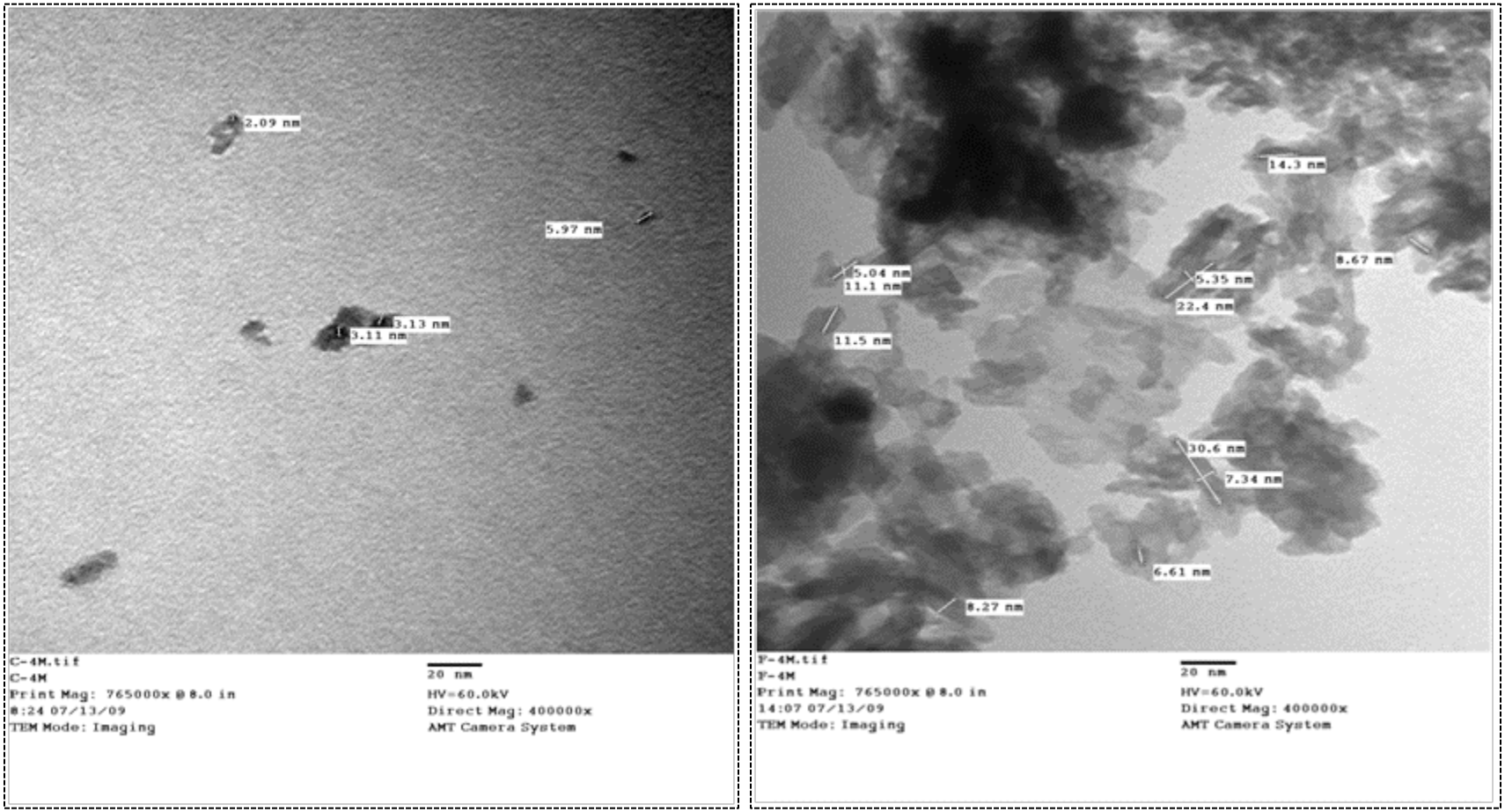

Figure F.7: Transmission electron micrographs of (A) W/γ-Al_2O_3 and (B) 4%-P nitride catalysts. Conditions: 30 wt% W, 4 wt% Ni, 4 wt% P and T_N, 700 °C.

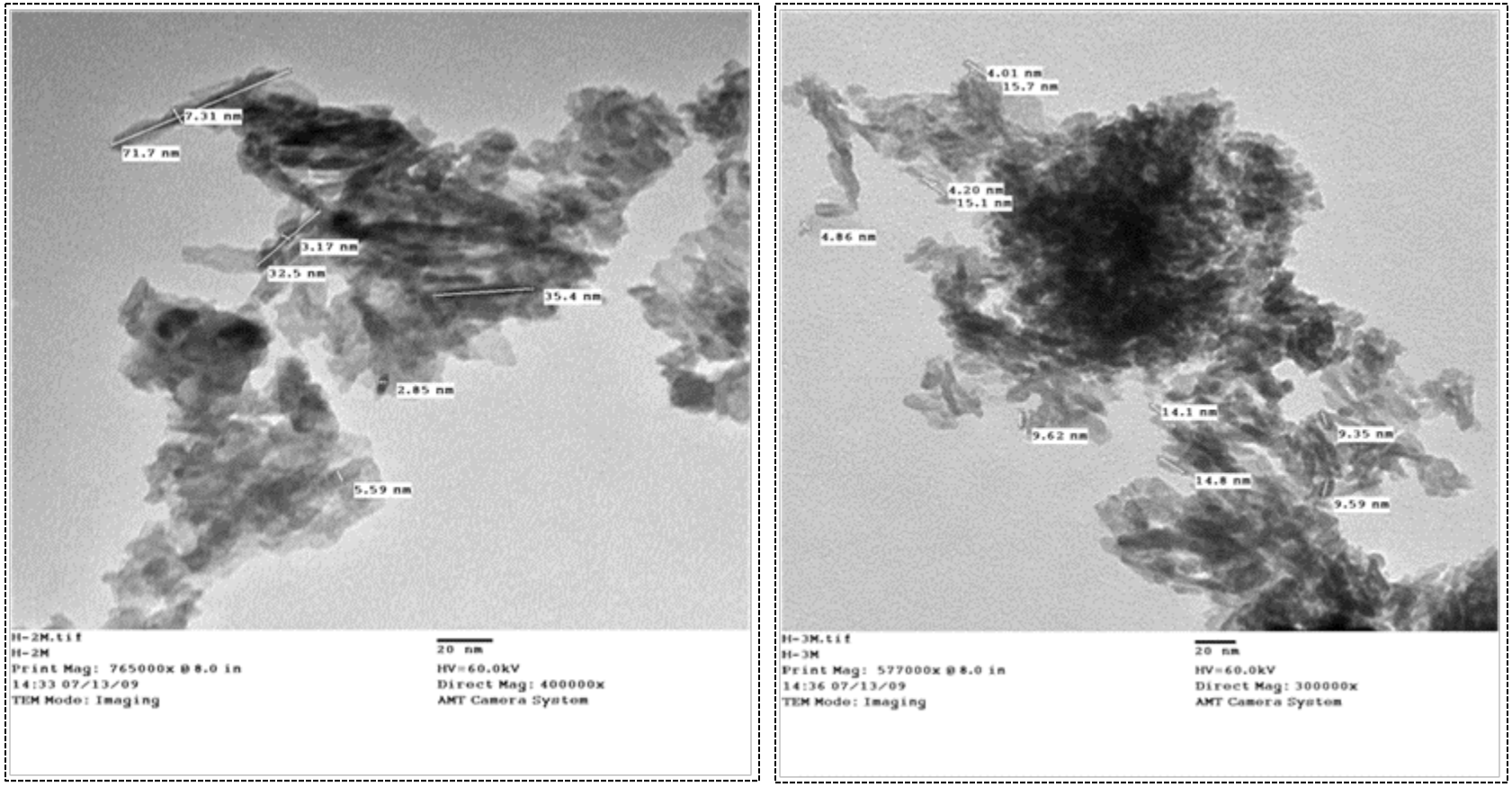

Figure F.8: Transmission electron micrographs of 2%-Ni nitride catalyst. Conditions: 30 wt% W, 2 wt% Ni, 2 wt% P and T_N, 700 °C.

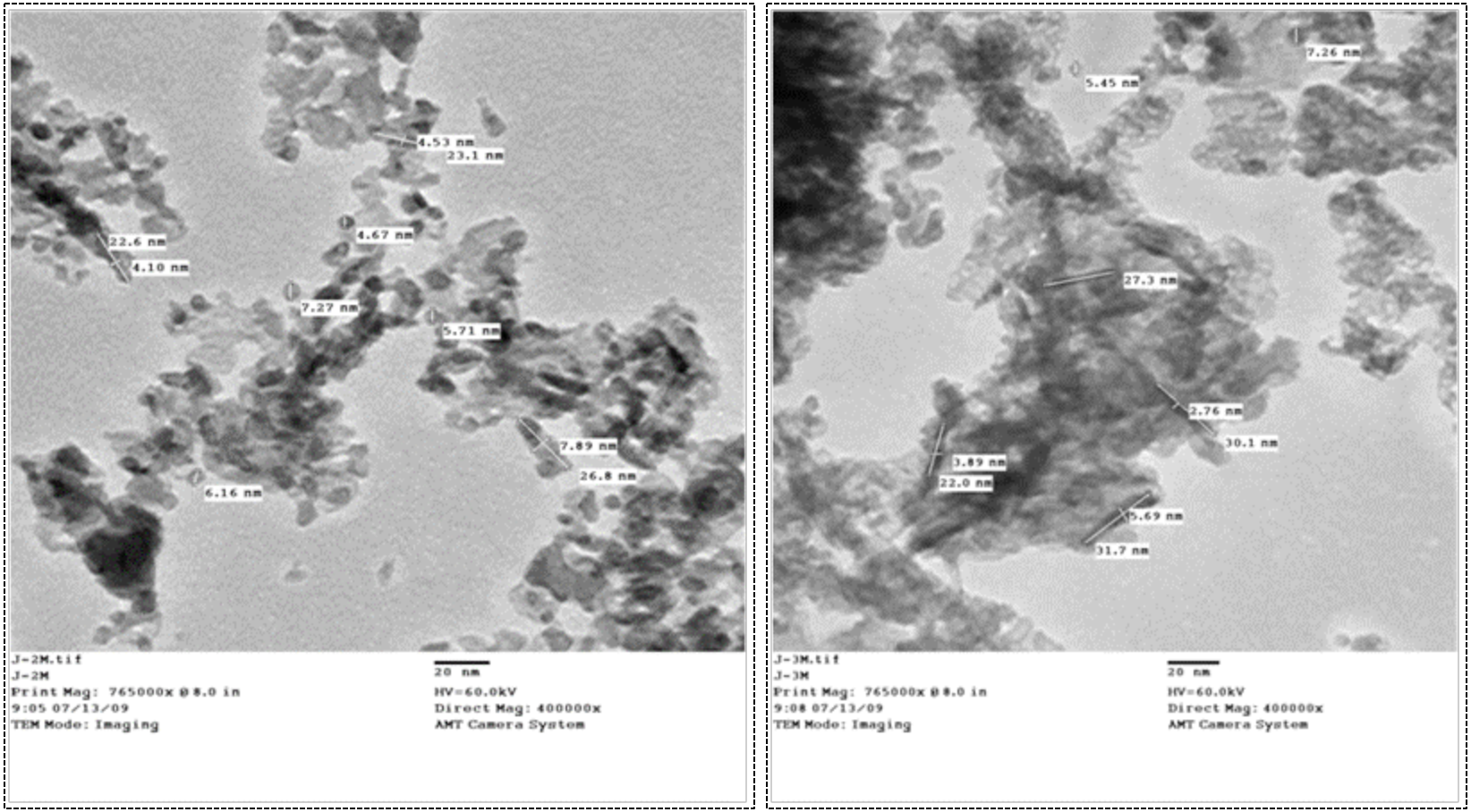

Figure F.9: Transmission electron micrographs of 40% W nitrides catalyst. Conditions: 40 wt% W, 4 wt% Ni, 2 wt% P and T_N of 700 °C.

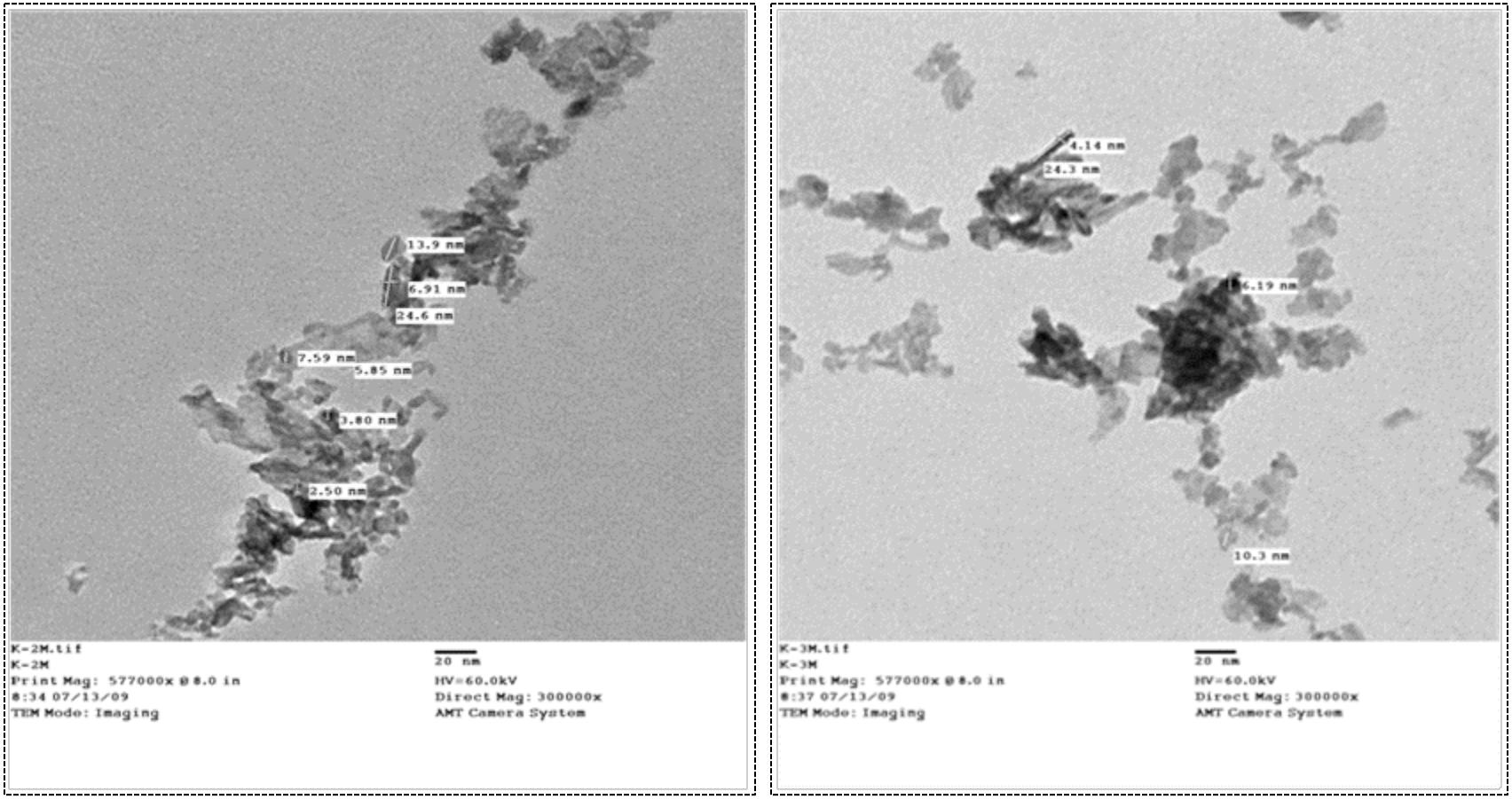

Figure F.10: Transmission electron micrographs of 500°-T_N nitrides catalyst. Conditions: 30 wt% W, 4 wt% Ni, 2 wt% P and T_N of 500 °C.

F.4 Infrared Spectroscopy Results

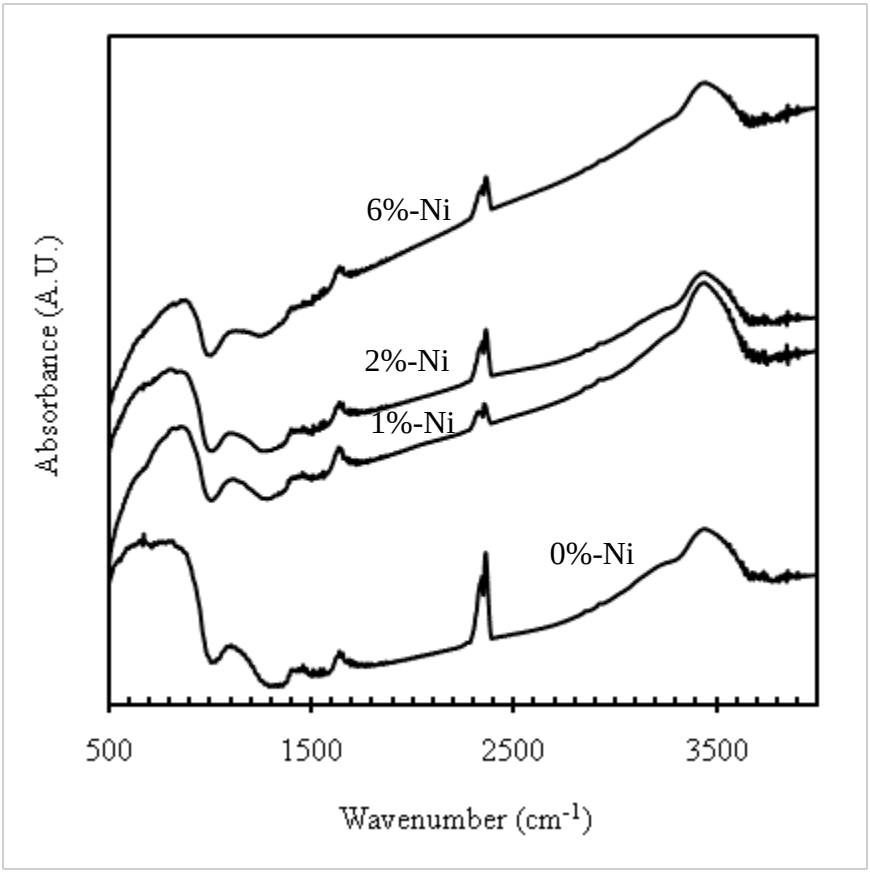

Figure F.11: Infrared spectra of Cat-Ni nitride samples in the 400-4000 cm^{-1} region. Conditions: W, 30 wt%; P, 2 wt%; T_N, 700 °C.

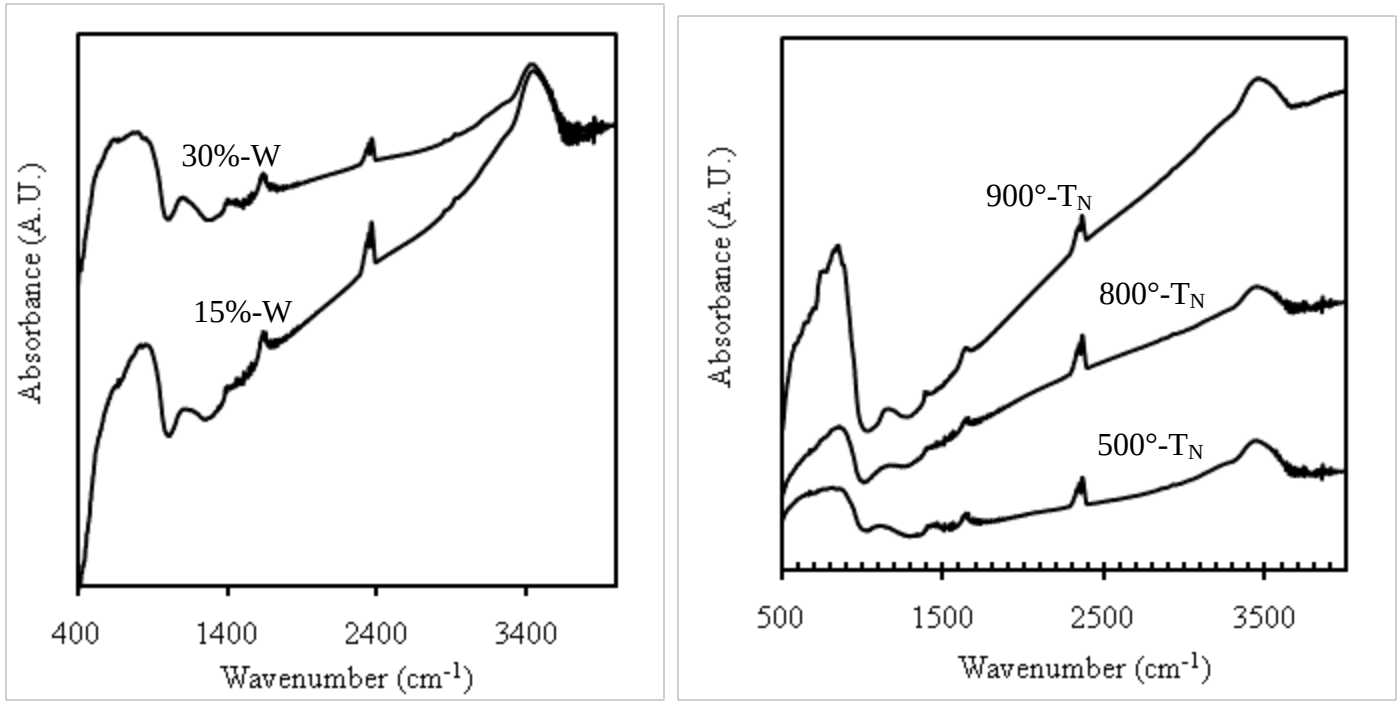

Figure F.12: IR spectra of (A) Cat-W and (B) Cat-T_N nitride samples in the 400-4000 cm^{-1} region. Conditions: 4 wt% Ni, 2 wt% P, (A) T_N of 700 °C, (B) 30 wt% W.

Table F.1: HDS, HDN and HDA responses for nitride catalyst activity screening studies.

Catalyst Name	Ni Loading (wt %)	P Loading (wt %)	T_N (°C)	HDS	HDN	HDA
R-1	6.4 (0.6)	4.0 (-0.6)	561 (-0.6)	68.1	18.0	40.0
R-2	6.4 (0.6)	1.0 (0.6)	739 (0.6)	74.3	14.8	52.0
R-3	4.0 (0.0)	2.5 (0.0)	650 (0.0)	84.1	37.0	61.0
R-4	1.6 (-0.6)	4.0 (-0.6)	739 (0.6)	74.2	32.3	43.1
R-5	1.6 (-0.6)	1.0 (0.6)	561 (-0.6)	90.5	62.0	45.4
R-6	4.0 (0.0)	2.5 (0.0)	650 (0.0)	84.7	34.5	59.0
R-7	6.4 (0.6)	4.0 (-0.6)	739 (0.6)	80.0	24.7	50.7
R-8	1.6 (-0.6)	1.0 (0.6)	739 (0.6)	63.4	12.2	36.8
R-9	6.4 (0.6)	1.0 (0.6)	561 (-0.6)	78.0	25.5	30.8
R-10	4.0 (0.0)	2.5 (0.0)	650 (0.0)	84.0	36.4	61.0
R-11	1.6 (-0.6)	4.0 (-0.6)	561 (-0.6)	78.3	28.4	41.5
R-12	4.0 (0.0)	2.5 (0.0)	650 (0.0)	83.9	33.3.0	58.0
R-13	4.0 (0.0)	2.5 (0.0)	650 (0.0)	84.5	31.6	58.2
R-14	0.0 (-1.0)	2.5 (0.0)	650 (0.0)	70.0	22.0	48.0
R-15	4.0 (0.0)	2.5 (0.0)	800 (1.0)	72.5	18.6	37.1
R-16	4.0 (0.0)	2.5 (0.0)	500 (-1.0)	84.1	24.0	41.0
R-17	8.0 (1.0)	2.5 (0.0)	650 (0.0)	71.2	20.5	44.0
R-18	4.0 (0.0)	2.5 (0.0)	650 (0.0)	86.0	37.0	59.0
R-19	4.0 (0.0)	0.0 (-1.0)	650 (0.0)	73.9	20.1	37.6
R-20	4.0 (0.0)	5.0 (1.0)	650 (0.0)	75.0	24.0	30.0